UNIVERSIDAD AUTÓNOMA DE MADRID
Facultad de Ciencias
Departamento de Física Teórica

A spectroscopic study of the nearby late-type stellar population: Properties of members of stellar kinematic groups and stars with circumstellar dusty debris discs.

PhD dissertation submitted by

Jesús Maldonado Prado

for the degree of Doctor in Physics

Supervised by

Dr. Carlos Eiroa de San Francisco

Madrid, June 2012

UNIVERSIDAD AUTÓNOMA DE MADRID
Facultad de Ciencias
Departamento de Física Teórica

Estudio espectroscópico de la población estelar fría cercana: Propiedades de estrellas en grupos cinemáticos estelares y de estrellas con discos circunestelares de tipo debris.

Memoria de tesis doctoral presentada por

Jesús Maldonado Prado

para optar al grado de Doctor en Ciencias Físicas

Trabajo dirigido por el

Dr. Carlos Eiroa de San Francisco

Madrid, Junio de 2012

A mis padres y hermanos

Agradecimientos

La finalización de una tesis doctoral es siempre un momento para el balance y la reflexión. Confío que estas breves palabras sirvan de pequeño reconocimiento a todas las personas que durante todo este largo, y no siempre fácil, período de tiempo han tenido a bien brindarme su ayuda, su apoyo y, en muchos casos, su simpatía. A todos los que de alguna manera me habeís ayudado, *gracias*.

Las primeras palabras de estas notas deben ser para mi supervisor de tesis, Carlos Eiroa, por su confianza, su apoyo y dedicación y sobre todo por esa mirada crítica tan suya que, desde siempre, ha tratado de transmitirme. A Benjamín Montesinos debo agradecerle muchas cosas, en particular su cercanía y su forma de ser, a David Montes y a Raquel Martínez, su esfuerzo y dedicación. A Alcione Mora y a Eva Villaver quisiera agradecerles su confianza, sus consejos y lo mucho que he disfrutado trabajando con ellos.

A lo largo de estos años he tenido la oportunidad de conocer y trabajar con mucha gente, de todos ellos he aprendido y con todos ellos he compartido buenas experiencias, en especial, Jonathan Marsall, Amelia Bayo, Gwendolyn Meeus, Alexander Mustill, Aurora Sicilia, todos los "DUNERs" y, por supuesto, Ignacio Mendigutía con el que llevo tantos años compartiendo amistad. En especial, a Ralf Lahunhardt debo agradecerle la estancia que hice en Heidelberg y su ayuda con los espectros FEROS.

Quisiera igualmente mencionar a mis amigos y compañeros del 301, al personal del departamento de Física Teórica, de la Universidad Autónoma de Madrid, y de los observatorios de Calar Alto y La Palma, así como a todos mis amigos en Bolaños, en Madrid y en otros muchos sitios.

Las palabras más importantes, como casi siempre suele ocurrir, se dejan para el final y, como no puede ser de otra manera, han de ser para mi familia, mis padres y mis hermanos, porque me han querido, me han animado, han cuidado de mí desde pequeñíto y siempre han dado todo lo que tienen (e incluso lo que no tienen) por mí.

Jesús Maldonado Prado

Acknowledgements

This Ph.D. Thesis is based on observations made with the 2.2 m telescope at the Centro Astronómico Hispano-Alemán (CAHA) at Calar Alto (Spain), operated jointly by the Max-Planck Institute für Astronomie and the Instituto de Astrofísica de Andalucía (CSIC); the Italian Telescopio Nazionale Galileo (TNG), operated on the island of La Palma by the Fundación Galileo Galilei of the INAF (Istituto Nazionale di Astrofisica) at the Spanish Observatorio del Roque de los Muchachos of the Instituto de Astrofísica de Canarias; and the Nordic Optical Telescope (NOT), operated on the island of La Palma jointly by Denmark, Finland, Iceland, Norway, and Sweden, in the Spanish Observatorio del Roque de los Muchachos of the Instituto de Astrofísica de Canarias. Complementary data has also been taken from the ESO Science Archive facility at http:://archive.eso.org/cms/.

This work has been supported by the Spanish Ministerio de Ciencia e Innovación (MICINN), Programa Nacional de Formación de Personal Investigador FPI 2006, and Plan Nacional de Astronomía y Astrofísica, under projects AYA2005-00954, and AYA2008-01727. The author also acknowledges support from the Department of Theoretical Physics of the Universidad Autónoma de Madrid, via an assistant teacher position. Additional funding for the Comunidad de Madrid project ASTRID S-0505/ESP/00361 is acknowledged.

This research has made use of the SIMBAD database and the VizieR catalogue access tool both operated at CDS, Strasbourg, France. The Spanish Virtual Observatory team is acknowledged for the development of the DAMA (Darwin Archive MAdrid) and DUNES Virtual Observatory Tools. This research also made use of the NASA's Astrophysics Data System Bibliographic Services.

Abstract

Understanding how stars and planetary systems form and evolve is one of the major goals of modern Astrophysics. Given that their stellar properties resemble those of our Sun, main-sequence, late-type stars usually constitute primary targets in exo-planet search programs, as well as surveys seeking for dusty debris discs similar to the Solar System's zodiacal light and the Edgeworth Kuiper Belt. Nearby stars have the additional advantage that high-resolution observations can be obtained for large samples, allowing a precise determination of their properties. In this dissertation, the results of a high-resolution ($\lambda/\Delta\lambda \sim 57000$), optical spectra study of a sample of nearby (distance less than 25 pc), main-sequence, late-type (spectral type FGK) stars are presented. The specific objective of this project is the spectroscopic characterisation of the nearby late-type stellar population, in particular the stars hosting debris discs.

In order to analyse the temporal evolution of debris discs, stellar ages as accurate as possible are required. However, stellar age is one of the most difficult parameters to determine, in particular for solar-type field stars. Therefore, in the first part of this dissertation a comparison between different methods to derive ages is performed. Young stars are identified on the basis of their kinematics and plausible membership to stellar kinematic groups. Radial velocities are derived by using the cross-correlation technique and galactic spatial-velocity components (U, V, W) are computed. The young nature of the candidates selected by their kinematics is confirmed or rejected by analysing their lithium abundances, rotation periods, and levels of chromospheric and coronal emission. Our results show that roughly 25% of the stars analysed show a kinematics in agreement with some of the known kinematic groups. Nevertheless, when age diagnostics are considered, most of these stars are too old to be members of kinematic groups, and only 25.5% of the candidates (6.5% of the total stars) can be considered as probable members of a kinematic group. The results of this study are published by Maldonado et al. (2010, Chapter 3).

In the second part of this dissertation, we study whether the presence or absence of debris discs correlate with the stellar properties of the host stars, in particular with the stellar age and metallicity, since the presence of planets (giant-planets) is known to correlate with the metal content of the host star. Fundamental stellar parameters, $T_{\rm eff}$, $\log g$, and [Fe/H] are calculated by measuring the equivalent width of a sample of isolated Fe I and Fe II lines and applying the iron excitation and ionisation equilibrium conditions. Data from the literature for those stars with debris disc not included in our spectroscopic observations are also used. We have found a smooth transition toward higher metallicities from stars with neither debris disc nor planets to stars hosting giant-planets. Stars with debris discs show a similar metallicity distribution to that of stars without discs. Stars harbouring

both debris discs and planets show the same metallicity behaviour as stars hosting planets. These results can be explained by core-accretion models of planet formation. In addition, we have also found that planets orbiting around stars with debris discs are usually cool. The data suggest that stars hosting debris and gas-giant planets tend to have low-dust luminosities, and that there seems to be an anticorrelation between the dust luminosity and the innermost planet eccentricity. These trends could be explained by recent simulations of dynamical instabilities produced by eccentric giant planets. This study is published by Maldonado et al. (2012, Chapter 4).

The confirmation or rejection of the apparent trends suggested in Chapter 4 requires the analysis of extended samples, i.e., the detection of new debris discs around stars with planets. The possibility of finding colder and fainter debris discs using the new capabilities offered by the *Herschel Space Telescope* is discussed in Chapter 5. This work was motivated as a preparatory activity for the DUNES (DUst around NEarby Stars, Principal Investigator: Carlos Eiroa) project, a *Herschel* Open Time Key Project aimed to detect circumstellar debris discs with IR excesses as low as the one of the Edgeworth-Kuiper belt. The work addresses how stellar photospheres are predicted at far-IR wavelengths, analysing the different sources of uncertainties and their influence in the detection of a debris discs: i) choice of the stellar atmosphere model (ATLAS9, PHOENIX, MARCS); ii) stellar parameters; and iii) choice of the photometric points used to match the models with the observed spectral energy distribution. This work played a central role to accurately fix the exposure time of each of the DUNES targets, achieving a compromise between the exposure time of each target and optimising, as much as possible, the total observing time granted for DUNES. This work has been submitted for publication (Chapter 5).

Key words. Open clusters and associations: general - Stars: abundances - Stars: activity - Stars: age - Stars: circumstellar matter - Stars: planetary systems - Stars: late-type - Technique: spectroscopy

Resumen

Entender la formación y evolución de las estrellas y los sistemas planetarios es uno de los mayores retos de la Astrofísica moderna. Las estrellas de la secuencia principal y tipo espectral tardío presentan unas propiedades similares a la de nuestro Sol y, a consecuencia de ello, a menudo son incluidas en programas destinados a la búsqueda de exo-planetas y discos circunestelares de tipo debris similares a la luz zodical o al cinturón de Kuiper en el Sistema Solar. Las estrellas más cercanas presentan la ventaja adicional de poder ser observadas en alta resolución lo que permite la determinación precisa de sus características. En este trabajo se presentan los resultados de un estudio basado en espectros ópticos de alta resolución ($\lambda/\Delta\lambda \sim 57000$) de una muestra de estrellas cercanas (distancia inferior a 25 pc), de clase secuencia-principal y tipo espectral tardío (F,G,K). El hilo conductor de esta disertación es la caracterización espectroscópica de la población fría cercana, en particular la de las estrellas que albergan discos circunestelares de tipo debris.

Los discos circunestelares evolucionan con el tiempo, por tanto, es necesario disponer de determinaciones lo más precisas posibles de las edades de las estrellas para poder entender las escalas de tiempo involucradas en la formación y evolución de los sistemas planetarios. Por eso, en primer lugar, este trabajo aborda el problema de obtener edades precisas en estrellas de tipo solar. Las estrellas jóvenes son identificadas a partir de su cinemática y posible pertenencia a grupos cinemáticos estelares. Para ello, se calculan velocidades radiales usando la técnica de la correlación cruzada y las componentes galácticas de la velocidad (U, V, W). La juventud de las estrellas seleccionadas por su cinemática es confirmada o rechazada mediante el análisis de sus abundancias de litio, periodos de rotación, así como de sus niveles de emisión cromosférica y coronal. Nuestros resultados muestran que aproximadamente un 25% de las estrellas analizadas muestran una cinemática que permite agruparlas como miembros de alguno de los grupos cinemáticos conocidos. No obstante, al aplicar los criterios de edad, la mayoría de estas estrellas son demasiado viejas para formar parte de estos grupos y sólo un 25.5% de los candidatos, (6.5% del total de estrellas estudiadas), son clasificados como miembros probables de algún grupo cinemático. Los resultados de este estudio han sido publicados por Maldonado et al. (2010, Capítulo 3).

En la segunda parte de este trabajo se analiza si existe algún tipo de correlación entre los discos debris y las propiedades de las estrellas, en particular con la edad estelar y la metalicidad. Esta última propiedad resulta de gran interés dado que las estrellas que albergan planetas gigantes tienden a ser ricas en metales. Los parámetros estelares básicos, $T_{\rm eff}$, $\log g$ y [Fe/H] son calculados a partir de espectros ópticos de alta resolución, midiendo la anchura equivalente de una selección de líneas aisladas de Fe I y Fe II, aplicando las condiciones de equilibrio de ionización y excitación para el hierro. El estudio se completa con datos de la literatura

para las estrellas con disco no observadas todavía. Los resultados muestran que la distribución de metalicidad de las distintas muestras analizadas presentan una transición hacia metalicidades más altas, desde las estrellas sin discos debris ni planetas hacia las estrellas con planetas gigantes. Las estrellas con discos debris muestran una distribución de metalicidad similar a la de las estrellas sin discos. Por otro lado, las estrellas con discos y planetas muestran un comportamiento similar al de las estrellas que albergan planetas. Estos resultados pueden explicarse mediante modelos de formación de planetas que implican la acrección de material. Hemos encontrado que los planetas alrededor de estrellas con discos debris son mayoritariamente de tipo frío. Los datos sugieren que las estrellas con debris y planetas fríos gigantes tienden a mostrar bajos valores de la luminosidad del polvo. Además, parece existir una anticorrelación entre la luminosidad del polvo y la excentricidad del planeta más cercano a la estrella. Estas tendencias podrían ser explicadas por simulaciones recientes de inestabilidades dinámicas producidas por la presencia de planetas gigantes. Este estudio ha sido publicado por Maldonado et al. (2012, Capítulo 4).

Para poder confirmar las tendencias encontradas en el Capítulo 4 es necesario el análisis de muestras más amplias, esto es, detectar más discos debris y planetas. En el Capítulo 5 se discute la posibilidad de buscar discos debris más fríos y menos luminosos usando las nuevas capacidades que ofrece el *Telescopio Espacial Herschel*. Este trabajo fue motivado como una actividad preparatoria para el proyecto DUNES (DUst around NEarby Stars, Investigador Principal: Carlos Eiroa), un proyecto clave para *Herschel* con el objetivo de detectar discos circunestelares de tipo debris con excesos infrarrojos tan bajos como el exceso debido al cinturón de Edgeworth-Kuiper. El trabajo analiza en detalle la predicción de flujos fotosféricos en el infrarrojo lejano, las distintas fuentes de incertidumbre y su influencia en la detección de un posible disco: i) la elección del modelo de atmósfera estelar (ATLAS9, PHOENIX, MARCS); ii) incertidumbres en los parámetros estelares de las estrellas; y iii) la elección de los puntos fotométricos que se utilizan para normalizar el modelo a la distribución espectral de energía observada. Como aplicación, se obtienen flujos en las longitudes de onda de *Herschel* para las estrellas DUNES. Este trabajo desempeñó un papel importante a la hora de fijar el tiempo de exposición de las estrellas DUNES, alcanzando así un compromiso entre asegurar la posible detección de un disco y optimizar, en la medida de lo posible, el tiempo de observación concedido para el proyecto. Este estudio ha sido enviado para su publicación (Capítulo 5).

Palabras clave. Cúmulos abiertos y asociaciones: general - Estrellas: abundancias - Estrellas: actividad - Estrellas: edad - Estrellas: material circunestelar - Estrellas: sistemas planetarios - Estrellas: tipo espectral tardío - Técnicas: espectroscopía

Contents

List of Figures

LIST OF FIGURES

List of Tables

LIST OF TABLES

1 Introduction

The discovery of planets beyond the Solar System orbiting other stars similar to our Sun is one the most significant discoveries of modern Astrophysics. Main-sequence, late-type stars are the closest "twins" to our Sun in the Universe so they usually constitute primary targets in ground based and space exo-planet search programmes. This thesis, entitled *"A spectroscopic study of the nearby late-type stellar population: Properties of stellar kinematic groups and stars with circum-stellar dusty debris discs"* was originally designed in the framework of a long-term observational project aiming at a characterization of the F, G, and K-type stars in the solar neighbourhood. Besides their capabilities as potential planets hosts, the late-type stellar population largely determines the local properties of the Galaxy, so understanding the properties of these stars is of importance in many fields of investigations.

The specific topic of this dissertation mainly deals with the properties of the stars known to host circumstellar dusty debris discs. Observations made with *IRAS*, *ISO* and *Spitzer* reveal that main-sequence stars are often surrounded by planetesimal material, the so-called "debris-discs". Debris discs host stars are valuable tools to shed light in our understanding on how planetary systems do form and evolve, their diversity, and to place our own Solar System into a complete astrophysical context. Through this chapter the current status of the research fields most relevant for this thesis are reviewed, while the structure of this dissertation is outlined in Section 1.5

1.1 The debris discs phenomena

Young forming stars are often surrounded by an accretion circumstellar disc of gas and dust (e.g. Shu et al. 1987; Hartmann 2000). These discs are usually referred as protoplanetary discs since they consitute the places where we expect planets and small objects like comets or asteroids to be formed (e.g Ruden 1999). In their early stages, protoplanetary discs are composed of material coming from the primordial

molecular cloud, mainly gas (hydrogen and helium) which consitutes 99% of the disc mass, while the other 1% is due to small dust particles (e.g. Hollenbach et al. 2005). These dust particles produce a strong IR emission which can be detected as flux excesses over the stellar photospheric emission.

The infall from the molecular cloud onto the star and disc system diminishes with time and most of the disc mass is accreted onto the central star. Some dust grains can coagulate and grow to form planetesimals, low-mass planets or the rocky cores of giant planets. Over 6 Myr most solar-type stars have lost their protoplanetary discs. In more massive stars (A-type stars) disc's lifetimes are even shorter, between 3-5 Myr (e.g. Wyatt 2008, and references therein). In addition, many mechanisms can deplete the dust grains, including collisions, Poynting-Robertson drag, and radiation pressure. All these processes operate in relatively short timescales, and in $\sim 10^7$ yr most of the primordial gas and dust have disappeared (e.g. Hollenbach et al. 2005; Pascucci et al. 2006). In the early 80s, *IRAS* observations revealed the presence of dusty discs around stars older than $\sim 10^7$ yr, like Vega (Aumann et al. 1984), Fomalhaut and β Pic. Since the age of these stars is much larger than the lifetime of the dust particles, it was concluded that the circumstellar material surrounding these stars could not be primordial (part of the same molecular cloud where the star once formed) but a second generation dust coming from ongoing collisional events within a large population of (undetected) planetesimals, like the asteroids, comets and Kuiper Belt Objects (KBOs) in our Solar System (Backman & Paresce 1993). In other words, *debris discs are evidence of the formation of planetesimals around other stars*.

Since the discovery of the first debris discs, *IRAS*, *ISO*, and *Spitzer* observations have allowed the detection of debris discs around more than 300 stars, of which 32 are resolved [1], in either optical/near infrared wavelengths (tracing the dust scattered light) or at infrared/millimeter wavelengths (revealing the thermal emission of the dust), confirming that debris discs resemble dust belts, with peak densities at tens to hundreds of AUs from the central star, and estimated masses from (sub-)millimetre unresolved observations of only a few Moon masses (e.g. Schütz et al. 2005; Nilsson et al. 2010).

1.1.1 Debris disc frequency and evolution

Although the first debris discs were discovered with the *IRAS* and *ISO* satellites, most of our current knowledge on this phenomenon is due to *Spitzer*. In the following, a brief summary of the results from *Spitzer* debris discs surveys is given.

Early-type stars (spectral-type A) show an incidence of IR-excess of 32% at

[1] Un updated list can be found in the Catalog of Resolved Circumstellar Disks, http://circumstellardisks.org/

24 μm and $\geq$ 33% at 70 μm (Su et al. 2006). The data show that the strength of the IR-excess diminishes with the stellar age, albeit a significant scatter in the fractional dust luminosities at similar ages occurs. Atempts to fit the data suggest a decay on the dust luminosity of the form $1/t$ (Rieke et al. 2005; Su et al. 2006). For solar-type stars (spectral-types FGK), the frequency of 24 μm excesses steeply decreases with the age (Siegler et al. 2007) from 30-40% for stars younger than 50 Myr to only 1.2% for stars older than 1 Gyr. This suggests that warm asteroid belt-like discs are rare at old ages, a result also seen in *Spitzer*-IRS data (Beichman et al. 2006b). On the other hand, Bryden et al. (2006) and Trilling et al. (2008) found that $\approx$ 16% of the main-sequence F5-K5 mature (older than 1 Gry) stars show IR-excess at 70 μm, tracing cold dust $\sim$ 30-100 K at Kuiper Belt distances (tens of AUs), with fractional dust luminosities, $L_{dust}/L_{\star}$, of the order of 10^{-5} and higher. In constrast to the case of young stars, the frequency of excess remains fairly constant with the stellar age (1 - 10 Gyr). This different behaviour has been interpreted as the result of different evolutionary processes. The dynamics of young systems could be dominated by episodes of collisional events similar to the Solar System's late-heavy bombardment, producing large quantities of dust. After a billion years, such processes have almost ceased. Then, debris should be mainly produced by the steady grinding down of planetesimals (Trilling et al. 2008). Finally, debris discs around M-type stars still remain elusive. Thus, although some young M stars show a debris disc (e.g., AU Mic, $\sim$ 12 Myr) not clear IR-excess have been detected around old M-type stars (Gautier et al. 2007). The lack of excesses around old M-type stars could be an observational bias.

Debris discs have been found to be also common around binary systems. Trilling et al. (2007) found an incedence of debris discs around early (A and F spectral type) binary stars of 9% at 24 μm and 40% at 70 μm. The excess rate increases up to nearly 60% for binary systems with small (< 3 AU) separations. On the contrary, the frequency of debris discs around mature solar-type binary stars does not seem to be higher than around single stars (DUNES team, private communication). There is, in addition, evidence of the presence of planetesimals around more than 20 white dwarfs with atmospheres polluted with heavy elements (see e.g. Steele et al. 2011, and references therein). The presence of such discs are usually explained by the tidal disruption of planetesimals. Models require the presence of at least one planetary companion around the white dwarf's progenitor. During the asymptotic giant branch evolution of the withe dwarf's progenitor, the orbits of the planetary system became unstable and part of the planetesimal material could acquire high eccentricity, entering the white dwarf's Roche radius and being tidally disrupted (Jura 2003).

1.1.2 The Solar System debris disc

Our own Solar System also harbours a dusty disc produced by collisions of minor bodies like asteroids, comets, and Kuiper belt objects. Small dust particles in the inner Solar System are heated by the Sun and re-emit that energy at infrared wavelengths producing a diffuse glow in the sky nigth, a phenomenon known as zodiacal light. Observations with *IRAS*, *ISO*, and *COBE* satellites reveal that the zodiacal light is produced by rapidly-rotating grains composed of a mixture of amorphous silicates and carbon, 10-100 μm in size, placed at a typical distance of 1 AU (Reach et al. 2003). According to Nesvorný et al. (2010), roughly 85% of the dust grains in the inner Solar System are produced by Jupiter-family comets. The estimated fractional dust luminosity of the inner Solar System dust is $L_{dust}/L_{\star} \sim 10^{-8}$-$10^{-7}$ (Dermott et al. 2002), between two and three orders of magnitude less luminous than the faintest debris disc detected with *Spitzer*.

In the outer Solar System, the region beyond the orbit of Neptune, built up by small icy planet-scale objects remnants of the Solar System's formation, is known as the Edgeworth-Kuiper Belt (EKB). About 10^5 objects with diameters greater than 100 km are estimated to be in the EKB between 30 and 50 AU (Jewitt & Luu 2000). The thermal emission from the EKB dust disc has not yet been observed; nevertheless, impacts of dust grains were registered in-situ by the *Pioneer* 10 and 11 spacecrafts (Humes 1980) as well as by the *Voyager* mission (Gurnett et al. 1997). The estimated fractional luminosity of the EKB is $L_{dust}/L_{\star} \sim 10^{-7}$ (Vitense et al. 2012).

It is assumed that the early Solar System asteroid belt and EKB contained much more solid mass than today (e.g. O'Brien et al. 2007, and references therein). Models of dust evolution suggest that after $\sim 10^4$ yr, large planetesimals of $\sim$ 1000-2000 km have already been formed. These large bodies disturb the population of smaller planetesimals triggering a collisional cascade which produces large quantities of dust (Kenyon & Bromley 2005, Figure 4). After that, the dust production rate decreases and the dust luminosity slowly decays with time, following a power-law of the form $\sim 1/t$. Stochastic collisional events can alter the dust evolution, producing large spikes in the dust luminosity. The most important event of this type in the Solar System happened between 3.8 and 4.1 Gyr ago, a period known as the Late Heavy Bombardment (LHB), during which a large number of impact craters are believed to have formed on the surface of the Moon and the terrestrial planets. The LHB seems to have its origin in the orbital migration of the giant-planets which produced a severe ejection of asteriods towards the inner Solar System (Strom et al. 2005). The EKB has also been sculpted by the presence of the giant-planets, indeed, current models place its origin as a result of Neptune's outward migration (Gomes 2003; Levison & Morbidelli 2003).

1.2 Kinematics and age of solar-type stars

Nowdays, much effort is being developed to improve empirical age-relationships of main-sequence late-type stars. Quoting Mamajek & Hillenbrand (2008), one of the main motivations for such work is the need of accurate ages in order to understand the timescales involved in the formation and evolution of planetary systems and debris discs. Solar-type stars evolve too slowly to be dated by their position in the Hertzsprung-Russell diagram. Alternatively, membership to stellar associations and kinematic groups has been used as a methodology to identify young stars and to assign ages, specially after the release of the *Hipparcos* data. Today, high-resolution spectrographs allow us to date solar-type stars by the temporal decline of their levels of stellar activity, rotation, and lithium surface abundance, providing not only accurate ages, but also additional criteria (independent of kinematics) for assessing the likelihood of membership to a given stellar kinematic group.

1.2.1 Kinematic groups

Kinematic streams, stellar streams or moving groups are unbound group of stars that share common motions around the Galaxy. The study of kinematic groups has a long history, coming back in time to the works of Kapteyn (1905). Most of the recent works on kinematic groups are, however, due to O. Eggen, who postulated that such structures should have their origin in the dispersion of clusters, constituting the "link" between stars in clusters and field stars (e.g. Eggen 1994). According to Eggen, during the cluster's disruption their members are streched out forming a stream-like structure. Clusters' members are dispersed all over the sky but they still maintain a common motion which allow their identification as a group. Clusters are disintegrated on a time scale of about 0.2 Gyr (Wielen 1971) by effect of internal relaxation, tidal processes of the galactic field and encounters with massive objects such as giant molecular clouds. Therefore, kinematic groups should be young. Nevertheless, most of the kinematic groups idenfied by Eggen (usually referred to as "classical" groups) are older than several 10^8 yr (Table 1.1). This led to an important controversy on the existence of kinematic groups (e.g. Griffin 1998; Taylor 2000). It was not clear how stellar streams could survive against the galactic differential rotation over periods of time as long as 10^8-10^9 yr. In addition, the effect known as *disc heating* (the increase of the velocity dispersion of disc stars with the age) constituted another factor acting against the survival of a possible kinematic group.

The publication of the data from the ESA *Hipparcos Space Astrometry Mission* (ESA 1997) changed our understanding of stellar streams, providing positions and trigonometric parallaxes with unprecedented accuracy for tens of thousands of stars near the Sun. Statistical unbiased studies of large samples of stars

carried out by Chereul et al. (1999) and Asiain et al. (1999) showed that the velocity space is full of structures. The four most prominent ones can be identified with the classical Eggen's groups, namely Pleiades, Hyades, Ursa Major and Coma Berenices. At smaller velocity scales these groups split into distinct substructures with smaller velocity dispersions. Evidence for the existence of "old" kinematic groups were found by Dehnen (1998), who showed that the less prominent structures in the (U, V) planes were mainly composed of redder (and hence, on average older) stars. These older groups were more widespread in their U, V components and followed non circular orbits. To explain their eccentric orbits, Dehnen (1998) suggested that moving groups could have their origin in stars trapped into a resonance with a nonaxisymmetric force field like that of the galactic bar. Although these works were based on early (spectral-types A-F) stars, Skuljan et al. (1999) found a similar strucuture in two samples of early and late-type stars (Figure 1.1), showing that many late-type stars could be members of moving groups.

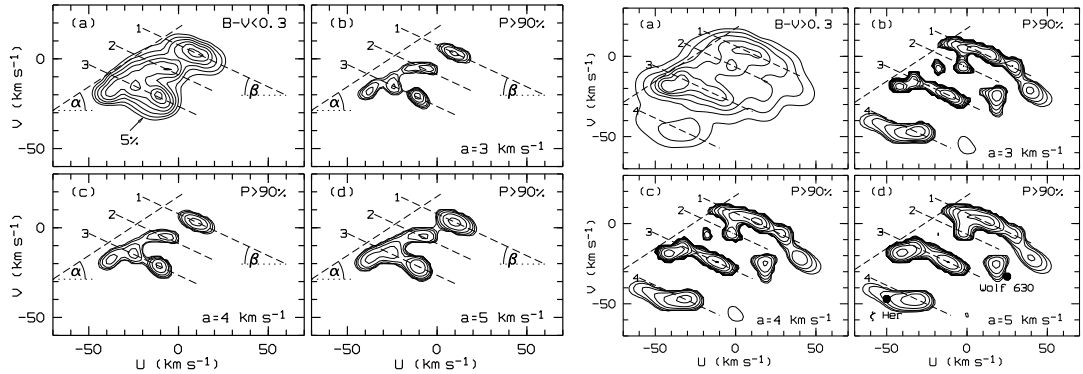

Figure 1.1: Example of velocity structures in the galactic (U, V) plane of early-type stars (left) and late-type stars (right). Taken from Skuljan et al. (1999, Figures 8 and 10). In each case (a) shows the velocity distribution and (b-d) the corresponding wavelet transforms at different scales. Both early and late-type stars show a stream-like structure (dashed lines) with several streams running diagonally with a negative slope relative to the U-axis.

These studies confirmed the existence of the classical moving groups but, at the same time, questioned the classical view of stellar streams as halos of evaporating clusters. Famaey et al. (2007, 2008) argue that if moving groups are systems trapped at a resonance, their mass distribution should be similar to the distribution of the disc' stars. On the other hand, in the evaporating cluster theory, the mass distribution should be the initial mass function of the cluster (modified by star evaporation as a function of mass). Their results for the Hyades moving group show that only a small fraction of the moving group stars were associated with the

Hyades cluster in the past, the rest being old field stars trapped at a resonance.

The topic is developing rapidly, and more statistical analysis of large-samples of stars are being conducted (e.g. Antoja et al. 2008; Klement et al. 2008; Bovy et al. 2009; Francis & Anderson 2009; Zhao et al. 2009). *Hipparcos* data are, therefore, providing us a new view of the concept of stellar stream, whose main features are:

- The velocity-space is richly populated with overdensity-regions. The positions of these overdensities agree reasonable well with the positions of the classical moving groups suggested by Eggen.

- At smaller velocity scales, moving groups split into different substructures with different ages, that in several cases can be related to the kinematic properties of nearby open clusters or associations. The velocity dispersion of the moving groups are large (up to $\sigma_U \sim$ 5-6 kms^{-1}), suggesting that moving groups can survive for long periods of time.

- Studies favour a dynamical (resonant) nature of stellar streams, in which only a given percentage of the members (stars in structures with coherent kinematics) arises from the evolution and dissolution of an initially gravitationally bound cluster.

An updated list of the known stellar kinematic groups is given in Table 1.1, while Figure 1.2 shows their positions in the galactic-(U, V) plane.

The richness of the galactic velocity space is completed with the presence of young, nearby associations or young moving groups. Examples of such associations are β Pictoris, TW Hydrae, ϵ Chamaleonis, Tucana-Horologium, or AB Doradus. An updated list is given in Table 1.1. These associations are located at distances of 50-100 pc and have a relatively small number of members (20 - 40) with derived ages between 6 and 200 Myr. In the velocity diagrams, young associations are located in the boundaries of the Eggen's Local Association of stars (Figure 1.2, right panel). In contrast to the "classical" groups, it is widely accepted that young associations have their origin in recent events of star formation (Zuckerman & Webb 2000; Zuckerman & Song 2004). In this regard, Makarov (2007) trace back the three-dimensional galactic orbits of possible members of young associations concluding that the majority of nearby young stars were formed during close passages or encounters of their natal clouds with the OB associations in Scorpius-Centaurus and the dense clouds in Ophiuchus and Corona Australis. These triggered star formation events resulted in small co-moving groups of 20 - 40 stars.

Table 1.1: Kinematics groups and associations in the solar neighbourhood, ordered by increasing V component (in absolute value). They are divided into three categories according to their age: "young associations", "moderately young", and "old" moving groups.

Name	U (kms^{-1})	V (kms^{-1})	W (kms^{-1})	Age (Myr)	Ref.
Young Associations					
Octans	-14.5	-3.6	-11.2	20?	Torres et al. (2008)
Young Sco-Sgr Ass.	-4.0	-13.4	-8.0	8	Torres et al. (2003)
Argus A	-22.0	-14.4	-5.0	40	Torres et al. (2008)
HD 141569	-5.4	-15.6	-4.4	~ 5	Aarnio et al. (2008)
Cha-Near	-11.0	-16.0	-8.0	10?	Zuckerman & Song (2004)
β Pictoris	-10.1	-15.9	-9.2	10	Torres et al. (2008)
TW Hydrae Association	-10.5	-18.0	-4.9	8	Zuckerman & Song (2004)
Carina-Near	-26.0	-18.0	-2.0	~ 200	Zuckerman et al. (2006)
32 Ori (Mamajek 3)	-12.0	-19.0	-9.0	~ 25	Mamajek (2007)
ϵ Chamaleonis	-11.0	-19.9	-10.4	6	Torres et al. (2008)
Tucana / Horologium	-9.9	-20.9	-1.4	30	Torres et al. (2008)
Columba	-13.2	-21.8	-5.9	30	Torres et al. (2008)
Carina	-10.2	-23.0	-4.4	30	Torres et al. (2008)
μ Oph (Mamajek 2)	-12.5	-24.1	-4.9	$\sim$120	Mamajek (2006)
AB Doradus	-6.8	-27.2	-13.6	70	Torres et al. (2008)
Classical "moderately young" Moving Groups					
Ursa Major	+14.9	+1.0	-10.7	300-500	Soderblom & Mayor (1993b)
Castor	-10.7	-8.0	-9.7	200	Barrado y Navascués (1998)
IC 2391	-20.6	-15.7	-9.1	35-55	Montes et al. (2001b)
Hyades	-39.7	-17.7	-2.4	650	Montes et al. (2001b)
Local Association	-11.6	-21.0	-11.4	20-150	Montes et al. (2001b)
Hercules-Lyra	-15.4	-23.4		150-300	Fuhrmann (2004)
Classical "old" Moving Groups					
γ Leonis	+78	-4	-1		Eggen (1959b,a)
Wolf 630	+25	-33	+13	2700	Eggen (1965, 1969)
					Bubar & King (2010)
ϵ Indi	-78	-38	+4		Eggen (1958b, 1971b)
ζ Herculis	-52	-47	-27		Eggen (1958b, 1971b)
61 Cygni	-90	-53	-8		Eggen (1958b, 1964)
HR 1614	-4	-58	-11	2000	Feltzing & Holmberg (2000a)
σ Puppis	-75	-88	-21		Eggen (1971b)
η Cephei	-33	-97	+10		Eggen (1964, 1971b)
Arcturus	+25	-115	-14	10000	Eggen (1971a, 1987)
					Williams et al. (2009)
Groombridge 1830	+227	-157	-14		Eggen & Sandage (1959)
Kapteyn's Star	+19	-288	-53		Eggen (1964)
					Wylie-de Boer et al. (2010)

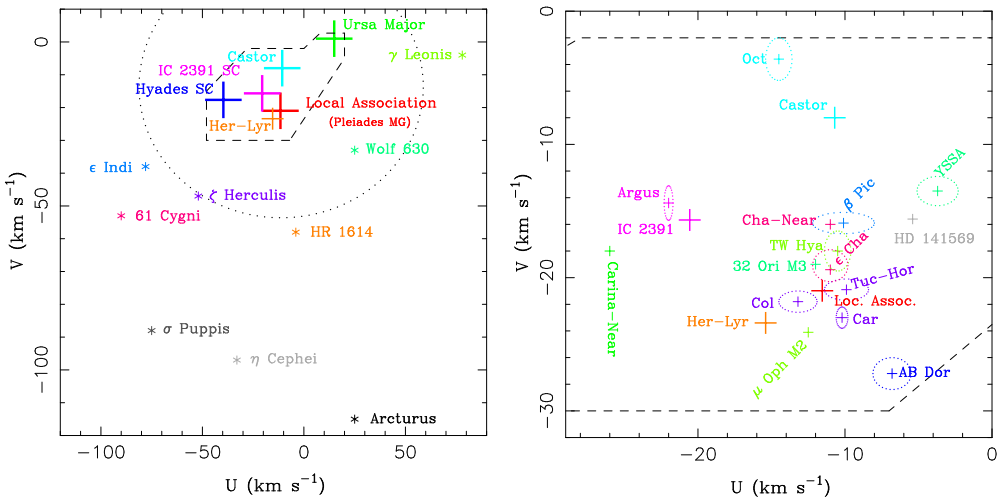

Figure 1.2: Left: (U, V) plane showing the position of the known kinematic groups in the solar neighbourhood. Large crosses represent the convergence point of the classical "moderately-young" moving groups. Asterisks show the position of the so-called "old" moving groups. The dashed line represents the boundary of the young disc population as defined by Eggen (Eggen 1984, 1989). The dotted line represents the velocity ellipsoid determined by Francis & Anderson (2009). Right: Zoom of the region of the (U, V) plane around the Local Association where the young moving groups or associations are found.

1.2.2 On the age of solar-type stars

Age determination for isolated (non-cluster's members) solar-type stars constitutes an important challenge in many research areas. Usual dating-methods for these stars are their levels of rotation, chromospheric activity, and lithium abundance, properties which can be quantified by observable features in the stellar spectra.

Stellar activity & rotation rate

In solar-type stars, stellar activity has its origin in the presence of a convective zone and it is generated by the stellar magnetic dynamo mechanism, the strength of which scales with the stellar differential rotation (Kraft 1967; Noyes et al. 1984; Montesinos et al. 2001). Stellar activity is observed in X-rays, the UV, and as emissions in the cores of strong absorption lines. The use of rotation and activity as age-diagnostics dates back to the works of Kraft (1967) and Skumanich (1972) who quantified their time decay with a power-law of the form $t^{-1/2}$. Since then, the Ca II H & K (3968.47, 3933.66 Å) resonance lines have become the most

observed manifestation of chromospheric activity in optical spectra, and a huge amount of papers with published Ca II H & K observations and their reduction to the R'_{HK} index is available in the literature (see references in Appendix A). Using the Sun as one anchor point and data from open clusters (with ages derived from other methods) several R'_{HK}-age relations have been described and discussed in the literature (Soderblom et al. 1991; Soderblom 2010; Donahue 1993; Rocha-Pinto & Maciel 1998; Lachaume et al. 1999; Mamajek & Hillenbrand 2008).

Kraft (1967) already noticed that the evolution of the rotational period had a dependence on the stellar mass - or colour (see also Mamajek & Hillenbrand 2008, Figure 4), but none of the available R'_{HK}-age calibrations have been able to provide stellar age as a function of activity and colour simultaneously. Barnes (2007) proposed that the influence of the mass and age are independent effects, so they can be separeted as follows:

$$P(B-V,t) = f(B-V)g(t) \tag{1.1}$$

$$f(B-V) = a[(B-V)_0 - c]^b \tag{1.2}$$

$$g(t) = t^n \tag{1.3}$$

Where the power-law $g(t)$ models the decay of the stellar rotation with age, and the dependence on the stellar mass is taken into account multiplying by the function $f(B-V)$. These curves in the colour-period-age space are known as "gyrochronology" curves. Slightly different values for the coefficients a, b, c, and n have been provided by Barnes (2007), Mamajek & Hillenbrand (2008), and Meibom et al. (2009), who fit the colour dependence (coefficients a, b, and c) using data from well known clusters. The index n is derived from the Sun's rotation and colour.

The use of gyrochronology as an age-estimator is limited by the lack of accurate rotational stellar periods for most stars. To overcome this problem, Mamajek & Hillenbrand (2008) derive empirical calibrations to transform the easier measurable R'_{HK} and L_X quantities into rotation periods via the Rossby number. The Rossby number, R_0, is defined as the ratio between the stellar rotation period, P, and the convective turnover time, τ_c. An estimate of τ_c can be obtained from the stellar colour following the prescriptions given in Noyes et al. (1984, Equation 4). In this way, gyrochronology can be appied to large samples of stars provided their R'_{HK} or L_X values are available.

X-ray fluxes constitutes another stellar activity database which can be used for age estimations. Sterzik & Schmitt (1997) demonstrated that the fractional X-ray luminosity, $\log(L_X/L_{Bol})$, derived from *ROSAT* soft X-ray (0.2- 2.4 keV) data, scales with chromospheric activity, while Guedel et al. (1997) found that

X-ray emission decays with time following a dependence of the form $L_X \propto t^{-1.5}$, a result which has been lately confirmed by Garcés et al. (private communication).

Lithium abundance

Photospheric lithium abundances are usually derived from the 6708 Å resonant doublet. Although some empirical Li abundance-age relations have been provided (Soderblom 1983; Boesgaard 1991), the physical processes that drive Li depletion depend not only on the stellar age, but also on the mass and chemical composition of a star. Even stars in a given open cluster show a high dispersion in their Li abundances (e.g. Soderblom et al. 1993). Therefore, Li abundance is usually applied as an additional methodology which gives a range of ages, instead of an specific value (e.g. Montes et al. 2001a). Recent works (e.g. Takeda et al. 2007, 2010) suggest that rotation may play a key role in controlling the surface Li of a star, being the depletion more efficient as the stellar rotation decreases.

Before analysing further properties of the debris discs host stars, Chapter 3 of this thesis deals with the problem of the kinematic and age estimates in low-mass stars.

1.3 The relationship between debris discs and planets

1.3.1 Frequency of debris discs among stars with planets

A relationship between the presence or absence of planets and debris discs should be expected. After all, debris discs are, strictly speaking, signatures of planetesimal systems, i.e., the raw material from which planets are formed. A first step to establish a possible connection is to check whether the presence of debris correlates with the presence of planets. In this regard, Beichman et al. (2005) analysed *Spitzer-MIPS* data for a sample of stars known to host close-in giant planets detected by radial-velocity techniques, finding a debris disc detection rate of 24 ± 10%. This percentage was higher than the average debris occurrence rate for non-host stars, 13 ± 5% (Bryden et al. 2006), so a "tentative" correlation between debris and planets was suggested.

With the number of known exoplanets and debris discs growing, the possible correlation debris-planets was discarded by Moro-Martín et al. (2007), a result which has been confirmed in more recent works. Bryden et al. (2009) and Kóspál et al. (2009) found a debris disc detection rate at 70 μm among stars hosting giant planets of 9 ± 3% and 15%, respectively. Nevertheless, the lack of a correlation presence of planets - presence of debris could be a trace that debris and planets

are indeed related phenomena. The presence of gaseous giant planets can affect the dynamical evolution of a disc producing warps, cavities, asymmetries or rings (e.g. Wyatt 2008, and references therein), and can also influence the dust production rates. Moro-Martín et al. (2007) argued that giant planets may clear out part of an initially massive debris disc by grinding or ejecting away planetesimals, maybe in processes similar to the LHB in our own Solar System (Section 1.1.2). As a consecuence, the brightness density of the disc diminishes, making the disc more difficult to detect.

Since 2009, new debris discs and planets have been discovered, in particular low-mass planets, reaching now objects with masses as low as ~ 1.94 $M_{\oplus}$ (Gl 581e). The number of stars harbouring both debris and planets has increased by $\sim 50\%$ with respect to the latest works. Given these numbers, it is worth to review the properties of the stars with debris discs and planets, in order to provide improved statistics. This objective will be addressed in Chapter 4 of this thesis.

1.3.2 Metallicity of planets and debris discs host stars

Another aspect that should be investigated is if debris production depends on the stellar properties, in particular the stellar age (Section 1.1.1) and the metallicity.

Establishing any possible trend with the stellar metallicity is crucial since it is well known that the presence of gaseous giant planets correlates with the stellar metallicity (e.g. Santos et al. 2001, 2004; Fischer & Valenti 2005; Bond et al. 2006). Data show that the percentage of stars with detected Jupiter-like planets with orbital periods shorter than 4 yr rises with the Fe abundance from less than 3% for the FGK stars with subsolar metallicity, up to 25% for stars with [Fe/H] $\geq$ +0.3 dex, the probability of harbouring a giant planet being nearly proportional to the square of the number of iron atoms (Figure 1.3, black histogram). On average, the metallicity distribution of stars with planets is shifted by 0.12 dex relative to that of stars without planets. It has also been found that high metallicity plays a role in the fraction of stars with multiple planets (Fischer & Valenti 2005).

Less massive planets (Figure 1.3, red histogram), more like Neptune or a super Earth ($M_p < 30$ $M_{\oplus}$, hereafter SEN), do not follow the same metallicity trend than their jovian counterparts, i.e, they do not form preferentially in higher-metallicity environments (Udry et al. 2006; Sousa et al. 2008; Ghezzi et al. 2010b; Mayor et al. 2011). Indeed, the median metallicity for solar-type stars hosting SEN planets is close to -0.1 dex, and a significant number of SEN planets are orbiting around stars with metallicities as low as -0.4 dex (Mayor et al. 2011).

These observational results have implications in our understanding on how planets form. Current models of giant planet formation can be divided into two main categories: core-accretion models and discs instability models. In core-accretion models, giant planets are formed by the runaway accretion of gas around

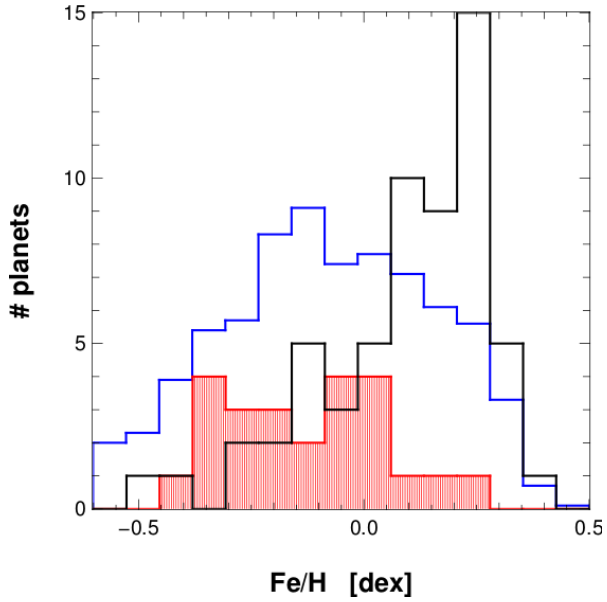

Figure 1.3: Number of planet host-stars as a function of stellar metallicity (taken from Mayor et al. 2011, Figure 16). The increasing trend in the number of stars with giant-planets as a function of metallicity is clearly seen (black histogram). On the contrary, the frequency of SEN planets (red histogram) is not correlated with high metallities. The histogram for both types of planets is shown in blue (multiplied by 0.1 for visual comparison purposes).

a previously formed rocky/icy core, the higher the grain content of the parental molecular cloud, the easier to build metal cores (e.g. Pollack et al. 1996; Rice & Armitage 2003; Alibert et al. 2004). On the contrary, in low-metal content protostelar clouds, the timescale needed to form cores would be longer, so by the time the cores are massive enough to start a runaway accretion of gas, the gas has already been depleted and, therefore, only low-mass planets could be formed. On the other hand, in the disc instability scenario, a gravitationally unstable region of the protoplanetary disc forms self-gravitating clumps of gas and dust (Boss 1997, 2006). Disc instabilities models do no depend on the metallicity of the primordial disc (Boss 2002), so, in these models, the metal-rich nature of the host stars is explained by an external origin not related to the properties of the parental molecular cloud, but to late-stage accretion of gas-depleted material.

Using metallicities from the literature, Beichman et al. (2005) discarded a relationship between debris discs and stellar metallicity; a result which was lately confirmed by Chavero et al. (2006) and Greaves et al. (2006), although statistics in both works are poor with only 42 FG debris discs stars analysed in the former, and 18 FGK in the latter work. The lack of such a correlation was interpreted

by Greaves et al. (2007) within the framework of core-accretion models: the outcome of a planetary system is classified from most to least successful, from the large supply of refractories and short evolutionary time-scales needed to form hot-gas giant planets, to systems with sparse refractories and long timescales, mainly characterized by planetesimal formation. The authors point out that the total mass of metals in the primordial disc is the key factor which determines the outcome of the system; their basic hypothesis is that the current metallicity of the stars reflects the original metal content of the young star and its disc.

As far as we know, the only work aimed to determine homogeneous metallicities for large samples of stars with debris disc is the one of Saffe et al. (2008), although $\sim$ 60% of the stars analysed are non solar-type objects (spectral types B, A, and early F). In this regard, part of the analysis presented in Chapter 4 of this thesis constitutes a first step towards a systematic characterization of a large sample of late-type stars with dusty debris discs.

1.4 Towards the detection of colder and fainter discs. Contribution to the *Herschel*-DUNES OTKP

Sptizer results show that the frequency of debris discs detection decreases steeply as smaller fractional dust luminosities are considered (Bryden et al. 2006, Figure 10). The less luminous debris disc detected by *Sptizer* surveys have dust luminosities, $L_{dust}/L_{\star}$, of the order of $\sim 10^{-5}$, which are within the sensitivity limits of the observatory (Figure 1.4, blue curve). These debris discs are around two orders of magnitude brighter than that of the Solar System EKB (Section 1.1.2). Extrapolating the *Spitzer* results, Bryden et al. (2006) concluded that the luminosity of the EKB is between 0.1 and 10 times the luminosity of an average solar-type star. That is to say, observational results suggest that debris discs at flux levels as low as the EKB should be common, but they have remained undetected because of their low fractional luminosities.

The launch on May 2009 of the ESA *Herschel Space Observatory* (Pilbratt et al. 2010) opened the possiblity of probing the frequency of disc detections for fainter discs. This is the main objetive of the on-going *Herschel* debris disc surveys DUNES (Eiroa et al. 2010) and DEBRIS (Matthews et al. 2010). In particular, DUNES (DUst around NEarby Stars)[2] aims to detect extra-solar analogues to the EKB around a sample of 239 nearby stars using as an optimal reference wavelength PACS (Poglitsch et al. 2010) 100 μm. DUNES observing strategy is to integrate for as long as needed to detect the 100 μm photospheric flux, subject only to confusion noise limitations. This constitutes an important difference with

[2]http://www.mpia-hd.mpg.de/DUNES/

the DEBRIS project which is a flux-limited survey[3]. The choice of PACS/100 is illustrated in Figure 1.4, where the discovery space of *Herschel* (cross-hatched area) is shown in comparison with previous facilities (*Spitzer*, SCUBA2, and Keck Interferometer). It is clear from the figure that PACS/100 μm is the most suitable wavelength for the detection of dust with temperatures in the range 20-100 K and dust luminosities, $L_{dust}/L_{\star} \sim 10^{-6}$.

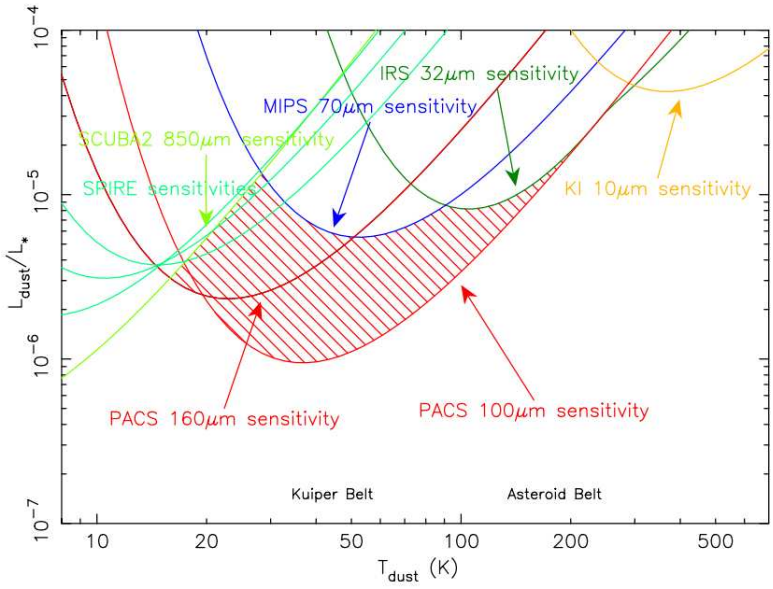

Figure 1.4: Detection limits for a G5V star at 20 pc, over a range of assumed dust temperatures following the Bryden et al. (2006) approach, where 3σ detection limits are shown in terms of the dust's fractional luminosity, $L_{dust}/L_{\star}$. The assumed 1σ fractional flux accuracies are 20% for *Spitzer*/MIPS at 70 μm, 2.5% for *Spitzer*/IRS at 32 μm, 10% for PACS 100 μm (i.e. SNR = 10) and 100% for PACS 160 μm (SNR = 1). Figure taken from the DUNES-OTKP proposal.

Figure 1.5 shows the expected PACS/100 μm IR-excesses around FGK stars compared to the *Spitzer* detection rates, as a function of the disc to star flux ratio. The figure shows that DUNES observations are expected to double the number of known debris discs around solar-type stars. DUNES estimations indicate that PACS 100 μm images with a SNR of 5-100 should provide a minimum detection rate of 20%.

Before *Herschel* data were provided, a lot of preparatory work was needed in order to assess the success of the project. Among this work, one of the most important task was the estimation of the stellar photospheres at *Herschel* wavelengths.

[3]Each target is observed to a depth of 1.2 mJy beam^{-1} at 100 μm.

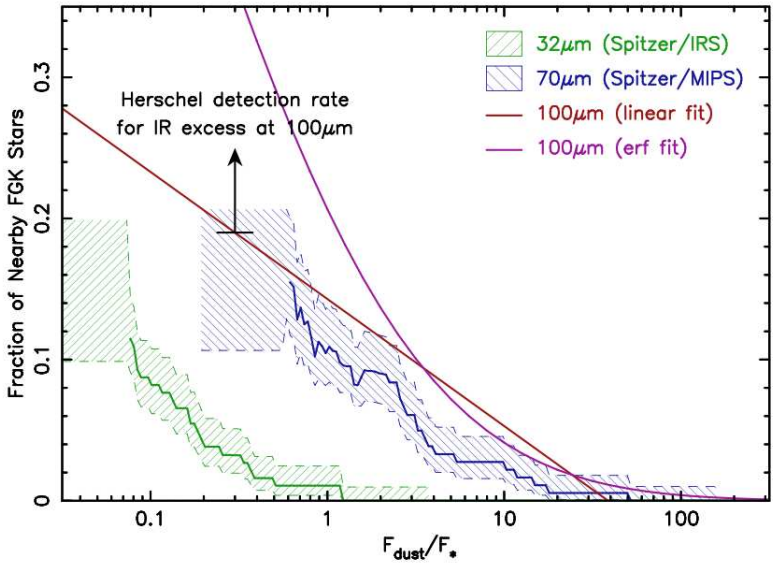

Figure 1.5: *Spitzer* detection rates of IR excess as a function of the fractional monochromatic dust, $F_{dust}/F_{\star}$ (blue and green curves). Uncertainties in the underlying distribution due to small number statistics (shaded regions) are large below the detection limits of each instrument/wavelength. The expected PACS/100 μm detection rates are overplotted in red (assuming a log-linear underlying distribution of debris disc fluxes) and purple (assming a log-normal relationship). Figure taken from the DUNES-OTKP proposal.

It is worth to note that DUNES aims to detect very low IR-excesses (a dusty EKB analogue at a 10 pc distance would have a ~ 5-10 mJy flux at PACS wavelengths), over similar photospheres (see photospheric predictions in Appendix C), which are only a few times the uncertainties in the measurements [4]. In other words, photospheric predictions as accurate as possible are essential to conclude the presence of a debris discs around a specific star as well as to optimize the total amount of observing time granted to the project. However, when predicting phostospheric fluxes several questions arise: what family of model atmospheres do better reproduce the observed SED of our targes, how to extrapolate to IR-wavelengths, which stellar parameters should be used, how uncertainties on the stellar parameters should be taken into account, which photometric points should be used to normalize the photosphere, etc. All these questions are discussed in

[4]Only 1.6 and 3.0 mJy, corresponding to the instrumental central area point-source 1σ rms-noise at 100 and 160 μm, for scans of 3.0 arcmin leg length and 3 repetitions. Release note PICC-ME-TN-036 at http://herschel.esac.esa.int/

detail in Chapter 5 of this thesis, where predictions at *Herschel* wavelengths for the DUNES targets are also given.

DUNES first results find an occurrence rate of debris disc around FGK stars of $\sim$ 24% (roughly 9% more than previous results). Nearly 38% of these excesses are new (not previously detected). The frequency of debris among planet-host stars is around 30% (DUNES team, private communication). One of the most interesting DUNES results is the discovery of a new class of cold and faint debris discs, $T_{dust} \lesssim 22$ K, $L_{dust}/L_{\star} \sim 10^{-6}$ (Eiroa et al. 2011). These new discoveries, togheter with the expected detection of further planets, in particular low-mass planets around stars with debris discs, will allow us to extend the samples analysed in this thesis, confirming or rejecting the apparent trends discussed in this work.

1.5 Scope and objectives of this thesis

This Ph.D. thesis is the result of the work carried out during the last years at the Universidad Autónoma de Madrid. Such work was planned as part of a long-term observational project designed to characterize the local late-type population following two main lines of research: *i)* the spectroscopic characterization of the stars by using high-resolution optical spectra, and *ii)* the study of the presence of circumstellar dusty debris discs and the properties of their host stars. The work done during this research in order to achieve the general objetives can be briefly summarised as follows:

(a) Several observing proposals were written and submitted in order to obtain the observational data required.

(b) Data were reduced using standard procedures.

(c) Accurate radial velocities and galactic spatial velocity components were computed. A preliminar identification of kinematic groups' members was performed using kinematics criteria.

(d) Different age diagnostics were studied and analysed, results were compared with kinematics, and lists of kinematic groups members were provided.

(e) A list of solar-type stars with known debris discs was compiled by analysing the previous *IRAS*, *ISO*, and *Spitzer* data.

(f) Stellar parameters were computed by applying the iron ionisation and equilibrium condition to a set of isolated Fe I and Fe II lines. A comparison with literature data was performed.

(g) The metallicity distribution of the stars was studied taken into account the presence/absence of debris discs and/or planets.

(h) Possible trends between the presence of debris and planets were investigated.

(i) Available photometry and stellar parameters in the literature were compiled for the DUNES targets.

(j) A comparison between different model atmospheres was performed. The influence of the stellar parameters and the photometric points in predicting stellar photospheres at IR-wavelengths was also studied.

(k) Photospheric predictions at *Herschel* wavelengths were computed for the DUNES targets.

Points (a) to (d) contributed fo fullfil objective *i)*, while objective *ii)* was addressed by points (e) to (k). The structure of this thesis is as follows:

- Chapter 2 includes all the information related to the observations and data reduction.
- Chapter 3 includes the kinematic and age study of the stars observed.
- Chapter 4 consists of the work about the metallicity distribution of stars with circumstellar dusty debris discs, and possible trends between the presence of debris and planets.
- Chapter 5 contains the work performed within the framework of the DUNES project.
- Chapter 6 contains the conclusions obtained in this Ph.D. thesis, as well as, prospects for future work.
- Chapter 7 is the Spanish version of Chapter 6.
- Appendices A, B, and C include the tables generated in Chapters 3, 4, and 5, respectively.

2

Observations and data reduction

Between 2005 and 2009, 12 observing runs were carried out in 2.2 and 3.5 meter telescopes. More than 500 stars were observed using several high-resolution échelle spectrographs. In Section 2.1 the telescopes and the configuration of the spectrographs are described. Once the observations were obtained, several operations in order to extract the stellar signal from the CCD frames were performed, a process known as data reduction. The calibration frames needed to reduce the data and the full procedure are explained in detail in Section 2.2.

2.1 Telescopes and instruments

An *échelle* is a grating designed to operate in high interference orders, n $\sim$ 100, each of them covering a small region of the spectra, typically $\lambda_{max} - \lambda_{min} \sim 100$ Å (e.g., Schroeder 2000). Spatial overlap may occur between contiguous orders, so a cross-dispersing grating or prism is used to separate and stack the orders on the detector.

A summary of the telescopes and instruments used in this thesis is given in Table 2.1, while Figure 2.1 shows an example of spectra of calibration light sources with flat spectral energy distribution (Flat-fields).

2.1.1 2.2m-FOCES

The FOCES spectrograph, Fibre Optics Cassegrain Echelle Spectrograph, (Pfeiffer et al. 1998) attached to the 2.2 m telescope in the Centro Astronómico Hispano-Alemán de Calar Alto (CAHA) was used in six observing runs. FOCES was used in unique fibre modus, with a CCD SITe♯1d (2048×2048, 0.24 μm/pixel) as detector. This configuration provides a resolution of $\approx$ 57000 and a spectral range from 3800 to 10000 Å in a total of 111 orders.

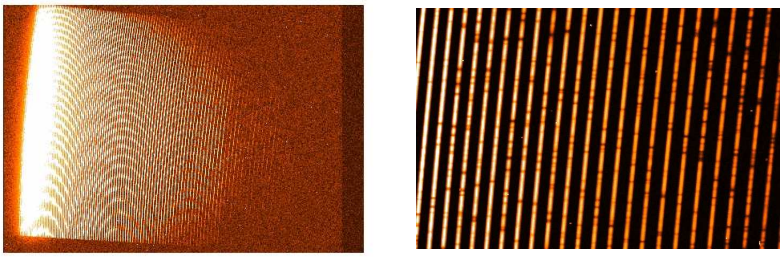

Figure 2.1: Spectral layout of frames of FOCES. Flat-Field frames are shown. The cross-dispersion direction is perpendicular to the frames. Left: The full frame is shown. The high brithness differences between the different regions of the CCD produces a moiré pattern which should not be confused with the location of the spectral orders. Right: Zoom of a region of the CCD showing several spectral orders.

2.1.2 TNG-SARG

The SARG spectrograph, Spectrografo ad alta risoluzione Galileo, (Gratton et al. 2001) on the Telescopio Nazionale Galileo (TNG) operated on the island of La Palma was used in four observing runs. SARG provide a resolution of $\approx$ 57000 and a spectral range covering from 4960 to 10110 Å in 50 orders. The detector is a mosaic of 2000 $\times$ 4000 EEV CCDs with a pixel size of 13.5 μm.

2.1.3 NOT-FIES

Two observing runs were carried with the FIES instrument, the high-resolution FIbre-fed Echelle Spectrograph, (Frandsen & Lindberg 1999) on the Nordic Optical Telescope (NOT) on the island of La Palma. FIES was used with the fibre bundle B (100 micron high-res fibre), a slit of 1.3 arcsec, and a 2000 $\times$ 2000 E2V CCD as detector. With this configuration, the resolution, $\lambda/\Delta\lambda$, is $\approx$ 67000 and the wavelength range covers from 3640 Å to 7360 Å in 80 orders.

2.1.4 Additional data from public archives

Available spectra in public libraries and archives constitute powerful data sets that allow us to optimize our own collection of observations, avoiding duplications and maximizing the observing time granted. In particular, since our observations were done from northern observatories, most targets have $\delta >$ -25^o and spectra

Table 2.1: Description of the telescopes and instruments.

	FOCES 2.2m-CAHA	**SARG** TNG	**FIES** NOT
Telescope			
Latitude	37^{o}13'23.8" N	28^{o}45'28.3" N	28^{o}45'26.2" N
Longitude	02^{o}32'45.7" E	17^{o}53'37.9" W	17^{o}53'06.3" W
Altitude (sea level)	2168 m	2387.2 m	2382 m
Telescope (aperture)	2.2 m	3.58 m	2.56 m
Focus	Cassegrain	Nasmyth	Primary
Spectrograph			
Configuration	Unique fibre modus	Red crossdisperser	Fibre bundle B
Slit size (μm)	120	150	50†
Orders (extracted)	106-111	50	80
Spectral range (Å)	3470-10700	5600-10000	3640-7360
CCD			
Manufacturer	SITe♯1d	2×EEV	E2V
♯ Pixels	2048^2	2048×4096	2048^2
Resolving power	≈ 57000	≈ 57000	≈ 67000
Pixel size (μm)	24	13.5	13.5
Observing runs			
	July 2005	February 2006	September 2008
	January 2006	January 2007	May 2009
	December 2006	April 2007	
	07A*, 08B*, 09B*	November 2008	

† A 100-micron slit with a 50 micron exit slit.
* Service mode.

from public archives were needed to partially cover the lack of southern targets. Specifically, data were taken from the following libraries/archives:

- FEROS spectra were retrieved from the ESO/ST-ECF Science Archive Facility [1]. FEROS is the ESO's Fibre-fed, extended range, prism-crossdispersed

[1] http://archive.eso.org/cms/

échelle spectrograph (Kaufer et al. 1999). It is mounted on the MPG/ESO-2.2 m telescope at La Silla Observatory. FEROS is fed by two fibres providing simultaneous spectra of *object* plus either *sky* or one of the two *calibration lamps*, wavelength calibration or flat-field ($R \sim 42000$, $\lambda\lambda$ 3500-9200 Å).

- "S^{4}N, A Spectroscopic Survey of Stars in the Solar Neighbourhood" (Allende Prieto et al. 2004), which is based on spectra taken with the 2d coudé spectrograph at McDonald Observatory (Tull et al. 1995), and the FEROS instrument on the ESO 1.52 m telescope in La Silla. McDonald spectra has a resolution of ~ 60000, covering a spectral range from 3400 to 10900 Å.

2.2 Data reduction

2.2.1 Calibration frames

In addition to the scientific stellar observations, several calibration frames are needed to recover the stellar signal:

- **Bias frames:** In order to avoid negative signals due to the read-out noise, a constant signal is applied to the CCD, the so-called *bias level*. This signal has to be determined from the *bias frames*. These frames are obtained by mere read-out, i.e., zero seconds of exposure time with the camera shutter closed.

- **Dark frames:** Another signal that should be subtracted is the *dark current* (electrons released in the CCD by the action of the thermal energy of the body of the detector). This signal increases with the exposure-time. Dark frames are also taken with the shutter closed but the exposure time used is the same to that selected for the object frames.

- **Flat-field frames:** The sensitivity varies across the CCD and strongly depends on the wavelength. Also, pixel-to-pixel changes in sensitivity can occur. Furthermore, the light measured depends on the wavelength-dependent efficiency of the instruments. To correct for these effects the images are divided by the so-called *flat-field frames*. These are obtained by illuminating the instrument with a source of light having a continuous spectrum. FOCES, SARG and FIES use an internal lamp which is moved into the light-path in front of the fibre.

- **Calibration lamps frames:** To make the identification of the pixel positions on the CCD frame with the wavelength of the incoming light, i.e.

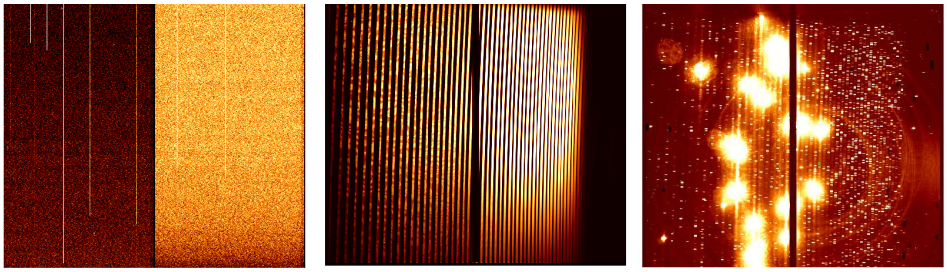

Figure 2.2: Example of calibration frames taken with the SARG spectrograph: bias (left), flat-field (center) and calibration lamp (right). The separation between the two CCDs is visible in all frames. Each CCD has its own bias level (left frame). Red wavelengths are to the left and the cross-dispersion direction is perpendicular to the frame (flat frame). The calibration lamp frame shows the Th-Ar emission lines, some of them are clearly saturated. Several cosmetic effects (bad columns and hot pixels) are also visible in the bias frame.

the *dispersion relation*, a frame of a calibration lamp is needed. FOCES, SARG and FIES are equipped with Thorium-Argon (Th-Ar) calibration lamps which provide sharp emission lines at known wavelengths covering the optical and the near-infrared spectral range.

All calibration frames are taken during day-time (before observations) and at the end of the night, so that the night-time can be devoted to the science observations. Figure 2.2 shows an example of these calibration frames for the SARG spectrograph.

2.2.2 Reduction procedure

The data reduction extracts the required information from the CCD frames, i.e. the stellar spectrum versus wavelength. It can be done in a mostly standardized process using specifically designed computational environments for the reduction and analysis of astronomical data. The IRAF [2] package *echelle* was used to reduce the data, following the steps summarized in Figure 2.3:

1. **Overscan:** Since the dark frame includes the bias level, it is possible to correct for both effects simultaneously by using the *overscan* region of the detector. The overscan regions are not physical rows or columns on the CCD, but “empty” pixels generated by sending additional clock cycles to the CCD

[2]IRAF is distributed by the National Optical Astronomy Observatory, which is operated by the Association of Universities for Research in Astronomy, Inc., under contract with the National Science Foundation.

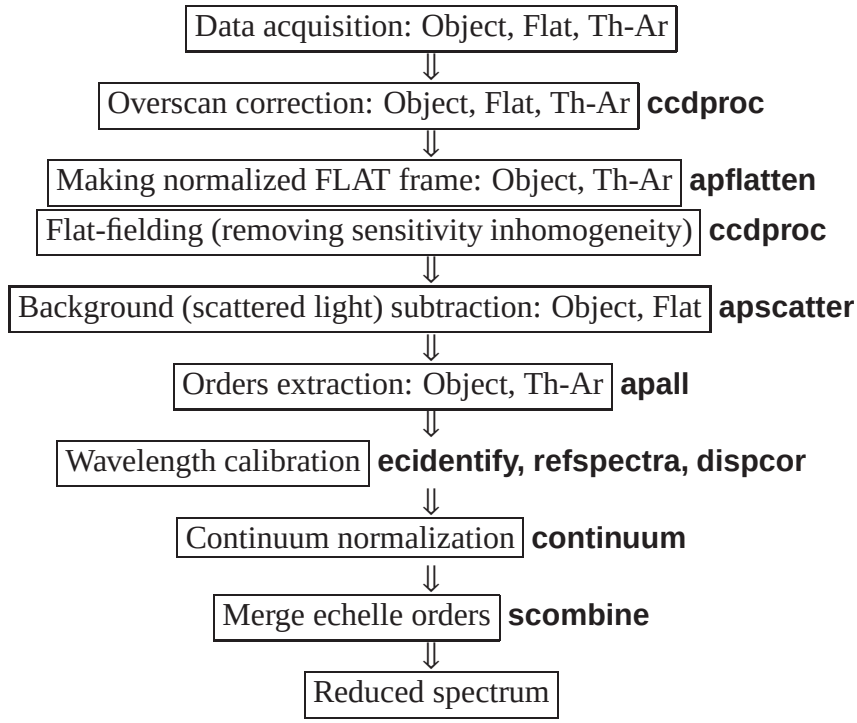

Figure 2.3: Flow chart of the reduction procedure with the IRAF package *echelle*.

output electronics. On an image display, overscan regions appear as a band along one of the edges of the image (see Figure 2.1, left frame). We used this method in our reduction. The trimming of the overscan columns and the correction for bias and dark current were done in the same step using the task *ccdproc*. This correction was applied to all frames, i.e, flat-field frames, Th-Ar frames and science frames.

2. **Flat-field correction:** Around 5-10 flat-field frames per night were combined by using the task *flatcombine*. This led to a "combined" flat-field frame. Before dividing the science frames by the combined flat-field, it was normalized, in order to keep the counts of the object data. This was done order by order, fitting a function for each order separately, so the number of rows in each image does not change. This process was done with the task *apflatten*.

3. **Scattered-light subtraction:** The spectrographs have many imperfections which originate additional sources of illumination on the CCD. Therefore, the light collected by the CCD is the sum of the astronomical spectrum and a scattered light continuum. Dispersed light is visible in an image display as a "bright" background signal (see Figure 2.1, left frame). Figure 2.4

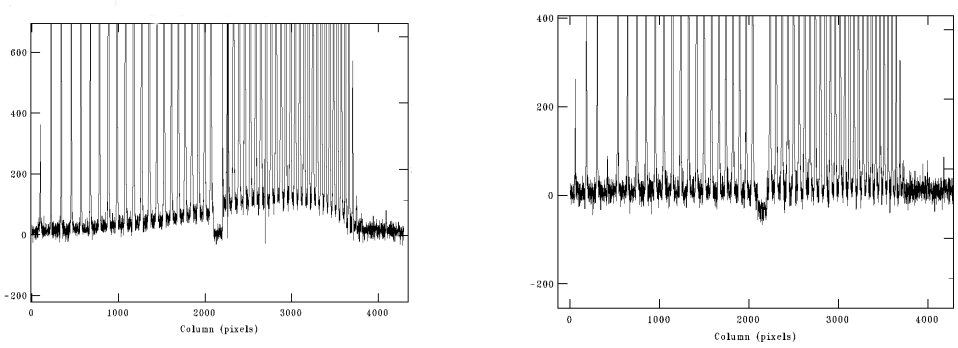

Figure 2.4: Example of scattered-light subtraction. Left: A cross section of an échelle spectrum in the spatial direction is shown. The scattered-light appears as a continuum which varies smoothly across the spatial direction. The spectral orders can be identified as narrow profiles superimposed over the continuum. In order to remove the scattered-light, the continuum is fitted in both the spatial and spectral directions. Right: A cross section of the same spectrum after scattered-light has been subtracted.

shows a cross section of an échelle spectrum in the spatial direction. The spectral orders appear as narrow profiles superimposed over a continuum of smooth spatial variability. The IRAF task *apscatter* can be used to fit the scattered light in both directions (spatial and spectral) making a two-dimensional image for each object.

4. **Order extraction:** The extraction is the generation of a one-dimensional spectrum for each order in the input image (i.e. adding up all of the data along the spatial profile). Each one-dimensional spectrum contains a portion of the complete stellar spectrum. It was performed with the task *apall* which provides functions for defining, modifying, tracing, and extracting apertures from two-dimensional spectra. An example is shown in Figure 2.5.

5. **Wavelength calibration:** The Th-Ar calibration frames' orders are extracted and used to derive the wavelength scale by fitting all orders simultaneously to a polynomial function. The IRAF task *ecidentify* is used to interactively identify the emission features of the Th-Ar calibration frames. Additional features from line lists included in IRAF can also be used. Once the Th-Ar frame is calibrated, the tasks *refspectra* and *dispcor* are used to link the stellar spectra to the Th-Ar frame and to replace pixels by wavelengths.

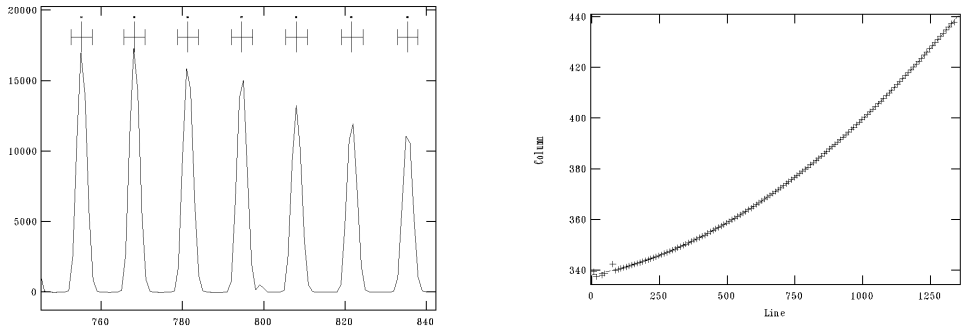

Figure 2.5: Left: A cut along the spatial profile of an échelle spectrum is shown. Several apertures are identified. Right: for one of these orders, the the trace of the spectrum along the detector is shown.

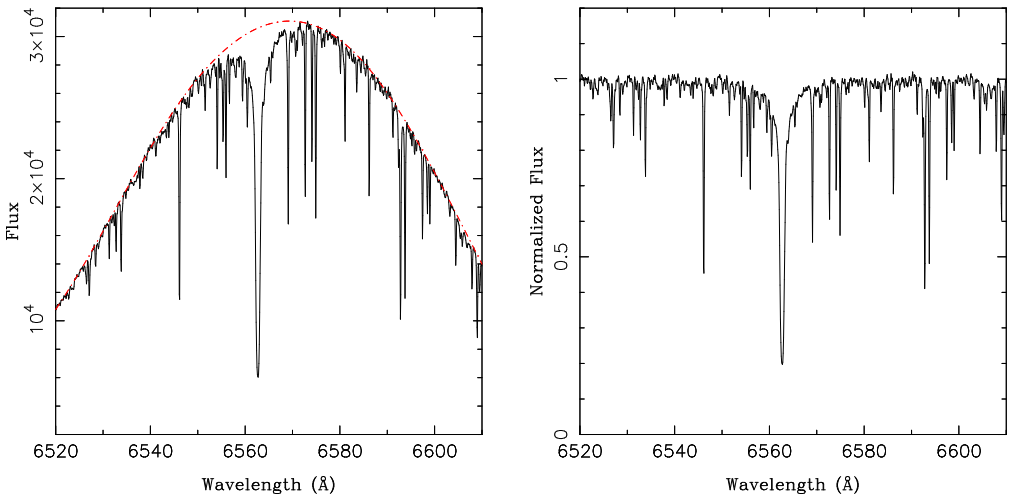

Figure 2.6: Example of normalization to the continuum. Left: The order displayed shows the spectrum of HD 3651 around H_α. The stellar continuum is fitted to a function (dashed red line) whose parameters (type of function, order, low rejection level, high rejection level, number of iterations) can be changed interactively by the user. Right: The same spectrum after the normalization.

6. **Normalization to the continuum:** An absolute flux calibration is difficult and not necessary for this work. The spectral analysis described later only requires the line profiles with respect to a relative continuum. The continuum in each spectral order is fitted with a spline cubic function. Spectral regions with chromospheric lines or prominent telluric lines have been excluded. Therefore a "flat" spectrum with the continuum flux set to the unit is obtained for each spectral order. In this way, equivalent widths of lines can be measured and lines profiles can be compared. Figure 2.6 shows an example of the normalization process.

7. **Merge of echelle orders:** For the analysis, the orders can be merged to have one single spectrum spanning the whole wavelength range. This is done with the task *scombine*. The most simple method is to average the normalized spectra in the overlapping regions. However, the orders' ends usually suffer from high noise as well as bad normalization, which lead to a "degraded" spectrum in the overlapping region, therefore it is convenient to cut the orders' ends before merging or applying low and/or high thresholds to the input pixels.

Some examples of representative stars in different spectral regions are given in Figure 2.7.

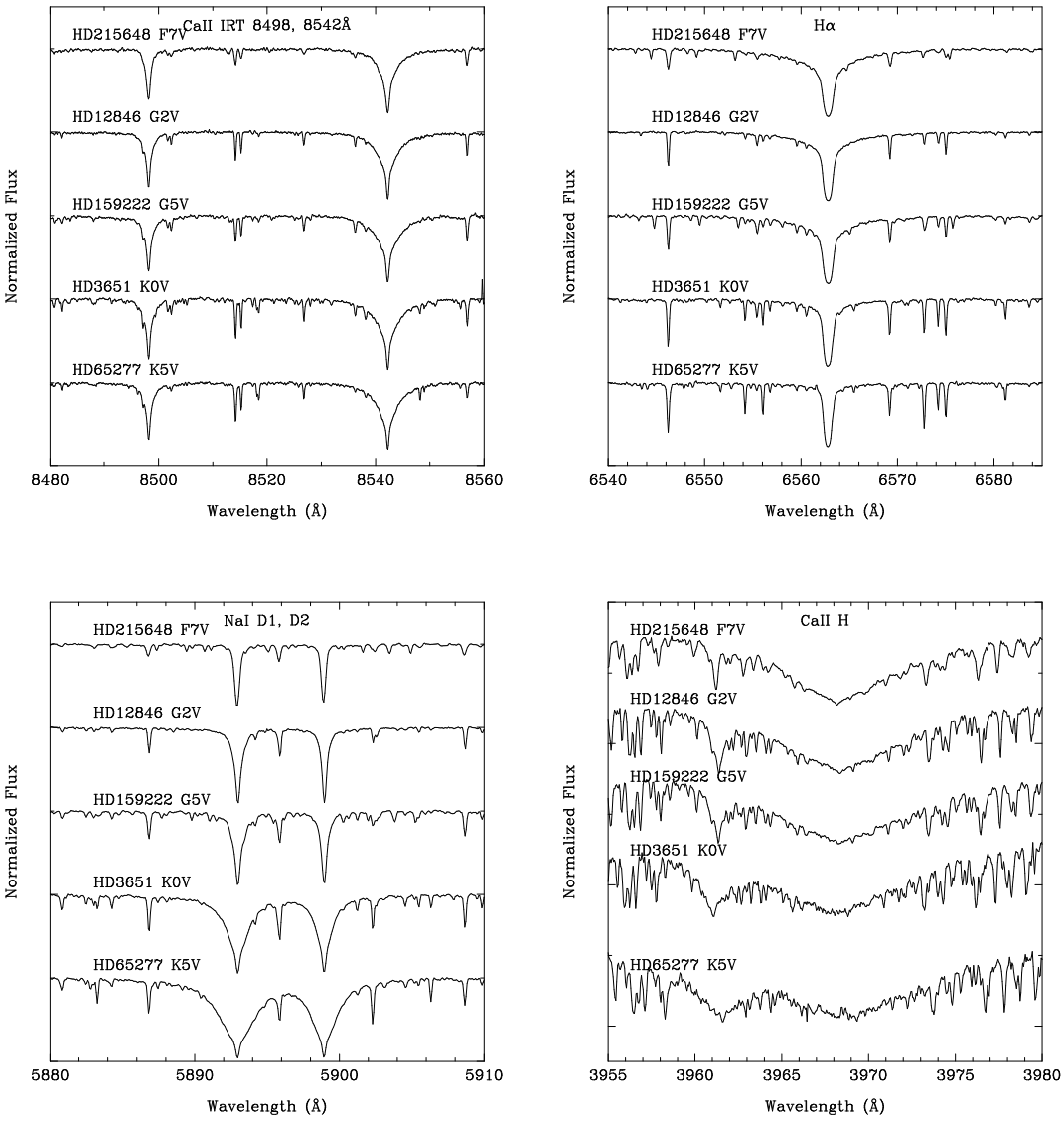

Figure 2.7: FOCES spectra of representative stars in the Ca II IRT regions, $H\alpha$, Na I D_1, D_2, and Ca II H & K regions.

3

A spectroscopy study of nearby late-type stars, possible members of stellar kinematic groups

J. Maldonado[1], **R.M. Martínez-Arnáiz**[2], **C. Eiroa**[1], **D. Montes**[2] **and B. Montesinos**[3]

[1] Universidad Autónoma de Madrid, Dpto. Física Teórica, Módulo 15, Facultad de Ciencias, Campus de Cantoblanco, E-28049 Madrid, Spain
[2] Universidad Complutense de Madrid, Dpto. Astrofísica, Facultad Ciencias Físicas, E-28040 Madrid, Spain
[3] Laboratorio de Astrofísica Estelar y Exoplanetas, Centro de Astrobiología, LAEX-CAB (CSIC-INTA), ESAC Campus, P.O. BOX 78, E-28691, Villanueva de la Cañada, Madrid, Spain

Originally published in *Astronomy and Astrophysics* **521**, A12 (2010)
Submitted: 6 May 2010 / Accepted: 1 June 2010

ABSTRACT

Context. Nearby late-type stars are excellent targets for seeking young objects in stellar associations and moving groups. The origin of these structures is still misunderstood, and lists of moving group members often change with time and also from author to author. Most members of these groups have been identified by means of kinematic criteria, leading to an important contamination of previous lists by old field stars.
Aims. We attempt to identify unambiguous moving group members among a sample of nearby-late type stars by studying their kinematics, lithium abundance, chromospheric activity, and other age-related properties.

Methods. High-resolution echelle spectra ($R \sim 57000$) of a sample of nearby late-type stars are used to derive accurate radial velocities that are combined with the precise *Hipparcos* parallaxes and proper motions to compute galactic-spatial velocity components. Stars are classified as possible members of the classical moving groups according to their kinematics. The spectra are also used to study several age-related properties for young late-type stars, i.e., the equivalent width of the lithium Li I 6707.8 Å line or the $R'_{\rm HK}$ index. Additional information like X-ray fluxes from the ROSAT All-Sky Survey or the presence of debris discs is also taken into account. The different age estimators are compared and the moving group membership of the kinematically selected candidates are discussed.
Results. From a total list of 405 nearby stars, 102 have been classified as moving group candidates according to their kinematics. i.e., only ~ 25.2 % of the sample. The number reduces when age estimates are considered, and only 26 moving group candidates (25.5% of the 102 candidates) have ages in agreement with the star having the same age as an MG member.

Key words. stars: activity -stars: ages -stars: late-type -stars: kinematics -open clusters and associations: general

3.1 Introduction

Last years have been very productive in identifying small associations and kinematic groups of young late-type stars in the solar vicinity. Although the study of moving groups (MGs) goes back more than one century, their origin and evolution remain still unclear, and this term is commonly used in the literature to indicate any system of stars sharing a common spatial motion. The best-studied MGs are the so-called *classical* MGs. Examples are Castor, IC 2391, Ursa Major, the Local Association and the Hyades (e.g. Montes et al. 2001b; López-Santiago et al. 2006, 2009, 2010, and references therein).

In the classical theory of MGs developed by O. Eggen (Eggen 1994), moving groups are the *missing link* between stars in open clusters and associations on one hand and field stars on the other. Open clusters are disrupted by the gravitational interaction with massive objects in the Galaxy (like giant molecular clouds), and as a result, the open cluster members are stretched out into a "tube-like" structure and dissolve after several galactic orbits. The result of the stretching is that the stars appear, if the Sun happens to be inside the "tube", all over the sky, but they may be identified as a group through their common space velocity.

Clusters disperse on time scales of a few hundred years (Wielen 1971); therefore, most of these groups should be moderately young (~ 50 - 650 Myr). However, Eggen's hypothesis is controversial and some of the MGs may also be the

result of resonant dynamical structures. For instance, Famaey et al. (2007) studied a large sample of stars in the Hyades MG, and determined that it is a mixture of stars evaporated from the Hyades cluster and a group of older stars trapped at a resonance. MGs may also be produced by the dissolution of larger stellar aggregates, such as stellar complexes or fragments of old spiral arms.

The *young* MGs (8 - 50 Myr) are probably the most immediate dissipation products of the youngest associations. Examples of such associations are TW Hya, β Pic, AB Dor, η Cha, ϵ Cha, Octans, Argus, the Great Austral complex (GAYA), and the Hercules-Lyra association (Zuckerman & Song 2004; Torres et al. 2008; Fuhrmann 2004; López-Santiago et al. 2006; Montes 2010).

Some of the young MGs are in fact related to star-forming regions like the Scorpius-Centaurs-Lupus complex (Zuckerman & Song 2004), Ophiuchus or Corona Australis (Makarov 2007).

The availability of accurate parallaxes provided by the *Hipparcos* satellite became a milestone in the study of MGs. Statistical, unbiased studies of large samples of stars have confirmed the existence of the classical MGs and have given rise to new clues and theories about the origin of such structures. Examples of these studies are those by Chereul et al. (1999), Asiain et al. (1999), Skuljan et al. (1999), and Antoja et al. (2008).

Identifying a star or group of stars as members of an MG is not a trivial task, and in fact, lists of members change among different works. Most members of MGs have been identified by means of kinematic criteria; however, this is not sufficient since many old stars can share the same spatial motion of those stars in MGs. For example, López-Santiago et al. (2009) show that among previous lists of Local Association members, roughly 30% are old field stars. The membership issue can be partially solved if high-resolution spectroscopy is used. Recent studies have shown that stars belonging to a given MG share similar spectroscopic properties (e.g. Montes et al. 2001a; López-Santiago et al. 2009,2010). These studies exploit the many advantages of the nearby late-type stars. First, spectra of late-type stars are full of narrow absorption lines, allowing determination of accurate radial velocities. In addition, it is unlikely that an old star by chance shares chromospheric indices or a lithium abundance similar to those of young solar-like stars, which provides means for assessing the likelihood of membership of a given star that are independent of its kinematics (e.g. Soderblom & Mayor 1993b).

In this chapter we present a search for classical MG members by analysing the kinematic and spectroscopic properties of a sample of nearby late-type stars. Section 3.2 describes the stellar sample. A detailed analysis of the kinematic properties of the stars is given in Section 3.3. Age indicators for solar-like stars are analysed in Section 3.4. A combination of the results from Sections 3.3 and

3.4 is used in Section 3.5 to analyse the MG membership of the stars. Section 3.6 summarizes our results.

3.2 The stellar sample

Our reference stellar sample consists of main-sequence (luminosity classes V/IV-V) FGK stars located at distances less than 25 pc. The stars have been selected from the the *Hipparcos* catalogue (ESA 1997), since it constitutes a homogeneous database especially for distance estimates - parallax errors are typically about 1 milliarcsec. In this work we have taken the revised parallaxes computed by van Leeuwen (2007) from *Hipparcos*' raw data. No other selection criteria have been applied to the sample.

The sample is most likely complete for FG-type stars; i.e., it constitutes a volume-limited sample since the *Hipparcos* catalogue is complete for these spectral types. In the case of K-type stars, *Hipparcos* is incomplete beyond $\sim$ 15 pc; however, the number of the K-type stars is high enough for our purposes. The final selection contains 126, 220, and 477 stars of spectral types F,G and K respectively. In this contribution we present our first results for an observed subsample of 405 stars. The completeness of the observed sample can be seen in Figure 3.1 where the number of objects is plotted as a function of distance, and the distribution fits well a cubic law, which indicates that they are homogeneously distributed. M-type stars have in principle been excluded from this study; nevertheless, six M-type stars, members or candidate member of MGs, which exhibit high levels of chromospheric activity and are suspected to be young, have been included in order to better understand the properties of such stellar groups.

The observed stars are listed in A.1, and Figure 3.2 shows the HR diagram of the sample. Several stars are clearly under the main sequence: HIP 4845, HIP 42525, HIP 49986, HIP 57939, HIP 72981, and HIP 96285. *Hipparcos*' spectral types for these stars are quite similar to those reported in other catalogues such as Wright et al. (2003), Skiff (2009), or SIMBAD. Only for HIP 72981 is incomplete, giving simply 'K:', whereas SIMBAD gives M1 and the most updated reference in Skiff (2009) gives M2. However, the colour index $B - V = 1.17$ suggests an early type, around K5. HIP 42525 is a star in a double system and has a large uncertainty in the parallax ($\sigma_\pi = \pm 15.51$ mas). Stars with uncertainties over 10 milliarcsec are identified with a symbol † in Table A.1. The original selection (and therefore the observations) of the sample was made before the release of the revised *Hipparcos* parallaxes (van Leeuwen 2007), and some of our stars are now out of the 25 pc distance because their revised parallaxes are slightly smaller.

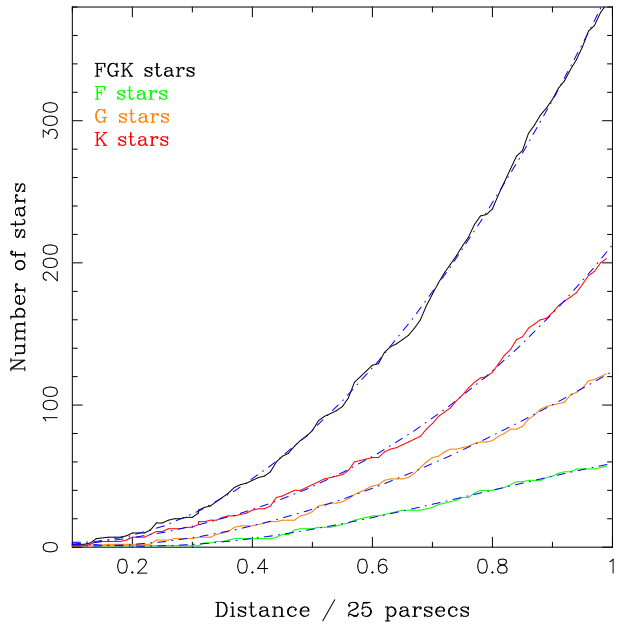

Figure 3.1: Number of stars versus distance (normalized to 25 pc) for the F stars (green), G stars (orange), K stars (red) and for the observed 405 stars. Fits to cubic laws are plotted in blue.

These stars are identified with a symbol ‡ in Table A.1. The most “extreme” case is HIP 1692 whose parallax has changed from 43.42 ± 1.88 mas to 3.23 ± 1.43 mas. This new parallax places the star in the giant branch as is clearly shown in Figure 3.2 (square in the upper right corner).

The reader is referred to Chapter 2 for details on the observing runs and data reduction.

3.3 Kinematic analysis

3.3.1 Radial velocities

Radial velocities were measured by cross-correlating order by order, using the IRAF routine *fxcor*, the spectra of our programm stars with spectra of radial velocity standard stars of similar spectral types (Table 3.1), taken from Barnes et al. (1986), Beavers et al. (1979), and Udry et al. (1999a,b). Spectral orders with chromospheric features and prominent telluric lines were excluded when determining the mean radial velocity. Typical uncertainties are between 0.15 and 0.25 km/s, while maximum uncertainties are around 1-2 km/s. Column 7 of Table A.1, gives

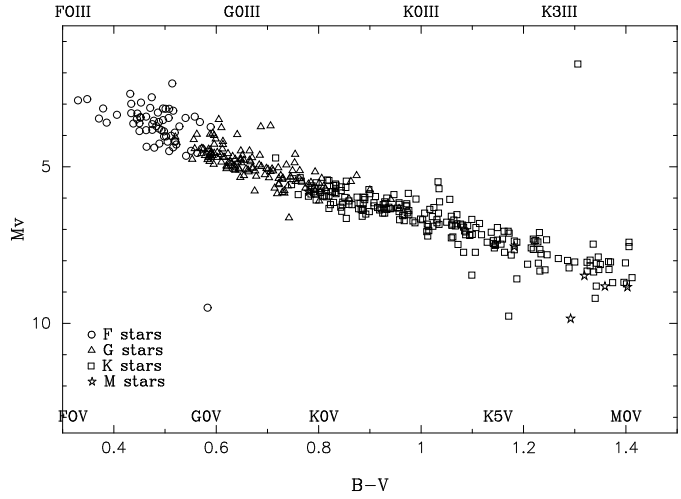

Figure 3.2: HR Diagram for our sample of nearby late-type stars. F-type stars are plotted with circles; G-type stars with triangles; K-type stars with squares and M-type stars with stars.

our results for the radial velocities. A large number of stars in our sample (51) are known spectroscopic binaries and are listed in *The 9th catalogue of spectroscopic binaries* (Pourbaix et al. 2004, hereafter SB9) and *The 3rd Catalogue of Chromospherically Active Binary Stars* (Eker et al. 2008). They are identified in Table A.1 with the label 'Spec. Binary'. For those stars we have considered the radial velocity of the centre of mass of the system.

We have compared our results with radial velocity estimates by Kharchenko et al. (2007, hereafter KH07), Nordström et al. (2004, hereafter NO04), Valenti & Fischer (2005, hereafter VF05), and Nidever et al. (2002, hereafter NI02).

These values are also given columns 8 to 11 of Table A.1. Of the 405 stars in our sample, 366 are found in KH07, and the differences among the radial velocity values in that work and our results are less than 2 km/s for 290 stars, i.e., 79.2% of the common stars. A comparison with the NO04 data shows that, for 215 out of 251 common stars (i.e. 85.6%), the corresponding differences between the radial velocities are less than 2 km/s. A similar result, 85.3% (177 out of the 151 common stars), is found when considering VF05 data. The comparison with NI02 is even better, because 179 out of 190 stars (i.e. 94.2 %) show differences lower than 2 km/s.

Figure 3.3 illustrates these comparisons. One can see that the differences are slightly greater with KH07, likely because of the non-homogeneous origin of their radial velocities values, mainly taken from *The general catalogue of radial velocities* (Barbier-Brossat & Figon 2000).

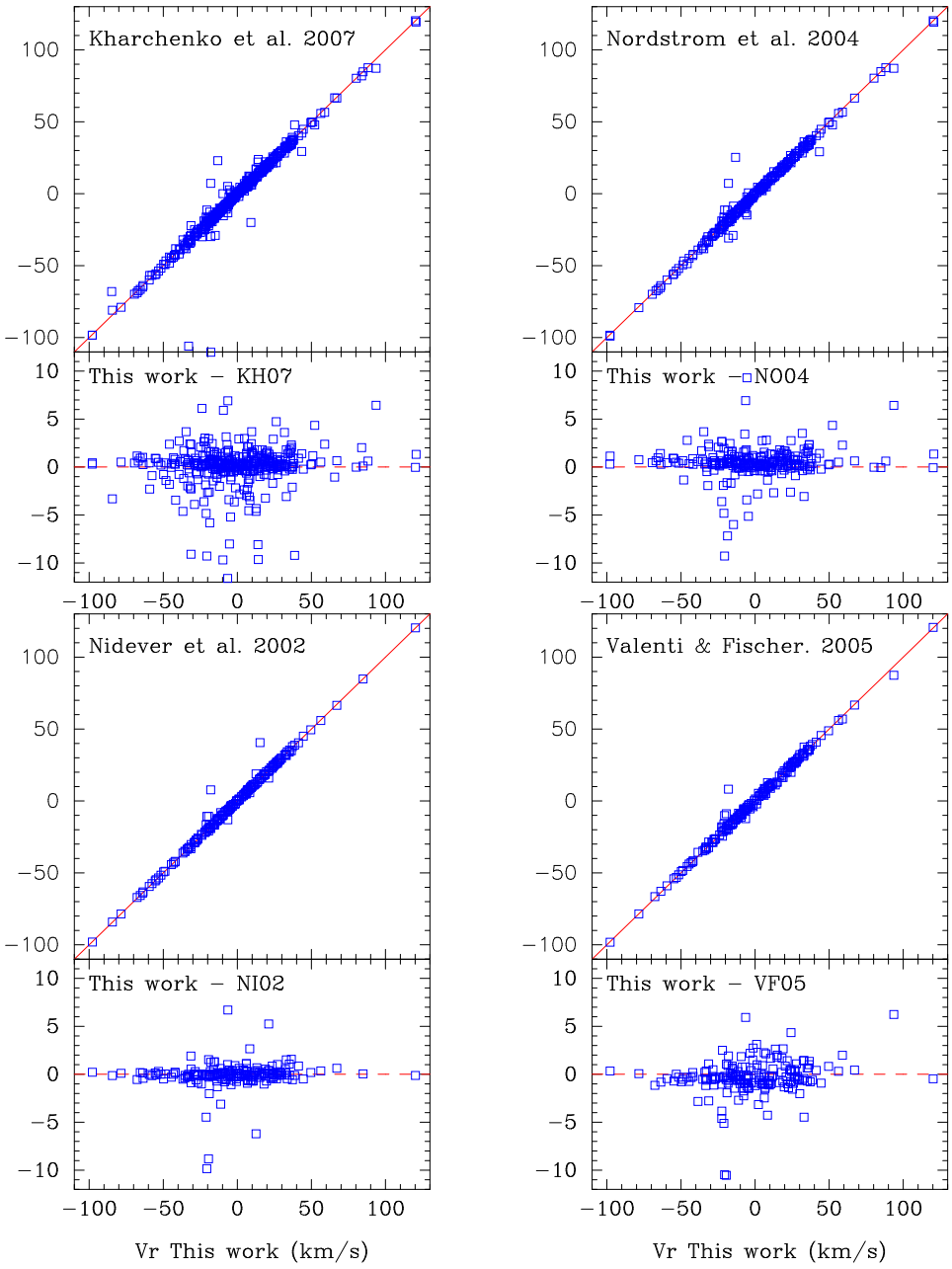

Figure 3.3: Comparison of radial velocities taken from the literature and obtained in this work. Top left panel: Kharchenko et al. (2007); top right panel:Nordström et al. (2004); bottom left panel: Nidever et al. (2002); bottom right panel: Valenti & Fischer (2005)

Table 3.1: Radial velocity standard stars

Star	SpT	$V_r \pm \sigma_{V_r}$ (km/s)	Reference
HD 102870	F8V	4.30	a
HD 50692	G0V	−15.05	a
HD 84737	G0.5	6.0 ± 1.1	b
HD 20630	G5V	18.0 ± 1.0	b
HD 159222	G5V	−51.60	a
HD 82885	G8III	14.40	a
HD 65583	G8V	14.80	a
HD 144579	G8V	−59.45	a
HD 182488	G8V	−21.55	a
HD 102494	G9IV	−22.1 ± 0.3	c
HD 62509	K0III	3.2 ± 0.3	c
HD 100696	K0III	0.2 ± 0.5	b
HD 3651	K0V	−32.96 ± 0.8	b
HD 38230	K0V	−29.25	a
HD 136442	K0V	−45.6 ± 0.8	b
HD 92588	K1IV	43.5 ± 0.3	d
HD 10476	K1V	−33.9 ± 0.9	b
HD 73667	K1V	−12.10	a
HD 124897	K2III	−5.3 ± 0.3	c
HD 4628	K2V	−10.1 ± 0.4	d
HD 82106	K3V	29.75	a
HD 139323	K3V	−67.20	a
HD 29139	K5III	54.29 ± 0.2	c

a Udry et al. (1999b)
b Barnes et al. (1986)
c Udry et al. (1999a)
d Beavers et al. (1979)

3.3.2 Identification of moving group candidates

Soderblom & Mayor (1993a) argued that, in order to be convincingly classified as a kinematic group, a group of stars should be moving through space at the same rate and in the same direction, and they should share the same velocity in the direction of the Galactic rotation V. This is because while motions in U and W lead to oscillations of the star about the mean motion of the group, diffusion in V removes the star from its cohort forever. However, stars identified as group members show different structures tilted in the (U, V) plane, i.e., do not form flat bars o ellipses with small σ_V (e.g. Skuljan et al. 1997), and therefore both U, V

velocity components must be used to define more realistic membership criteria.

Galactic spatial-velocity components (U, V, W) were computed using our radial velocity results listed in Table A.1, together with *Hipparcos* parallaxes (van Leeuwen 2007) and *Tycho-2* proper motions (Høg et al. 2000). To compute (U, V, W) we followed the procedure of Montes et al. (2001b) who updated the original algorithm of Johnson & Soderblom (1987) to epoch J2000 in the International Celestial Reference System (ICRS) as described in Section 1.5 of *The Hipparcos and Tycho Catalogues'* (ESA 1997). To take the possible correlation between the astrometric parameters into account, the full covariance matrix was used in computing the uncertainties. To identify possible members of MGs we proceeded in two steps:

- *i) Selection of young stars.* Young stars are assembled in a specific region of the (U, V) plane with (-50 km/s $<$ U $<$ 20 km/s; -30 km/s $<$ V $<$ 0 km/s), although the shape is not a square, see Figure 3.4.
- *ii) Selection of possible members of MGs with small V dispersion.* Considering previous results (Skuljan et al. 1997, 1999; Montes et al. 2001b), a dispersion of 8 km/s in the U, V components with respect to the central position of the MG in the (U, V) plane is allowed. The same dispersion is considered when taking the W component into account.

One hundred two stars of the sample have been classified as possible members of the different MGs: 29 for the Local Association, 29 for the Hyades, 18 for the Ursa Major, 19 for IC 2391, and 7 for Castor. Column 2 of Table 3.2 lists these numbers, while the specific stars are listed in Tables A.2 to A.6. Their contents are described in Appendix A. Another 78 stars have been selected as *young disc stars*. These stars are inside or in the boundaries that determine the young disc population, but their possible inclusion in one of the stellar kinematic groups is not clear. The identified young disc stars are given in Table A.7. Figure 3.4 shows the (U, V) and (W, V) planes, usually known as Bottlinger's diagrams, for these stars.

3.3.3 Eggen's astrometric criteria

To test whether a star "belongs" to a kinematic group, Eggen tried to establish "strict" criteria for MG-membership (Eggen 1958a, 1995). Eggen's criteria basically treat MGs, whose stars are extended in space, like open clusters whose stars are concentrated in space. Therefore, it is assumed that the total space velocities of the stars in the MG are parallel and move towards a common convergent point.

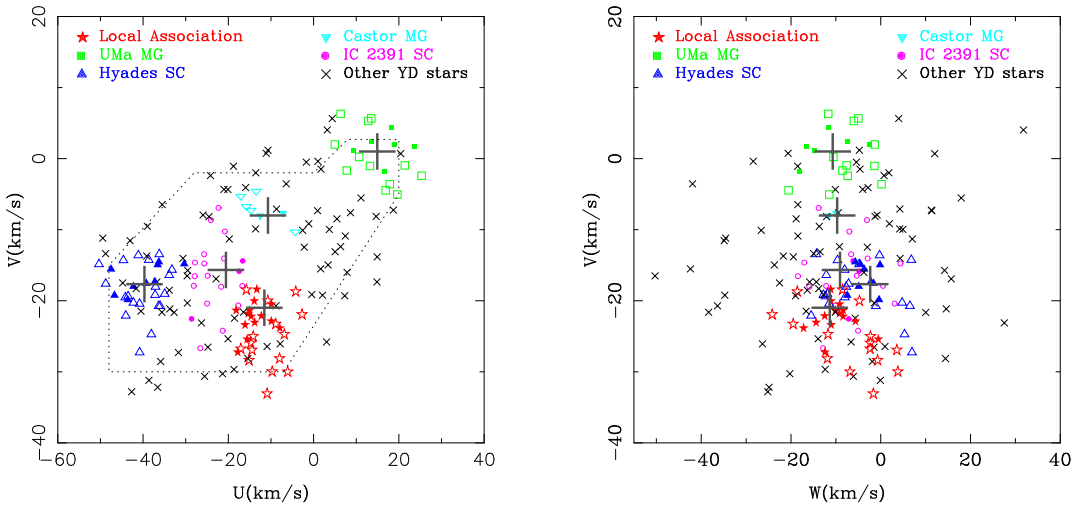

Figure 3.4: (U, V) and (W, V) planes for the observed stars. Different colours and symbols indicate membership to different MGs. Large crosses represent the convergence point of the young MGs shown in the figure. The dotted line represents the boundary of the young disc population as defined by Eggen (Eggen 1984, 1989). Stars that satisfy both Eggen's criteria are shown with filled symbols, while open symbols indicate stars that do not satisfy at least one of the Eggen's criteria.

The same relations of the moving-cluster method for the total and tangential velocities are applied, but taking into account only the components of the proper motion (μ) oriented towards the convergence point (v) and the component of the proper motion oriented perpendicularly to the great circle between the star and the convergence point (τ). The total (V_T) and tangential velocity (denoted as Peculiar Velocity, PV, by Eggen) can be combined to define a predicted radial velocity (ρ_c).

The first membership criterion, namely the *peculiar velocity criterion*, is to compare the proper motion of the candidate to the proper motion expected if the star were a member of the MG; i.e., the candidate is accepted as an MG member if the ratio τ/v or $PV/V_{\rm Total}$ is "sufficiently small". Eggen (1995) considered a candidate to be a member if its peculiar velocity is less than 10% of the total space velocity.

The second membership criterion, the *radial velocity criterion*, compares the observed and the predicted radial velocities. Eggen (1958a) considered a star to be a member if the difference between both radial velocities is less than 4-8 km/s. A more detailed discussion of these criteria can be found in Montes et al. (2001b).

Table 3.2 gives the number of stars in each MG that satisfy both criteria (column 3), only the peculiar velocity criterion (column 4), and only the radial velocity criterion (column 5). Only a low percentage of the MGs members selected in the previous section satisfies both criteria (from $\approx$ 49% in the Local Association to roughly 16% in the IC 2391 MG). The results for individual stars are given in columns 8 and 9 of Tables A.2 to A.6. For both *PV* (column 8) and ρ_c (column 9) criteria, there is a label, 'Y' or 'N', which indicates if the star satisfies the criteria.

Eggen's criteria are not conclusive since they assumed a constant V within the stars of a given MG. Anticipating some of the results in Section 3.5, some stars for which both age estimates and (U, V, W) components indicate that they are probable MG members do not satisfy these criteria.

Table 3.2: Number of MGs candidates according to Eggen's criteria.

Group	Total stars	Both criteria	Only *PV*	Only ρ_c
Local Association	29	14	9	1
IC 2391	19	3	7	5
Castor	7	2	0	4
Ursa Major	18	6	1	7
Hyades SC	29	9	5	9

3.4 Age estimates

Members of a given MG should be coeval and moderately young (only several Myr old, see Section 3.1) therefore it is expected that MGs members share age related-properties, such as similar chromospheric emission or lithium abundance. This provides the means of assessing the likelihood of membership for a given star that is independent of its kinematics.

3.4.1 Lithium abundance

Lithium abundance in late-type stars is a well-known age indicator since this element is destroyed as the convective motions gradually mix the stellar envelope with the hotter ($T \sim 2.5\times10^6 K$) inner regions. However, it should only be regarded as an additional age indicator when compared with others since Li I equivalent width has a wide spread at a given age and mass, and consequently, the relation lithium-age is poorly constrained. Furthermore, for late K, M-type stars, lithium is burned so rapidly that it is only detectable for extremely young stars. Thus, the

use of Li I as an age tracer is biased toward young stars, and it only provides low limits for stars of the age of the Hyades or older.

An age estimate of the stars in our sample can be carried out by comparing their Li I equivalent width, with those of stars in well known young open clusters of different ages (e.g. Montes et al. 2001a; López-Santiago et al. 2006). Lithium EWs have been obtained using the IRAF task *sbands*, performing an integration within a band of 1.6 Å centred in the lithium line. At the spectral resolution of our observations, the Li I 6707.8 Å line is blended with the Fe I 6707.41 Å line. To correct for a possible contamination by Fe I, Soderblom et al. (1990) obtained an empirical relationship between the colour index ($B - V$) and the Fe I equivalent width, measured in stars that showed only the Fe I feature and no Li I. Soderblom's equation was obtained by using main-sequence and subgiant stars, so it does not account for possible luminosity-class effects. Therefore we have built a new relationship, using only main-sequence stars without lithium detected in the spectrum:

$$\text{Fe I (EW)} = (0.020 \pm 0.005)(B - V) - (0.003 \pm 0.0015)(\text{Å}). \quad (3.1)$$

Which is fairly similar to the one obtained by Soderblom:

$$\text{Fe I (EW)} = 0.040(B - V) - 0.015(\text{Å}). \quad (3.2)$$

The EWs obtained are shown in column 10 in Tables A.2 to A.6, for each individual MG and in column 6 in Tables A.7 to A.8 for the stars classified as *Other young disc stars* and for the stars not selected as possible MGs, respectively.

Figure 3.5 shows the EW Li I versus colour index ($B - V$) diagram. We have overplotted the upper envelope of the Li I EW of IC 2602 (10-35 Myr) given by Montes et al. (2001a), the Pleiades cluster (78-125 Myr) upper envelope determined by Neuhaeuser et al. (1997), and the lower envelope adopted by Soderblom & Mayor (1993a), as well as the Hyades open cluster (600 Myr) envelope adopted by Soderblom et al. (1990). These clusters cover the range of ages of the MGs studied here (35-600 Myr).

Nearly 4 % of the stars are between the Pleiades envelopes, consistent with an age of $\sim$ 80 Myr. Roughly 8% of the stars are between the Hyades and the Pleiades lower envelope with an age similar to those stars in the Ursa Major $\sim$ 300 Myr. Stars with lithium EW below the Hyades envelope are likely to be older than 600 Myr. They are around the 23% of the sample. Thus, approximately 35% of the stars are moderately young (younger than 1 Gyr). Roughly 50% of the stars lie below the Pleaides lower envelope (but not below the Hyades' one). For these stars we can only state that they should be older than the Pleiades. Finally, stars

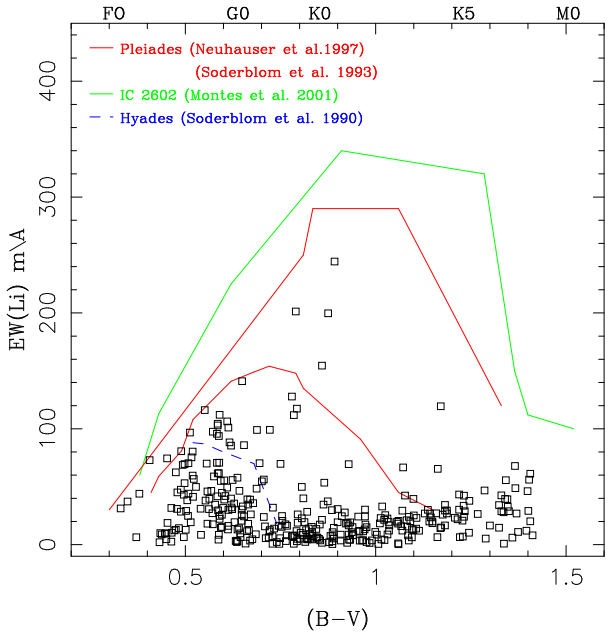

Figure 3.5: Li I vs $(B - V)$ diagram. Lines indicate the envelopes for the IC2602 (green), Pleiades (red), and Hyades (dashed blue).

with no photospheric Li I detected are expected to be older than 1 Gyr (around 15% of the whole sample).

Concerning spectral types, the majority of the F stars are in the Hyades-like region of the diagram, with only five out of 61 stars in the Pleiades-like region. For G-type stars, 71 out of 129 are in the Hyades-like region, 34 in the Ursa Major-like region and only HIP 63742 shows an EW comparable to those stars in the Pleiades. Finally, six out of 209 K-type stars are in the Pleiades-like region and 15 in the Ursa Major-like.

The stars with the largest Li I EW are HIP 46816, HIP 46843, HIP 13402, HIP 63742 HIP 75809, HIP 75829 (in this order). According to their kinematics, HIP 46816 has been classified in the *young discs stars* category, whereas the three other stars have velocity-components (U, V, W) in the boundaries of the Local Association (discussed in some detail in Section 3.5.1).

3.4.2 Stellar activity indicators

It is well known that for cool stars with convective outer-layers, chromospheric activity and rotation are linked by the stellar dynamo (e.g. Kraft 1967; Noyes et al. 1984; Montesinos et al. 2001) and both (activity and rotation) diminish as the stars

evolve. Thus, activity/rotation tracers, such as $R'_{\rm HK}$, $L_{\rm X}$ or rotational periods are often used to estimate stellar ages (for a recent detailed work on this subject see Mamajek & Hillenbrand 2008).

Chromospheric emission: Ca II H & K lines

The stellar chromospheric activity is usually quantified by the $R'_{\rm HK}$ index, defined as the ratio of the chromospheric emission in the cores of the broad Ca II H & K absorption lines to the total bolometric emission of the star (e.g. Noyes et al. 1984). The $R'_{\rm HK}$ values used in this work were taken from Martínez-Arnáiz et al. (2010) since they were obtained from the spectra in this thesis. For those stars with no $R'_{\rm HK}$ value in Martínez-Arnáiz et al. (2010), the $R'_{\rm HK}$ values have been taken from the literature (see references in Appendix A).

Several relations between $\log R'_{\rm HK}$ and stellar chromospheric age are available in the literature (e.g. Soderblom et al. 1991). In this chapter we take those given by Mamajek & Hillenbrand (2008, Eq.3):

$$\log(\tau/{\rm yr}) = -38.053 - 17.912 \log {\rm R}'_{\rm HK} - 1.6675 \log {\rm R}'^{2}_{\rm HK}, \qquad (3.3)$$

which is valid between $\log R'_{\rm HK}$ values of -4.0 and -5.1 (i.e. $\log \tau$ of 6.7 and 9.9). Although the stars used in the calibration of Eq. 3.3 are all stars with $(B-V) < 0.9$, we assume it holds for the entire (B-V) range of our stars. As in the case of the lithium abundance, activity indicators are also biased towards younger stars. The accuracy of Mamajek's relation is 15-20% for young stars (younger than 0.5 Gyr), but beyond this age, uncertainties can grow up to more than 60%. The $\log R'_{\rm HK}$ values and derived ages are shown in columns 11 and 12 in Tables A.2 to A.6, and columns 7 and 8 in Tables A.7 to A.8.

Figure 3.6 shows the $\log R'_{\rm HK}$ versus $(B-V)$ diagram of stars in clusters of known ages. Following Henry et al. (1996), we used $\log R'_{HK}$ to classify stars into "very inactive" ($\log R'_{\rm HK} < -5.1$), "inactive" ($-5.1 < \log R'_{\rm HK} < -4.75$), "active" ($-4.75 < \log R'_{\rm HK} < -4.2$), and "very active" if $\log R'_{\rm HK} > -4.2$. The percentages of stars in each region are 8%, 47%, 41%, and 4%, respectively. Mean $\log R'_{\rm HK}$ value for inactive stars is -4.93 with a standard deviation of 0.09, and $< \log R'_{\rm HK} >= -4.53$ with a standard deviation of 0.13 for active stars. These numbers are quite similar to those found by Henry et al. (1996) and Gray et al. (2003).

Most of the stars in the "very active" category are, according to their kinematics, candidate members to MGs. HIP 46843 and HIP 86346 (Local Association), HIP 21482, and HIP 25220 (Hyades), HIP 8486 (Ursa Major), HIP 66252 (IC

2391) HIP 33560 and HIP 46816 (young disc population). Three of the stars in this "very active" region, namely HIP 45963, HIP 21482 and HIP 91009 are well-known variable chromospherically active binaries (included in The 3rd Catalogue of chromospherically active binary stars (Eker et al. 2008)). In those systems, stellar activity/rotation are enhanced by tidal interaction with the companion star, leading to high levels of chromospheric and coronal emission, up to two orders of magnitude higher than the level expected for a single star with the same rotation period (Basri et al. 1985; Simon & Fekel 1987; Montes et al. 1996). Therefore their $\log R'_{\rm HK}$ values cannot provide any information on their age or membership to MGs. Lithium abundance is also affected in this kind of systems, showing over-abundances with respect to the typical values for single stars of the same mass and evolutionary stage (Barrado y Navascués et al. 1997).

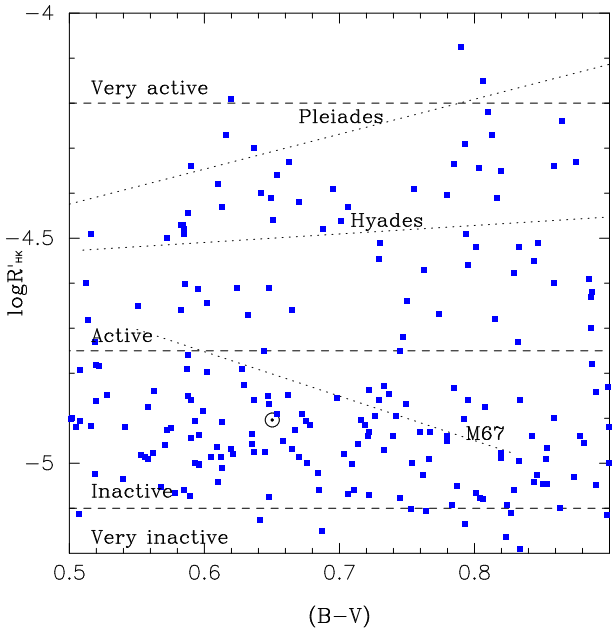

Figure 3.6: $\log R'_{\rm HK}$ vs $(B-V)$ colour. The position of the Pleiades (~ 120 Myr), Hyades (600 Myr), and M67 (4 Gyr) stars are indicated with dotted lines (Mamajek & Hillenbrand 2008). The position of the Sun is also shown with a dotted circle. Dashed lines are the limits for very active, active, inactive, and very inactive stars, according to Henry et al. (1996).

Coronal emission: ROSAT data

In addition to their chromospheric activity, the rapid rotation of young stars drives a vigorous stellar dynamo, producing a strong, coronal X-ray emission. Even

though there are L_X values already published in several catalogues (e.g. Hünsch et al. 1999), in order to be self-consistent we have re-computed them with the revised *Hipparcos* parallaxes (van Leeuwen 2007) used in this work.

To compute L_X, we searched for X-ray counterparts in the ROSAT All-Sky Survey Bright Source Catalogue (Voges et al. 1999) and the Faint Source Catalogue (Voges et al. 2000). To determine the X-ray fluxes we used the count rate-to-energy flux conversion factor (C_X) relation given by Fleming et al. (1995):

$$C_X = (8.31 + 5.30\ \mathrm{HR1})10^{-12}\mathrm{erg\ cm^{-2}\ counts^{-1}}. \quad (3.4)$$

Where HR1 is the hardness ratio of the star in the ROSAT energy band 0.1-2.4 KeV. Combining the X-ray count rate, f_X(counts s^{-1}), and the conversion factor C_X with the distance D, the stellar X-ray luminosity L_X(erg s^{-1}) can be estimated:

$$L_X = 4\pi D^2 C_X f_x. \quad (3.5)$$

Figure 3.7 shows the fractional X-ray luminosity L_X/L_{Bol} versus the colour index $(B-V)$. Bolometric corrections were derived from the $(B-V)$ colour by interpolating in Flower (1996, Table 3). Data for the Pleaides (Stauffer et al. 1994) and Hyades (Stern et al. 1995) clusters have been overplotted for a comparison. Approximately 23% of the stars are in the Pleiades region of the diagram, 51% of the stars are in the Hyades region, and $\sim$ 26% of the stars are below the Hyades' sequence.

To compute the stellar age from the X-ray luminosity, we followed the work by Garcés et al. (private communication):

$$\begin{aligned} L_X &= 6.3\times10^{-4}\ L_{Bol} \quad (\tau < \tau_i) \\ L_X &= 1.89\times10^{28}\ \tau^{-1.55} \quad (\tau > \tau_i). \end{aligned} \quad (3.6)$$

With $\tau_i = 2\times10^{20}L_{Bol}^{-0.65}$, and both L_X and L_{Bol} are expressed in erg/s and τ is given in Gyr. Columns 13 and 14 in Tables A.2 to A.6 show the L_X/L_{Bol} values and derived ages, while in Tables A.7 to A.8 these data are in columns 9 and 10.

The critical parameter τ_i marks the change from a non-saturated regime in which there is an inverse relation between the stellar rotation and L_X and the saturated regime in which the star reaches a maximum L_X such that $L_X/L_{Bol} \approx 10^{-3}$ (e.g. Pizzolato et al. 2003, and references therein). Only one star, HIP 86346, is in the saturated regime. For this star, Eq. 3.6 only provides an upper limit to the age, close to the "real" age of the star. This star is discussed in some detail in Section 3.5.1.

Most of the stars included in the "very inactive" category defined before do not have ROSAT data, and for the few of them that do, X-ray data place them

below the Hyades' sequence (Fig 3.7). Lithium abundance shows a similar behaviour, and these stars are below the Hyades' envelope or do not show lithium at all. Although some of them have been identified by means of their kinematics as young disc stars or MG members, age diagnostics show that they are, however, old stars. For the stars in the "very active" category, the situation is the opposite one. All of them have ROSAT data, and most of them have fractional X-ray luminosities similar to those of the Pleiades (Fig 3.7). They also show higher lithium abundances than the "very inactive" or the "inactive" stars.

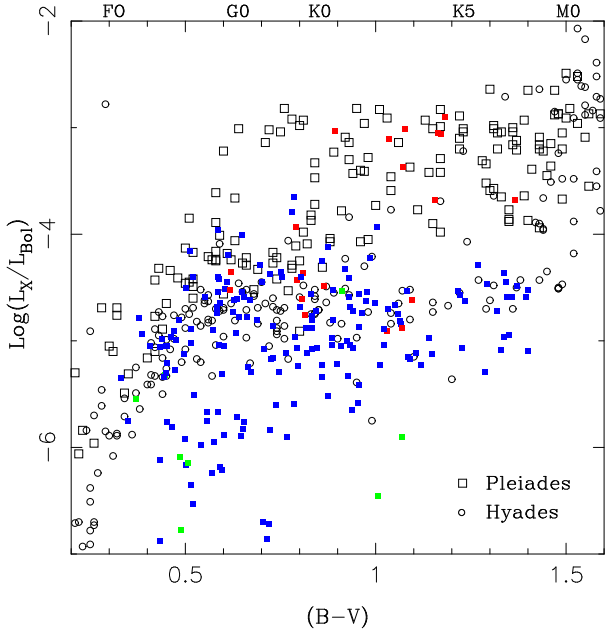

Figure 3.7: Fractional X-ray luminosity $\log(L_X/L_{Bol})$ vs colour index $(B-V)$. Stars classified as "very active" and "very inactive" according to their $\log R'_{HK}$ value are plotted in red and green colours, respectively.

Age from stellar rotation: Gyrochronology

Stars are born with relatively high rotational velocities. In the course of their evolution, rotation decreases due to the loss of angular momentum with stellar winds and magnetic breaking (Weber & Davis 1967; Jianke & Collier Cameron 1993; Aibéo et al. 2007). Thus stellar rotation can be used to estimate stellar ages, and it is well known that solar-type stars follow a law of the form $P_{Rot} \propto t^{1/2}$ (Skumanich 1972). Subsequent works have refined this relationship, e.g., by establishing a mass dependence in the evolution of rotational periods (e.g. Kawaler 1989) or deriving a rotation-age relationship as a function of the stellar colour (Barnes 2007; Mamajek & Hillenbrand 2008).

To compute ages, we follow the relationship given by Mamajek & Hillenbrand (2008):

$$P_{\rm Rot} = 0.407((B-V) - 0.495)^{0.325} \times t^{0.566}. \quad (3.7)$$

With the age of the star, t, given in Myr and the period in days.

Rotational periods have been taken from Noyes et al. (1984); Baliunas et al. (1996); Saar & Osten (1997) and Messina et al. (2001) Unfortunately, only 17.3% of the stars have measured rotational periods. Rotational periods and derived ages are given in columns 15 and 16 in Tables A.2 to A.6 and columns 11 and 12 in Tables A.7 to A.8. Figure 3.8 shows the rotation period for the stars of our sample as a function of the colour index $(B-V)$. Percentages of Pleiades-like, Hyades-like, and older stars are 22%, 28%, and 50% respectively. All stars with rotation periods lower than seven days are MGs candidates. The fastest rotator is HIP 86346 with a period of only 1.8 days, while the slowest ones are HIP 3093 and HIP 104217 with 48 days.

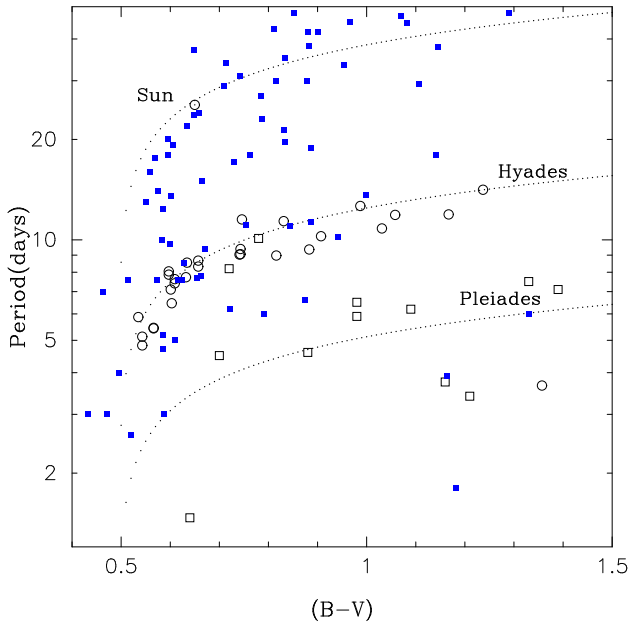

Figure 3.8: Rotation periods vs $(B-V)$ colour. Data from the Pleiades were taken from Prosser et al. (1995), whereas data from the Hyades are from Radick et al. (1987). Three gyrochrones (at the ages of the Pleiades, Hyades, and the Sun) have been overplotted for a comparison.

Discussion

Figure 3.9 shows the age distribution for the different activity indicators. The results can be compared with those of Mamajek & Hillenbrand (2008, Figure 14). Chromospheric age shows an enhancement of the star formation rate in the last 2 Gyr, then the distribution becomes more or less flat. We do not find a clear minimum at 2 Gyr, the so-called *Vaughan-Preston gap* (Vaughan & Preston 1980). ROSAT ages are biased towards stars younger than 3-4 Gyr; i.e., older stars have negligible (or undetectable) X-ray emission, and therefore their distribution does not offer information on the stellar formation history. As far as rotational ages are concerned, there are not enough stars with measured rotational periods to draw robust conclusions.

Although the agreement between the ROSAT and the chromospheric distribution is overall good, when considering individual stars there can be discrepancies, which can for to different reasons. For example, some stars present variability in their levels of activity, which leads to very different age estimates if the activity indicators are taken in different epochs of the activity cycle. For example, HIP 37349 is a known variable observed three times: $\log R'_{\rm HK}$ values are -4.54, -4.57, and -4.28 (Martínez-Arnáiz et al. 2010), which lead to ages 800, 950, and 115 Myr, respectively, while the ROSAT-derived age is 1.17 Gyr, which is compatible with 800-950 Myr but not with 115 Myr. In addition, stellar rotation can be influenced by tidal interaction in binary systems, leading to completely different ages. Finally there could be other aspects like possible mismatches of X-ray sources with their optical counterparts.

3.4.3 Additional criteria

Presence of debris discs

It is now well established that debris discs are more common around young stars (e.g. Habing et al. 2001; Zuckerman et al. 2004; Siegler et al. 2007). As stars age they are on average orbited by increasingly fewer dust particles so a high value of the fractional dust luminosity, $f_{\rm d}$, can be used as an additional indicator of youth. There is evidence that debris systems of high infrared luminosity are more intimately linked to young stellar kinematic groups than the majority of normal stars (e.g Moór et al. 2006); indeed, several of the stars with the strongest infrared excesses are members of MGs (e.g., β Pic, Barrado y Navascués et al. 1999).

However, $f_{\rm d}$ is a rather inaccurate age diagnostic. First, the amount of excess emission shows large differences among stars within the same age range (e.g Siegler et al. 2007, Fig. 7). Even though stars with significant excess emissions should in principle be young, no further information can be given without addi-

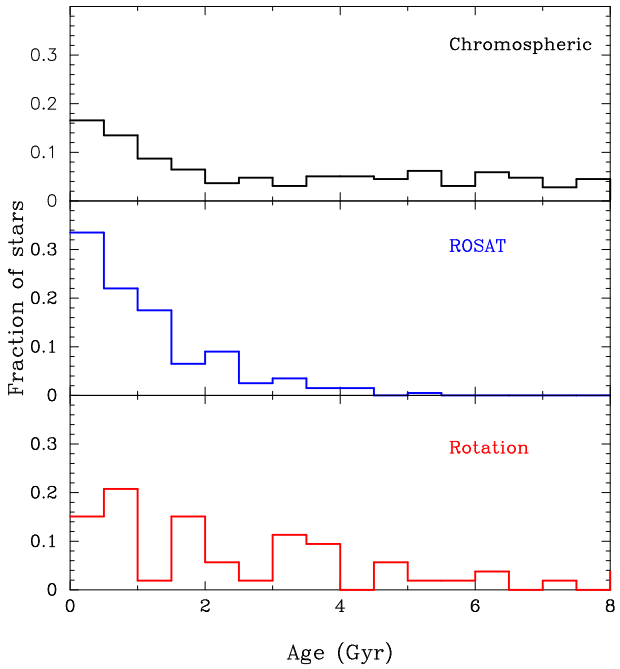

Figure 3.9: Age distribution for chromospheric-derived ages (black solid line), ROSAT ages (blue line), and rotational ages (red line).

tional age estimates. Moreover, there are relatively old systems (age $\gtrsim$ 500 Myr) with high $f_{\rm d}$ values ($f_{\rm d} \simeq 10^{-3}$) possibly associated with stochastic collisional events.

Stars with known infrared excesses and their inclusion to MGs are given Table 3.3. As shown in that table, the IR excesses of those stars are relatively moderate ($f_{\rm d} \simeq 10^{-5}$) and most stars with excess are not related to MGs. For example, the three stars with the largest IR-excess (HIP 76375, HIP 40693, and HIP 32480) are old field stars. Both kinematics and activity-derived age confirm this.

Metallicity

Moving group members are supposed to have formed in the same molecular cloud, so, they should have similar metallicity. Local Association and Ursa Major members are expected to have metallicities compatible with the solar value. Recently, Soderblom et al. (2009) have obtained [Fe/H] = +0.03 for a sample of 20 Pleaides' stars with statistical and systematic uncertainties of +0.002 and +0.05, respectively. For members of the Ursa Major Group, Boesgaard & Friel (1990) found [Fe/H] = −0.085, σ = 0.021. Hyades' members should be slightly metal rich [Fe/H] = +0.14, σ = 0.05. Therefore we discard very metal-poor stars as "good" MG candidates. Considering that the "old" (2 Gyr) and metal-rich MG

Table 3.3: Stars with known debris discs

HIP	HD	f_d (10^{-5})	Reference	MG	Age (Myr)
544	166	5.9	[4]	LA	20-150
1599	1581	0.2-1.6	[4]		
13402	17925	2.2-4.4	[4]	LA	20-150
15371	20807	0.4-1.5	[4]		
16537	22049	8.3	[3]		
16852	22484	1.2-4.3	[4]	YD	
18859	25457	10±2	[2]	LA	20-150
19335	25998	2.7	[1]	HS	600
22263	30495	2.0-3.0	[4]	IC 2391	35-55
23693	33262	0.2-1.1	[4]		
27072	38393	0.77	[3]	UMa	300
27435	38858	10	[1]	YD	
28103	40136	2.04	[3]		
32480	48682	11	[1]		
40693	69830	20	[2]		
42430	73752	3.21	[3]		
42438	72905	0.6-1.5	[4]	UMa	300
43726	76151	0.4-1.0	[4]	HS	600
51502	90089	0.85	[1]		
62207	110897	1.4-2.3	[4]		
64924	115617	1.9-3.3	[4]		
65721	117176	1.8-7.7	[4]		
71284	128167	0.49	[3]		
71395	128311	1.3-2.7	[4]	UMa	300
76375	139323	78.6	[3]		
85235	158633	4.1	[1]		
107350	206860	0.6-1.5	[4]	LA	20-150

[1] Beichman et al. (2006a); [2] Moór et al. (2006)
[3] Rhee et al. (2007); [4] Trilling et al. (2008)

HR 1614 has a mean metallicity of [Fe/H] = +0.19 ± 0.06 (Feltzing & Holmberg 2000b), stars with metal overabundances over ≈ +0.20 should also be discarded.

Reliable spectroscopic determinations of the metallicity for our stars were taken from the literature (Fuhrmann 2008, 2004; Santos et al. 2004; Sousa et al. 2008; Takeda et al. 2005; Valenti & Fischer 2005). When no spectroscopic metallicities were found there, they were computed from Strömgren indices (Hauck & Mermilliod 1997) by using the calibrations given by Schuster & Nissen (1989).

These values are given in columns 17 (Tables A.2 to A.6) and 13 (Tables A.7 to A.8).

An inspection of the metallicities obtained reveals that there are no MGs candidates among the most metal-poor stars. However, some MGs candidates have positive metallicities. This is especially evident in the Hyades MG where the 45% of the candidates are more metal-rich than the Sun. Between them we find HIP 43587 and HIP 67275, which are among the most metal rich in our sample, [Fe/H] = +0.35, [Fe/H] > +0.30, respectively, and they both are known to have planets. As we will see in Section 3.5.2, their age estimates confirm that they are old stars and not "good" Hyades' members.

3.5 Comparison between kinematic and age estimates. Final membership.

Tables A.2 to A.6 show a summary of the kinematic and spectroscopic properties, as well as age estimates, of the stars which are candidate members to the different MG, according to their (U, V, W) velocity components. Each table refers to one specific MG. This summary classifies the MGs candidates into three different categories, which are similar to the ones by Soderblom & Mayor (1993a):

- *Probable non-member:* If the derived ages from the different indicators agree, but they are in conflict with the object having an age as an MG member.
- *Doubtful member:* If there is important disagreement among the different age indicators, including here the assigned age of the corresponding MG, or there is lack of information (i.e., some age indicators are not available)
- *Probable member:* If age indicators agree and also do with the position of the star in the (U, V) plane.

The following subsections describe the membership of the stars studied in this work and the properties of each MG individually

3.5.1 Membership and properties of the Local Association candidates

The concept of a Local Association of stars was introduced by Eggen (e.g. Eggen 1975). This association, also known as Pleiades MG or Pleiades stream, includes stars in the Pleiades, α Persei, and IC 2602 clusters, as well as stars in

the Scorpius-Centaurus star-forming region. In the past years, small associations or groups of very young stars have been detected among Local Association members (AB Dor, TW Hydrae, β Pic, and others). The spatial motions of these new associations are quite similar, but they present a wide range in ages and distributions around the Sun (e.g. Zuckerman & Song 2004), which leads to the question of whether it is reasonable to consider the Local Association as a single entity. Addressing this problem is beyond the scope of this thesis, so we consider the Local Association as a single MG.

There are 29 stars (Table A.2) that have velocity components (U, V, W) consistent with the stars being candidates to the Local Association. Eight out of the 29 stars do not satisfy other criteria; i.e., their age estimates suggest that they are older than 20-150 Myr commonly adopted for the Local Association, and we consider them to be non-members; Seven out of the 29 stars are considered as doubtful members while, 14 are good candidates, i.e., probable members. Although the number of candidates is too small to draw robust conclusions we can infer that the contamination by old main-sequence stars vary from roughly 25% to 50%.

Table 3.4 lists the candidates and our final classification (column 3) for the Local Association stellar membership. Some of our candidates have already been classified as members of the young association around the star AB Dor or members of the so-called Hercules-Lyra association introduced by Fuhrmann (2004), which are listed in columns 4 to 6 of Table 3.4. All the previously proposed members of AB Dor or Hercules-Lyra fall into our classification of probable Local Association members, with the only exception of HIP 62523, which we have classified as a "doubtful member". Thirteen out of our 29 candidates have not been included in these previous studies.

Among the Local Association members there are some interesting stars:

- HIP 13402 (HD 17925): Although it is classified as an RS CVn variable (Eker et al. 2008), Cutispoto et al. (2001) shows that the binary hypothesis does not seem to be consistent with the *Hipparcos* photometric data. The estimated EW Li I = 182.52 ± 4.63 mÅ agrees with the 208 mÅ given by Montes et al. (2001a) and the 197 mÅ given by Favata et al. (1995), which suggests an age similar to the Pleaides ($\approx$ 80 Myr). In addition, the different age estimates agree very well and confirm that it is a young star; furthermore, the star is known to have IR-excess at 70 μm, see Table 3.3 (Trilling et al. 2008). Thus, we consider that it is a reliable member of the Local Association.

- HIP 18859 (HD 25457): This star is classified as a weak-line T Tauri (e.g. Li et al. 2000), and has a remarkable infrared excess of $f_d = 1.0 \pm 0.2 \times 10^{-4}$,

Table 3.3 (Moór et al. 2006). The EW Li I and age estimates confirm its young evolutionary state.

- HIP 86346 (HD 160934): This star is one of the few *Hipparcos*' M-type stars we have observed in this project. Available spectral types in the literature vary between K7 to M0 (Reid et al. 1995; Zuckerman et al. 2004). This object is a flare star identified as a spectroscopic binary by Gálvez et al. (2006). A close companion was detected using lucky imaging techniques by Hormuth et al. (2007). Our radial velocities vary between -25.37 and -28.39 km/s. In all epochs the main optical activity tracers (Ca II IRT, H_α, Na I D_1, D_2, Ca II H & K) are in emission. This star is a very rapid rotator (for an M-type star) with $v \sin i$ between 21 and 23 km/s. Our EWs Li I measurements vary from 11.1 to 55.7 mÅ and agree with the 40 mÅ reported by Zuckerman et al. (2004). ROSAT-age indicates a star younger than 100 Myr (it is in the "saturated" regime in the $\log L_X/L_{Bol}$ vs age diagram), the position of the star in a colour-magnitude diagram ($M_V = 7.55 \pm 0.15$; $(V-I) = 2.58 \pm 0.91$) suggests it is a pre-main sequence star.

3.5.2 Membership and properties of the Hyades candidates

The Hyades MG group or Hyades Supercluster [1] has a venerable history in the study of MGs since references to the Hyades MG group go back in time to the first works in this area (Proctor 1869). It is commonly related with the Hyades and Praesepe clusters, both of them with ages around 600 Myr. Recently, Famaey et al. (2007) has found that the MG is in reality a mixture of two different populations: a group of coeval stars related to the Hyades cluster (the evaporating halo of the cluster) and a second group of old stars with similar space motions. Age diagnostics analysed in Section 3.4 allow us, in principle, to distinguish between the two populations.

There are 29 stars in the region of the (U, V, W) planes occupied by the Hyades MG. Eleven out of these 29 candidates have been classified as probable members [2], nine as probable non-members, whereas the classification of the other nine stars remains unclear (Table A.3).

Our selection contains 14 stars in common with López-Santiago et al. (2010). A comparison between our final classification and those given by López-Santiago et al. (2010) is shown in Table 3.5. There is good agreement with two exceptions, HIP 17420 (for which our age estimates suggest an old star) and HIP 19335 (discussed below).

[1] The terms moving group and supercluster are used here without distinction.

[2] To avoid confusion we recall that by "probable member" of the Hyades supercluster we mean member of the group of coeval stars evaporated from the primordial Hyades cluster

Table 3.4: Comparison between our final membership for the Local Association and previous studies.†

			Hercules-Lyra		AB Dor
HIP	HD	This work	FU04	L06	ZU04
544	166	Y	Y	Y	
3979	4915	N			
7576	10008	Y		Y	
7751	10360	N			
12929	17230	N			
13402	17925	Y	Y	?	
18859	25457	Y			Y
19422	25665	?			
26779	37394	N			
37288		?			
46843	82443	Y		?	
54155	96064	Y		?	
54745	97334A	Y	Y		
57494	102392	?			
62523	111395	?	Y	?	
63742	113449	Y	?		Y
65515	116956	Y	Y	?	
69357	124106	N			
72146	130004	?			
73695	133640	?			
75809	139777	Y	Y	?	
75829	139813	Y	Y	?	
77408	141272	Y	Y	?	
79755	147379	N			
86346	160934	Y			Y
105038	202575	?			
107350	206860	Y		Y	
108156	208313	N			
115341	220221	N			

FU04: Fuhrmann (2004); ZU04:Zuckerman et al. (2004)
L06: López-Santiago et al. (2006)

†Label 'Y' indicates probable members, '?' doubtful members and 'N' probable non-members, respectively.

We briefly describe some interesting stars concerning this MG:

- HIP 19335 (HD 25998): This F7V star has been identified as a T-Tauri star

in the surroundings of the Taurus-Auriga star formation region (Li & Hu 1998), although it is located at a significantly shorter distance, 21 pc, than the commonly accepted distance of ∼ 140 pc to that star forming region. The Li I EW = 93.1 ± 3.0 mÅ confirms its youth and agrees well with the rest of age indicators, between 96 and 300 Myr. The star has infrared-excesses at both *Spitzer* 24 μm and 70 μm MIPS bands (Beichman et al. 2006a). All this information also confirms the youth of this star, but it is likely too young to be a member of the Hyades MG.

- HIP 43726 (HD 76151): The Li I EW of 31.42 ± 3.66 mÅ of this star, as well as the estimated chromospheric and rotational ages of ∼ 1.0 Gyr, suggests that it is not a member of the Hyades MG. Interestingly, this is a relatively old star with a debris disc (Trilling et al. 2008; Beichman et al. 2006a).

- HIP 67275 (HD 120136, τ Boo): τ Boo is one of the first cases where an exoplanet was found (Butler et al. 1997). There is a strong disagreement between the X-ray age estimate, 0.36 Gyr, and the chromospheric age, 4.78 Gyr. Li I EW also suggests an old star. This agrees with other published ages, 1.3 Gyr (Valenti & Fischer 2005), 2.1 Gyr (Nordström et al. 2004), and 2.52 Gyr (Saffe et al. 2005). It is therefore unlikely that HIP 67275 is a member of the Hyades MG.

3.5.3 Membership and properties of the Ursa Major moving group

The concept of a group of stars sharing the same kinematic as Sirius goes back more than one century ago. Nowadays the group includes more than 100 stars (Eggen 1992; Soderblom & Mayor 1993b; King et al. 2003; Fuhrmann 2004; Ammler-von Eiff & Guenther 2009). Eighteen stars have velocity components (U, V, W) consistent with the star being a candidate for Ursa Major (Table A.4). Four out of the 18 stars do not satisfy other criteria, and their age estimates indicate that they are older than the 300 Myr commonly adopted for the Ursa Major MG. Another eight out of the 18 stars are considered as doubtful members, while six stars are probable members.

Table 3.6 shows a comparison between our classification and those reported in the literature. There is good agreement specially in the stars classified as good members. Three candidates of this MG are of special interest:

- HIP 42438 (HD 72905): This star is known to have infrared excesses at 60 and 70 μm (Spangler et al. 2001; Bryden et al. 2006). All age estimates

Table 3.5: Comparison between our final memberships for the Hyades MG and those given by López-Santiago et al. (2010).[†]

HIP	HD	This work	LS10
1803	1835	Y	Y
4148	5133	N	
12709	16909	Y	
13976	18632	Y	?
16134	21531	Y	?
17420	23356	N	Y
18774	24451	?	
19335	25998	N	Y
21482	283750	?	
25220	35171	?	Y
40035	68146	N	
42074	72760	Y	Y
42333	73350	Y	
43587	75732	?	?
43726	76151	N	
44248	76943	?	
46580	82106	Y	
47592	84117	N	
48411	85488	?	?
63257	112575	?	
66147	117936	N	
67275	120136	N	?
69526	124642	?	
72848	131511	Y	
90790	170657	N	
94346	180161	Y	?
96085	183870	?	?
104239	200968	Y	?
116613	222143	Y	?

[†]Label 'Y' indicates probable members, '?' doubtful members and 'N' probable non-members, respectively.

agree with an age of ≈ 300 Myr, which indicate that it is a probable member of the group.

- HIP 71395 (HD 128311): This object is an example of a star with a planetary system (Butler et al. 2003; Vogt et al. 2005) in a debris disc (excess at 70 μm found by Trilling et al. 2008). Our chromospheric-derived age of

430 Myr agrees with the 390 Myr given by Saffe et al. (2005) and confirms that this star is a probable member of the Ursa Major group.

- HIP 80337 (HD 147513): This star is also known to have a planet (Mayor et al. 2004). Due to a problem with the header's spectra, no radial velocity could be obtained so we have adopted the value given by NO04. Measured Li I EW = 35.51 ± 3.5 mÅ suggests that it is older than the Hyades, which agrees with both chromospheric and rotational ages, around 700 Myr. However the ROSAT age is much shorter, only 370 Myr. Therefore, we have classified this star as a "doubtful" member.

Table 3.6: Comparison between our final memberships for the Ursa Major MG and those previously reported in the literature. †

HIP	HD	This work	SO93	KI03	FU04	LS10
5944	7590	Y			Y	
8486	11131	Y	Y	Y?	Y	Y
27072	38393	N	?	Y?		Y
27913	39587	?	Y	Y	Y	
33277	50692	N	N	?		
36827	60491	?		N?/?		?
37349	61606A	?		N?		Y
42438	72905	Y	Y	Y?	Y	?
60866	108581	?				
71395	128311	Y		?		Y
72659	131156A	Y	Y	?	Y	?
73996	134083	N		N?		Y
74702	135599	N		?	Y	
80337	147513A	?	Y	N?/?		Y
80686	147584	?		Y		
96183	184385	?				
102485	197692	Y				
108028	208038	?				

S093: Soderblom & Mayor (1993b); KI03: King et al. (2003)
FU04: Fuhrmann (2004); LS10: López-Santiago et al. (2010)

†Label 'Y' indicates probable members, '?' doubtful members and 'N' probable non-members, respectively.

3.5.4 Membership and properties of the IC 2391 moving group

The identification of an MG related to the IC 2391 cluster is from Eggen (1991, 1995). Most of the stars listed as members of this MG are in fact early-type star members of the cluster. By using the member's position in colour-magnitude diagrams Eggen obtained an age of ~ 100 Myr, within an interval spreading from 80 to 250 Myr. Recently, López-Santiago et al. (2010) has suggested the presence of two subgroups mixed in the (U, V) plane with ages of 200-300 and 700 Myr.

Table A.5 summarizes our membership criteria for the IC 2391 MG. Five out of 19 candidate stars have been classified as probable members, 10 as doubtful, and four as probable non-members. Our sample contains three stars in common with López-Santiago et al. (2010). We confirm that HIP 11072 is a doubtful member and HIP 59280 is a member of the old subgroup, but our age estimates for HIP 25119 disagree with López-Santiago et al. (2010). We therefore consider this star as a "non" member instead of a member of the old subgroup since both chromospheric and ROSAT ages are around 3 - 5 Gyr.

We have identified four new stars as probable-members of the young subgroup: HIP 19076, HIP 22263, HIP 29568, and HIP 66252. In addition, HIP 71743 has been classified as a probable member of the old subgroup. HIP 66252 (HD 118100, EQ Vir) is known to have flares, and therefore chromospheric and ROSAT ages can be greater than our estimates, although the lithium abundance confirms that it is a young star. HIP 34567 (ages between 320 and 470 Myr) should remain in the "doubtful category" since it is a known chromospherically active binary (Eker et al. 2008).

3.5.5 Membership and properties of the Castor moving group

The Castor MG was originally suggested by Anosova & Orlov (1991). This group includes, among other stars, three spectroscopic binaries (Castor A, Castor B, and YY Gem) and two prototypes of the β Pic stars (Vega and Fomalhaut). Barrado y Navascués (1998) estimated an evolutionary age for this association of 200 ± 100 Myr.

Only seven stars have been identified on the basis of their kinematics as candidate members of this group (Table A.6). Four were classified as probable members and three as doubtful members. HIP 29067 and HIP 109176 have been previously studied in detail by Barrado y Navascués (1998), and since we obtain similar results, we concentrate on the rest of candidates:

- HIP 12110 (HD 16270): There is a strong discrepancy between ROSAT and chromospheric ages, therefore the star remains as a doubtful member.

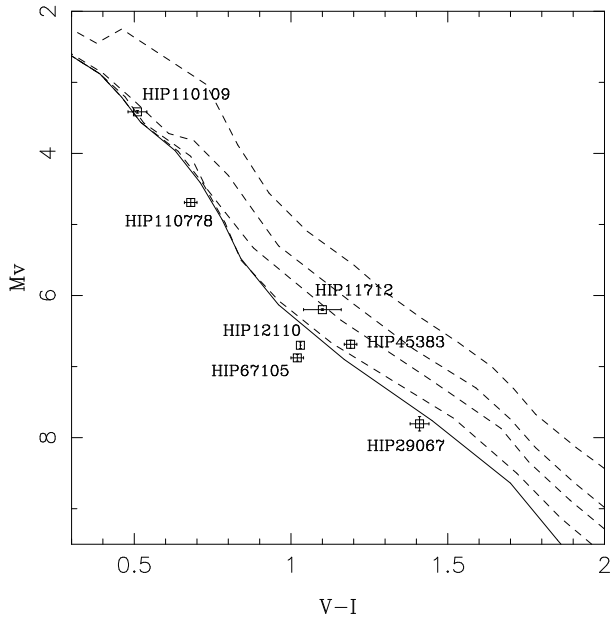

Figure 3.10: Colour-magnitude diagram for the Castor MG candidates. Pre-main sequence isochrones from Siess et al. (2000) are plotted at 10, 20, 30 and 50 Myr.

- HIP 45383 (HD 79555): This star is a long-period astrometric binary (Mason et al. 2001). Both ROSAT and chromospheric ages agree with the star being coeval with Castor MG members. As an additional test of youth, we plotted the star in a M_V vs $(V - I)$ diagram (Figure 3.10). The position of the star in this diagram suggests an age around 35 Myr. Therefore we conclude that HIP 45383 is a young star and a probable Castor member.

- HIP 67105 (HD 119802): There is a strong discrepancy between ROSAT and chromospheric ages, therefore the star remains as doubtful member.

- HIP 110778 (HD 212697): Both ROSAT and calcium ages agree with the star being coeval with the Castor MG. Since this is a star in a multiple system, we have confirmed its youth nature by using colour-magnitude diagrams.

- HIP 117712 (HD 22378): This star is a known spectroscopic binary. Chromospheric ages suggest a moderately young star, between 600 and 860 Myr. The position of the star in colour magnitude diagrams suggests also it is a young star, and hence a probable Castor MG member.

3.6 Summary

In this chapter we have addressed the problem of identifying unambiguous MG members. Making use of a large quantity of data from the literature and data from our own spectroscopic observations, we were able to study the kinematics and age of the nearby late-type population, identifying a considerable group of stars that are members of moderately young (35-600 Myr) kinematic groups. Based on both the kinematics and different age estimates, our results allow us to identify new members, confirm previously suggested members of MGs, and discard previously claimed members.

We find that approximately $\sim$ 25% of the nearby stars can be classified as members of MGs according to their kinematics, but that only 10% have ages that agree with the accepted ages of the corresponding MG members. Specifically, we find that among the stars studied in this work, the bona fide members for each MG are 14 stars (out of 29 kinematic candidates) for the Local Association, 11 (29 of kinematic candidates) for the Hyades MG, six (out of 18 kinematic candidates) for the Ursa Major MG, six (out of 19 kinematic candidates) for IC 2391, and four (out of seven kinematic candidates) for the Castor MG.

Some of the bona fide members identified here have not been reported before (at least to our knowledge), especially when considering the less-studied groups: Hyades (four new probable members), IC 2391 (five new probable members), and Castor (three new probable members). We find discrepancies with previously reported lists in eight stars. Additional observations are required to identify new bona fide members in each group and to address further investigations as suggested below.

3.7 Further applications of MGs members

Lists of nearby MGs members constitute promising targets for a wide variety of further investigations. We briefly summarized some of them:

First, we investigated whether there is a connection between the so-called "solar-analogues" (e.g. Porto de Mello & da Silva 1997; Meléndez et al. 2009; Ramírez et al. 2009) and MGs members. Taking as a reference the list of analogues published by Gaidos et al. (2000), we have found 25 matches between their list and our sample, where 22 out of these 25 stars, have been classified as bona fide MG members. Another three stars, HIP 29525, HIP 80337, and HIP 116613, also candidates for MGs, satisfy Gaidos' criteria for being considered as solar analogues. These stars are listed in Table 3.7. These "young-suns" are essential to study the history and formation of our own Solar System, indeed three of them, namely HIP 15457, HIP 42438, and HIP 64394, are included in the am-

Table 3.7: Solar analogues and their ascription to MGs. Label 'Y' indicates probable members, '?' doubtful members, and 'N' probable non-members, respectively.

HIP	MG	Membership	HIP	MG	Membership
544	LA	Y	46843	LA	Y
1803	HS	Y	54745	LA	Y
5944	UMa	Y	63742	LA	Y
7576	LA	Y	65515	LA	Y
8362	IC2	N	71743	IC2	Y
8486	UMa	Y	72567		
15457	YD	Y	74702	UMa	N
22263	IC2	Y	77408	LA	Y
26779	LA	Y	80337	UMa	?
29525	YD	Y	82588		
29568	IC2	Y	94346	HS	Y
42074	HS	Y	107350	LA	Y
42333	HS	Y	115331		
42438	UMa	Y	116613	HS	Y

LA: Local Association; HS: Hyades; UMa: Ursa Major
IC2: IC 2391; Cas: Castor

bitious project *The Sun in Time* aimed at reconstructing the spectral irradiance evolution of the Sun (e.g Ribas et al. 2005).

As we have shown in Section 3.4.3, debris discs are linked to stars in MGs. It is therefore natural to check if there is a similar relation between stars with known planets and MGs. Nineteen stars of our sample have detected planets [3], and seven of them are MGs candidates: HIP 21482 (Hyades MG, but it is doubtful member and in addition the planet is not confirmed); HIP 43587 (Hyades MG, but it is a doubtful member); HIP 71395 (Ursa Major MG, probable member); HIP 80337 (Ursa Major, doubtful member); HIP 95319 (IC 2391 MG, but doubtful member and the planet is not confirmed); HIP 49669 and HIP 53721 (young disc stars according to their kinematics, but their calcium ages suggest that they are old stars).

Other applications are related to activity studies, i.e., flux-flux and rotation-activity-age relationships (e.g Martínez-Arnáiz et al. 2010), or search programmes to detect stellar and substellar companions (e.g Hormuth et al. 2007). Finally, we point out that an important fraction of the stars analysed in this thesis are being observed in the framework of the DUNES (DUst around NEarby Stars) programme,

[3]The Extrasolar Planets Encyclopedia, http://www.obspm.fr/encycl/es-encycl.html

an approved *Herschel* Open Time Key Project with the aim of detecting cool faint dusty discs, at flux levels as low as the Solar EKB (see Section 1.4).

4

Metallicity of solar-type stars with debris discs and planets

J. Maldonado[1], **C. Eiroa** [1], **E. Villaver**[1], **B. Montesinos**[2], **and A. Mora**[3]

[1] Universidad Autónoma de Madrid, Dpto. Física Teórica, Módulo 15, Facultad de Ciencias, Campus de Cantoblanco, E-28049 Madrid, Spain
[2] Centro de Astrobiología (INTA-CSIC), LAEFF Campus, European Space Astronomy Center (ESAC), P.O. Box 78, E-28691 Villanueva de la Cañada, Madrid, Spain
[3] ESA-ESAC Gaia SOC. P.O. Box 78, E-28691 Villanueva de la Cañada, Madrid, Spain

Originally published in *Astronomy and Astrophysics* **541**, A40 (2012)
Submitted: 10 January 2012 / Accepted: 6 February 2012

ABSTRACT

Context. Around 16% of the solar-like stars in our neighbourhood show IR-excesses due to dusty debris discs and a fraction of them are known to host planets. Determining whether these stars follow any special trend in their properties is important to understand debris disc and planet formation.
Aims. We aim to determine in a homogeneous way the metallicity of a sample of stars with known debris discs and planets. We attempt to identify trends related to debris discs and planets around solar-type stars.
Methods. Our analysis includes the calculation of the fundamental stellar parameters $T_{\rm eff}$, $\log g$, microturbulent velocity, and metallicity by applying the iron ionisation equilibrium conditions to several isolated Fe I and Fe II lines. High-resolution échelle spectra ($R \sim 57000$) from 2-3 meter class telescopes are used. Our derived metallicities are compared with other results in the literature, which finally allows us to extend the stellar samples in a consistent way.

Results. The metallicity distributions of the different stellar samples suggest that there is a transition toward higher metallicities from stars with neither debris discs nor planets to stars hosting giant planets. Stars with debris discs and stars with neither debris nor planets follow a similar metallicity distribution, although the distribution of the first ones might be shifted towards higher metallicities. Stars with debris discs and planets have the same metallicity behaviour as stars hosting planets, irrespective of whether the planets are low-mass or gas giants. In the case of debris discs and giant planets, the planets are usually cool, - semimajor axis larger than 0.1 AU (20 out of 22 planets), even ≈ 65% have semimajor axis larger than 0.5 AU. The data also suggest that stars with debris discs and cool giant planets tend to have a low dust luminosity, and are among the less luminous debris discs known. We also find evidence of an anticorrelation between the luminosity of the dust and the planet eccentricity.
Conclusions. Our data show that the presence of planets, not the debris disc, correlates with the stellar metallicity. The results confirm that core-accretion models represent suitable scenarios for debris disc and planet formation. These conclusions are based on a number of stars with discs and planets considerably larger than in previous works, in particular stars hosting low-mass planets and debris discs. Dynamical instabilities produced by eccentric giant planets could explain the suggested dust luminosity trends observed for stars with debris discs and planets.

Key words. techniques: spectroscopic - stars: abundances - stars: circumstellar matter -stars: late-type -stars: planetary systems

4.1 Introduction

Understanding the origin and evolution of planetary systems is one of the major goals of modern astrophysics. The unexpected discovery by the *IRAS* satellite of infrared excesses around main-sequence stars (Aumann et al. 1984) was attributed to the presence of faint dusty discs, produced by collisional events within a significant population of invisible left-over planetesimals. The discovery of these so-called *debris discs* demonstrated that planetesimals are more common than had been previously thought, revealing that the initial steps of planetary formation are ubiquitous (e.g. Backman & Paresce 1993). This realisation has been complemented in the past 15 years with the detection of more than 700 exoplanets orbiting stars other than the Sun [1].

More recent studies have found that more than 50% of solar-type stars harbor at least one planet of any mass with a period of up to 100 days, and about 14%

[1] http://exoplanet.eu/

of this type of stars have planetary companions more massive than 50 $M_{\oplus}$ with periods shorter than 10 years (Mayor et al. 2011). It is well-established that the percentage of stars hosting gas-giant planets increases with the metal content, up to 25% for stars with metallicities higher than +0.30 dex (e.g. Santos et al. 2004; Fischer & Valenti 2005). On the other hand, stars that host less massive planets, Neptune-like or super Earth-like planets ($M_p < 30\ M_{\oplus}$), do not tend to be metal-rich (Ghezzi et al. 2010b; Mayor et al. 2011; Sousa et al. 2011, and references therein). In terms of the metallicity of evolved stars (late-type subgiants and red giants) hosting planets, previous results have been based on the analysis of small and inhomogeneous samples that even produce contradictory results, while these stars are metal-poor in the cases of Pasquini et al. (2007) and Ghezzi et al. (2010a), they show metal enrichment according to Hekker & Meléndez (2007).

Debris discs are, strictly speaking, signatures of planetesimal systems. About 16% of the main-sequence solar-like (spectral types F5-K5) stars are known to show an excess at 70 μm (e.g. Trilling et al. 2008). If planetesimals were the building blocks of planets and, at the same time, the raw material from which debris discs form, their host stars might be expected to have similar properties. However, the incidence of debris discs is no higher around planet-host stars than around stars without detected planets (Kóspál et al. 2009), and several works do not find any correlation between the presence of a debris disc and the metallicity, or any other characteristic, of the stars with planets (e.g. Beichman et al. 2005; Chavero et al. 2006; Greaves et al. 2006; Moro-Martín et al. 2007; Bryden et al. 2009; Kóspál et al. 2009).

In this chapter, we revisit the analysis of the properties of solar-type stars hosting planets and/or debris discs. One of the motivations is the increase with respect to previous works of $\sim 50\%$, in the number of stars with known debris discs and planets, in particular those associated with low-mass planets ($M_p \lesssim 30 M_{\oplus}$). We distinguish three different categories: stars with known debris discs but no planets (SWDs hereafter), stars with known debris discs and planets (SWDPs), and stars with known planets but no discs (SWPs). In addition, we consider a comparison sample of stars with no detected planets and no detected debris discs (SWODs). We use our own high-resolution échelle spectra to homogeneously determine some of the stellar properties, particularly metallicity, and in a second step we compare our spectroscopic results with published results. This allows us to increase coherently the stellar samples analysed in this work.

4.2 Observations

4.2.1 The stellar sample

A list of stars with known debris discs, SWDs, was compiled by carefully checking the works of Habing et al. (2001), Spangler et al. (2001), Chen et al. (2005), Beichman et al. (2006a), Bryden et al. (2006), Moór et al. (2006), Smith et al. (2006), Moro-Martín et al. (2007), Rhee et al. (2007), Trilling et al. (2007), Trilling et al. (2008), Bryden et al. (2009), Kóspál et al. (2009), Plavchan et al. (2009), Tanner et al. (2009), Koerner et al. (2010), Dodson-Robinson et al. (2011), and Moór et al. (2011). These debris discs were discovered by the *IRAS*, *ISO*, and *Spitzer* telescopes. We compiled a total list of 305 stars, from which we retained for study only the solar-type stars (*Hipparcos* spectral type between F5 and K2-K3), leading to a total of 136 stars. Most of the debris discs around these stars were detected at *Spitzer*-MIPS 70 μm, with fractional dust luminosities of the order of 10^{-5} and higher (Trilling et al. 2008).

To build the *comparison* sample of stars without discs (SWODs), we selected from the aforementioned works stars in which IR-excesses were not found at 24 and 70 μm by *Spitzer*. As before, only solar-type stars were considered, leading to 150 stars. Since *Spitzer* is limited up to fractional luminosities of $L_{dust}/L_{\star} \gtrsim 10^{-5}$, we cannot rule out the possibility that some of these stars have fainter discs.

To avoid the effects of planets, planet-hosting stars in both the SWD and SWOD samples were removed, after checking the Extrasolar Planets Encyclopedia[2]. The final number of stars in the SWDs sample is 107: 49 F-type stars, 37 G-type stars, and 21 K-type stars. The SWODs sample contains 145 stars: 62 F-type stars, 65 G-type stars, and 18 K-type stars. Table B.1 lists the stars in the SWD and SWOD samples, their properties, and references to debris disc detection.

4.2.2 Possible biases

Metallicity reflects the enrichment history of the ISM (see e.g. Timmes et al. 1995). It is, therefore, important to determine whether the SWD and SWOD samples have randomly selected stellar hosts in terms of age and distance, which are the parameters most likely to affect the metal content of a star. In this respect, we compared the distances and stellar ages of both samples; the results are given in Table 4.1. Distances are from the updated *Hipparcos* parallaxes (van Leeuwen 2007) and stellar ages were computed from the $\log R'_{HK}$ values given in Chapter 3 or from the literature if no value was available in that Chapter. The relationship

[2]http://exoplanet.eu/

provided by Mamajek & Hillenbrand (2008, Eq. 3) was used to compute the ages. This relationship has an accuracy of 15-20% for young stars, i.e. younger than 0.5 Gyr, and at older age, uncertainties can grow by up to 60%. The age distributions are shown in Figure 4.1.

Table 4.1: Comparison between the properties of the SWDs and the SWODs samples.

	SWDs			**SWODs**		
	Range	Mean	Median	Range	Mean	Median
Distance (pc)	3.6/134	32.0	24.6	5.8/53	24.1	20.6
log[Age (yr)]	7.2/9.9	9.0	9.0	7.6/9.9	9.2	9.6
SpType (%)	45.8 (F); 34.6 (G); 19.6 (K)			42.8 (F); 44.8 (G); 12.4 (K)		

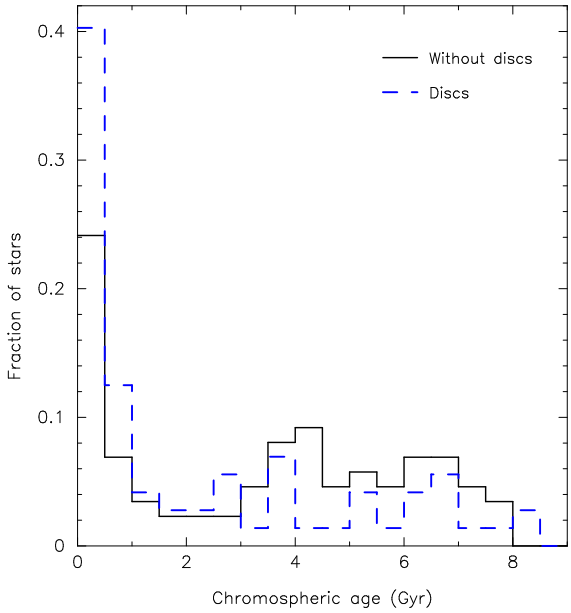

Figure 4.1: Age distribution for stars in the SWOD (continuous-black line) and the SWD (dotted-blue line) samples.

We found a difference between the two samples in terms of the age, with the SWDs containing 15% more stars younger than 500 Myr. Type II and Type Ia supernova (SNe) are the two sources of Fe production, each operating on different timescales and accounting for very different amounts of the total Fe injected into the ISM. While Type Ia SNe are the major producers of Fe in galaxies (see e.g.

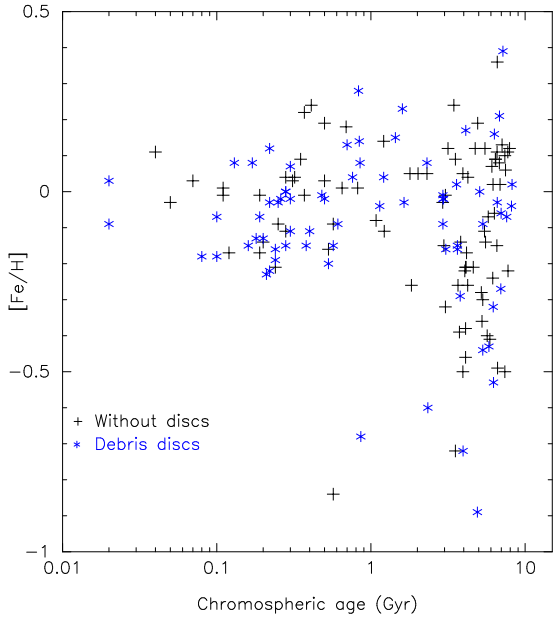

Figure 4.2: [Fe/H] versus age for the stars in the SWOD (black crosses) and in the SWD (blue asterisks) samples.

Matteucci & Greggio 1986), their injection timescales are, according to the most recent estimates, longer than 1 Gyr (Matteucci et al. 2009). In the solar neighbourhood, this 1 Gyr timescale, although uncertain, is the time at which the Fe production from SNe Ia starts to become important (Matteucci & Recchi 2001). On the other hand, Type II SNe are expected to account for only 30% of the total yield of Fe (Matteucci & Greggio 1986) but are expected to do so on a shorter timescale (3-5 Myr). A high rate of local SN type II explosions has been estimated to explain the local bubble (Maíz-Apellániz 2001), namely 20 SN type II explosions within 150 pc of the Sun in the past 11 Myr (Benítez et al. 2002). The youngest stars in the SWD and SWOD samples have ages of 15 Myr and 35 Myr, respectively, with a larger number of young SWDs in the first 500 Myr bin. The paucity of SNe type II in the Galaxy (typical rate of ≈ 1 SNe Myr^{-1}) and all the stars being at relatively close distances from the Sun (less than 130 pc) make it very unlikely that the two samples have experienced different enrichment histories. We have, however, explored this possibility in Figure 4.2, where we plot the metallicity versus age (Section 4.3) for the two samples. As we can see, the SWDs and SWODs have similar behaviours. Young stars in the SWDs sample do not seem to have higher metallicities, so we can rule out a possible chemical evolution in the SWD sample.

We have also checked whether there is a difference between the SWD and

SWOD samples in terms of distance that might affect their metallicity distributions. After all, the SWD sample contains stars out to a larger volume than that of the SWODs and could possibly include stars with a different chemical evolution. Garnett & Kobulnicky (2000) studied the scatter in the age-metallicity relation for F and G dwarf stars in the solar neighbourhood up to 80 pc, and found that their stars at distances 30-80 pc from the Sun are more metal-poor than those within 30 pc. Garnett & Kobulnicky (2000) attributed this difference to the possible consequence of a selection bias in the analysed sample.

We certainly cover the same volume of stars in our homogeneous SWD and SWOD subsamples (see Section 4.3.1), since they are located within 25 pc of the Sun (Chapter 2) We do not find any chemical distinction between these two subsamples. If in the full sample (see Section 4.3.3) we had a selection bias due to the larger distance of the SWODs, we would expect its metallicity distribution to show a larger dispersion owing to a possible contamination by stars not born in the solar neighbourhood. We have the opposite case, where the full samples of both SWODs and SWDs have a smaller dispersion than the volume-limited homogeneous SWDs and SWODs subsamples (see Figure 4.3).

In short, we believe that we have a randomly selected sample of stars in terms of their chemical history, although the SWD and SWOD samples show some differences in age and distance.

4.2.3 Spectroscopic observations

The high-resolution spectra used in this work are the same as in Chapter 2, where a complete description of the observing runs and the reduction procedure can be found. The number of stars covered by these spectra are 35 (33%) and 58 (40%) for the SWD and SWOD samples, respectively. Thus, we consider additional data from the literature to analyse the whole set of stars in both samples (see Section 4.3.3).

4.2.4 Analysis

The stellar parameters $T_{\rm eff}$, $\log g$, microturbulent velocity (ξ_t), and [Fe/H], are determined using the code TGV developed by Takeda et al. (2002), which is based on iron-ionisation equilibrium conditions, a methodology that is widely applied to solar-like stars (spectral types F5/K2-K3). Iron abundances are computed for a well-defined set of Fe I and Fe II lines. Basically, the stellar parameters are adjusted until: i) no dependence is found between the abundances derived from Fe I lines and the lower excitation potential of the lines; ii) no dependence is found between the abundances derived from the Fe I lines and their equivalent widths; and iii) the derived mean Fe I and Fe II abundances are the same. We list the

lines used in Table 4.2. We are aware that ideally all our targets should have been observed with the same spectrograph using the same configuration. Nevertheless, all the spectra used here have a similar resolution, and cover enough Fe lines to provide a high-quality metallicity determination. Only for the SARG spectra is the number of Fe II lines slightly lower (6 out of 13, begining in the 6432.68 Å line).

Table 4.2: Fe I and Fe II lines used to compute abundances. Wavelengths are given in Angstroms (Å).

Fe I			Fe II
4389.25	6173.34	6699.14	4576.34
4445.48	6180.21	6739.52	4620.52
5225.53	6200.32	6750.16	4656.98
5247.06	6219.29	6752.71	5234.63
5250.22	6232.65	6793.27	5264.79
5326.15	6240.65	6804.00	5414.08
5412.79	6265.14	6804.28	5525.13
5491.84	6271.28	6837.01	6432.68
5600.23	6280.62	6854.83	6516.08
5661.35	6297.80	6945.21	7222.40
5696.09	6311.51	6971.94	7224.46
5701.55	6322.69	6978.86	7515.84
5705.47	6353.84	7112.17	7711.73
5778.46	6481.88	7401.69	
5784.66	6498.95	7723.21	
5855.08	6518.37	7912.87	
5909.98	6574.23	8075.16	
5956.70	6581.21	8204.11	
6082.72	6593.88	8293.52	
6120.26	6609.12	8365.64	
6137.00	6625.03		
6151.62	6667.72		

Equivalent widths are obtained by fitting the lines with a Gaussian profile using the IRAF task *splot*. Stars with significant rotational velocities, $v \sin i$, have lines affected by blending, complicating the application of this method. Stars with $v \sin i \gtrsim$ 15-20 kms^{-1} typically do not have enough isolated lines to obtain accurate parameters. This has a small impact on our estimates since we consider stars with spectral types F5 or later, with typical vsini values in the range 3-9

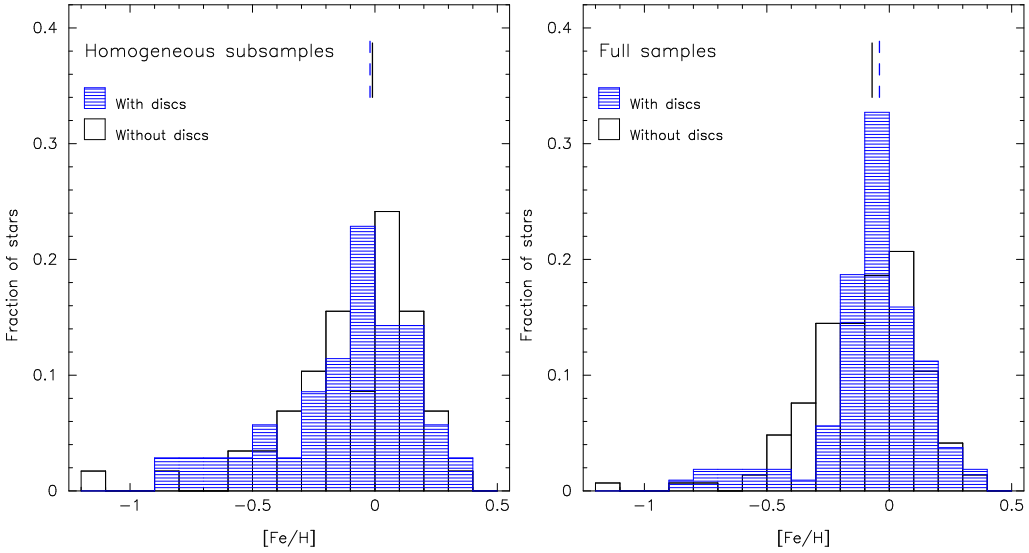

Figure 4.3: Normalized metallicity distribution of the stars without debris discs (SWODs, empty histogram), and the stars with debris discs (SWDs, blue histogram shaded at 0 degrees). Median values of the distributions are shown with vertical lines. Left panel: distributions of the stars in the homogeneous sample, i.e., metallicities computed from our own spectra. Right panel: distributions of the full stellar sample (see text).

kms^{-1} (Martínez-Arnáiz et al. 2010). The estimated stellar parameters and iron abundances are given in Table B.2.

4.3 Results

4.3.1 Homogeneous analysis

In a first step, we consider the 35 SWDs and 58 SWODs whose metallicities were estimated directly in this work. The stars in these *homogeneous samples* are listed in Table B.2, and are marked in Column 7 of Table B.1 as well. Figure 4.3 (left panel) shows the normalized distribution of these stars. Both distributions are very similar. The metallicity distribution of the SWOD sample spreads over a large range containing both metal-poor and metal-rich stars, from -1.12 to 0.36 dex. The mean metallicity of the distribution is -0.09 dex with an RMS dispersion of 0.27 dex. The distribution of the SWDs spans a slightly narrower range, from -0.89 to 0.35 dex, with a mean value of -0.10 dex and a dispersion of 0.28 dex. Since the mean of a distribution is strongly affected by the presence of outliers, we consider the median as a more representative value. The median values for

the SWOD and SWD distributions are -0.01 and -0.02, respectively. To assess whether both distributions are equal from a statistical point of view, a two-sample Kolmogorov-Smirnov (K-S) test was performed (details about how the K-S test is applied in this chapter are given in Appendix B). The maximum difference between the SWD and SWOD cumulative distribution functions is only ~ 0.11, while the likelihood that both samples have the same parent distribution is around 94%.

4.3.2 Comparison with previous works

The spectroscopic observations performed in Chapter 2 were limited to 25 pc in distance and, therefore, do not cover all SWDs and SWODs in Table B.1. Thus, we use the data of Nordström et al. (2004, NO04), Valenti & Fischer (2005, VF05) and Takeda et al. (2005, TA05) to analyse the full samples. To ensure that we did not introduce any bias resulting from estimates based on different analysis techniques, a comparison between our metallicities and the ones reported in these papers is shown in Figure 4.4. Our sample contains 72 stars in common with NO04. Our metallicities are slightly higher, by a factor ~ 0.07 dex (in median), than those given by NO04; the differences are largest for stars with positive metallicities. The agreement with VF05 is very good, with no apparent bias for the 64 stars in common; the mean difference is only -0.01 dex with a standard deviation of 0.09 dex. The VF05 metallicities are also higher than the NO04 values by a factor ~ 0.08 dex. The agreement with TA05 is excellent, better than ± 0.10 dex for most of the 49 common stars. The latter result is expected because the same method and lines were used to estimate the metallicity; it can thus be considered a consistency double check.

4.3.3 Full sample

To set the VF05 and NO04 metallicities on our own metallicity scale, we used the stars in common to obtain a linear transformation (Figure 4.4). Where possible, VF05 values were selected because they have been obtained from high-resolution spectra similar to those used in this work. The metallicities in NO04 are based on Strömgren *uvbyβ* photometry. The adopted final metallicity values for each star of the SWD and SWOD samples are given in Table B.1.

Some statistical diagnostics for the SWD and SWOD full samples are summarised in Table 4.3. Both samples have similar distributions. The *full* SWD distribution has a median of -0.04 dex, very close to the value obtained in the *homogeneous* analysis (-0.02 dex). In the case of the SWOD sample, the *full* sample has a median of -0.07 dex that, when compared with the value of -0.01 dex for the *homogeneous* subsample, means a difference of 0.06 dex. We note that 0.06

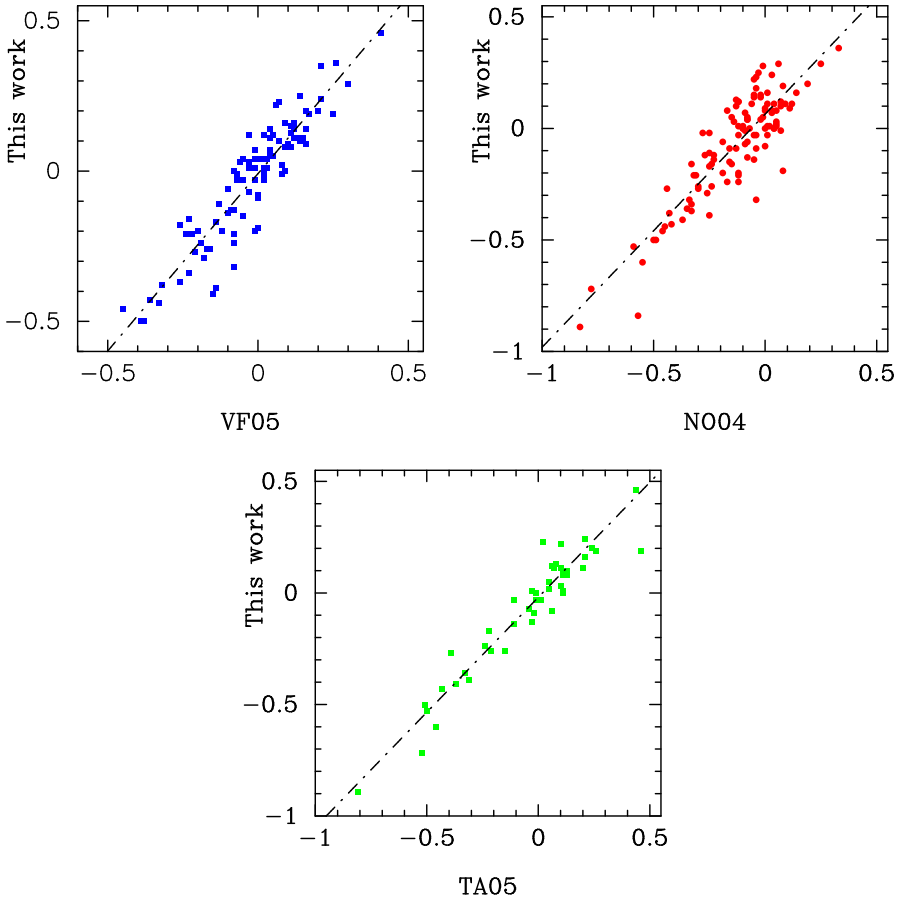

Figure 4.4: Comparison between the metallicities from the literature and those obtained in this work. Top left panel: VF05; top right panel: NO04; bottom panel: TA05. Dashed lines represent the best linear fit (y = m*x + b) between our metallicities and those given in the corresponding works. The coefficients are: m=1.18 ± 0.05, b = -0.008 ± 0.008 for VF05; m=1.04 ± 0.05, b = 0.064 ± 0.013 for N04; and m=0.99 ± 0.05, b = -0.017 ± 0.011 for TA05.

dex is of the order of the individual uncertainties in metallicity. The SWD and SWOD distributions have a smaller dispersion when we consider the whole sample (Figure 4.3, right panel). Using a K-S analysis, we tested the possibility of both distributions to differing within a 98% confidence level; our results cannot exclude that both samples come from the same parent distribution at this confidence level. Nevertheless, the likelihood that both samples are drawn from the same parent distribution diminishes significantly with respect to the homogeneous sample case (9%, see Appendix B). An interesting aspect is that there seems to be a “deficit” of stars with discs in the metallicity range -0.50 < [Fe/H] < -0.20. This

Table 4.3: [Fe/H] statistics of the stellar samples

Sample	*Mean*	*Median*	*Deviation*	*Min*	*Max*	*N*
SWODs	-0.09	-0.07	0.22	-1.12	0.36	145
SWDs	-0.08	-0.04	0.26	-1.49	0.39	107
SWDPs	0.08	0.05	0.17	-0.34	0.36	29
SWPs	0.10	0.15	0.22	-0.70	0.43	120

deficit is not explicit in the homogeneous case (Figure 4.3, see also Section 4.4 and Figure 4.7).

4.3.4 Stars with known debris discs and planets

At the time of writting[3], there are, to our knowledge, 29 solar-type stars known to host both a debris disc and at least one planet (SWDPs). This figure represents an increase of $\sim$ 50% with respect to the most recent works (Bryden et al. 2009; Kóspál et al. 2009) [4]. These stars are listed in Table 4.4.

Among the 29 SWDPs, 11 stars host known multiplanet systems, which represents an incidence rate of 38%. Wright et al. (2009) found a rate of 14% confirmed multiple planetary systems, and it could be 28% or higher when they include cases with a significant evidence of being multiple[5]. Mayor et al. (2011) found a rate exceeding 70% among their 24 systems with planets less massive than 30 $M_{\oplus}$. In our SWDP sample, there are five stars with low-mass planets in multiple systems, but this might be a lower limit, as pointed out by Mayor et al. (2011). This suggests that the multiplanet system rate in SWDPs approaches that of the low-mass planet case.

There are seven of 29 SWDPs that host at least one low-mass planet, $M \lesssim 30$ $M_{\oplus}$. These stars are HD 1461, HD 20794, HD 38858, HD 45184, HD 69830, 61 Vir (HD 115617), and HD 215152; in all cases, but in HD 1461, their metallicity is [Fe/H] ≤ 0.0, consistent with the metallicity trend for stars with low-mass planets (e.g. Mayor et al. 2011; Sousa et al. 2011).

Wright et al. (2009, Figure 9) and Currie (2009, Figure 1) showed that there is an enhanced frequency of close-in gas giant planets with semimajor axes $\lesssim 0.07$ AU (hot Jupiters). Among the 22 SWDPs that are currently known to host only

[3]December 26, 2011

[4]For the 22 stars with debris discs and planets given by Kóspál et al. (2009), HD 33636 has a substellar companion that has been retracted as a planet (Bean et al. 2007), GJ 581 is a M star, and HD 137759 is a giant star. In addition, Bryden et al. (2009) listed HD 150706 as hosting a planet and a debris disc, but the planet is not confirmed (http://exoplanet.eu).

[5]See also for comparison http//exoplanet.eu

Table 4.4: Stars with known debris discs and planets.

HIP	HD	SpType	[Fe/H]† (dex)	Ref‡	Planet⋆
522	142	F7V	0.09 (b)	9:	gc
1499	1461	G0V	0.18 (b)	11	mlh
7978	10647	F8V	-0.09 (a)	3	gc
14954	19994	F8V	0.19 (a)	8	gc
15510	20794	G8V	-0.34 (a)	10	mlc
16537	22049	K2V	-0.08 (a)	1	gc
27253	38529	G4V	0.31 (b)	6	mgc
27435	38858	G4V	-0.27 (a)	4	lc
28767	40979	F8	0.13 (b)	10:	gc
30503	45184	G2V	0.03 (b)	11	lh
31246	46375	K1IV	0.23 (b)	10:	gh
32970	50499	G1V	0.29 (b)	10:	gc
33212	50554	F8	-0.09 (b)	8	gc
33719♯	52265	G0V	0.18 (b)	8	gc
40693	69830	K0V	0.00 (a)	2	mlh
42282	73526	G6V	0.22 (b)	10:	mgc
47007	82943	G0	0.23 (b)	8	mgc
58451	104067	K2V	0.04 (b)	11	gc
61028	108874	G5	0.17 (b)	12	mgc
64924	115617	G5V	0.00 (a)	8	mlh
65721	117176	G5V	-0.03 (a)	8	gc
71395	128311	K0	0.04 (a)	8	mgc
72339	130322	K0V	-0.07 (b)	12	gh
94075	178911B	G5	0.29 (b)	10:	gc
97546	187085	G0V	0.05 (b)	10:	gc
99711	192263	K2	-0.01 (a)	5	gc
104903	202206	G6V	0.36 (b)	10	mgc
112190	215152	K0	-0.10 (c)	11	mlh
113044	216435	G3IV	0.24 (b)	10	gc

† (a) This work; (b) Valenti & Fischer (2005)
(b) values are set into our metallicity scale as described in Section 4.3.2.
(c) Metallicity for this star is from Sousa et al. (2008) since no value were found in VF05 or NO04.

‡ (1) Habing et al. (2001); (2) Bryden et al. (2006);
(3) Moór et al. (2006); (4) Beichman et al. (2006a);
(5) Smith et al. (2006); (6) Moro-Martín et al. (2007);
(7) Rhee et al. (2007); (8) Trilling et al. (2008);
(9) Bryden et al. (2009); (10) Kóspál et al. (2009);
(11) Koerner et al. (2010); (12) Dodson-Robinson et al. (2011)
The symbol ":" means that non-excess is attributed to the corresponding star in (9) or (10).

⋆ m = multiplanet system; l = low-mass planet;
g = gas giant planet; c = cool planet;
h = hot planet (semimajor axis ≤ 0.1 AU, see text);

♯ Spectral type from Montes et al. (2001b)

gas-giant planets, HD 46375 is the only star harbouring such a close-in planet, semimajor axis of 0.041 AU, while HD 130322 has a hot Jupiter at 0.088 AU; five more stars have giant planets with semimajor axes smaller than 0.5 AU (HD 38529, HD 104067, HD 117176, HD 178911B, and HD 192263). On the other hand, the semimajor axes of the low-mass planets are $\lesssim 0.07$ AU in all cases, but

in HD 20794 and HD 38858 .

The statistical properties of the SWDP metallicity distribution are shown in Table 4.3, while Figure 4.5 (left) compares the corresponding SWDP histogram with the SWDs. The figure clearly shows the distinct metallicity distributions of both the SWDPs and the SWDs; a K-S test confirms that both distributions differ within a confidence level of 98% (the likelihood of being the same distribution is 0.7%).

Summarizing, although there may be some bias related to the planet detection methods as well as the sensitivity in detecting debris discs, our results suggest that SWDPs i) have higher metallicities than both SWDs and SWODs (see Figures 4.5 and 4.7), ii) they tend to have a higher incidence of multiplanet systems, most likely at a rate close to the one of stars with low-mass planets, iii) many of them host low-mass planets, and iv) in the cases with only gas-giant planets, these planets tend to be cool Jupiters (only two out of 22 stars harbour one hot Jupiter).

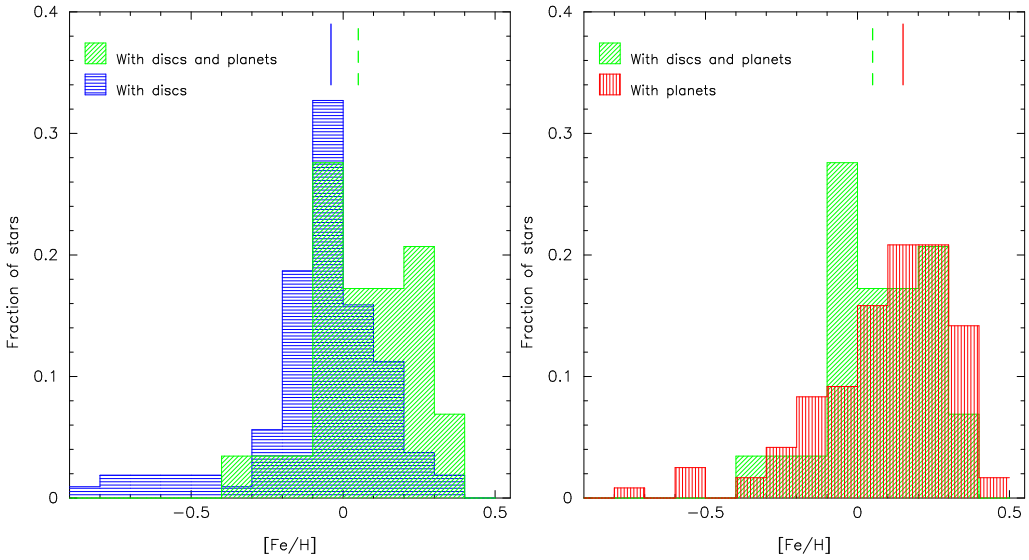

Figure 4.5: Normalized metallicity distribution of the SWDP sample (light green histogram) versus stars with debris discs (left) and stars with giant planets (right). Median values of the distributions are shown with vertical lines.

4.3.5 Comparison with stars with giant planets

Figure 4.5 (right) shows the metallicity distributions of both SWDPs and SWPs. The SWPs sample contains 120 stars and corresponds to stars hosting exclusively giant planets from Santos et al. (2004), Valenti & Fischer (2005), Sousa et al. (2011), and Mayor et al. (2011), where we have removed the stars with retracted

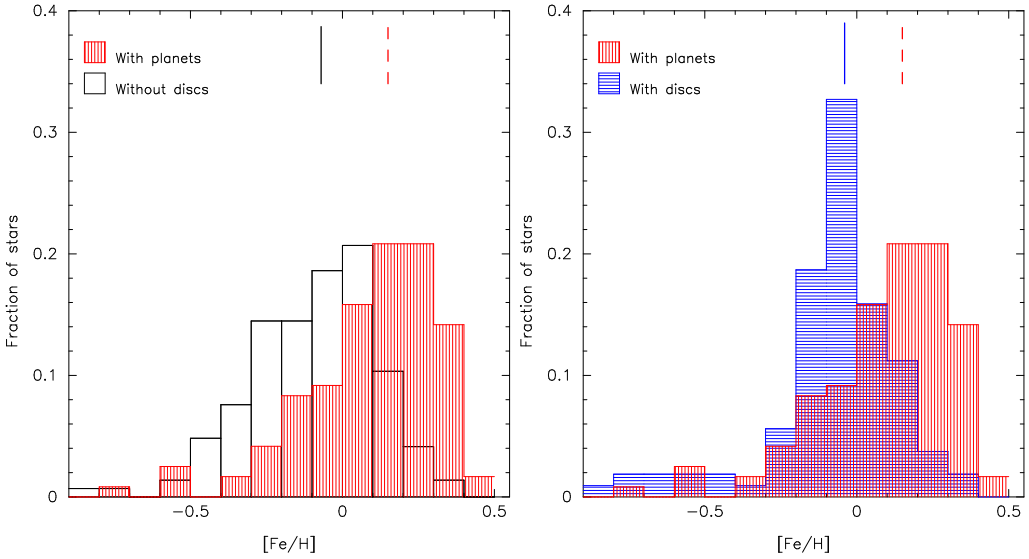

Figure 4.6: Normalized metallicity distributions of planet host-stars (red histogram) versus stars without debris discs (left) and stars with debris discs (right). Median values of the distributions are shown with vertical lines.

or not-confirmed exoplanets. Both histograms clearly show that the stars in the SWP and SWDP samples tend to have high metallicity. The K-S tests cannot rule out that both distributions are the same (p-value = 49%).

With the aim of completeness, Figure 4.6 compares the metallicity distribution of the SWPs, with those of the SWODs and SWDs samples, where the well-known trend of SWPs (gas-giant planets) to higher metallicities is clearly reproduced.

4.4 Discussion

The results presented in the previous section suggest that a transition toward higher metallicities occurs from SWODs to SWPs. The cumulative metallicity distributions, presented in Figure 4.7, allow us to get an unified overview of the metallicity trends. As pointed out before, the distribution of SWDs is similar to that of SWODs, but there seems to be a deficit of SWDs at low [Fe/H], below approximately -0.1 (see also the histogram for the full samples in Figure 4.3 (right panel) and the median [Fe/H] value in Table 4.3). The distribution of SWDPs can be clearly distinguished from that of SWDs and is similar to that of SWPs. Thus, planets are clearly the main drivers of the trend in stellar metallicity in SWDPs; this is true for both the low-mass and the giant planets in the SWDP sample. The metallicity distribution of SWPs was divided into hot and cool Jupiters because

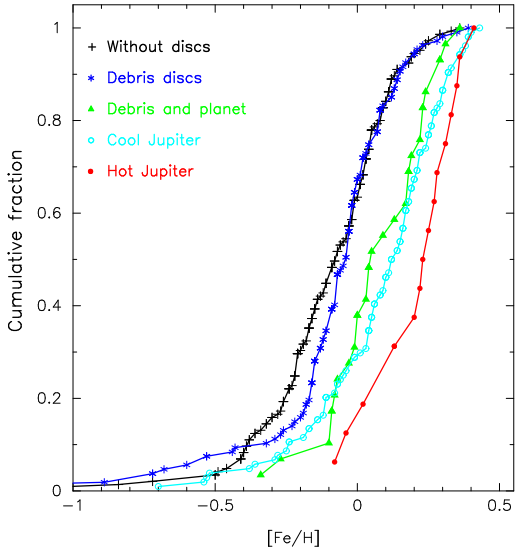

Figure 4.7: Histogram of cumulative frequencies for the different samples studied in this work.

most of the SWDPs hosting giant planets are associated with cool planets. Figure 4.7 suggests that the frequency of hot giant planets is lower for low metallicities than the frequency of cool ones. We point out that a similar trend is obtained, when the data refer to all known solar-type stars hosting giant planets, i.e., stars with close-in giant planets tend to be more metal-rich.

These trends can be explained by core-accretion models (e.g. Pollack et al. 1996; Ida & Lin 2004; Hubickyj et al. 2005; Mordasini et al. 2009, 2012), and are consistent with the view that the mass of solids in proto-planetary discs is the main factor controlling the formation of planets and planetesimals (Greaves et al. 2007; Moro-Martín et al. 2007). Thus, the rapid build-up of a core in a metal-rich proto-planetary disc would allow giant planets to form before the dissipation of the gas, while the formation of planetesimals could proceed slowly after the gas dissipation and also in a less metal-rich environment. We note that planetesimals could form regardless of the giant planet formation, and that the timescale for Earth-like planet formation is long and can proceed in a relatively metal-poor environment.

Figure 4.8 shows the fractional dust luminosity, $L_{dust}/L_{\star}$, of the SWDs and SWDPs versus the metallicity. The plot distinguishes between low-mass and gas giant planets. Values of $L_{dust}/L_{\star}$ are taken from the references in Section 4.2.1; we plot the mean value of $L_{dust}/L_{\star}$ for the stars from Trilling et al. (2008). It is found that the SWDPs as a whole span approximately two orders of magnitude in $L_{dust}/L_{\star}$ and are well-mixed with SWDs, while most of the stars hosting debris

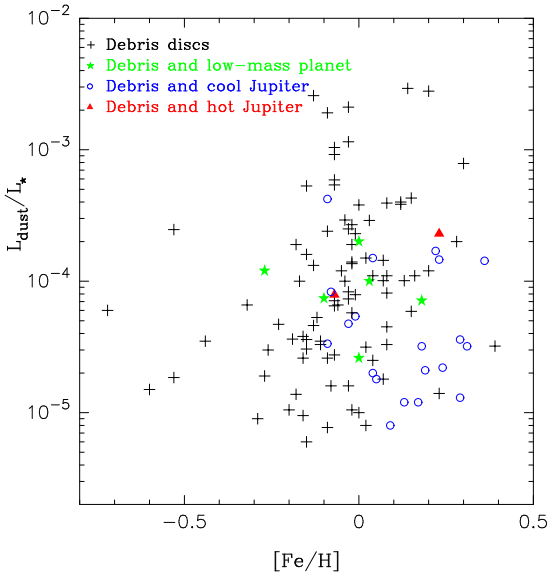

Figure 4.8: Fractional dust luminosity, $L_{dust}/L_\star$, versus [Fe/H] for those stars hosting a debris discs. Stars are plotted with different symbols and colours depending on the presence/absence of low-mass or cool/hot Jupiter planets.

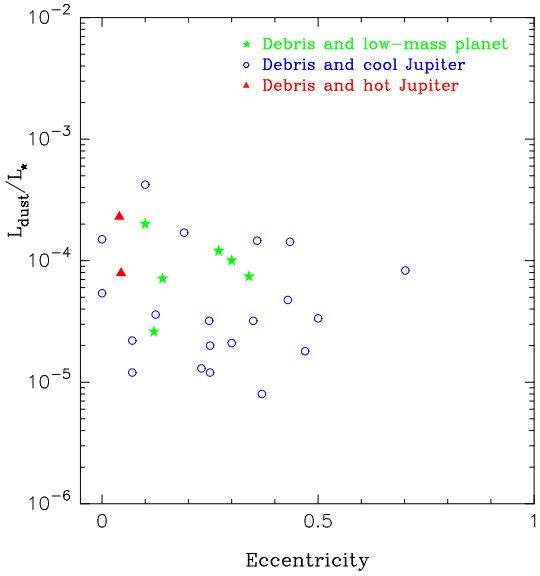

Figure 4.9: Fractional dust luminosity, $L_{dust}/L_\star$, versus eccentricity.

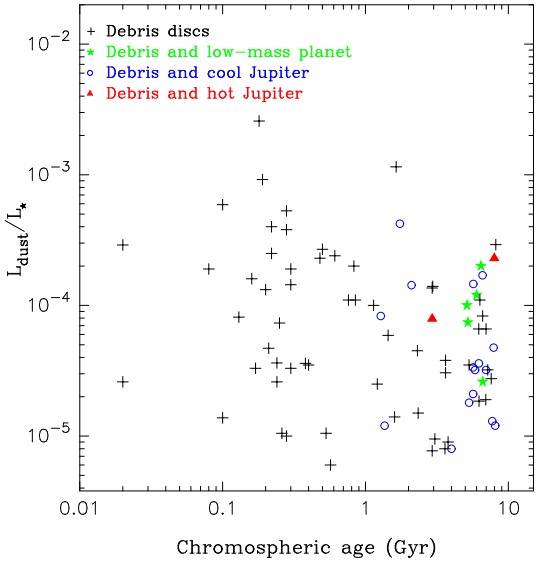

Figure 4.10: Fractional dust luminosity, $L_{dust}/L_\star$, versus stellar age.

discs and cool giant planets tend to have low dust luminosities, $L_{dust}/L_\star < 10^{-4}$; more than 50% of SWDPs of this type are indeed concentrated in the low-dust luminosity/high-metallicity corner of Figure 4.8. In addition, there seems to be a trend of larger eccentricities (we take as reference the innermost planet) while the luminosity of the dust decreases, albeit with a large scatter (Figure 4.9). Such an anticorrelation may be the result of dynamical instabilities produced by eccentric giant planets, which clear out the inner and outer regions of the planetary discs (Raymond et al. 2011). On the other hand, there is no trend with the semimajor axis of the planet (not shown), although it seems that low-mass planets tend to be predominantly hot but most of the giant planets are cool (Section 4.3.4). Furthermore, while the SWDs span the ∼10 Myr - 10 Gyr range, the SWDPs are mature stars (older than 1 Gyr), although low-mass planet host stars tend to group at old ages, > 5 Gyr, and the cool giant-planet stars span a larger range of 1 - 10 Gyr (Figure 4.10). This age behaviour reflects a bias introduced by current planet-detection techniques. Young stars are usually excluded from planet-search programmes owing to their high-levels of chromospheric activity, although much effort is being applied to overcome this problem (e.g. Dumusque et al. 2011a,b). Finally, we can exclude a dust luminosity evolution with age in the SWDP sample, in line with the results of Trilling et al. (2008) for solar-type stars surrounded by debris discs.

4.5 Conclusions

The number of debris disc stars known to host planets has increased in the past few years by a factor of ~ 50 % , particularly those associated with low-mass planets. This has motivated us to revisit the properties of these stars and to compare them with stars with planets, stars with debris discs, and stars with neither debris nor planets.

We have identified a transition toward higher metallicities from SWODs to SWPs. The SWDs have a metallicity distribution similar to those of SWODs, although the distribution of the first ones might be slightly shifted towards higher metallicities. The SWDPs follow the same metallicity trend as SWPs, irrespective of whether the planets are low-mass or gas giants; thus, it is the planet which reveals the metallicity of the corresponding stars. There is a high rate of incidence of multiplanet systems in SWDPs. Their innermost planets are usually cool giants, but the planets are close-in when the debris disc stars only host low-mass planets. It cannot be excluded that this latter result could be biased by the planet detection techniques. These results support the scenario of core accretion for planet formation and the previous view that the mass of solids in proto-planetary discs is the main factor determining the outcome of planet formation processes.

In addition, we have found that debris disc stars hosting cool giant planets tend to have the lowest dust luminosities, and that there is an anticorrelation between the dust luminosity and the innermost planet eccentricity. A plausible explanation of these suggested trends is provided by recent simulations of dynamical instabilities produced by eccentric giant planets. These apparent trends will likely be either confirmed or rejected by the various programmes dealing with planets and debris discs, currently being carried out with the *Herschel Space Observatory*, together with the expected detection of further planets, particularly low-mass planets, around the debris disc stars.

Finally, no other trend has been found relating debris disc and planet (e.g. period or semimajor axis) properties.

5

The influence of stellar parameters, normalization and atmosphere models on the detection of faint cold circumstellar debris discs.

J. Maldonado[1], B. Montesinos[2], A. Mora[3], A. Bayo[4], and C. Eiroa[1].

[1] Universidad Autónoma de Madrid, Dpto. Física Teórica, Módulo 15, Facultad de Ciencias, Campus de Cantoblanco, E-28049 Madrid, Spain
[2] Centro de Astrobiología (INTA-CSIC), LAEFF Campus, European Space Astronomy Center (ESAC),
P.O. Box 78, E-28691 Villanueva de la Cañada, Madrid, Spain
[3] ESA-ESAC Gaia SOC. P.O. Box 78, E-28691 Villanueva de la Cañada, Madrid, Spain
[4] European Space Observatory, Alonso de Cordova 3107, Vitacura, Casilla 19001, Santiago 19, Chile

Submitted for publication in Montly Noticies of the Royal Astronomical Society

ABSTRACT

Many main-sequence stars are surrounded by dusty-debris discs, signatures of planetesimals systems. The *Herschel Space Observatory* is detecting very faint debris discs, with infrared excesses only few mJy over the photospheric fluxes, which also amount a few mJy at the relevant wavelengths. Thus, predictions as accurate as possible of the photospheric flux levels are essential to determine the presence of a dusty debris disc around a specific star. In this chapter we analyze how the predicted stellar flux of a given star is affected by the choice of the stellar parameters, the photometric bands used to normalize the photosphere, and

the choice of the stellar model. For solar-like stars we find differences of the order of 2% at 70 μm between predictions based on different models. For M-type stars, PHOENIX predicts fluxes around 5-7% larger than ATLAS9. In addition, small variations in the stellar parameters can lead to significant differences in the prediction of the stellar photosphere, higher than the *Herschel* absolute flux calibration at 70 and 100 μm. We have applied our analysis to a sample of 239 nearby stars which are being observed with *Herschel* in the framework of the Open Time Key Project DUNES, and have predicted their fluxes in several photometric bands ranging from V Johnson to SPIRE 500 μm.

Key words. -stars: circumstellar matter -stars: late-type -stars: planetary systems

5.1 Introduction

The question of the origin and evolution of planetary systems is of fundamental importance for astrophysics. Dusty debris discs are generated by collisions of large solid bodies orbiting main sequence stars (Backman & Paresce 1993). They constitute a direct signature of planetesimal systems and an indirect one of planetary systems, providing therefore valuable tools to understand the formation and evolution of planets, as well as the history of our own Solar System. Current data show that around 16% of mature (older than 1 Gyr) stars are surrounded by debris discs (e.g. Trilling et al. 2008).

Debris discs are detected as flux excesses over the stellar photospheric emission at IR wavelengths, which requires a prediction of the stellar photospheric flux at IR wavelengths. This is normally done by fitting a photospheric spectrum to the star's SED and extrapolating it from visible/near-IR to longer wavelengths (e.g. Beichman et al. 2005; Bryden et al. 2006; Trilling et al. 2008). The presence of a debris disc is inferred if (F_{obs} - F_{pred}) $\geq 3\sigma$, where F_{pred} is the predicted flux, F_{obs} is the observed flux, and σ is the uncertainty of the measurement (e.g. Su et al. 2006).

To estimate the stellar photospheric fluxes at IR-wavelengths several input data are needed: i) the stellar parameters (T_{eff}, $\log g$, [Fe/H]); ii) a model atmosphere; and iii) at least one photometric point.

The selection of the photospheric models is an important step. Several works have attempted to compare different families of model atmospheres. Bertone et al. (2004) compared ATLAS9 and PHOENIX-NextGen models, concluding that both theoretical models accurately reproduce the SED of early-type stars, although at low T_{eff} both ATLAS9 and PHOENIX codes fail to properly reproduce the contribution of molecular features in the observed SED of K-M stars. Those authors also concluded that ATLAS better reproduced early-type stars while NextGen is more

accurate for M stars. In a recent work, Sinclair et al. (2010) revisited the topic, analyzing how the use of ATLAS9, MARCS and PHOENIX-NextGen model spectra could affect the prediction of stellar photospheres at *Spitzer*-MIPS wavelengths. These authors conclude that the predicted photospheres could differ from 5% for solar-like stars (spectral-type FGK) up to 15% for M dwarfs.

To our knowledge, however, the influence of the specific stellar parameters and the choice of the photometric bands, in the detection of a debris disc have not been discussed in detail yet. In this chapter we discuss these issues. We use the results to predict the stellar photosphere at *Herschel* (Pilbratt et al. 2010), PACS 70, 100, and 160 μm (Poglitsch et al. 2010), and SPIRE 50, 350 and 500 μm (Griffin et al. 2010). Our analysis is used to predict the expected stellar photospheric fluxes of the stars observed in the framework of the *Herschel Space Observatory* - DUNES[1] Open Time Key Programme (Eiroa et al. 2010). A detailed description of the DUNES targets and their properties (e.g. age, binarity, kinematics, ...) is out of the scope of this thesis, the reader is referred to Eiroa et al. (in prep) for details. The DUNES objectives are the detection of cold and faint debris discs, which would produce excesses of the order of few mJy i.e., few times the measurement uncertainties, on top of photospheres with similar flux levels. Therefore, the analysis proposed in this chapter is of the utmost importance to assess the possible detection of a debris disc around those stars.

The chapter is organised as follows. Section 5.2 shows a comparison between the different families of stellar models atmosphere. The impact of the stellar parameters is studied in Section 5.3. In Section 5.4 we describe the procedure to predict the photospheric fluxes, and test our procedure with the stars in the DUNES sample. Our conclusions are given in Section 5.5.

5.2 Comparison between different stellar models atmosphere: ATLAS9, PHOENIX, and MARCS

ATLAS9 (Castelli & Kurucz 2003), PHOENIX-GAIA (Brott & Hauschildt 2005), and MARCS (Gustafsson et al. 2008) are the photospheric models more commonly used to fit the observed photospheres of stars. Thus, we have carried out a comparison between the three families of synthetic spectra with the objective of evaluating which one is the best to be used for fitting the observed spectral energy distributions of stars. Specific information on each family of models can be found in Table 5.1 and in the corresponding web pages[2].

[1] DUst around Nearby Stars project (DUNES), http://www.mpia-hd.mpg.de/DUNES/

[2] ATLAS9: http://www.user.oat.ts.astro.it/castelli/grids.html; MARCS: http://marcs.astro.uu.se/; Unfortunately, the version of the PHOENIX-GAIA models used

Table 5.1: Some comparative information on the three sets of models.

	ATLAS9	PHOENIX	MARCS
Physics	LTE (NLTE limited)	LTE and NLTE	LTE
Opacity	ODF	Opacity sampling	Opacity sampling
Lines	Kurucz (1997)	> 300,000,000 lines	Updated 2008
	Molecules (new)		(several sources)
Grid points	1221 points	~ 52000 points	100724 points
Temperatures	3,500 - 50,000 K	2,000 - 50,000 K	2,500 - 8,000 K
$\log g$	0.00 - 5.00 cgs	-0.5 - 5.5 cgs	-1.00 - 5.00 cgs
Metallicity	-5.5 - +0.5 dex	-4.0 - +0.5 dex	-5.0 - +1.0 dex
v_{turb}	0, 2 km/s	2 km/s	0, 1, 2, 5 km/s
Mixing length	1.25	1.5	2.0
Geometry	Plane-parallel	Plane-parallel	Plane-parallel
		Spherical	Spherical
Code	Public	Not public	Not public

The ATLAS9 models have a fixed amount of wavelength points (1221), whose step changes with the wavelength. They cover the range 0.009-160 μm. Each PHOENIX model has a different amount of wavelength points (around 52000) and covers the interval 0.001-50 μm. The MARCS models have a fixed amount of wavelength points (100724), and the wavelength step is also not constant. They cover the spectral range between 0.13-20 μm. Figure 5.1 shows a first comparison among the three sets of models for effective temperatures 6000, 5000, 4000 and 3500 K. Values of $\log g$ = 4.0 and [Fe/H]=0.0 have been used. In those figures the models have been plotted superimposed to each other without any normalization, i.e., we show the original energy distributions [3].

The conclusions from this comparison are:

1. For $T_{eff} \geq 5000$ K the three sets of models are virtually identical (see Fig. 5.1, bottom panels).

2. For 4000 K $\lesssim T_{eff} <$ 5000 K the models start to show some differences, which are more pronounced towards lower temperatures and shorter wavelengths. Fig. 5.1, top right panel, shows the differences in the optical and in

in this work (v2.6.1) is not longer available in the web. Other PHOENIX models can be found at ftp://ftp.hs.uni-hamburg.de/pub/outgoing/phoenix/

[3]The original PHOENIX and MARCS spectra were degraded to the resolution of the ATLAS9 models by smoothing them with a gaussian filter with FWHM=0.005, after taking the decimal logarithm of the wavelengths in Å. Then, the wavelength scale was put back in physical units.

Table 5.2: Differences in magnitudes at V, I_c, and J, H, K_s 2MASS photometric bands between PHOENIX and ATLAS9 models atmosphere and MARCS and ATLAS9 models atmosphere.

PHOENIX / ATLAS9					
T_{eff} (K)	V	I_c	J	H	K_s
3500	0.06	0.03	0.04	0.02	-0.08
4000	0.05	-0.03	-0.02	0.02	-0.02
5000	-0.01	-0.03	-0.01	0.01	0.00
6000	-0.01	-0.02	-0.01	0.01	0.00
7000	0.00	-0.02	-0.02	0.00	-0.01
MARCS / ATLAS9					
T_{eff} (K)	V	I_c	J	H	K_s
3500	0.19	0.06	0.07	-0.04	-0.12
4000	0.03	0.00	0.01	-0.01	-0.04
5000	-0.01	-0.01	0.00	0.01	0.00
6000	-0.01	0.00	0.00	0.01	0.00
7000	-0.01	0.00	0.00	0.01	0.00

the near-IR for the temperature of 4000 K. We note that for this temperature ATLAS9 and PHOENIX are quite similar around 1 μm, while MARCS is slightly lower. At 2-3 μm PHOENIX and MARCS are similar while ATLAS9 is lower. For $\lambda > 4$ μm the three sets of models are virtually identical, apart from some very small discrepancies (e.g. around 4.5 and 6.5 μm).

3. Models with $T_{eff} \lesssim 4000$ K present relative large discrepancies. Fig. 5.1, top left panel, shows that the ATLAS9 models are very different from PHOENIX and MARCS in the optical and near-IR ranges, whereas these two are fairly similar. Fig. 5.1 also shows that the ATLAS9 model runs slightly below PHOENIX and MARCS up to ~10 μm.

In order to quantify how different ATLAS9, PHOENIX, and MARCS models are, we integrated all models in the most commonly used photometric filters in the optical (V, I_c), and near-IR wavelengths (J, H, and K_s 2MASS) [4]. The differences are shown in Table 5.2. They are given in magnitudes ($\Delta m = -2.5 \times \log(F_1/F_2)$). We see that for $T_{eff} > 5000$ K the differences in the five photometric bands are almost zero, and even for $T_{eff} = 4000$ K differences are below 0.05 magnitudes

[4]Filters passbands were taken from Bessell (1990) for V, and I_c and Cohen et al. (2003) for 2MASS.

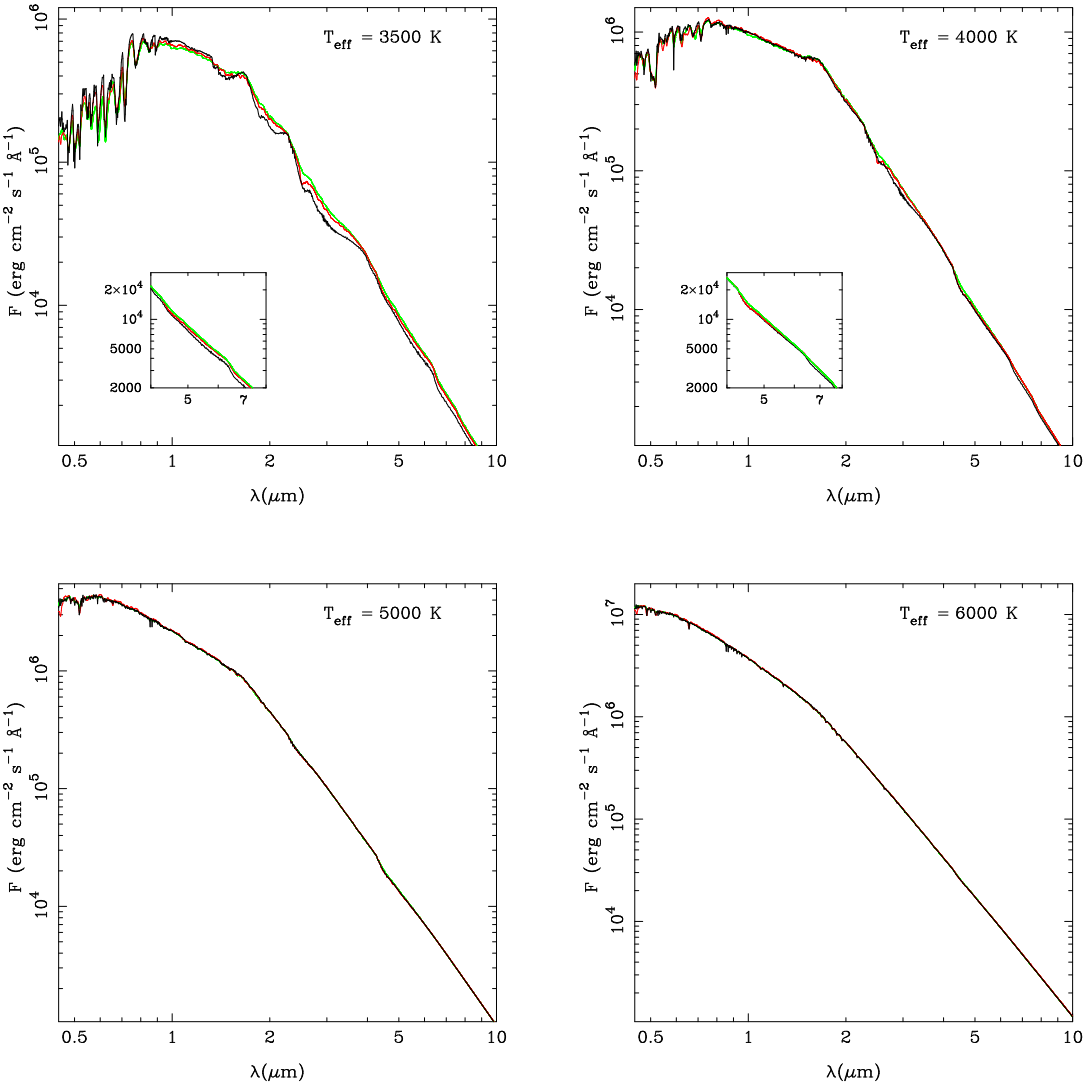

Figure 5.1: Models with T_{eff} = 3500 K (top left panel), 4000 K (top right panel), 5000 K (bottom left panel), and 6000 K (bottom right panel). In all cases $\log g_*$=4.0 and [M/H]=+0.00. ATLAS9 models are plotted in black, PHOENIX models in red, and MARCS models in green. Left corner panels show a zoom of the 4-8 μm region.

in all bands. For T_{eff} = 3500 K, the models are significantly different at V and K_s bands. PHOENIX models differ from ATLAS9 in 0.06 and -0.08 magnitudes, respectively, while MARCS differ in 0.19 and -0.12 magnitudes.

5.2.1 Deviations from the Rayleigh-Jeans regime

PHOENIX and MARCS models extend up to wavelengths much shorter than *Herschel*-PACS (70, 100, and 160 μm), whereas ATLAS9 models do not cover *Herschel*-SPIRE wavelengths (250, 350, and 500 μm). It is therefore, mandatory to use the Rayleigh-Jeans tail to predict stellar photospheres at PACS/SPIRE wavelengths. This leads to the question of whether models atmosphere are themselves consistent with the Rayleigh-Jeans regime.

In order to study how models atmosphere deviate from the Rayleigh-Jeans regime, we compare fluxes at 24 μm (one of the *Spitzer*-MIPS wavelengths) with fluxes at 45 μm. If models followed a "pure" Rayleigh-Jeans law, the ratio between flux densities per frequency unit at 24 and 45 μm should be 3.516[5].

The choice of 45 μm is due to the fact that PHOENIX models extend up to only 50 μm. MARCS models end at 30 μm, so they are excluded from this exercise.

Figure 5.2 shows the distribution of that ratio for ATLAS9 (left) and PHOENIX models (right) as a function of T_{eff}.

It is clear from the figure that models with lower temperatures deviate more from the Rayleigh-Jeans tail that models for hotter stars. These deviations could be produced by the presence of molecular bands which become more prominent at lower temperatures. In the case of ATLAS9 models, those with T_{eff} = 3500 K show a median deviation from a "pure" Rayleigh-Jeans tail of 5% [6], which diminishes to only 0.35% for 5000 K models. For stars with T_{eff} > 5000 K, the overall median deviation is only 0.08%. $\log g$ effects become negligible when considering stars hotter than 5500 K, and models at a given T_{eff} show different deviations only depending on their metallicity. Models with [Fe/H]=+0.5 show slightly larger deviations. For example, at T_{eff} = 6000 K, the median deviations are 0.31%, 0.13% and 0.56% for metallicities -0.50, +0.00, and +0.50 dex, respectively.

When considering PHOENIX, median deviation for 3500 K models is 4.6%, while for 5000 K models is 0.02%. Overall median deviation for T_{eff} > 5000 K is around 0.15%. For T_{eff} > 5500 K, at a given T_{eff}, models with [Fe/H] = +0.5 and +0.0 practically give the same ratio, almost independently of $\log g$. However, models with [Fe/H] = -0.5 show a small different ratio depending on their $\log g$.

If we consider longer wavelengths, for example 70 μm instead of 45 μm, the deviations with respect to the Rayleigh-Jeans law are larger, 5.3%, 1.5%, and 0.6% for stars with 4000 K < T_{eff}, 4000 K ≤ T_{eff} < 5000 K, and T_{eff} ≥ 5000 K, respectively (only ATLAS9 models).

Because PHOENIX and MARCS models are almost identical for $\lambda \gtrsim 10$ μm, in the following sections only ATLAS9 and PHOENIX models are considered.

[5] Although MIPS reference wavelength is 23.675 μm, for simplicity we consider 24 μm in this exercise.

[6] Computed as 100×(|ratio - theoretical ratio|/theoretical ratio)

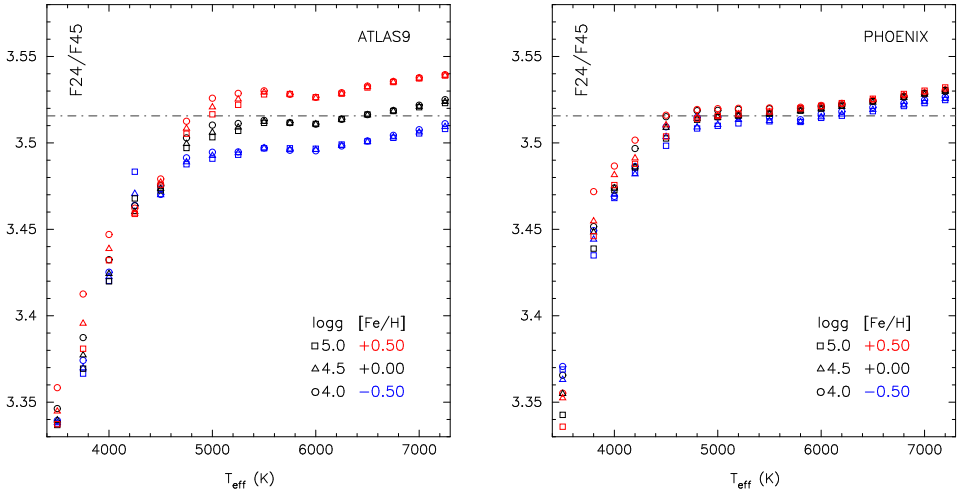

Figure 5.2: Ratio F24/F45 for ATLAS9 models (left panel) and PHOENIX models (right panel) as a function of the effective temperature. Ratios are plotted with different colours and symbols depending of the $\log g$ and [Fe/H] of the model. The horizontal dashed line represents the expected value if models followed the canonical Rayleigh-Jeans law.

5.3 Stellar parameters and their influence

Stellar photospheres are mainly characterized by their effective temperatures, surface gravities and metallicities, while other properties such as e.g. rotation or turbulence velocity play a secondary role. Due to this, it is therefore interesting to study how variations of those fundamental parameters affect the photospheric models and the predicted fluxes and what happens for stars with "extreme" stellar parameters.

5.3.1 T_{eff} effects

To study the effect of the T_{eff}, four sets of models are used. Each set contains five models: a "reference model" chosen at T_{eff}^{ref} = 4000, 5000, 6000, and 7000 K, respectively; and four models with $T_{eff} = T_{eff}^{ref} \pm 250$ K, and $T_{eff} = T_{eff}^{ref} \pm 500$ K, respectively. In the case of the PHOENIX models, since their T_{eff} step is ±100 K, we use ± 200 K, instead of ± 250 K. $\log g$ and [Fe/H] are fixed in all models to 4.5 dex and +0.00 dex. Each model in each set is compared with its respective "reference model", normalized at 2MASS K_s flux, i.e, for each model the following ratio is computed:

Table 5.3: Sensitivity in flux determination at *Herschel-PACS* wavelengths, in %, computed from the *r* values defined in equations 5.1, 5.3, and 5.4. For each set of models atmosphere, and for different temperatures, ranging from 3500 to 7000 K: Column 2 shows the uncertainties when changes in T_{eff} of ±250/200K are considered; Column 3 shows the uncertainties when changes in T_{eff} of ±500K are considered; Column 4, and 5 show, respectively, the uncertainties when changes in [Fe/H] and logg are studied.

ATLAS9 models				
T_{eff} (K)	Δ_{Teff} ±250 K	Δ_{Teff} ±500 K	$\Delta_{[Fe/H]}$ ±0.5 dex	$\Delta_{\log g}$ ±0.5 dex
7000	<0.1%	<0.1%	2.5%	0.2%
6000	<0.1%	0.2%	2.6%	0.4%
5000	1%	3%	2.1%	0.5%
4000	13%	25%	4.1%	5%
3500			7.3%	5%
PHOENIX models				
T_{eff} (K)	Δ_{Teff} ±200 K	Δ_{Teff} ±500 K	$\Delta_{[Fe/H]}$ ±0.5 dex	$\Delta_{\log g}$ ±0.5 dex
7000	0.3%	0.5%	0.5%	0.4%
6000	0.1%	0.4%	0.6%	0.4%
5000	0.2%	0.1%	0.8%	0.5%
4000	9%	20%	6%	6%
3500			5%	6%

$$r = \frac{F(T_{\rm eff})}{F(T_{\rm eff}^{\rm ref})} \times \frac{F_{\rm Ks}(T_{\rm eff}^{\rm ref})}{F_{\rm Ks}(T_{\rm eff})} \tag{5.1}$$

where the ratio *r*, is computed at each wavelength and $F \equiv F_\nu$ is the flux at the stellar surface. The ratios are shown in Figure 5.3. To transform the ratios into uncertainties, the following expression is used:

$$\Delta F = \frac{\left|1 - r\left(T_{eff}^{ref} - 250\,K\right)\right| + \left|1 - r\left(T_{eff}^{ref} + 250\,K\right)\right|}{2} \tag{5.2}$$

and a similar one for $\Delta T_{\rm eff} = \pm 500$ K. These uncertainties are given in Columns 2 and 3 of Table 5.3. They are computed at the *Herschel*-PACS wavelengths of 70, 100, and 160 μm. The value given in the table refers to the wavelength for which

the uncertainty is larger [7].

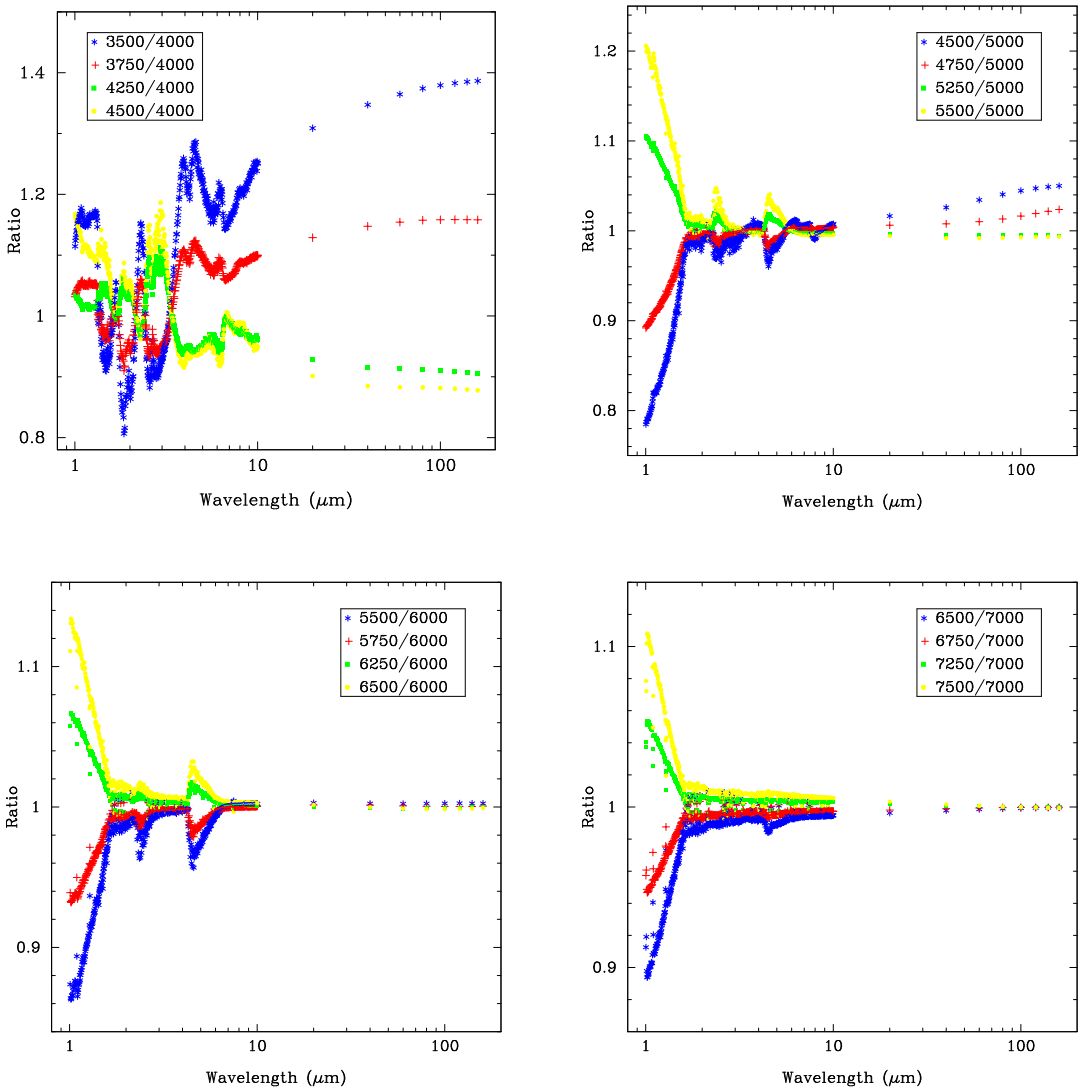

Figure 5.3: Variations in the SEDs when T_{eff} is changed ± 250 K and ± 500 K. Top left panel: T_{eff}=4000 K; top right panel: T_{eff}=5000 K; bottom left panel: T_{eff}=6000 K; bottom right panel: T_{eff}=7000 K. ATLAS9 models are shown.

The results show that the uncertainties for stars with $T_{eff} \gtrapprox 5000$ K (spectral types hotter than K0) are small. For the coolest stars, even small variations in

[7]The uncertainties show small variations, less than 1% from one wavelength to the another, due to the deviations of the ATLAS9 models from the canonical Rayleigh-Jeans law. For PHOENIX models, since they have been extrapolated to *Herschel*-PACS wavelengths using Rayleigh-Jeans, the obtained uncertainties are equal for the three wavelengths.

the temperature (200-250 K), can lead to important differences in the predicted photospheric fluxes between 9 and 13%, depending on the model used, which are larger than 5%, the *Herschel* absolute flux calibration uncertainty[8] at 70 and 100 μm, (10% absolute flux calibration, at 160 μm) and can seriously affect the detection/non-detection of a debris discs. It is important to notice that the effect is more pronounced for lower temperatures, for example, going from 4000 to 3500 K implies a flux variation of 39%, the same temperature difference but assuming 4500 instead of 4000 K has an impact of only 12% (ATLAS9 models).

5.3.2 $\log g$ and [Fe/H] effects

A similar approach is used to study the effect of the gravity. [Fe/H] is fixed to the solar value, and for different temperatures (3500, 4000, 5000, 6000, and 7000 K) five models with $\log g$ values of 3.0, 3.5, 4.0, 4.5, and 5.0 dex are considered. For each temperature the reference model is the one with $\log g = 4.5$:

$$r = \frac{F(\log g)}{F(\log g = 4.5)} \times \frac{F_{\rm Ks}(\log g = 4.5)}{F_{\rm Ks}(\log g)} \tag{5.3}$$

To study the effect of the metallicity, $\log g$ is fixed to 4.5 dex, and for each temperature, four models of metallicities -1.0, -0.5, +0.0, and +0.5 dex are considered. For each temperature the reference model is set to the one with solar metallicity:

$$r = \frac{F([{\rm Fe/H}])}{F([{\rm Fe/H}] = [{\rm Fe/H}]_\odot)} \times \frac{F_{\rm Ks}([{\rm Fe/H}] = [{\rm Fe/H}]_\odot)}{F_{\rm Ks}([{\rm Fe/H}])} \tag{5.4}$$

Results are summarized in Columns 4 and 5 of Table 5.3. $\log g$ or metallicity produce small variations in the fluxes, unless we consider the cooler stars ($T_{\rm eff} \lessapprox 4000$ K). In these cases variations in $\log g$ or [Fe/H] can change the fluxes around 5%, which is a significant percentage, although still below the variations due to the effective temperature. ATLAS9 and PHOENIX models, the former showing uncertainties much larger, show a different behaviour in metallicity. Indeed, metallicity is the most important source of flux variations in ATLAS9 models for $T_{\rm eff} \gtrapprox 5000$ K.

5.3.3 "Extreme" values

Finally, the effect of a combination of "extreme" stellar parameters has been studied. First, the influence of variations in [Fe/H] on the fluxes when both $T_{\rm eff}$ and $\log g$ are extreme. For $T_{\rm eff} = 3500$ and 7000 K we consider models with $\log g =$

[8]Technical Note PICC-ME-TN-036 in http://herschel.esac.esa.int

3.5 and 5.0 dex, and [Fe/H] = +0.5, +0.00 and -1.0 dex, respectively. The models with solar metallicity are considered as the reference ones. The comparisons are shown in Figure 5.4. In the case of low gravities, the effect of the metallicity is quite dependent on the temperature. For 7000 K, variations in metallicity lead to small differences in the fluxes, approximately 3%, 4% for Δ [Fe/H]= +0.5 and -1.0 dex, respectively. In the lower temperature regime (3500 K), the situation is the opposite and variations in metallicities of $\pm$ 0.5 dex can vary our predictions up to more than 15%.

In a second test, metallicities were fixed to the extreme values of -1.0 and +0.5 dex, (with T_{eff} = 3500 and 7000 K) and $\log g$ was changed to values from 3.5 to 5.0 dex. In this case, models with $\log g$ = 4.5 are chosen as reference. Similarly to the previous test, significant variations are only found for the coolest stars (3500 K). The effect is larger for lower gravities and higher metallicities. For [Fe/H]=-1.0 dex, changing $\log g$ from 4.5 dex to 3.5 dex produces differences in fluxes of 5%, In contrast, for [Fe/H]=+0.5, the same change in $\log g$ leads to a difference in flux up to 13%. Increasing the gravity from $\log g$ = 4.5 dex to $\log g$ = 5.0 dex, also produces significant changes (although smaller than in the previous case), up to 7.5% in the case of metal overabundance, while less than 1% in the case of [Fe/H]=-1.0 dex. Figure 5.5 illustrates these cases.

5.4 Predicting photospheric fluxes. Application to the DUNES sample

In the previous sections we have analyzed the behaviour of different models atmosphere at mid/far IR wavelengths, and how uncertainties in the stellar parameters can alter photospheric predictions at such wavelengths. Through this section we consider a practical case, predicting the photospheric fluxes at *Herschel* wavelengths, and computing the spectral energy distribution of a sample of 239 nearby AFGKM-spectral type stars, which have been observed in the framework of the *Herschel*-DUNES Open Time Key Programme. 106 of the targets are shared with the complementary *Herschel* OTKP-DEBRIS (Matthews et al. 2010).

Stellar parameters for these stars are taken from Eiroa et al. (in prep). T_{eff} values for the DUNES targets are mainly between 3700 and 7600 K, $\log g$ values are within 3.7 and 5.0 dex, and metallicity values range from -1.0 to 0.5 dex. Typical T_{eff} differences between values from different catalogues, archives or individual papers are within 100 K for roughly 80% of the sample, while differences in $\log g$ and [Fe/H] are usually in the range 0.1-0.2 dex. Around 9% of the stars, are in the low temperature regime (4000 K $\leq T_{eff}$) in which parameters should be known with high precision (ΔT_{eff} < 200 K) in order to be confident in the photosphere's

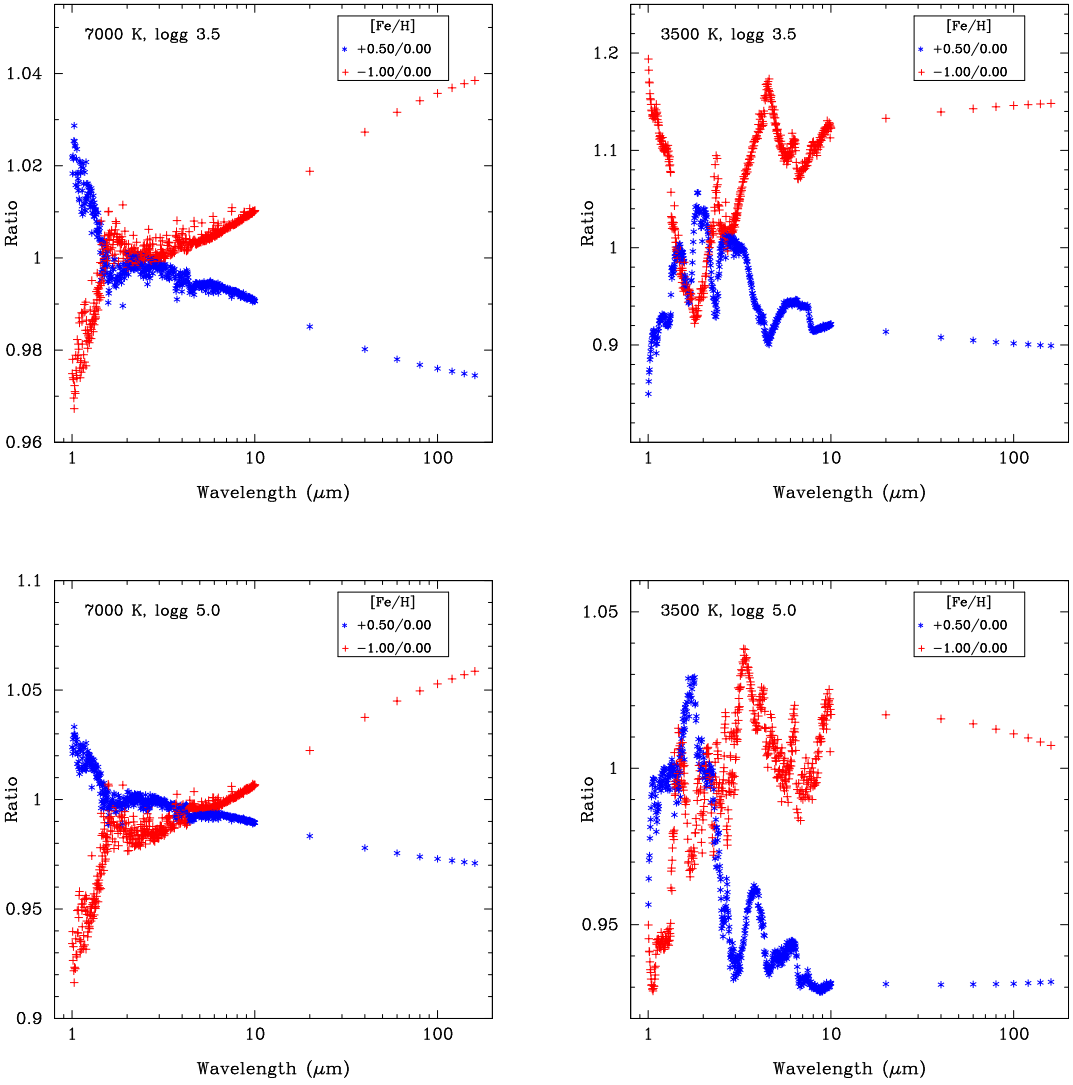

Figure 5.4: Metallicity effects when both T_{eff} and $\log g$ have extreme values. Top left panel: T_{eff}=7000 K $\log g$=3.5 dex; top right panel: T_{eff}=3500 $\log g$=3.5 dex; bottom left panel: T_{eff}=7000 K $\log g$=5.0 dex; bottom right panel: T_{eff}=3500 K $\log g$=5.0 dex. Ratios of models with [Fe/H]=+0.50 and [Fe/H]=-1.00, normalized to [Fe/H]=+0.00 are plotted in blue and red, respectively. ATLAS9 models are shown.

predictions.

A set of Linux scripts and FORTRAN 90 programs were written to predict the photospheric fluxes at *Herschel* wavelengths. The procedure is slightly different from ATLAS9 to PHOENIX models, so it is necessary to describe it with some

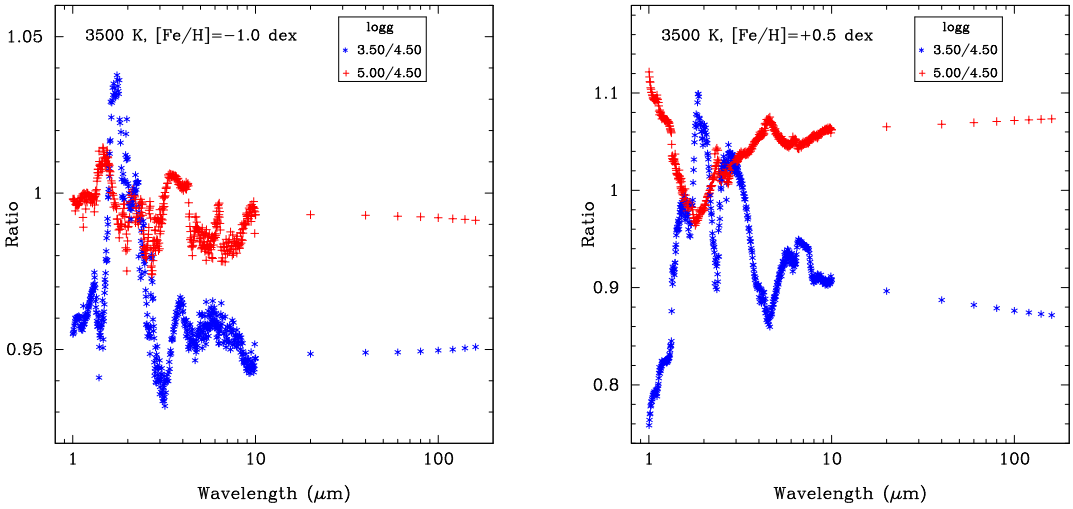

Figure 5.5: $\log g$ effects when both T_{eff} and [Fe/H] have extreme values. Only T_{eff}=3500 K is shown, since for higher temperatures the variations in the fluxes are negligible. Left panel: [Fe/H]=-1.0 dex; right panel: [Fe/H]=+0.5 dex. Ratios of models with $\log g$=3.5 and $\log g$=5.0, normalized to $\log g$=4.5 are plotted in blue and red, respectively. ATLAS9 models are shown.

detail.

5.4.1 ATLAS9 models

A FORTRAN90 code was written to predict the stellar flux in several photometric bands within the spectral range from *V* Johnson to SPIRE 500 μm. The program was applied to a grid of ATLAS9 low-resolution spectra covering the interval in T_{eff} from 3500 to 8000 K, from 3.5 to 5.0 dex in $\log g$, and from -1.0 to +0.5 dex in [Fe/H].

Models usually do not contain the fluxes at the effective wavelength of the desired photometric bands, for example, there is no estimate flux at 0.55 μm (V band) or 0.79 μm (I_c). In these cases, an interpolation between the corresponding adjacent wavelengths is performed in logarithmic space.

ATLAS9 models extend up to 160 μm, i.e., PACS-160 μm flux is already computed in the last row of the model. Fluxes at SPIRE wavelengths are extrapolated from the 160 μm flux, according to the Rayleigh-Jeans tail:

$$\begin{aligned} &F_\nu \sim \lambda^{-2} \\ &\log F_\nu = \log F_\nu(160\ \mu\text{m}) + 2 \times \log\left(\tfrac{160\ \mu\text{m}}{\lambda}\right) \end{aligned} \tag{5.5}$$

Finally, for each star in the target list, an interpolation in T_{eff}, $\log g$, and [Fe/H],

was carried out in order to obtain the stellar fluxes.

5.4.2 PHOENIX models

When using PHOENIX models there are several particularities that need to be taken into account:

- Given the large quantity of points in PHOENIX models (around 52000, which varies from one model to the other, see Section 5.2), all models are rebinned to the same number of points and wavelengths
- To obtain a model with a given set of stellar parameters, an interpolation is performed in the three-dimensional space (T_{eff}, $\log g$, [Fe/H]).
- Since PHOENIX models cover up to only 50 μm, the Rayleigh-Jeans law is used to extend the models beyond this point.

5.4.3 Setting the photospheric level

Fluxes obtained directly from the models atmosphere have to be scaled to match the observed SED of a target star. To fix the photospheric level we follow a procedure similar to the one used by Bertone et al. (2004) when more than one band is used. For each photometric point, the observed flux, $F(\lambda)$, is compared to the synthetic model, $S(\lambda)$, deriving a residual function:

$$X(\lambda) = \ln F(\lambda) - \ln S(\lambda) + \alpha \tag{5.6}$$

where

$$F(\lambda) = F_0(\lambda) \times 10^{-0.4 \times m(\lambda)} \tag{5.7}$$

The fluxes at zero magnitude, for the optical (*Hipparcos* B, V, I_c) and near-IR (2MASS) photometry, are given in Table 5.4. The constant offset α is such that:

$$\sum_{i=1}^{n\ bands} X(\lambda)_i = 0 \tag{5.8}$$

so:

$$\alpha = < \ln S(\lambda) - \ln F(\lambda) > \tag{5.9}$$

Table 5.4: Effective wavelengths and fluxes at zero magnitude.

Filter	λ μm	F_ν (Jy)
B, V, I_c photometry[†]		
B	0.44	4260
V	0.55	3640
I_c	0.79	2550
2MASS photometry[‡]		
J	1.235	1594
H	1.662	1024
K_s	2.159	666.8

[†]Bessell (1979)
[‡]Cohen et al. (2003)

5.4.4 Reference photometry

To analyze how the choice of a reference flux among the available photometric bands, affects our predictions, we consider the following five normalizations:

1. Only 2MASS K_s
2. 2MASS J, H, K_s
3. I_c, and 2MASS J, H, K_s
4. B, V, I_c, and 2MASS J, H, K_s
5. B, V, I_c

Optical and near-IR photometry for the DUNES targets are compiled from *Hipparcos* (ESA 1997) and 2MASS catalogues (Cutri et al. 2003). Following the procedure described in Section 5.4.3 we predict photospheric fluxes at 70 μm for each star in our target list, using normalizations (i) to (v) and both ATLAS9 and PHOENIX models.

Figure 5.6 shows the predicted fluxes at 70 μm when normalizations (ii) to (v) are used, compared with those predicted when a normalization at only the 2MASS K_s magnitude is done.

For each normalization, the distribution Predicted Flux - Predicted Flux (normalization at K_s only) is constructed. Table 5.5 shows the median and standard deviation of each distribution. It is clear from Table 5.5 that the normalization at

Table 5.5: Statistics of *(Predicted Flux - Predicted Flux (normalization using only K_s))* when different photometric bands are used in the normalization. All values refer to the fluxes predicted at 70 μm.

ATLAS9 models						
Bands	$\overline{\Delta F}$ (mJy)	$\sigma_{\Delta F}$ (mJy)	$< 1\sigma$ %	1-2σ %	2-3σ %	$> 3\sigma$ %
JHK_s	-1.7	3.4	49	29	11	11
I_cJHK_s	-1.6	5.0	61	22	4	12
BVI_cJHK_s	-1.8	7.2	64	18	4	14
BVI_c	-1.6	11.0	53	19	7	21
PHOENIX models						
Bands	$\overline{\Delta F}$ (mJy)	$\sigma_{\Delta F}$ (mJy)	$< 1\sigma$ %	1-2σ %	2-3σ %	$> 3\sigma$ %
JHK_s	-1.6	3.4	50	28	12	10
I_cJHK_s	-1.6	5.0	60	24	6	10
BVI_cJHK_s	-1.9	7.2	60	23	3	14
BVI_c	-2.0	11.0	56	16	6	22

only K_s gives slightly larger predictions than the others, with mean differences of the order or less than 2 mJy.

Columns 4 to 7 in Table 5.5 show the percentage of stars for which the difference between using the normalization at K_s only and other normalizations is less than 1 σ, between 1 and 2σ, between 2 and 3σ, and more than 3 σ, where σ is the *Herschel* photometric error at 70 μm [9]. For roughly 55% of the stars the predicted fluxes are independent of the normalization choice (differences lower than 1 σ). For around 10-14% of the stars, differences between normalization at only 2MASS K_s and others are larger than 3 σ. When we consider the normalization to BVI_c, the percentage of stars with differences larger than 3 σ increases up to 21-22%. We note that most of these stars have 2MASS K_s quality flags "D", i.e, low quality.

5.4.5 PHOENIX vs ATLAS9 predictions

In this subsection we compare ATLAS9 and PHOENIX predictions at *Herschel*-PACS 70 μm. The normalization uses the six photometric bands B, V, I_c, J, H, K_s. A "relative difference" is computed as:

[9]Taken as 1.3 mJy, corresponding to the instrumental central area point-source 1-σ rms-noise at 70 μm, for scans of 3.0 arcmin leg length and 3 repetitions. Release note PICC-ME-TN-036.

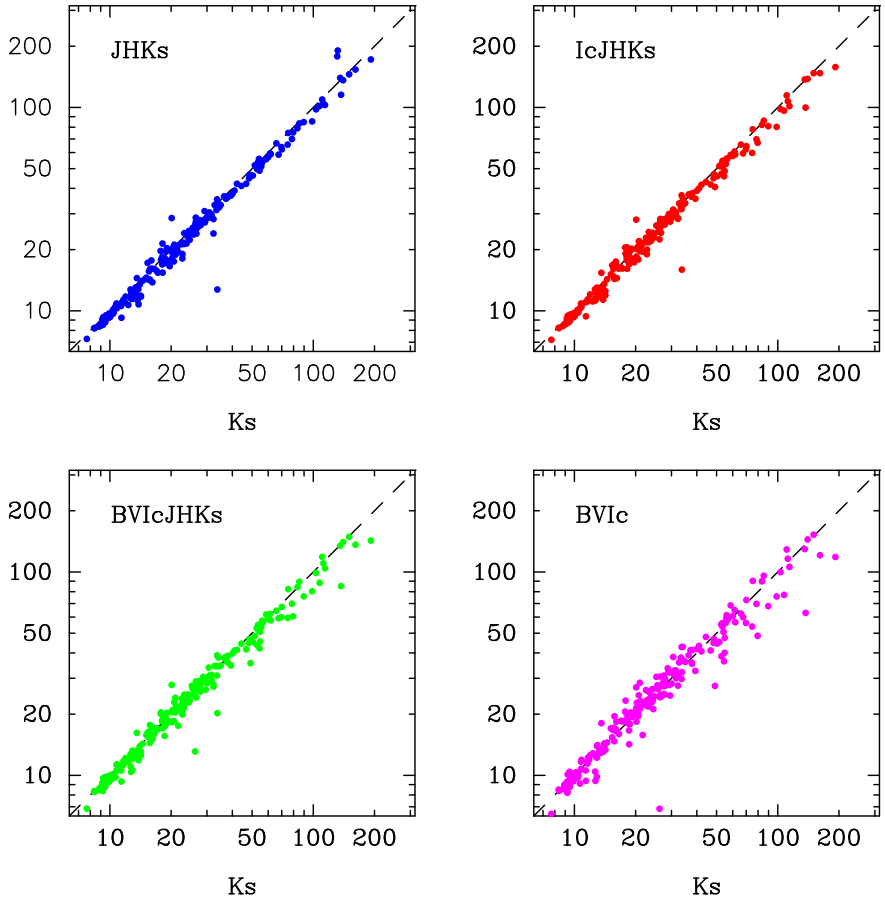

Figure 5.6: Comparison between the predicted fluxes at 70 μm (mJy) using different normalizations versus using only the 2MASS K_s band for the normalization. ATLAS9 predictions are shown.

$$100 \times \frac{\text{PHOENIX\_prediction} - \text{ATLAS9\_prediction}}{\text{ATLAS9\_prediction}} \tag{5.10}$$

Figure 5.7 illustrates the behaviour of the relative difference with the effective temperature of the stars. There is a clear dependence of the relative difference with the temperature: For stars with $T_{eff} \leq 4200$ K, ATLAS9 models run below PHOENIX (as seen in Section 5.2) and therefore PHOENIX predictions are larger than those obtained using ATLAS9 models. For stars with temperatures in the range 4200 - 6300 K, ATLAS9 models predict slightly larger fluxes (maximum difference $\sim$ -2%). There is a change in the slope of the curve around 5000 K, from which differences begin to decrease. For stars with $T_{eff} > 6300$ K, PHOENIX predictions are larger than ATLAS9, and the difference rise up to $\sim$ 2%.

The median relative difference for stars in the lower temperature regime is around 6.8%. There are four stars in this regime with differences close to 10%, these stars do not seem to follow the general tendency, if we consider them as outliers, then the median relative difference reduces to ∼ 5.4%. Independently of these four stars, relative differences in this regime (spectral-types later than ∼ K9-M0) are of the order of or larger than the 5% *Herschel* absolute flux calibration at 70 μm and can affect the interpretation of a possible excess. For the rest of targets, mainly solar-type stars, differences are within ± 2%, with a median value of only -0.7%, below the *Herschel* absolute flux calibration uncertainty. For these stars, the choice of the model atmosphere should not affect the detection (or non-detection) of a possible debris disc.

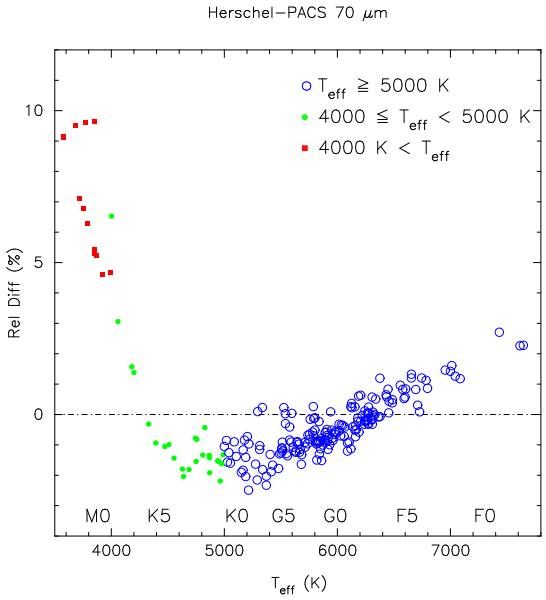

Figure 5.7: Relative difference in %, computed following Equation 5.10, between ATLAS9 and PHOENIX predictions for *Herschel*-PACS 70 μm, versus the effective temperature of the stars. Stars in different T_{eff} regimes are plotted with different colours and symbols.

5.4.6 Comparison with previous work

Table C.1 gives the predicted fluxes in mJy for the DUNES targets at PACS 70, 100, and 160 μm; and SPIRE 250, 350 and 500 μm. PHOENIX predictions are given.

We compare our predictions at 70 μm with photospheric predictions and *Spitzer*-MIPS data provided by Bryden, G. (private communication). Figure 5.8 (right

panel) illustrates this comparison. Since MIPS reference wavelength is 71.42 μm, Bryden fluxes were converted to *Herschel*-PACS 70 μm by applying Rayleigh-Jeans ($(71.42/70)^2 \approx 1.041$). The agreement is better than 2 mJy for 141 stars which represent the 61% of the whole sample. For an agreement interval better than 4 mJy then, the percentage rises up to 78% of the sample. Nevertheless, we note than, in general, Bryden fluxes are slightly larger than ours by roughly 1.5-2 mJy.

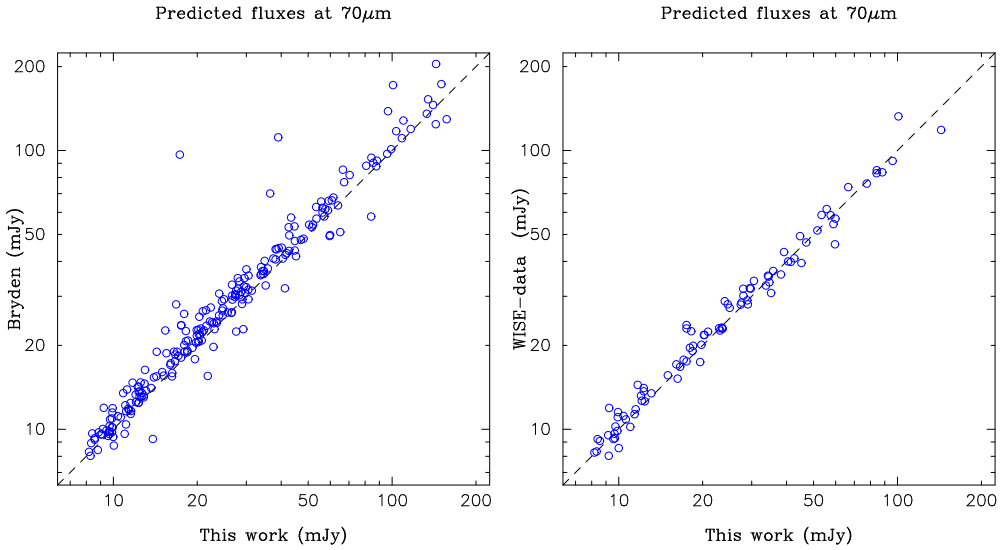

Figure 5.8: Left panel: Predicted fluxes at 70 μm provided by Bryden, G. (private communication) versus the ones obtained in this work. Right panel: Predicted fluxes at 70 μm using WISE 22 μm magnitudes versus those predictions obtained in this work.

An alternative to the use of models atmosphere is to use mid-IR photometry to predict far-IR fluxes by applying the Rayleigh-Jeans law. In order to estimate how different are predictions based on a simple extrapolation of mid-IR data from predictions based on models atmosphere, we compiled the available *WISE* (Wright et al. 2010) W4 magnitudes (λ=22.0883 μm, F^0_ν=8.363 Jy) for our targets, and used the Rayleigh-Jeans equation to predict photospheric fluxes at 70 μm. The comparison is illustrated in the right panel of Figure 5.8.

Simple Rayleigh-Jeans extrapolation predicts fluxes at 70 μm which differs from our predictions by a median residual of 0.35 mJy, although the standard deviation is high, 8 mJy. The agreement between our prediction and those based on *WISE* data is better than 2 mJy for almost 67% of the stars having W4 magnitudes. For 80% of the stars the differences are within 4 mJy. Only four stars (roughly 4%) deviate more than 3 σ.

5.4.7 Uncertainties

Under the assumption that the different sources of uncertainty are independent, we can obtain an estimate of the total uncertainty in our predictions, adding cuadratically the uncertainties due to the different error sources:

$$(\Delta F)^2 = (\Delta F \text{ models atmosphere})^2 + (\Delta F \ T_{\rm eff})^2 + (\Delta F \ \log g)^2 + (\Delta F \ [\rm Fe/H])^2 + (\Delta F \text{ photometry})^2 \quad (5.11)$$

Several comments should be made for each source of uncertainty:

- Atmosphere models: it is not easy to study "how well" models atmosphere reproduce real stars and such a study is out of the scope of this thesis. The best estimate possible is the flux variations in the predictions when using one or other family of models. Taking into account the results given in Section 5.4.5, we adopt a value of 2%. For stars with $T_{\rm eff} \leq 4000$ K, we consider a 5%.
- Stellar parameters: errors are taken from Table 5.3.
- Uncertainties in the photometry: errors in the optical and near-IR photometry used to fix the photospheric level constitute another source of uncertainty, whose contribution can be computed from the expressions given in Section 5.4.3:

$$\Delta F \text{ photometry} = \frac{0.4 F \ln 10}{N} \times \sqrt{\sum_{i=1}^{n \ bands} (\Delta m_i)^2} \quad (5.12)$$

This expression assumes that the uncertainties in the synthetic model are zero. The obtained uncertainties are given in Table C.1.

Final uncertainties spread a range between 6 and 30% with a median of 11% and a standard deviation of 5%. The coolest stars show the largest deviations.

5.5 Summary

In this chapter we have analyzed how stellar parameters, models and photometry can affect the detection of debris discs. Our conclusions can be useful for further disc-search projects, and are summarized as follows:

- ATLAS9, PHOENIX, and MARCS models are virtually identical for stars with $T_{\rm eff}$ between 5000 and 7500 K. At lower temperatures models start to show differences. At $T_{\rm eff} \leq 4000$ K, although quite different in the optical, PHOENIX and MARCS are fairly similar at mid/far-IR wavelengths.

- In the low temperature regime, differences in the stellar parameters can lead to important variations in the predicted photospheres. Effective temperatures should be known with an accuracy better than ± 200 K in order to obtain accurate predictions. $\log g$ and [Fe/H] have a smaller impact, although small variations can alter the predictions in percentages higher than 5% (equal to the *Herschel* absolute flux calibration at 70 and 100 μm).

- Relative differences between predicted fluxes using ATLAS9 and PHOENIX depend on T_{eff}. For stars with $T_{eff} > 4000$ K, differences are within 2% and the choice of one or other model atmosphere do not affect the detection of a possible debris disc. For stars cooler than K9-M0, PHOENIX predicts larger photospheric fluxes than ATLAS9. Mean differences are of the order of 5.4%, and can affect the interpretation of a possible excess.

- For stars with $T_{eff} > 4500$ K (spectral types hotter than K4) the combined effect of stellar parameters and the choice of the model atmosphere lead to uncertainties in the predictions around 2.1%. When considering stars in the range 4000 K < T_{eff}, 4500 K uncertainties are about 10.15%, which rise up to 11.1% for stars with T_{eff} lower than 4000 K (spectral types cooler than K9-M0).

- Errors in the photometry used to fix the photospheric level constitute another source of uncertainty which dominates the overall uncertainty in the predictions.

As an application, we computed the expected fluxes at *Herschel* wavelengths for those stars which are being observe in the framework of the DUNES project. The methodology used here played a central role to estimate exposure times and to optimize the total observing time granted for DUNES.

6

General conclusions and prospects for future work

In this chapter, the most relevant conclusions derived in this thesis are summarized. Some of them have already been given in Sections 3.6, 4.5 and 5.5.

6.1 General conclusions

- High-resolution échelle spectra were obtained for more than 500 nearby solar-type stars. This unique set of data has allowed the determination of accurate radial velocities, lithium abundances, effective temperatures, gravities and metallicities among other parameters. All the spectra are reduced and can be of utility for a wide range of astronomers in many kind of studies. It is our intention to make them public and available to the community following the Virtual Observatory standards.

- A systematic search for stars in kinematic groups were performed by a detailed analysis of the kinematics of the stars. Around 25% of the stars are located in the same region of the velocity-space diagram which is occupied by kinematic groups. Only 40% of these stars share a similar age, in agreement with the corresponding kinematic group (~10% of the total sample). The numbers of probable members of each kinematic group studied here are: 14 out of 29 for the Local Association; 11 out of 29 for the Hyades; 6 out of 18 for the Ursa Major moving group; 6 out of 19 for the IC 2391 moving group; and 4 out of 7 for the Castor moving group. This result confirms that not all stars sharing a similar kinematics, do also share a common age, and therefore a dynamical (resonant) mechanism is needed to explain the origin of kinematic streams.

- Most stars in the solar neighbourhood are old, only $\sim$ 22% of the stars are younger than 300 Myr, according to their *ROSAT* and rotational ages. A

slightly lower percentage, $\sim$ 15% is obtained when using chromospheric indices or lithium abundances.

- Stars with debris discs are more related to stellar kinematic groups than stars without debris disc: $\sim$ 27% of the stars with debris discs share both a similar kinematics and age. In general, stars with planets do not seem to be related to kinematic groups.

- Spectroscopic values of $T_{\rm eff}$, $\log g$, microturbulent velocity ($\xi_{\rm t}$), and [Fe/H] were obtained in an homogeneous and consistent way for a sample of 119 stars. The metallicity distribution of these stars was studied according to the presence or absence of debris discs and planets.

- The analysis of the metallicity distribution of the different samples studied in this work shows a smooth transition towards higher metallicities, from stars with neither debris discs nor planets to the stars hosting gaseous hot-Jupiters.

- Stars with and without debris discs show similar metallicity distributions, although that of the former seems to be slightly shifted towards higher metallicity values. In addition, it seems to be a "deficit" of stars with debris discs below -0.1 dex.

- Stars harbouring both debris discs and planets have a metallicity distribution which behaves in the same way as the distribution of those stars hosting giant planets.

- Previous statements show that it is the presence of the planets, and not the debris discs, which correlates with the stellar metallicities. These results can be explained in the framework of core-accretion models.

- Stars with known debris discs and planets show a high rate of multiplanet systems (38%) and a significant rate of low-mass planets (24%).

- Giant planets around stars with debris discs are usually cool (a > 0.1 AU), even $\sim$ 65% have orbits whose semimajor axis is larger than 0.5 AU. The data suggest that stars with known debris discs and cool giant planets tend to have low values of the fractional dust luminosity ($10^{-5} < L_{\rm dust}/L_{\star} < 10^{-4}$) and higher metallicities when comparing with other stars hosting only debris discs. This trend is not seen in stars with debris discs and low-mass planets.

- An anticorrelation between the fractional dust luminosity, $L_{dust}/L_{\star}$, and the eccentricity of the innermost planet is suggested. Such a trend could be explained by dynamical instabilities produced by eccentric giant planets. No relation was found between the dust luminosity and other planet properties (period or semimajor axis).

- Uncertainties in the stellar parameters have a small impact in the prediction of stellar photospheres at far-IR wavelengths, unless we consider stars with temperatures of the order of 4000 K and lower. In these cases, errors in T_{eff} of ± 200 K can lead to differences in the predicted photospheric fluxes up to 13%, errors in $\log g$ and [Fe/H] can vary the fluxes around 5%. For these stars also the choice of the model atmosphere is crucial, since PHOENIX models predict fluxes between 5% and 10% larger than ATLAS9 models. For solar-like stars, differences in the predictions due to the use of ATLAS9 or PHOENIX models are within 2%.

- Photospheric fluxes at *Herschel* wavelengths were predicted for a sample of 239 AFGKM stars which are being observed in the framework of the DUNES OTKP, playing a major role in fixing the exposure times and optimizing the total time granted for the project.

6.2 Future work

The natural extension of the present work consists in the determination of accurate chemical individual abundances of different elements.

In particular, abundance patterns in stars with debris discs and low-mass planets constitute a case of remarkable astrophysical interest. It has been recently suggested that terrestrial planet formation could let a fingerprint in the spectra of the host star in the form of a "deficit" of refractory elements relative to volatiles (Meléndez et al. 2009; Ramírez et al. 2009, 2010). An hypothesis which has, however, been disputed by González Hernández et al. (2010). The solar-type stars with known debris discs and planets listed in this thesis are excellent benchmark targets to test whether solar-type stars show or not any chemical anomaly, and if such anomaly is related to low-mass planet formation. The key aspect of this investigation consists in determining differences in abundances as low as ~ 0.08 dex, i.e, of the same order of the uncertainties in the abundances of the individual elements. Such an accuracy is difficult to obtain and several changes with respect to the analysis presented in this thesis are required: strictly differential analysis, account for non-LTE effects, and spectral synthesis for some elements like Zr or Nd whose lines are blended with other features. To overcome this project, further observations were carried out last year in two observing runs at the MERCATOR

telescope using the HERMES spectrograph, $\lambda/\Delta\lambda \approx 85000$, $\lambda\lambda \sim 3700$-9000 Å (Raskin et al. 2011). The observations include additional solar-type stars with debris discs, stars with debris discs and giant-planets, and stars with debris discs and low-mass planets.

The chemical composition of evolved stars hosting planets is another open question that requires further investigation in order to clarify the origin of the planet-metallicity correlation (e.g. Hekker & Meléndez 2007; Pasquini et al. 2007; Ghezzi et al. 2010a). To address this problem, 77 evolved stars (giant and subgiants) with planets, and other 87 control stars without planets were observed at the MERCATOR and NOT telescopes in several observing runs between February and August 2011. Again, the analysis should be more detailed than the one presented in this work since for evolved stars both non-LTE corrections and sphericity effects could be significant.

7

Conclusiones de la tesis y proyectos de trabajo futuro.

En este capítulo se resumen las conclusiones más relevantes que se derivan de esta tesis. Algunas de ellas han sido ya expuestas en las Secciones 3.6, 4.5 y 5.5.

7.1 Conclusiones generales

- Durante el desarrollo de esta tesis se han obtenido espectros ópticos de alta resolución para más de 500 estrellas cercanas de tipo solar. Esta colección única de datos ha permitido la determinación de velocidades radiales, abundancias de litio, temperaturas efectivas, gravedades y metalicidades, entre otros parámetros. Todos los espectros se encuentran reducidos y pueden resultar de gran interés para un amplio rango de astronónomos en numerosos campos de estudio. Es nuestra intención que los espectros estén públicamente disponibles para su uso siguiendo los formatos estándares del Observatorio Virtual.

- Se ha llevado a cabo una búsqueda sistemática de posibles miembros de grupos cinemáticos estudiando en profundidad la cinemática de las estrellas. Aproximadamente un 25% de las estrellas se sitúan en la misma región del espacio de velocidades en la que se agrupan los grupos cinemáticos. No obstante sólo un 40% de éstas estrellas muestran una edad similar, en concordancia con el correspondiente grupo cinemático ($\sim$ 10% de la muestra total). El número de probables miembros para cada grupo cinemático que ha sido objeto de estudio es: 14 de 29 candidatos en la Asociación Local; 11 de 29 en las Híades; 6 de 18 en el grupo de Ursa Major; 6 de 19 en el grupo de movimiento IC 2391; y 4 de 7 en el grupo de movimiento de Castor. Este resultado confirma que no todas las estrellas que muestran una cinemática similar son coétaneas, por tanto, mecanismos de carácter

dinámico (resonancias) son necesarios para poder explicar el origen de los grupos cinemáticas estelares.

- La mayor parte de las estrellas en la vecindad solar son de avanzada edad, solamente un $\sim$ 22% presentan edades inferiores a los 300 millones de años de acuerdo con las edades inferidas por sus emisiones en rayos-X cuantificadas por el satélite *ROSAT* o a partir de sus períodos rotacionales. El porcentaje es ligeramente inferior, 15% cuando se utilizan índices de actividad cromosférica o la presencia de litio como indicadores de edad.

- Existe una mayor relación entre los grupos cinemáticos y las estrellas con discos circunestelares de tipo debris, que con las las estrellas sin discos: $\sim$ 27% de las estrellas con discos debris muestran una cinemática y edad común a algún grupo cinemático. En general, las estrellas que albergan planetas no parecen estar relacionadas con grupos cinemáticos.

- Se ha utilizado un procedimiento homogéneo y consistente para obtener valores espectroscópicos de $T_{\rm eff}$, $\log g$, velocidades de microturbulencia ($\xi_{\rm t}$) y metalicidad para 119 estrellas. La distribución de metalicidad de éstas estrellas ha sido estudiada en detalle teniendo en cuenta la presencia/ausencia de discos debris y/o planetas.

- El análisis de la distribución de metalicidad de las distintas muestras estelares estudiadas en este trabajo muestra una suave transición hacia metalicidades más altas, comenzando desde las estrellas sin discos ni planetas conocidos hacia las estrellas que albergan planetas gaseosos de tipo Júpiter caliente.

- Las estrellas con discos de tipo debris presentan una distribución en su metalicidad similar a la de las estrellas que no albergan este tipo de discos, aunque la distribución de las primeras está ligeramente desplazada hacia metalicidades más altas. Además, parece existir un “déficit” de estrellas con disco con metalicidades por debajo de aproximadamente -0.1 dex.

- Las estrellas que albergan simúltanemanete discos debris y planetas tienen una distribución de metalicidad similar a la de las estrellas que únicamente albergan planetas gigantes.

- Los postulados anteriores muestran que es la presencia de planetas, y no de debris, el factor que correlaciona con la metalicidad estelar. Estos resultados pueden explicarse dentro de los modelos de formación de planetas mediante mecanismos de acrección.

- Las estrellas que albergan simúltanemanete discos debris y planetas se caracterizan por una alta frecuencia de sistemas múltiples (38%) así como por una elevada fracción de planetas de baja masa (24%).

- Los planetas gigantes alrededor de estrellas con discos de tipo debris son típicamente fríos (a > 0.1 UA), incluso ∼ 65% de ellos tienen semiejes mayores más grandes que 0.5 UA. Los datos sugieren que las estrellas con debris y planetas gigantes fríos tiene valores especialmente bajos de la luminosidad del polvo ($10^{-5} < L_{polvo}/L_{\star} < 10^{-4}$) así como metalicidades mayores cuando se comparan con las estrellas que sólo presentan discos debris. Este comportamiento no se encuentra en las estrellas con discos de tipo debris y planetas de baja masa.

- Parece existir una anticorrelación entre la luminosidad fraccional del polvo, $L_{polvo}/L_{\star}$, y la excentricidad del planeta más cercano a la estrella. Este comportamiento podría deberse a inestabilidades de tipo dinámico producido por planetas gigantes en órbitas excéntricas. No se han encontrado relaciones entre la luminosidad del polvo y el período o semieje mayor del planeta.

- Los errores en los parámetros estelares poseen una pequeña influencia a la hora de predecir las fotosferas estelares en las longitudes de onda correspondientes al infrarrojo lejano, salvo que estemos considerando estrellas con temperaturas de 4000 K e inferiores. En dicho caso, errores en T_{eff} de ± 200 K pueden conducir a diferencias en los flujos fotosféricos predichos de hasta un 13%, mientras que errores en $\log g$ y [Fe/H] pueden variar los flujos en un 5%. Para éstas estrellas la elección del modelo de atmósfera también resulta crucial, dado que los modelos PHOENIX predicen flujos fotosféricos entre un 5 y un 10% mayores que los obtenidos usando modelos ATLAS9. Para estrellas de tipo solar, las diferencias en los flujos predichos usando modelos ATLAS9 y usando modelos PHOENIX se sitúa dentro del 2%.

- Se han obtenido flujos fotosféricos en las longitudes de onda de *Herschel* para una muestra de 239 estrellas con tipos espectrales A, F, G, K y M, que están siendo observadas dentro del proyecto clave de tiempo abierto DUNES. Dichas predicciones desempeñaron un papel importante a la hora de estimar los tiempos de exposición de los objetos, optimizando así el total de tiempo concedido para el proyecto.

7.2 Trabajo futuro

La extensión natural del trabajo presentado consiste en la determinación de las abundancias químicas de diferentes elementos de manera individual.

En particular, las abundancias en estrellas con discos de tipo debris y planetas de baja masa constituyen un caso científico de gran intéres. Recientemente, ha sido sugerido que la formación de planetas terrestres puede dejar una "huella" en el espectro de las estrellas en forma de una "deficiencia" de elementos refractarios con respecto de los volátiles (Meléndez et al. 2009; Ramírez et al. 2009, 2010), hipótesis que, sin embargo, ha sido puesta en cuestión por González Hernández et al. (2010). Las estrellas de tipo solar con discos de tipo debris y planetas de baja masa presentadas en esta tesis constituyen excelentes objetos en los que comprobar si las estrellas de tipo solar muestran o no una composición química anómala, y si dicha anomalía esta relacionada con la formación de planetas de baja masa. El aspecto clave en una investigación de este tipo consiste en determinar diferencias en abundancias tan bajas como $\sim$ 0.08 dex, esto es, del mismo orden que las incertidumbres en las abundancias individuales de los distintos elementos. Tal precisión es complicada de obtener y algunos cambios con respectos al análisis presentado en esta tesis pueden ser necesarios: análisis estrictamente diferencial, desviaciones con respecto al equilibrio termodinámico local y síntesis espectral para algunos elementos como el Zr o el Nd cuyas líneas espectrales se encuentran mezcladas con las de otros elementos. Para llevar a cabo tal investigación, se llevaron a cabo observaciones adicionales a lo largo del pasado año en dos campañas de observación en el telescopio MERCATOR usando el espectrógrafo HERMES, $\lambda/\Delta\lambda \approx 85000$, $\lambda\lambda \sim$ 3700-9000 Å (Raskin et al. 2011). Las observaciones incluyeron estrellas de tipo solar con discos debris, estrellas con discos debris y planetas gaseosos así como estrellas con discos debris y planetas de baja masa.

Otra cuestión abierta que requiere un estudio más detallado es la composición química de estrellas evolucionadas con planetas (e.g. Hekker & Meléndez 2007; Pasquini et al. 2007; Ghezzi et al. 2010a). Aclarar este aspecto es de vital importancia para entender el origen de la correlación planeta-metalicidad. En este caso, se observaron 77 estrellas gigantes y sub-gigantes con planetas y otras 87 estrellas de control sin planetas en los telescopios MERCATOR y NOT en varias campañas de observación entre febrero y agosto de 2011. De nuevo, el análisis de estos datos requiere de un detalle mayor ya que en estrellas evolucionadas tanto las desviaciones con respecto al equilibrio termodinámico local, así como los efectos de esfericidad pueden ser importantes.

A

Tables of Chapter 3

Results produced in Chapter 3 are published in electronic format only. Table A.1 is also available at the CDS via anonymous ftp to cdsarc.u-strasbg.fr (130.79.128.5) or via `http://cdsweb.u-strasbg.fr/cgi-bin/qcat?J/A+A/521/A12`

Table A.1 contains the following information: HIP number (column 1), right ascension and declination (ICRSJ2000) (columns 2 and 3), parallax and its uncertainty (column 4), proper motions in right ascension and declination with their uncertainties (columns 5 and 6), radial velocity used in this work and its uncertainty (column 7), and radial velocities reported in KH07, NO04, NI02, and VF05 works (columns 8 to 11) with their uncertainties, if available. Column 12 contains important notes: spectroscopic binaries ("Sb" label) radial velocities standards ("RV" label), and stars in chromospherically active binary systems ("Cab" label) are identified in this column. [1]

Tables A.2 to A.6 contain the properties of the potential candidates to MG members for the different MGs studied in this work. These tables give: HIP number (column 1), (B-V) colour (column 2), spatial-velocity components (U, V, W) with their uncertainties (columns 3, 4 and 5), $V_{\rm Total}$, V_T, PV and ρ_c as defined by Eggen (columns 6, 7, 8 and 9), measured Li I EW (column 10), $R'_{\rm H,K}$ value and derived age (columns 11 and 12), $log(L_{\rm X}/L_{\rm Bol})$ and derived age (columns 13 and 14), rotational period and derived age (columns 15 and 16) and metallicity (column 17). For each Eggen's criteria, PV and ρ_c (columns 8 and 9), there is label indicating if the star satisfies the criteria (label 'Y') or not (label 'N').

Tables A.7 and A.8 are similar to the previous ones, but they show the properties of the stars classified as *Other young disc stars* and stars not selected as possible MG members, respectively.

[1] The published table contains two extra-columns: the HD number, and the observing runs in which the star was observed. These columns were excluded here due to clarity reasons.

References in Tables A.2 to A.8 are indicated in parenthesis: (1) Martínez-Arnáiz et al. (2010) (2) Baliunas et al. (1996); (3) Duncan et al. (1991) calculated using equations in Noyes et al. (1984); (4) Gray et al. (2003); (5) Gray et al. (2006); (6) Hall et al. (2007); (7) Henry et al. (1996); (8) Jenkins et al. (2006); (9) Saffe et al. (2005); (10) Wright et al. (2004); (11) estimated form ROSAT-data using equation A1 in Mamajek & Hillenbrand (2008); (12) Noyes et al. (1984); (13) Saar & Osten (1997); (14) Messina et al. (2001).

Table A.1: Kinematic data and radial velocities for the observed stars

						Radial Velocity					
HIP	α (h,m,s)	δ (^{o},',")	π (mas)	$\mu_\alpha \times \cos\delta$ (mas/yr)	μ_δ (mas/yr)	*Thiswork* (km/s)	*KH*07 (km/s)	*NO*04 (km/s)	*NI*02 (km/s)	*VF*05 (km/s)	Notes
(1)	(2)	(3)	(4)	(5)	(6)	(7)	(8)	(9)	(10)	(11)	(12)
171	00 02 10.1552	+27 04 56.122	82.18 ± 2.23	829.90 ± 1.20	-989.40 ± 1.10	-37.90	-36.90 ± 5.24	-36.90 ± 0.40			Sb
544	00 06 36.7839	+29 01 17.406	73.16 ± 0.56	380.50 ± 0.90	-177.90 ± 0.90	-6.66 ± 0.07 -6.69 ± 0.04	-6.90 ± 0.22	-6.90 ± 0.10	-6.54	-5.8	
910	00 11 15.8573	-15 28 04.719	53.33 ± 0.64	-82.50 ± 0.90	-270.90 ± 1.00	16.70 ± 0.08	14.90 ± 0.71	14.90 ± 0.10			
1499*	00 18 41.8677	-08 03 10.805	43.02 ± 0.51	419.00 ± 1.00	-145.10 ± 0.90	-10.13 ± 0.10	-10.49 ± 0.43	-10.50 ± 0.10	-10.17	-9.9	
1532	00 19 05.5619	-09 57 53.474	47.43 ± 1.65	-36.50 ± 1.60	-305.30 ± 1.80	-10.88 ± 0.23	-11.10 ± 0.30				
1598	00 20 00.4085	+38 13 38.629	40.32 ± 0.59	-141.80 ± 1.00	-276.70 ± 1.10	15.27 ± 0.70	15.08 ± 2.62	15.10 ± 0.20			
1599	00 20 04.2601	-64 52 29.246	116.46 ± 0.16	1708.40 ± 0.80	1164.80 ± 0.80	10.47 ± 0.07	9.09 ± 0.36	9.10 ± 0.10		8.8	
1692‡	00 21 13.3193	-08 16 52.209	3.23 ± 1.43	12.90 ± 1.10	1.70 ± 1.20	18.22 ± 0.45					Giant
1803	00 22 51.7883	-12 12 33.977	47.93 ± 0.53	393.90 ± 1.10	61.00 ± 1.00	-2.71 ± 0.09	-2.72 ± 0.29	-2.70 ± 0.10	-2.41	-3.1	
2941	00 37 20.7007	-24 46 02.162	64.89 ± 1.84	1391.00 ± 2.30	-13.00 ± 2.30	18.44	18.47 ± 0.25	18.50 ± 0.20			Sb, Cab
3093*	00 39 21.8061	+21 15 01.701	90.43 ± 0.32	-460.60 ± 0.80	-369.80 ± 0.70	-32.96 ± 0.80	-33.42 ± 0.16	-33.50 ± 0.10	-32.96	-33.3	RV
3206	00 40 49.2696	+40 11 13.824	57.74 ± 0.80	357.60 ± 1.00	-668.60 ± 1.10	-63.62 ± 0.21	-63.87 ± 0.53	-63.90 ± 0.10	-63.20	-62.8	
3418	00 43 32.8596	+33 50 40.441	48.60 ± 0.92	-204.40 ± 1.00	-358.80 ± 1.00	-36.19 ± 0.19	-35.00 ± 1.00				
3535	00 45 04.8943	+01 47 07.876	46.37 ± 0.62	-47.80 ± 1.00	-571.90 ± 1.00	9.24 ± 0.80	7.80 ± 0.90		9.46	9.9	
3765	00 48 22.9772	+05 16 50.214	134.13 ± 0.51	757.30 ± 2.90	-1135.40 ± 2.80	-10.10 ± 0.40	-10.78 ± 0.63	-10.80 ± 0.10	-10.23	-9.6	RV
3810	00 48 58.7083	+16 56 26.318	42.64 ± 0.27	-1.90 ± 0.80	-200.60 ± 0.80	4.10	3.63 ± 1.84	3.10 ± 1.90			Sb
3821	00 49 06.2912	+57 48 54.674	168.01 ± 0.48	1086.60 ± 0.40	-559.42 ± 0.33		8.21 ± 0.71	8.20 ± 0.10	8.31	9.0	Sb
3979	00 51 10.8481	-05 02 21.402	46.46 ± 0.66	263.60 ± 1.20	-118.90 ± 1.20	-4.38 ± 0.17	-3.90 ± 0.10	-3.90 ± 0.10	-3.74	-2.9	
3998	00 51 21.7545	+18 44 21.306	46.78 ± 1.59	52.10 ± 1.10	-266.80 ± 1.10	6.16 ± 0.19	6.80 ± 1.30				
4148	00 53 01.1351	-30 21 24.895	70.57 ± 0.60	622.20 ± 1.20	31.80 ± 1.20	-6.37 ± 0.06	-13.28 ± 2.62	-13.30 ± 0.20	-13.07	-12.3	
4845	01 02 21.1317	-10 25 25.909	49.06 ± 1.88	27.00 ± 1.40	-176.20 ± 1.50	9.14 ± 0.18	-20.00				
5286	01 07 37.8719	+22 57 17.914	47.52 ± 0.94	101.70 ± 1.00	-491.60 ± 0.90	6.88 ± 0.90	4.80 ± 1.10				
5336	01 08 16.3942	+54 55 13.221	132.40 ± 0.82	3412.30 ± 6.60	-1600.10 ± 6.50	-98.00	-98.30 ± 7.59	-98.30 ± 0.20			Sb
5799	01 14 24.0398	-07 55 22.173	42.75 ± 0.30	124.60 ± 0.70	278.70 ± 0.80	22.08 ± 0.14	22.03 ± 0.43	22.00 ± 0.10			
5944	01 16 29.2530	+42 56 21.911	43.11 ± 0.45	-112.00 ± 1.10	-29.50 ± 1.10	-13.04 ± 0.11	-13.30 ± 0.20	-13.30 ± 0.20	-13.07	-12.6	
5957	01 16 39.3579	+25 19 53.309	42.31 ± 1.76	431.10 ± 1.50	-100.60 ± 1.50	-23.88 ± 0.22	-30.00				
6290	01 20 40.7457	+57 19 40.479	49.78 ± 2.10	-290.50 ± 3.40	435.80 ± 3.40	13.91 ± 0.15	22.00				
6917	01 29 04.8961	+21 43 23.397	42.14 ± 0.68	456.60 ± 0.80	-185.00 ± 0.80	21.83	21.70 ± 0.72	21.70 ± 0.20			Sb,Cab
7235	01 33 15.8087	-24 10 40.662	52.50 ± 0.46	272.70 ± 1.40	-159.40 ± 1.40	2.24 ± 0.07	2.20 ± 1.14	2.20 ± 0.20		5.4	
7339	01 34 33.2635	+68 56 53.293	48.41 ± 0.40	-376.80 ± 1.20	114.60 ± 1.30	-33.47 ± 0.05	-31.50 ± 0.80		-33.29	-33.0	
7513*	01 36 47.8428	+41 24 19.652	74.14 ± 0.19	-173.33 ± 0.20	-381.79 ± 0.13	-28.62 ± 0.03	-28.89 ± 0.71	-28.90 ± 0.10	-28.67	-28.4	
7576	01 37 35.4661	-06 45 37.525	41.74 ± 0.75	171.90 ± 1.40	-97.70 ± 1.40	11.67 ± 0.10	11.10 ± 0.10	11.10 ± 0.10			
7751	01 39 47.5430	-56 11 47.041	127.99 ± 2.29	302.60 ± 1.40	-14.10 ± 1.30	24.25 ± 0.06	21.35 ± 0.54	21.50 ± 0.20		19.9	
7918	01 41 47.1429	+42 36 48.128	78.52 ± 0.54	806.60 ± 1.00	-152.20 ± 1.00	3.12 ± 0.13	3.35 ± 0.30	3.00 ± 0.30			Sb
7981	01 42 29.7619	+20 16 06.616	132.76 ± 0.50	-300.60 ± 1.00	-673.70 ± 0.90	-33.90 ± 0.90	-34.12 ± 0.16	-34.20 ± 0.10	-33.65	-34.1	RV
8102	01 44 04.0829	-15 56 14.928	273.96 ± 0.17	-1721.05 ± 0.17	854.16 ± 0.15	-16.56 ± 0.04	-16.96 ± 0.16	-17.10 ± 0.10	-16.62	-16.7	
8275	01 46 38.7185	+12 24 42.378	41.63 ± 1.22	31.20 ± 1.20	-73.00 ± 1.10	21.62 ± 0.10	20.70 ± 0.80				
8362	01 47 44.8347	+63 51 09.004	99.34 ± 0.53	582.60 ± 1.00	-246.10 ± 1.10	2.73 ± 0.02	2.64 ± 0.22	2.50 ± 0.10	2.76	3.1	
8486	01 49 23.3569	-10 42 12.816	44.33 ± 3.02	-150.00 ± 0.90	-91.10 ± 0.90	-4.57 ± 0.07 -3.50 ± 0.08	-4.88 ± 1.28	-5.00 ± 0.40			
8768	01 52 49.1717	-22 26 05.484	90.86 ± 1.16	845.30 ± 1.80	0.40 ± 1.80	12.66 ± 0.24 12.67 ± 0.23	17.00 ± 1.70				
9269	01 59 06.6329	+33 12 34.849	40.06 ± 0.58	243.80 ± 1.00	-352.40 ± 1.10	-35.35 ± 0.06 -34.98 ± 0.07	-36.10 ± 1.50		-35.10	-34.7	

It follows in the next page

Table A.1 It cames from the previous page

						Radial Velocity					
HIP	α	δ	π	$\mu_\alpha \times \cos\delta$	μ_δ	*Thiswork*	*KH*07	*NO*04	*NI*02	*VF*05	Notes
	(h,m,s)	(^{o},',")	(mas)	(mas/yr)	(mas/yr)	(km/s)	(km/s)	(km/s)	(km/s)	(km/s)	
(1)	(2)	(3)	(4)	(5)	(6)	(7)	(8)	(9)	(10)	(11)	(12)
						-35.26 ± 0.05					
9829	02 06 30.2437	+24 20 02.375	43.89 ± 0.57	6.70 ± 1.00	-147.80 ± 1.00	-4.77 ± 0.60	-5.10 ± 0.20	-5.10 ± 0.20	-4.66	-4.3	
10138*	02 10 25.9342	-50 49 25.408	92.75 ± 0.32	2150.30 ± 2.50	673.20 ± 2.40	58.98 ± 0.07	56.60 ± 1.27	56.70 ± 0.30		57.0	
10337	02 13 12.1658	-21 11 47.235	44.87 ± 1.60	377.90 ± 2.00	55.00 ± 1.80	3.29 ± 0.15	3.20 ± 1.10				
10416	02 14 13.5703	-03 38 06.733	44.02 ± 1.02	-12.90 ± 1.00	-218.00 ± 1.30	-8.47 ± 0.06					
10644	02 17 03.2301	+34 13 27.232	92.74 ± 0.39	1153.80 ± 0.80	-245.10 ± 0.80	-5.90	-7.66 ± 0.72	-7.70 ± 0.20			Sb
10798	02 18 58.5045	-25 56 44.474	78.94 ± 0.35	-217.70 ± 0.90	445.20 ± 0.90	7.33 ± 0.03	7.19 ± 0.54	7.20 ± 0.20	7.38	5.2	
11072	02 22 32.5468	-23 48 58.774	45.52 ± 0.82	196.61 ± 0.81	-4.99 ± 0.58	12.62 ± 0.07	17.24 ± 2.05	15.30 ± 2.30	18.82		
11452	02 27 45.8620	+04 25 55.749	58.31 ± 1.07	86.73 ± 1.35	239.82 ± 0.95	5.28 ± 0.23	5.70 ± 0.30				
11565	02 29 01.6922	-19 58 44.994	51.15 ± 1.33	613.99 ± 1.01	189.11 ± 1.06	26.68 ± 0.08	26.10 ± 3.70				
12110	02 36 00.7765	-23 31 16.775	47.00 ± 0.94	87.10 ± 1.70	15.00 ± 1.40	16.65 ± 0.08					
12114	02 36 04.8937	+06 53 12.733	139.27 ± 0.45	1807.81 ± 0.89	1444.00 ± 0.40	25.79 ± 0.06	25.70 ± 0.10	25.10 ± 0.10	25.77	26.8	
						25.93 ± 0.06					
12709	02 43 20.9201	+19 25 45.279	52.95 ± 1.03	429.00 ± 1.10	-12.10 ± 1.10	32.20	32.20				Sb
12777	02 44 11.9863	+49 13 42.412	89.88 ± 0.23	334.66 ± 0.17	-89.99 ± 0.17	24.18 ± 0.04	24.35 ± 0.29	24.30 ± 0.10	24.45	23.7	
12843	02 45 06.1851	-18 34 21.225	70.31 ± 1.83	331.40 ± 1.00	34.50 ± 1.00		16.96 ± 0.91	25.90 ± 0.80			Sb
12929	02 46 17.2777	+11 46 30.864	62.46 ± 1.38	265.20 ± 1.20	-209.50 ± 1.20	10.97 ± 0.12	10.40 ± 3.00		11.06		
13081	02 48 09.1429	+27 04 07.075	40.58 ± 1.28	274.50 ± 1.10	-122.60 ± 1.10	9.34 ± 0.21	6.90 ± 0.90				Sb
13258	02 50 36.8923	+15 42 35.691	43.98 ± 0.91	343.50 ± 1.00	-395.50 ± 1.00	-28.90 ± 0.11	-25.00		-28.90		
13402	02 52 32.1287	-12 46 10.972	96.61 ± 0.40	397.30 ± 1.20	-189.90 ± 1.30	17.83 ± 0.07	17.61 ± 0.22	17.50 ± 0.10	18.07	16.4	Cab
						18.24 ± 0.05					
13642	02 55 39.0575	+26 52 23.580	42.52 ± 0.84	274.00 ± 1.70	-185.40 ± 1.60	31.88 ± 0.08	31.80		31.95	32.5	
13976	03 00 02.8130	+07 44 59.106	41.00 ± 1.12	330.60 ± 1.50	19.30 ± 1.50	28.78 ± 0.08	28.70 ± 0.20		28.83	29.3	
14150	03 02 26.0271	+26 36 33.263	48.46 ± 0.47	232.80 ± 1.00	-167.90 ± 1.00	9.58 ± 0.06	9.50 ± 1.91	9.50 ± 0.10	9.88	10.3	
14286	03 04 09.6364	+61 42 20.989	41.27 ± 0.58	722.00 ± 1.10	-693.70 ± 1.30	-5.63 ± 0.90	-2.22 ± 1.14	-2.20 ± 0.20			
14632	03 09 04.0197	+49 36 47.799	94.87 ± 0.23	1262.60 ± 0.80	-91.50 ± 0.80	49.63 ± 0.05	49.40 ± 0.43	49.40 ± 0.10	49.45	48.8	
14879	03 12 04.5277	-28 59 15.425	70.24 ± 0.45	370.88 ± 0.30	611.30 ± 0.42	-16.94 ± 0.05	-19.39 ± 0.60	-19.40 ± 0.60			
15099	03 14 47.2272	+08 58 50.851	44.13 ± 0.83	400.90 ± 1.30	-402.90 ± 1.30	-16.85 ± 0.70	-17.49 ± 0.92	-17.40 ± 0.20	-16.68	-16.5	
15330	03 17 46.1635	-62 34 31.159	83.29 ± 0.20	1338.40 ± 1.10	650.30 ± 1.10		12.10 ± 0.53	12.10 ± 0.10		12.3	
15371	03 18 12.8189	-62 30 22.907	83.11 ± 0.19	1330.74 ± 0.21	647.09 ± 0.19	12.16 ± 0.01	11.59 ± 0.54	11.60 ± 0.20		11.6	
15442‡	03 19 01.8932	-02 50 35.501	39.64 ± 0.74	254.70 ± 1.10	-101.50 ± 1.10	23.54 ± 0.07	22.49 ± 1.25	22.50 ± 0.10	22.69	23.1	
15457	03 19 21.6960	+03 22 12.712	109.39 ± 0.27	269.70 ± 0.60	93.60 ± 0.60	18.00 ± 1.00	18.76 ± 0.16	18.70 ± 0.10	19.02	17.8	
15510	03 19 55.6505	-43 04 11.221	165.48 ± 0.19	3038.20 ± 0.70	728.30 ± 0.70	93.63 ± 0.06	87.19 ± 0.49	87.20 ± 0.10		87.4	
15673	03 21 54.7559	+52 19 53.453	42.81 ± 1.03	-312.00 ± 1.20	-264.60 ± 1.20	-40.05 ± 0.08					
15919	03 24 59.7309	-05 21 49.520	64.95 ± 0.71	-229.28 ± 0.84	-769.03 ± 0.58	-13.21 ± 0.80	-13.68 ± 0.49	-13.70 ± 0.10	-13.11		
16134	03 27 52.4061	-19 48 16.137	80.06 ± 0.98	535.00 ± 1.40	304.10 ± 1.50	34.62 ± 0.17	33.91 ± 0.82	33.80 ± 0.60			
						35.12 ± 0.14					
						37.21 ± 0.14					
16537*	03 32 55.8442	-09 27 29.744	310.95 ± 0.16	-976.10 ± 0.30	18.10 ± 0.40	16.31 ± 0.05	16.15 ± 0.10	16.00 ± 0.10	16.33	17.3	
						16.52 ± 0.05					
16852	03 36 52.3832	+00 24 05.982	71.60 ± 0.54	-233.40 ± 0.70	-482.10 ± 0.70	27.99 ± 0.03	27.80 ± 0.53	27.80 ± 0.10	28.08	26.9	
17147‡	03 40 22.0645	-03 13 01.133	39.13 ± 0.57	691.60 ± 1.10	-212.80 ± 1.10	120.23 ± 0.11	120.26 ± 0.29	120.30 ± 0.10	120.36	120.7	
17420	03 43 55.3429	-19 06 39.238	71.67 ± 0.67	308.70 ± 1.50	156.70 ± 1.40	25.24 ± 0.04	25.20 ± 0.20		25.29	26.8	
17496	03 44 51.1263	+11 55 12.001	44.33 ± 1.11	314.40 ± 1.20	126.40 ± 1.10	83.92 ± 0.11	81.90				
17651	03 46 50.8875	-23 14 59.002	56.79 ± 0.19	-159.90 ± 0.60	-529.10 ± 0.50	6.89 ± 0.29	7.23 ± 0.45	7.30 ± 0.20			
18267	03 54 28.0332	+16 36 57.793	48.98 ± 0.70	220.10 ± 0.80	-166.60 ± 0.80	18.79 ± 0.70	18.51 ± 1.70	18.50 ± 0.10	18.94	19.5	
18324	03 55 03.8424	+61 10 00.508	47.60 ± 0.84	436.60 ± 1.20	-246.40 ± 1.40	38.69 ± 0.05	47.90		38.81	39.3	
18413	03 56 11.5211	+59 38 30.796	45.51 ± 0.62	-265.10 ± 0.90	169.70 ± 1.00	-18.16 ± 0.04	-18.80 ± 0.40	-19.00 ± 0.30			

It follows in the next page

Table A.1 It cames from the previous page

						Radial Velocity					
HIP	α (h,m,s)	δ (^{o},',")	π (mas)	$\mu_\alpha \times \cos\delta$ (mas/yr)	μ_δ (mas/yr)	*This work* (km/s)	*KH*07 (km/s)	*NO*04 (km/s)	*NI*02 (km/s)	*VF*05 (km/s)	Notes
(1)	(2)	(3)	(4)	(5)	(6)	(7)	(8)	(9)	(10)	(11)	(12)
18774	04 01 19.6235	+76 09 33.732	61.55 ± 0.70	330.80 ± 1.10	-546.80 ± 1.20	17.76 ± 0.07	17.20 ± 2.62	17.20 ± 0.10	17.67		
18859	04 02 36.7449	-00 16 08.123	53.09 ± 0.32	150.70 ± 0.90	-252.00 ± 0.90		17.74 ± 0.32	17.60 ± 0.20			
19076	04 05 20.2581	+22 00 32.059	59.03 ± 0.34	172.20 ± 0.70	-130.20 ± 0.70	24.16 ± 0.09	23.78 ± 0.22	23.80 ± 0.10	24.03	23.7	
19335	04 08 36.6163	+38 02 23.040	47.63 ± 0.26	166.80 ± 1.20	-203.10 ± 1.30	27.01 ± 0.27	26.23 ± 0.38	26.20 ± 0.20			
19422	04 09 35.0403	+69 32 29.013	53.33 ± 0.71	73.60 ± 1.00	-298.80 ± 1.10	-13.39 ± 0.07	-14.09 ± 1.25	-14.10 ± 0.10	-13.55	-13.3	
19832	04 15 09.5321	-04 25 05.940	48.07 ± 3.45	88.10 ± 1.60	-91.10 ± 1.60	24.32 ± 0.12					
19849	04 15 16.3201	-07 39 10.336	200.61 ± 0.23	-2240.12 ± 0.23	-3420.26 ± 0.20	-42.12 ± 0.05	-42.92 ± 0.16	-43.00 ± 0.10	-42.33	-42.3	
20917	04 29 00.1250	+21 55 21.727	87.78 ± 0.97	-65.70 ± 0.90	174.70 ± 0.80	-35.46 ± 0.15	-36.17 ± 0.63	-36.20 ± 0.10	-35.07		
21482*	04 36 48.2425	+27 07 55.897	55.65 ± 1.43	233.20 ± 0.80	-148.60 ± 0.80	36.00	35.19 ± 1.00				Sb, Cab
22263	04 47 36.2918	-16 56 04.042	75.33 ± 0.36	130.40 ± 1.00	169.80 ± 1.00	22.00 ± 0.05	21.66 ± 0.22	21.60 ± 0.10		23.0	
22449	04 49 50.4106	+06 57 40.592	123.94 ± 0.17	462.90 ± 0.50	11.80 ± 0.50	24.11 ± 0.08	24.29 ± 3.54	24.00 ± 5.00		24.9	
22498‡	04 50 25.0912	+63 19 58.625	34.53 ± 1.67	220.40 ± 3.30	-196.20 ± 3.30	59.22 ± 0.13					
23311	05 00 49.0001	-05 45 13.231	114.84 ± 0.50	550.40 ± 1.20	-1110.20 ± 1.10	21.72 ± 0.07	21.06 ± 0.43	21.00 ± 0.10	21.55	20.3	
23693	05 05 30.6558	-57 28 21.734	85.88 ± 0.18	-31.90 ± 0.80	118.10 ± 0.80		-1.26 ± 0.35	-0.80 ± 0.30			
23786	05 06 42.2177	+14 26 46.445	42.25 ± 0.92	282.80 ± 1.10	-239.90 ± 1.10	31.82 ± 0.90	28.22 ± 2.40	28.30 ± 2.20			
23835	05 07 27.0061	+18 38 42.188	64.81 ± 0.33	537.40 ± 0.70	19.30 ± 0.70	20.93 ± 0.07	20.40 ± 0.10	20.30 ± 0.10	20.56	21.2	
24786‡	05 18 50.4722	-18 07 48.182	39.97 ± 0.40	385.50 ± 0.90	62.50 ± 0.90	41.31 ± 0.06	40.40 ± 1.42	40.40 ± 0.10	40.45	40.9	
24813	05 19 08.4745	+40 05 56.586	79.18 ± 0.28	518.99 ± 0.26	-665.05 ± 0.13	67.14 ± 0.03	66.48 ± 0.36	66.50 ± 0.10	66.51	66.7	
24819	05 19 12.6591	-03 04 25.714	64.71 ± 1.11	696.90 ± 1.90	127.10 ± 2.00	88.22 ± 0.07	87.60 ± 1.25	87.60 ± 0.10			
24874	05 19 59.5765	-15 50 22.722	41.14 ± 1.14	174.30 ± 1.30	201.20 ± 1.40	-14.01 ± 0.06	-15.10 ± 0.20	-15.10 ± 0.20			
25119	05 22 37.4901	+02 36 11.486	49.44 ± 1.17	69.70 ± 1.30	-152.10 ± 1.30	36.42 ± 0.07	36.40 ± 0.20	36.40 ± 0.20			
25220	05 23 38.3810	+17 19 26.830	71.01 ± 1.34	251.90 ± 1.10	-3.30 ± 1.00	38.24 ± 0.10	37.89 ± 0.43	37.90 ± 0.10			
25623	05 28 26.0963	-03 29 58.399	76.78 ± 0.76	-305.70 ± 1.40	-796.90 ± 1.50	-55.39 ± 0.10	-56.30 ± 1.27	-56.30 ± 0.10	-55.53		
26505	05 38 11.8615	+51 26 44.664	49.59 ± 0.72	-549.60 ± 1.10	105.60 ± 1.10	-45.80 ± 0.80	-44.00			-45.5	
26779	05 41 20.3357	+53 28 51.808	81.44 ± 0.54	3.50 ± 1.10	-523.60 ± 1.10	1.27 ± 0.03	0.96 ± 0.16	0.90 ± 0.10	1.21	0.6	
27072	05 44 27.7904	-22 26 54.176	112.01 ± 0.18	-291.67 ± 0.14	-368.98 ± 0.15		-9.51 ± 0.54	-9.50 ± 0.20			
27207	05 46 01.8857	+37 17 04.735	45.79 ± 0.76	488.10 ± 1.00	-509.50 ± 1.10	-29.25 ± 1.10	-29.70 ± 0.78	-29.70 ± 0.10	-29.18	-28.7	
27435	05 48 34.9407	-04 05 40.732	65.90 ± 0.41	62.20 ± 0.70	-228.60 ± 0.70	33.05 ± 0.09	31.25 ± 0.22	31.20 ± 0.10	31.54	31.6	
27913	05 54 22.9825	+20 16 34.228	115.42 ± 0.27	-174.60 ± 0.70	-89.90 ± 0.70	-13.47 ± 0.30	-13.45 ± 0.20	-13.90 ± 0.20	-12.17	-13.2	Sb
28103	05 56 24.2929	-14 10 03.721	67.21 ± 0.25	-42.06 ± 0.19	139.25 ± 0.17	-1.12 ± 0.56	-1.65 ± 0.54	-1.60 ± 0.20			
28267	05 58 21.5357	-04 39 02.404	42.46 ± 0.63	73.60 ± 1.00	-206.50 ± 1.10	144.09 ± 0.07	143.30 ± 0.10	143.30 ± 0.10	143.62	144.1	
29067	06 07 55.2511	+67 58 36.544	40.90 ± 1.85	-48.80 ± 1.80	-113.80 ± 1.90	-2.03 ± 0.18	1.60				
29271	06 10 14.4735	-74 45 10.963	98.05 ± 0.14	122.00 ± 0.70	-212.70 ± 0.70		35.55 ± 0.54	35.60 ± 0.20		37.1	
29432	06 12 00.5665	+06 46 59.068	42.54 ± 0.55	197.10 ± 1.30	-253.30 ± 1.40	-53.20 ± 0.04	-53.69 ± 0.99	-53.70 ± 0.10	-53.50	-53.2	
29525	06 13 12.5028	+10 37 37.718	55.73 ± 0.44	77.30 ± 1.30	-297.30 ± 1.20	5.96 ± 0.80	5.70 ± 0.78	5.70 ± 0.10			
29568	06 13 45.2957	-23 51 42.977	59.81 ± 0.49	-45.40 ± 1.10	113.20 ± 1.20	22.23 ± 0.09	21.67 ± 0.22	21.60 ± 0.10			
29650	06 14 50.8767	+19 09 23.213	48.06 ± 0.34	-96.90 ± 0.70	-181.90 ± 0.70	36.65 ± 0.13	34.60 ± 0.25	34.30 ± 0.20		35.3	
29800	06 16 26.6196	+12 16 19.787	51.98 ± 0.27	81.90 ± 0.50	186.90 ± 0.60	9.50 ± 0.60	9.10 ± 0.47	9.50 ± 0.60			
29860	06 17 16.1377	+05 06 00.403	51.95 ± 0.40	-195.40 ± 1.00	164.60 ± 1.00	8.43 ± 0.05	9.68 ± 0.32	9.80 ± 0.20	5.78	12.7	
30422‡	06 23 46.5007	+04 35 44.925	26.77 ± 0.88	-16.90 ± 0.50	11.80 ± 0.40		16.30				
32010	06 41 15.7114	+23 57 27.774	57.32 ± 1.16	206.70 ± 1.00	-277.00 ± 1.00	-44.44 ± 0.08 -44.72 ± 0.10	-44.86 ± 0.29	-44.90 ± 0.10	-44.25	-43.8	
32423‡	06 46 05.0519	+32 33 20.437	38.12 ± 1.01	-453.60 ± 1.10	98.60 ± 1.10	-32.09 ± 0.11 -32.08 ± 0.11	-34.50				
32439	06 46 14.1506	+79 33 53.320	55.95 ± 0.27	-98.70 ± 0.60	-603.30 ± 0.60		15.31 ± 0.71	15.30 ± 0.10			Sb
32480	06 46 44.3388	+43 34 38.737	59.82 ± 0.30	-0.80 ± 0.70	165.30 ± 0.70	-23.90 ± 0.07	-23.98 ± 0.22	-24.00 ± 0.10	-23.93	-23.6	
32919	06 51 32.3922	+47 22 04.149	53.89 ± 0.98	-245.30 ± 1.10	-694.30 ± 1.10	19.12 ± 0.17 18.84 ± 0.15	22.20				

It follows in the next page

Table A.1 It cames from the previous page

						Radial Velocity					
HIP	α	δ	π	$\mu_\alpha \times \cos\delta$	μ_δ	*Thiswork*	*KH*07	*NO*04	*NI*02	*VF*05	Notes
	(h,m,s)	(^{o},',")	(mas)	(mas/yr)	(mas/yr)	(km/s)	(km/s)	(km/s)	(km/s)	(km/s)	
(1)	(2)	(3)	(4)	(5)	(6)	(7)	(8)	(9)	(10)	(11)	(12)
32984	06 52 18.0501	-05 10 25.367	114.81 ± 0.44	-544.20 ± 1.30	-2.50 ± 1.30	-7.65 ± 0.09	-7.72 ± 0.71	-7.70 ± 0.10	-7.08	-5.4	
33277	06 55 18.6677	+25 22 32.511	58.02 ± 0.41	-36.70 ± 0.70	25.30 ± 0.70	-15.05	-15.15 ± 0.22	-15.20 ± 0.10	-15.02	-14.9	RV
33373	06 56 28.1185	+40 04 27.584	40.67 ± 1.34	114.96 ± 1.31	-436.21 ± 0.89	50.89 ± 0.11	49.80 ± 0.60				
						51.17 ± 0.17					
33537	06 58 11.7499	+22 28 33.193	40.59 ± 0.53	48.10 ± 0.70	97.50 ± 0.70	-26.77 ± 0.05	-27.10 ± 0.20	-27.10 ± 0.20		-26.3	
33560	06 58 26.0503	-12 59 30.565	46.10 ± 1.23	57.01 ± 1.65	-147.14 ± 1.21	-4.43 ± 0.14	-3.10 ± 2.10				
33852	07 01 38.5885	+48 22 43.220	49.79 ± 0.85	545.00 ± 1.10	-432.50 ± 1.20	-21.62 ± 0.06	-22.80		-21.62		
33955	07 02 42.9176	-06 47 57.212	54.22 ± 0.94	-198.80 ± 1.20	-313.60 ± 1.40	-30.79 ± 0.14					
34017	07 03 30.4587	+29 20 13.491	52.27 ± 0.41	156.50 ± 0.70	-827.80 ± 0.60	24.60 ± 0.08	24.44 ± 0.16	24.30 ± 0.10	24.60	24.3	
34567‡	07 09 35.3899	+25 43 43.136	39.75 ± 0.54	-124.30 ± 0.80	-175.30 ± 0.80	19.80	19.72 ± 6.00	18.10 ± 8.30			Sb,Cab
35136	07 15 50.1385	+47 14 23.870	59.21 ± 0.33	29.60 ± 0.90	-186.10 ± 1.00	84.85 ± 0.05	84.75 ± 0.25	84.90 ± 0.20	84.81		
36357	07 29 01.7705	+31 59 37.824	56.62 ± 0.93	159.70 ± 1.00	175.80 ± 1.10	-3.79 ± 0.23	-4.30 ± 1.70		-3.95		
						-4.25 ± 0.11					
36366	07 29 06.7191	+31 47 04.381	55.41 ± 0.25	157.20 ± 0.60	186.90 ± 0.60		-3.00 ± 6.19	-19.00 ± 8.70			
36439	07 29 55.9561	+49 40 20.866	49.41 ± 0.36	109.60 ± 1.20	-83.00 ± 1.30	-27.13 ± 0.10	-27.50 ± 0.38	-27.60 ± 0.20			
36551	07 31 07.7109	+14 36 50.919	48.06 ± 1.13	76.50 ± 1.20	-288.10 ± 1.10	65.65 ± 0.12	66.70 ± 1.10				
36827	07 34 26.1657	-06 53 48.040	40.72 ± 1.00	-80.90 ± 1.10	-42.50 ± 1.10	-10.17 ± 0.10	-9.70 ± 0.20		-9.67	-9.2	
37279	07 39 18.1183	+05 13 29.975	284.52 ± 1.27	-714.56 ± 2.07	-1036.82 ± 1.15	-4.10	-4.20 ± 1.26	-4.20 ± 0.20		-2.7	Sb
37288	07 39 23.0386	+02 11 01.186	68.59 ± 1.47	-147.60 ± 1.60	-247.30 ± 1.50	18.90 ± 0.27	18.5				
						20.70 ± 0.21					
37349	07 39 59.3282	-03 35 51.026	70.38 ± 0.64	71.70 ± 1.20	-276.10 ± 1.30	-18.14 ± 0.50	-18.61 ± 0.49	-18.60 ± 0.10	-18.21	-17.6	
						-18.56 ± 0.08					
						-18.06 ± 0.04					
38382	07 51 46.3026	-13 53 52.903	60.58 ± 0.58	-60.00 ± 0.70	-338.90 ± 0.70	-21.20	-21.50 ± 0.79	-21.50 ± 0.50			Sb
38657	07 54 54.0671	+19 14 10.824	48.31 ± 0.86	94.50 ± 0.90	-456.40 ± 1.00	-19.44 ± 0.08	-18.70		-10.62	-8.9	
38784	07 56 17.2303	+80 15 55.953	58.17 ± 0.36	-474.80 ± 1.00	87.70 ± 1.10	-7.79 ± 0.05	-7.84 ± 0.22	-7.90 ± 0.10			
38931	07 57 57.7861	-00 48 51.903	56.14 ± 1.22	-164.40 ± 1.00	3.10 ± 1.00	-4.44 ± 0.06	-4.00		-4.42	-4.3	
39064	07 59 33.9341	+20 50 37.994	42.16 ± 0.71	180.10 ± 1.10	-550.80 ± 1.00	-28.43 ± 0.30	-29.34 ± 1.01	-29.40 ± 0.30	-28.71	-28.9	Sb
39157	08 00 32.1290	+29 12 44.481	59.64 ± 0.56	-171.50 ± 1.20	-1164.90 ± 1.30	14.80	14.48 ± 0.53	14.50 ± 0.10	14.83	13.0	RV
40035	08 10 39.8261	-13 47 57.146	44.68 ± 0.30	-250.30 ± 0.80	58.10 ± 0.70	34.19 ± 0.13	32.82 ± 1.25	32.80 ± 0.10			
40118	08 11 38.6440	+32 27 25.667	45.90 ± 0.55	-464.70 ± 0.80	-646.50 ± 0.80	29.67 ± 0.05	29.60 ± 0.57	29.60 ± 0.10	29.58	30.3	
40170‡	08 12 14.4328	+51 54 25.508	39.18 ± 2.11	-116.60 ± 2.00	-205.40 ± 2.00	5.70 ± 0.21					
						3.97 ± 0.23					
40375	08 14 35.9131	+13 01 22.170	53.10 ± 1.11	-421.30 ± 1.00	95.70 ± 1.00	21.19 ± 0.16					
40671	08 18 10.7804	+30 36 02.936	44.08 ± 1.22	-283.60 ± 1.40	-822.10 ± 1.30	13.08 ± 0.11	11.60				
						13.98 ± 0.12					
						13.12 ± 0.13					
40693⋆	08 18 23.9473	-12 37 55.824	80.04 ± 0.35	280.30 ± 1.00	-989.50 ± 0.90	30.18 ± 0.04	29.82 ± 0.49	29.80 ± 0.10		32.2	
40843	08 20 03.8603	+27 13 03.745	54.73 ± 0.32	-17.60 ± 0.60	-376.50 ± 0.60	32.87 ± 0.08	32.62 ± 0.29	32.60 ± 0.10	32.73	33.3	
41484	08 27 36.7855	+45 39 10.753	44.94 ± 0.46	-20.70 ± 1.10	-351.90 ± 1.10	-32.62 ± 0.11	-32.42 ± 0.16	-32.60 ± 0.10	-32.34	-32.0	
41926	08 32 51.4959	-31 30 03.070	81.91 ± 0.46	-1113.70 ± 1.00	763.10 ± 1.00	15.00 ± 0.05	14.42 ± 1.26	14.40 ± 0.20	14.79	13.0	
42074	08 34 31.6497	-00 43 33.840	47.31 ± 0.72	-197.50 ± 1.00	18.90 ± 0.90	36.50 ± 0.11	34.20 ± 0.10	34.20 ± 0.10	34.93	35.5	
						36.50 ± 0.11					
42173‡	08 35 51.2716	+06 37 21.993	38.08 ± 0.78	-133.50 ± 6.20	-132.20 ± 5.40	43.48 ± 0.90	29.34 ± 0.32	29.20 ± 0.20			
42333	08 37 50.2932	-06 48 24.786	41.71 ± 0.70	-298.20 ± 1.40	45.60 ± 1.40	35.29 ± 0.06	35.50 ± 0.20	35.50 ± 0.20	35.37	36.0	
42430	08 39 07.9003	-22 39 42.750	51.61 ± 0.63	-260.80 ± 3.50	429.70 ± 3.30	52.25 ± 0.11	47.90 ± 1.50	47.90 ± 1.50			
42438	08 39 11.7040	+65 01 15.264	69.67 ± 0.37	-28.90 ± 1.00	88.50 ± 1.00	-13.62 ± 0.05	-12.85 ± 0.51	-12.80 ± 0.20			
42499	08 39 50.7917	+11 31 21.621	55.12 ± 0.71	-108.60 ± 0.90	-500.30 ± 0.90	-12.10 ± 1.50	-12.50 ± 1.06	-12.50 ± 0.10	-12.09	-11.5	RV

It follows in the next page

Table A.1 It cames from the previous page

						Radial Velocity					
HIP	α (h,m,s)	δ (^{o},',")	π (mas)	$\mu_\alpha \times \cos\delta$ (mas/yr)	μ_δ (mas/yr)	*Thiswork* (km/s)	*KH*07 (km/s)	*NO*04 (km/s)	*NI*02 (km/s)	*VF*05 (km/s)	Notes
(1)	(2)	(3)	(4)	(5)	(6)	(7)	(8)	(9)	(10)	(11)	(12)
42525[†]	08 40 11.9441	+41 17 07.458	68.54 ± 15.51	-36.20 ± 1.40	-30.90 ± 1.30	58.85 ± 0.26					
						60.61 ± 0.21					
42808	08 43 18.0304	-38 52 56.566	89.76 ± 0.37	-300.40 ± 1.30	342.90 ± 1.20		12.51 ± 1.25	12.50 ± 0.10			
43557	08 52 16.3907	+08 03 46.513	41.64 ± 1.02	154.30 ± 1.30	-236.80 ± 1.30	3.50	3.85 ± 5.59	3.90 ± 2.80			Sb
43587[⋆]	08 52 35.8112	+28 19 50.947	80.55 ± 0.70	-484.80 ± 0.70	-233.50 ± 0.70	27.50 ± 0.08	27.80 ± 0.20		27.35	27.8	
43726	08 54 17.9475	-05 26 04.054	57.51 ± 0.39	-412.10 ± 1.20	28.20 ± 1.20	32.29 ± 0.04	31.80 ± 0.36	31.80 ± 0.10	32.00	31.1	
						33.64 ± 0.09					
44075	08 58 43.9331	-16 07 57.817	47.54 ± 0.31	244.50 ± 1.10	213.00 ± 1.00	120.65 ± 0.19	119.33 ± 0.53	119.30 ± 0.10			
44248	09 00 38.3707	+41 46 58.480	62.22 ± 0.67	-474.30 ± 0.85	-204.25 ± 0.68	27.20	27.99 ± 5.59	28.10 ± 2.80			Sb
44897	09 08 51.0705	+33 52 55.981	52.13 ± 0.33	-192.10 ± 1.40	-116.70 ± 1.50	27.14 ± 0.07	26.09 ± 0.22	26.00 ± 0.10	26.12	26.8	
45038	09 10 23.5455	+67 08 02.465	49.07 ± 0.37	7.10 ± 0.80	-95.10 ± 0.90	-2.00 ± 0.06	-2.91 ± 0.22	-3.00 ± 0.10			
45170	09 12 17.5488	+14 59 45.733	49.11 ± 0.55	-522.80 ± 0.80	245.80 ± 0.80	50.20	49.90 ± 5.24	49.90 ± 0.50			Sb
45333	09 14 20.5406	+61 25 23.943	51.11 ± 0.32	-9.80 ± 1.10	-30.60 ± 1.20	-14.60	-14.32 ± 5.79	-8.60 ± 8.00			Sb
45343	09 14 22.7935	+52 41 11.849	172.14 ± 6.32	-1555.60 ± 0.90	-570.00 ± 1.00	10.45 ± 0.30	10.84 ± 0.10	10.5 ± 0.10	11.14		
45383	09 14 53.6615	+04 26 34.440	55.67 ± 1.41	-114.40 ± 1.30	26.80 ± 1.30	10.02 ± 0.70	8.50 ± 1.70				
45617	09 17 53.4561	+28 33 37.861	57.93 ± 0.76	52.80 ± 1.20	-510.50 ± 1.10	-20.65 ± 0.90	-20.94 ± 0.43	-21.00 ± 0.10			
45839	09 20 44.3177	-05 45 14.293	42.81 ± 1.44	-364.60 ± 1.40	-111.50 ± 1.40	37.10 ± 0.11	39.20 ± 2.30				
45963	09 22 25.9452	+40 12 03.818	40.08 ± 0.65	-340.70 ± 0.80	-359.30 ± 0.80	-3.20	-3.71 ± 5.23	-3.70 ± 0.10			Cab
46509	09 29 08.8977	-02 46 08.270	57.70 ± 2.14	98.99 ± 2.34	-2.66 ± 1.39	10.85 ± 0.28	9.70 ± 0.30	10.90 ± 0.30			Sb
46580	09 29 54.8245	+05 39 18.484	77.47 ± 0.64	-502.40 ± 1.00	109.70 ± 1.10	29.75	29.58 ± 0.63	29.60 ± 0.10	29.84	30.3	RV
46816	09 32 25.5683	-11 11 04.685	53.70 ± 0.84	-247.50 ± 1.10	35.50 ± 1.10	5.81 ± 0.35	9.20 ± 1.20			8.7	
						7.67 ± 0.65					
46843	09 32 43.7592	+26 59 18.709	56.19 ± 0.60	-147.80 ± 1.40	-246.70 ± 1.30	8.00 ± 0.09	11.20 ± 1.30				
						9.49 ± 0.33					
						8.12 ± 0.12					
47080	09 35 39.5023	+35 48 36.481	87.96 ± 0.32	-723.00 ± 1.30	-247.80 ± 1.40	14.40	14.80 ± 0.20				RV
47592	09 42 14.4168	-23 54 56.048	66.62 ± 0.20	-400.30 ± 1.10	263.20 ± 1.00	35.97 ± 0.09	34.48 ± 0.32	34.40 ± 0.20		35.3	
48113	09 48 35.3714	+46 01 15.629	54.45 ± 0.28	222.00 ± 0.80	-93.50 ± 0.90	6.00 ± 1.10	4.96 ± 0.16	4.80 ± 0.10	4.90	6.1	RV
48411	09 52 11.3626	+03 13 18.631	48.86 ± 1.23	-425.60 ± 1.20	17.20 ± 1.10	29.65 ± 0.12	21.50 ± 1.00				
						21.58 ± 0.14					
49081	10 01 00.6566	+31 55 25.220	66.47 ± 0.32	-529.10 ± 0.60	-430.20 ± 0.70	56.31 ± 0.06	55.79 ± 0.71	55.80 ± 0.10	55.96	56.0	
49366	10 04 37.6601	-11 43 46.930	41.63 ± 0.95	-189.80 ± 1.00	-25.20 ± 1.00	-11.52 ± 0.07	-12.20 ± 0.20		-12.13	-11.8	
49699[⋆]	10 08 43.1395	+34 14 32.135	54.93 ± 0.54	-65.10 ± 1.20	-60.70 ± 1.30	9.35 ± 0.06	9.20 ± 0.20		9.25	10.1	
						8.94 ± 0.09					
49908	10 11 22.1411	+49 27 15.252	205.20 ± 0.54	-1359.80 ± 1.00	-505.70 ± 1.00	-26.58 ± 0.17	-26.73 ± 0.22	-26.80 ± 0.10	-25.73		
						-26.57 ± 0.20					
49986	10 12 17.6681	-03 44 44.384	127.06 ± 1.90	-150.70 ± 1.40	-245.20 ± 1.50	7.33 ± 0.11	9.0 ± 1.40		7.93		
50125	10 13 57.3822	+52 30 24.208	43.28 ± 1.36	86.30 ± 1.14	-760.67 ± 0.80	-21.78 ± 0.11	-24.80				
50384	10 17 14.5385	+23 06 22.391	43.82 ± 0.35	-412.70 ± 0.90	-97.90 ± 0.80	37.41 ± 0.09	37.40 ± 1.25	37.40 ± 0.10			
50505	10 18 51.9488	+44 02 53.962	49.40 ± 0.50	61.90 ± 0.80	-299.70 ± 0.90	-6.54 ± 0.07	-8.20 ± 1.27	-8.20 ± 0.30	-7.55	-7.3	
51248	10 28 03.8823	+48 47 05.644	43.67 ± 0.43	82.60 ± 1.50	-881.90 ± 1.50	-6.09 ± 0.17	-7.11 ± 0.29	-7.10 ± 0.10			
51459	10 30 37.5798	+55 58 49.931	78.26 ± 0.29	-177.70 ± 0.70	-32.80 ± 0.80	8.47 ± 0.04	8.60 ± 0.22	8.50 ± 0.10	8.53	9.4	
51502	10 31 04.6638	+82 33 30.915	46.51 ± 1.40	-82.20 ± 0.30	24.20 ± 0.30		7.93 ± 2.68	8.60 ± 3.70			
51525	10 31 24.2173	+45 31 33.783	63.52 ± 1.09	-568.30 ± 1.10	-595.90 ± 1.00	21.44 ± 0.16	20.10 ± 1.13	20.10 ± 0.10	21.05		
51933[‡]	10 36 32.3829	-12 13 48.436	39.86 ± 0.37	268.60 ± 0.70	-672.40 ± 0.70	-6.37 ± 0.11	-6.30 ± 1.25	-6.30 ± 0.10			
52369	10 42 13.3215	-13 47 15.768	41.96 ± 0.48	236.40 ± 1.20	-171.40 ± 1.20	-17.06 ± 0.08	-18.20 ± 0.10	-18.20 ± 0.10			
						-17.68 ± 0.08					
53486	10 56 30.7983	+07 23 18.506	57.79 ± 0.87	-256.80 ± 1.30	-77.30 ± 1.30	6.12 ± 0.06	5.40 ± 0.20		5.53	6.4	

It follows in the next page

Table A.1 It cames from the previous page

						Radial Velocity					
HIP	α	δ	π	$\mu_\alpha \times \cos\delta$	μ_δ	*Thiswork*	*KH*07	*NO*04	*NI*02	*VF*05	Notes
	(h,m,s)	(^{o},',")	(mas)	(mas/yr)	(mas/yr)	(km/s)	(km/s)	(km/s)	(km/s)	(km/s)	
(1)	(2)	(3)	(4)	(5)	(6)	(7)	(8)	(9)	(10)	(11)	(12)
53721*	10 59 27.9737	+40 25 48.925	71.11 ± 0.25	-317.20 ± 0.70	56.60 ± 0.70	11.39 ± 0.07	11.19 ± 0.22	11.10 ± 0.10	11.24	11.7	
54155‡	11 04 41.4733	-04 13 15.924	38.09 ± 0.99	-178.60 ± 1.20	-102.90 ± 1.20	20.03 ± 0.14	18.00 ± 0.20	18.00 ± 0.20			
						19.23 ± 0.08					
54426	11 08 14.0145	+38 25 35.873	44.29 ± 0.84	-214.30 ± 1.50	41.30 ± 1.60	-35.60 ± 0.05	-36.40 ± 0.90				
54646	11 11 05.1724	+30 26 45.662	84.22 ± 0.86	590.80 ± 1.10	-197.70 ± 1.10	-16.66 ± 0.17	-16.40 ± 0.10	-17.20 ± 0.10	-16.38		
						-15.12 ± 0.16					
						-16.02 ± 0.15					
54651	11 11 10.7010	-10 57 03.195	49.39 ± 0.96	-939.40 ± 1.70	593.40 ± 1.70	38.30 ± 0.19	36.80 ± 2.62	36.80 ± 0.10			
						37.72 ± 0.01					
54677	11 11 33.1223	-14 59 28.996	46.34 ± 1.31	716.80 ± 1.60	-596.90 ± 1.50	-10.49 ± 0.17	-11.30 ± 3.28	-11.40 ± 0.70			
						-12.17 ± 0.15					
54745	11 12 32.3508	+35 48 50.689	45.60 ± 0.44	-248.60 ± 1.40	-151.90 ± 1.40	-3.31 ± 0.06	-3.66 ± 0.22	-3.70 ± 0.10	-3.66	-5.5	
54810	11 13 13.2332	+04 28 56.443	54.71 ± 1.23	-315.50 ± 1.00	-35.70 ± 1.00	17.10 ± 0.18	15.90 ± 1.83	15.90 ± 0.10			
54906	11 14 33.1624	+25 42 37.385	47.36 ± 0.75	-106.00 ± 1.50	49.30 ± 1.30	-1.27 ± 0.07	0.90 ± 1.40		-1.65	-4.0	
54966†	11 15 20.8893	-18 08 42.152	70.25 ± 29.70	341.29 ± 24.49	-690.34 ± 20.14	7.44 ± 0.25	6.91 ± 2.62	6.90 ± 0.10			
55210	11 18 22.0115	-05 04 02.288	46.37 ± 0.64	794.60 ± 0.90	-151.50 ± 1.00	13.73 ± 0.06	12.89 ± 1.25	12.90 ± 0.10	13.33	11.1	
55848*	11 26 46.2771	+03 00 22.781	55.71 ± 1.45	-728.30 ± 1.00	185.70 ± 1.00	4.17 ± 0.08	3.10 ± 0.36	3.10 ± 0.10	3.73	4.1	
56242	11 31 44.9451	+14 21 52.218	42.87 ± 1.21	-328.40 ± 1.00	-190.10 ± 0.90	-4.68 ± 0.05	-4.87 ± 0.79	-4.90 ± 0.20	-4.85	-4.4	
56452	11 34 29.4871	-32 49 52.823	104.61 ± 0.37	-669.90 ± 1.10	825.20 ± 1.00	-21.99 ± 0.05	-22.31 ± 0.53	-22.30 ± 0.10	-21.96	-24.5	
56809	11 38 44.9009	+45 06 30.296	43.06 ± 0.73	-594.00 ± 1.20	15.10 ± 1.30	-18.93 ± 0.24	-16.32 ± 2.42	-17.30 ± 0.20	-16.91	-17.0	Sb
56997	11 41 03.0153	+34 12 05.888	104.03 ± 0.26	-12.80 ± 0.80	-380.60 ± 0.80	-5.55 ± 0.06	-5.82 ± 0.16	-5.90 ± 0.10	-5.57	-4.3	
57443	11 46 31.0720	-40 30 01.274	108.45 ± 0.23	-1530.10 ± 0.80	402.50 ± 0.70		16.77 ± 0.53	16.80 ± 0.10		17.3	
57494‡	11 47 03.8343	-11 49 26.573	39.44 ± 1.10	-191.00 ± 1.50	-64.80 ± 1.40	18.68 ± 0.10	18.30 ± 1.40				
						20.29 ± 0.22					
57757	11 50 41.7185	+01 45 52.985	91.50 ± 0.22	740.30 ± 0.40	-271.70 ± 0.40	4.30	4.11 ± 0.53	4.10 ± 0.10	4.45	5.3	RV
57939	11 52 58.7691	+37 43 07.239	109.98 ± 0.41	4003.98 ± 0.37	-5813.62 ± 0.23	-96.79 ± 0.29	-98.30 ± 0.10	-99.00 ± 0.10	-98.07	-98.2	
						-98.27 ± 0.18					
59000	12 05 50.6575	-18 52 30.915	45.44 ± 1.39	-13.50 ± 1.70	-314.00 ± 2.40	52.81 ± 0.19					
						12.19 ± 0.20					
59280	12 09 37.2563	+40 15 07.399	40.76 ± 0.66	-314.30 ± 0.70	-51.30 ± 0.80	-2.86 ± 0.06	-2.10 ± 1.50		-2.43	-1.7	
						-1.15 ± 0.15					
59750	12 15 10.5577	-10 18 44.641	44.77 ± 0.81	34.80 ± 1.00	-1014.80 ± 1.10	4.69 ± 0.14	7.07 ± 3.61	4.00 ± 5.00			Sb
60866	12 28 31.5943	-18 17 50.237	40.67 ± 1.05	170.00 ± 1.70	-175.50 ± 1.60	-5.42 ± 0.16	2.70				
						-5.24 ± 0.14					
61317	12 33 44.5446	+41 21 26.927	118.49 ± 0.20	-704.90 ± 0.60	292.40 ± 0.60		6.30 ± 0.71	6.30 ± 0.10	6.26	8.9	Sb
61901	12 41 06.4805	+15 22 35.991	70.52 ± 0.73	122.10 ± 0.70	-390.50 ± 0.70	24.17 ± 0.09	23.70 ± 1.10		24.60		
61941	12 41 39.6423	-01 26 57.750	85.00 ± 0.58	-614.29 ± 0.86	60.71 ± 0.46	-21.42 ± 0.66	-19.56 ± 0.75	-19.50 ± 0.80			
62207	12 44 59.4051	+39 16 44.099	57.55 ± 0.32	-360.20 ± 0.80	139.00 ± 0.80	80.01 ± 0.10	80.29 ± 0.71	80.30 ± 0.10			
						81.70 ± 0.23					
62505	12 48 32.3079	-15 43 10.103	41.95 ± 3.00	59.90 ± 1.90	39.20 ± 1.70	1.25 ± 0.15	0.20 ± 0.40		0.62		
62523	12 48 47.0484	+24 50 24.813	59.04 ± 0.45	-335.00 ± 1.20	-106.00 ± 1.10	-8.70 ± 0.70	-9.26 ± 0.29	-9.30 ± 0.10		-6.0	
						-7.95 ± 0.09					
						-7.92 ± 0.08					
						-7.38 ± 0.08					
63257	12 57 43.9570	-14 27 48.626	41.61 ± 1.55	-355.60 ± 1.40	22.20 ± 1.40	-6.51 ± 0.07	5.10				
63366	12 59 01.5624	-09 50 02.705	47.86 ± 0.91	-824.60 ± 1.10	197.70 ± 1.10	3.97 ± 0.12	3.69 ± 1.84	3.70 ± 0.20			
63742	13 03 49.6555	-05 09 42.524	46.09 ± 0.81	-189.60 ± 0.70	-223.20 ± 0.80	-13.08 ± 0.08	0.00				
						-2.56 ± 0.09					

It follows in the next page

Table A.1 It cames from the previous page

						Radial Velocity					
HIP	α (h,m,s)	δ (^{o},',")	π (mas)	$\mu_\alpha \times \cos\delta$ (mas/yr)	μ_δ (mas/yr)	*This work* (km/s)	*KH*07 (km/s)	*NO*04 (km/s)	*NI*02 (km/s)	*VF*05 (km/s)	Notes
(1)	(2)	(3)	(4)	(5)	(6)	(7)	(8)	(9)	(10)	(11)	(12)
64241	13 09 59.2766	+17 31 45.953	56.14 ± 0.90	-430.10 ± 0.90	137.80 ± 0.90	-18.58 ± 0.23	-12.76 ± 0.32	-11.40 ± 0.20			
64394	13 11 52.3935	+27 52 41.459	109.53 ± 0.17	-800.90 ± 0.50	882.20 ± 0.50	5.30 ± 0.05	5.04 ± 0.36	5.00 ± 0.10	5.30	6.2	
64792	13 16 46.5155	+09 25 26.963	56.93 ± 0.26	-334.90 ± 0.80	191.00 ± 0.70	-27.73 ± 0.13	-27.22 ± 0.16	-27.40 ± 0.10	-27.14	-26.6	
64797	13 16 51.0523	+17 01 01.857	90.36 ± 0.74	623.90 ± 1.20	-259.00 ± 1.10	7.71 ± 0.06	9.00				
64924*	13 18 24.3146	-18 18 40.306	116.89 ± 0.22	-1070.37 ± 0.23	-1063.69 ± 0.13	-5.80 ± 0.09	-8.10 ± 0.16	-8.20 ± 0.10	-7.85	-9.4	
						-8.96 ± 0.03					
65343	13 23 32.7842	+29 14 14.930	53.18 ± 0.98	-467.90 ± 1.70	244.70 ± 1.50	-39.37 ± 0.18	-38.60 ± 0.20				
65352	13 23 39.1545	+02 43 23.970	64.73 ± 1.33	13.30 ± 1.30	199.60 ± 1.30	28.69 ± 0.07	28.00 ± 0.20	28.00 ± 0.20	28.42	28.9	
65515	13 25 45.5321	+56 58 13.776	46.31 ± 0.51	-218.30 ± 0.90	10.70 ± 1.10	-12.72 ± 0.08	-12.60 ± 0.20	-12.60 ± 0.20			
						-12.70 ± 0.10					
65721*	13 28 25.8094	+13 46 43.634	55.59 ± 0.24	-234.00 ± 0.60	-575.70 ± 0.60	6.15 ± 0.14	4.72 ± 0.16	4.60 ± 0.10	5.04	3.9	
66147	13 33 32.4003	+08 35 12.351	52.46 ± 0.89	-509.00 ± 1.70	93.50 ± 1.60	-5.79 ± 0.07	-6.20 ± 0.20		-6.09	-5.7	
66252	13 34 43.2057	-08 20 31.333	49.47 ± 0.72	-288.70 ± 1.60	-87.40 ± 1.60	-21.05 ± 0.24	-23.00 ± 2.62	-23.00 ± 0.10			
66886	13 42 26.0357	-01 41 10.580	41.43 ± 1.20	-287.90 ± 1.20	-154.50 ± 1.10	-42.52 ± 0.09	-42.90 ± 0.30				
67105	13 45 14.7165	+08 50 09.515	47.65 ± 0.98	-67.30 ± 1.30	-97.90 ± 1.30	-12.76 ± 0.07	-13.20 ± 0.30				
67275	13 47 15.7429	+17 27 24.862	64.03 ± 0.20	-480.80 ± 0.40	50.40 ± 0.40	-21.02 ± 0.31	-16.18 ± 0.36	-16.20 ± 0.10	-16.54	-15.9	
67422	13 49 03.9957	+26 58 47.678	74.48 ± 0.77	-436.00 ± 1.90	-110.80 ± 1.80	-20.50 ± 0.06	-19.90 ± 0.50		-20.38	-20.3	
68030	13 55 49.9935	+14 03 23.411	40.23 ± 0.37	-290.60 ± 0.80	9.70 ± 0.80	-10.83 ± 0.18	-10.74 ± 0.86	-10.70 ± 0.20	-10.53	-10.2	
68184	13 57 32.0575	+61 29 34.301	99.37 ± 0.32	-31.40 ± 1.20	217.20 ± 1.40	-26.62 ± 0.08	-25.30		-26.47	-26.3	
68337	13 59 19.4025	+22 52 11.116	40.32 ± 0.96	-161.70 ± 1.00	13.60 ± 1.00	-57.59 ± 0.17	-56.70 ± 1.10		-57.44		
68682	14 03 32.3515	+10 47 12.404	58.87 ± 0.62	91.10 ± 1.20	-307.50 ± 1.20	-11.20 ± 0.30	-12.30 ± 2.66	-12.30 ± 0.70	-8.08	-8.5	Sb
69357	14 11 46.1709	-12 36 42.358	42.75 ± 1.21	-256.20 ± 1.10	-180.40 ± 1.10	3.10 ± 0.11	2.86 ± 1.26	2.80 ± 0.20	3.29	3.7	
69414	14 12 45.2397	-03 19 12.304	45.35 ± 0.54	-162.20 ± 1.00	-323.10 ± 1.20	37.20 ± 0.10	37.44 ± 0.71	37.50 ± 0.10	37.77	38.0	
69526	14 13 57.0781	+30 13 01.874	57.39 ± 1.06	-398.50 ± 1.40	173.80 ± 1.40	-16.47 ± 0.19	-16.30 ± 0.20		-16.24		
69701	14 16 00.8697	-06 00 01.968	44.98 ± 0.19	-26.32 ± 0.19	-419.38 ± 0.14	13.07 ± 0.42	12.46 ± 0.29	12.40 ± 0.10			
69962	14 18 58.2805	-06 36 13.125	45.97 ± 1.60	-15.60 ± 1.50	-425.60 ± 1.80	7.35 ± 0.17	12.30 ± 1.40				
						9.65 ± 0.37					
69972	14 19 04.8348	-59 22 44.533	84.74 ± 0.69	-454.37 ± 0.93	-809.50 ± 0.72	-22.50 ± 0.08	-18.89 ± 1.25	-18.90 ± 0.10		-17.9	
70016	14 19 34.8641	-05 09 04.302	47.91 ± 0.81	-632.70 ± 1.00	-121.70 ± 1.20	-9.74 ± 0.07	-10.19 ± 0.71	-10.20 ± 0.10	-9.81	-9.5	
70218	14 21 57.2165	+29 37 46.626	69.70 ± 0.83	-631.40 ± 1.10	-306.70 ± 1.10	-36.49 ± 0.13	-37.81 ± 0.29	-37.80 ± 0.10			
						-35.69 ± 0.13					
70319	14 23 15.2847	+01 14 29.648	58.17 ± 0.52	223.30 ± 1.10	-477.80 ± 1.20	-17.99 ± 0.17	-19.58 ± 0.53	-19.60 ± 0.10	-19.24	-19.9	
71284	14 34 40.8171	+29 44 42.468	63.16 ± 0.26	189.10 ± 0.70	131.60 ± 0.70	0.22 ± 0.25	0.58 ± 0.43	0.60 ± 0.10	0.14	1.4	
71395*	14 36 00.5607	+09 44 47.466	60.58 ± 0.83	204.50 ± 1.10	-250.10 ± 1.10	-9.98 ± 0.10	-15.30		-9.57	-8.8	
						-9.83 ± 0.10					
						-8.11 ± 0.11					
71681†	14 39 35.0803	-60 50 13.761	796.77 ± 25.82	-3614.38 ± 20.43	803.21 ± 19.48	-22.44 ± 0.00	-25.09 ± 5.24	-25.10 ± 0.30		-18.6	Sb
71683	14 39 36.4951	-60 50 02.308	754.85 ± 4.11	-3679.27 ± 3.88	473.67 ± 3.23	-22.44 ± 0.00	-25.09 ± 5.24	-25.10 ± 0.30		-21.4	Sb
71743	14 40 31.1061	-16 12 33.444	42.24 ± 0.54	-116.10 ± 1.70	-65.10 ± 1.40	-22.66 ± 0.09	-23.30 ± 0.20	-23.30 ± 0.20			
72146	14 45 24.1821	+13 50 46.734	52.90 ± 0.83	-230.80 ± 1.00	-226.70 ± 1.00	-19.41 ± 0.11	-10.00 ± 1.00				
						-10.19 ± 0.09					
						-10.17 ± 0.16					
						-8.21 ± 0.11					
72237	14 46 23.2809	+16 29 48.135	58.02 ± 1.00	-109.47 ± 1.07	-918.87 ± 0.88	43.25 ± 0.11	42.13 ± 0.49	42.10 ± 0.10			
						44.17 ± 0.17					
72567	14 50 15.8112	+23 54 42.639	55.01 ± 0.34	144.30 ± 1.20	30.60 ± 1.10	-1.60 ± 0.09	-2.79 ± 0.43	-2.80 ± 0.10	-2.50	-3.1	
72603	14 50 41.1813	-15 59 50.053	43.38 ± 0.39	-136.40 ± 0.40	-58.96 ± 0.26	-23.47 ± 0.15	-24.63 ± 0.83	-24.70 ± 0.40			Sb
72659	14 51 23.3785	+19 06 01.656	149.03 ± 0.48	154.93 ± 0.40	-66.40 ± 0.45	1.39 ± 0.08	1.50 ± 0.20		1.30	0.4	

It follows in the next page

Table A.1 It cames from the previous page

						Radial Velocity					
HIP	α	δ	π	$\mu_\alpha \times \cos\delta$	μ_δ	*This work*	*KH*07	*NO*04	*NI*02	*VF*05	Notes
	(h,m,s)	(^{o},',")	(mas)	(mas/yr)	(mas/yr)	(km/s)	(km/s)	(km/s)	(km/s)	(km/s)	
(1)	(2)	(3)	(4)	(5)	(6)	(7)	(8)	(9)	(10)	(11)	(12)
72848	14 53 23.7664	+19 09 10.074	86.87 ± 0.46	-441.00 ± 1.20	217.10 ± 1.10	-31.27 ± 0.30	-22.18 ± 0.76	-33.40 ± 1.00	-31.81	-28.5	Sb,Cab
72875	14 53 41.5709	+23 20 42.625	42.48 ± 1.12	-824.40 ± 0.80	11.00 ± 0.80	-32.48 ± 0.10	-31.87 ± 1.30	-32.00 ± 0.50			
72981	14 54 53.4814	+09 56 36.562	40.78 ± 2.48	-313.50 ± 2.70	-402.00 ± 2.70	-1.20 ± 0.24					
73184	14 57 27.9996	-21 24 55.710	171.21 ± 0.94	1035.70 ± 1.80	-1734.90 ± 1.90	26.49 ± 0.10	26.32 ± 0.71	26.30 ± 0.10	26.96	26.0	Cab
73457	15 00 43.4112	-11 08 06.464	51.69 ± 1.97	-16.90 ± 1.30	-482.00 ± 1.30	14.24 ± 0.24	14.00				
						12.47 ± 0.28					
						14.41 ± 0.21					
73695	15 03 47.3040	+47 39 14.616	79.90 ± 1.55	-443.70 ± 1.20	9.90 ± 1.20	-17.89 ± 0.40	-29.86 ± 0.35	-30.80 ± 0.30			Sb
73786	15 04 53.5267	+05 38 17.150	53.80 ± 2.80	-606.50 ± 1.90	-508.40 ± 1.90	-84.80 ± 0.23	-68.00				
73996	15 07 18.0659	+24 52 09.104	51.14 ± 0.31	184.90 ± 0.70	-163.80 ± 0.70	-9.36 ± 0.86	-8.92 ± 3.59	-10.00 ± 5.00		-11.2	
74537	15 13 50.8948	-01 21 04.995	56.62 ± 0.49	-1270.00 ± 1.10	-502.10 ± 1.20	-69.45 ± 0.10	-69.87 ± 0.63	-69.90 ± 0.10			
74702	15 15 59.1667	+00 47 46.905	63.11 ± 0.71	178.20 ± 1.00	-136.90 ± 1.10	-4.23 ± 0.08	-3.20 ± 0.20		-3.15	-2.8	
75201	15 22 04.1017	-04 46 38.836	52.92 ± 1.60	-296.70 ± 1.60	-13.60 ± 1.50	-20.06 ± 0.23	-17.40 ± 1.10				
75253	15 22 36.6948	-10 39 40.044	45.22 ± 1.12	-57.00 ± 1.00	-203.80 ± 1.10	-5.15 ± 0.12	-6.30 ± 0.30		-6.04	-5.7	
						-6.39 ± 0.08					
75277	15 22 46.8337	+18 55 08.257	51.02 ± 0.63	-230.90 ± 1.10	77.20 ± 1.10	-7.55 ± 0.90	-10.70		-7.04	-6.6	
75542	15 25 58.5030	-26 42 20.816	41.52 ± 1.26	-818.20 ± 1.50	-8.80 ± 1.40	-133.45 ± 0.18	-133.03 ± 7.43	-133.10 ± 0.30			
75718	15 28 09.6115	-09 20 53.050	52.06 ± 1.18	76.40 ± 1.00	-359.00 ± 1.00	6.82 ± 0.04	6.48 ± 0.89	6.60 ± 0.60	7.75	8.2	Sb
75722	15 28 12.2103	-09 21 28.296	48.77 ± 0.90	80.50 ± 1.10	-355.90 ± 1.10	9.01 ± 0.09	7.21 ± 0.49	7.20 ± 0.10	7.75	8.2	
						-39.30 ± 0.08					
75809	15 29 11.1826	+80 26 54.968	45.77 ± 0.37	-223.20 ± 1.20	107.80 ± 1.20	-16.40 ± 0.14	-16.67 ± 0.57	-16.70 ± 0.10		-15.4	
						-14.39 ± 0.14					
75829	15 29 23.5924	+80 27 00.961	46.48 ± 0.49	-218.00 ± 1.20	105.80 ± 1.20	-14.59 ± 0.07	-29.00 ± 3.70	-29.00 ± 3.70		-15.4	
						-16.39 ± 0.14					
						-14.61 ± 0.14					
76051†‡	15 31 54.0449	+09 39 26.904	13.46 ± 11.21	-39.30 ± 1.60	-4.20 ± 1.60	-34.62 ± 0.15	-38.30 ± 2.20	-38.30 ± 2.20			
76375	15 35 56.5661	+39 49 52.023	44.69 ± 0.58	-447.50 ± 0.80	50.70 ± 0.90	-67.65 ± 0.13	-68.80 ± 1.20		-67.10	-66.5	
76602	15 38 39.9468	-08 47 40.970	41.02 ± 3.75	18.20 ± 2.60	-23.80 ± 2.70	-4.54 ± 0.15	0.68 ± 1.27	0.60 ± 0.30			
76603‡	15 38 40.0817	-08 47 29.364	37.57 ± 4.31	20.30 ± 2.60	-34.00 ± 2.70	-1.26 ± 0.10	-1.25 ± 2.77	-1.40 ± 1.30			Sb
76779	15 40 34.5693	-18 02 56.498	64.28 ± 1.39	161.70 ± 1.70	88.80 ± 1.60	4.55 ± 0.18					
77052	15 44 01.8197	+02 30 54.624	68.21 ± 0.66	-48.00 ± 0.80	-147.20 ± 0.80	20.36 ± 0.11	18.70 ± 0.36	18.70 ± 0.10		19.5	
77257	15 46 26.6133	+07 21 11.063	82.48 ± 0.31	-224.50 ± 0.90	-69.20 ± 0.80		-66.20 ± 0.71	-66.80 ± 0.10	-66.42	-65.3	Sb
77408	15 48 09.4630	+01 34 18.262	46.96 ± 0.80	-176.50 ± 1.10	-165.80 ± 1.00	-26.58 ± 0.80	-26.92 ± 1.26	-26.90 ± 0.20			
						-24.70 ± 0.09					
						-25.06 ± 0.12					
78072	15 56 27.1828	+15 39 41.821	88.85 ± 0.18	310.93 ± 0.20	-1282.19 ± 0.18	6.53 ± 0.31	6.40 ± 0.63	6.40 ± 0.10	6.54	7.5	
						6.46 ± 0.10					
78709	16 04 03.7132	+25 15 17.436	44.99 ± 0.79	-532.90 ± 1.00	683.00 ± 1.10	-48.15 ± 0.04	-46.74 ± 1.23	-46.80 ± 0.40			Sb
78775	16 04 56.7932	+39 09 23.433	68.88 ± 0.33	-571.90 ± 0.90	52.20 ± 1.00	-59.45	-59.88 ± 0.53	-59.90 ± 0.10	-59.43	-59.0	RV
78843	16 05 40.4714	-20 27 00.216	53.42 ± 1.23	300.20 ± 1.60	-349.10 ± 1.60	36.66 ± 0.09	36.67 ± 2.34	36.60 ± 0.30			Cab
79190	16 09 42.7934	-56 26 42.536	68.16 ± 0.64	-135.24 ± 0.62	333.39 ± 0.58	33.03 ± 0.09	36.11 ± 2.62	36.10 ± 0.20		37.5	
79492	16 13 18.4525	+13 31 36.880	42.03 ± 1.12	183.07 ± 0.94	-420.12 ± 0.93	18.27 ± 0.80	18.20 ± 1.00		18.42	16.3	
						18.97 ± 0.08					
79672	16 15 37.2703	-08 22 09.990	71.93 ± 0.37	231.10 ± 0.80	-494.60 ± 0.80	12.05 ± 0.05	11.62 ± 0.29	11.60 ± 0.10	11.75	12.2	
79755	16 16 42.7461	+67 14 19.847	93.57 ± 0.95	-493.80 ± 1.30	83.80 ± 1.30	-19.09 ± 0.20	-20.7 ± 1.40		-18.79		
80337⋆	16 24 01.2899	-39 11 34.729	78.27 ± 0.38	72.30 ± 0.70	3.30 ± 0.70		12.56 ± 0.53	12.60 ± 0.10		14.8	
80366	16 24 19.8100	-13 38 29.973	46.47 ± 1.07	-220.10 ± 1.50	-205.70 ± 1.40	6.66 ± 0.11	9.00		7.34	8.2	
80644	16 27 56.9082	+07 18 19.618	57.09 ± 1.26	-247.60 ± 1.80	-262.00 ± 1.80	-36.72 ± 0.15	-32.10 ± 2.90		-36.21		

It follows in the next page

Table A.1 It cames from the previous page

						Radial Velocity					
HIP	α (h,m,s)	δ (^{o},',")	π (mas)	$\mu_\alpha \times \cos\delta$ (mas/yr)	μ_δ (mas/yr)	*Thiswork* (km/s)	*KH*07 (km/s)	*NO*04 (km/s)	*NI*02 (km/s)	*VF*05 (km/s)	Notes
(1)	(2)	(3)	(4)	(5)	(6)	(7)	(8)	(9)	(10)	(11)	(12)
80686	16 28 28.1435	-70 05 03.843	82.54 ± 0.52	197.80 ± 0.70	111.50 ± 0.70	7.60	5.48 ± 3.01	4.80 ± 2.10			Sb,Cab
80725	16 28 52.6657	+18 24 50.597	50.96 ± 0.80	-339.90 ± 1.20	383.30 ± 1.30	-31.45 ± 0.13	-31.90 ± 0.60				
81300	16 36 21.4493	-02 19 28.501	102.55 ± 0.41	455.00 ± 0.70	-308.10 ± 0.70	-12.73 ± 0.06	-13.27 ± 0.29	-13.30 ± 0.10	-12.86	-12.7	
81375	16 37 08.4277	+00 15 15.631	49.18 ± 0.62	92.40 ± 0.90	74.60 ± 1.10	9.68 ± 0.70	6.00		10.39	10.8	
82588	16 52 58.8026	-00 01 35.116	57.96 ± 0.66	-709.30 ± 1.40	-1483.70 ± 1.40	45.08 ± 0.90	44.80 ± 0.29	44.80 ± 0.10	45.07	45.5	
						44.57 ± 0.11					
83591	17 05 03.3941	-05 03 59.427	93.41 ± 0.94	-915.60 ± 0.70	-1139.20 ± 0.80	33.69 ± 0.14	33.60 ± 0.71	33.60 ± 0.10	34.15		
83601	17 05 16.8193	+00 42 09.213	48.39 ± 0.40	-16.80 ± 0.90	-334.80 ± 0.90	-15.44 ± 0.10	-17.01 ± 0.53	-17.00 ± 0.10	-16.74	-16.3	
84195	17 12 37.6225	+18 21 04.295	47.70 ± 0.93	101.90 ± 1.10	-117.50 ± 1.00	19.20 ± 0.11	20.10 ± 0.90				
						19.32 ± 0.08					
84478	17 16 13.3626	-26 32 46.128	167.50 ± 0.61	-480.40 ± 0.90	-1123.30 ± 0.90	-0.59 ± 0.13	-0.49 ± 0.71	-0.50 ± 0.10	0.15		
84720	17 19 03.8337	-46 38 10.444	113.67 ± 0.69	1053.50 ± 2.10	144.00 ± 2.00	-13.14 ± 0.07	23.0	25.3 ± 0.10			
84862	17 20 39.5672	+32 28 03.876	69.80 ± 0.25	135.80 ± 0.70	-1039.90 ± 0.70	-78.44 ± 0.07	-78.96 ± 0.16	-79.20 ± 0.10	-78.55	-78.5	
85235	17 25 00.0985	+67 18 24.137	78.11 ± 0.30	-529.40 ± 1.20	2.10 ± 1.30	-38.53 ± 0.05	-39.09 ± 0.43	-39.10 ± 0.10		-35.7	
85295	17 25 45.2321	+02 06 41.120	129.87 ± 0.73	-579.10 ± 0.90	-1183.20 ± 1.00	-24.21 ± 0.11	-24.40 ± 1.34	-24.40 ± 0.10	-23.20		
85561	17 29 06.5570	-23 50 10.020	53.04 ± 1.73	-289.90 ± 2.40	-74.70 ± 2.30	-32.90 ± 0.18	-106.00				
85810	17 32 00.9926	+34 16 16.128	41.81 ± 0.35	-240.00 ± 1.30	63.30 ± 1.50	-51.60	-51.80 ± 0.16	-52.00 ± 0.10	-51.61	-51.3	RV
86036	17 34 59.5940	+61 52 28.394	70.48 ± 0.38	265.40 ± 3.30	-520.90 ± 3.20	-16.30	-14.85 ± 0.20	-14.60 ± 0.20			Sb
86346[‡]	17 38 39.6261	+61 14 16.125	30.19 ± 2.00	-21.80 ± 3.00	43.70 ± 3.00	-25.69 ± 0.35					
						-26.48 ± 0.37					
						-26.56 ± 0.37					
						-26.66 ± 0.42					
						-27.99 ± 0.28					
						-28.37 ± 0.51					
						-28.39 ± 0.35					
						-25.37 ± 0.45					
						-27.84 ± 0.36					
						-27.65 ± 0.44					
86400	17 39 16.9159	+03 33 18.860	90.91 ± 0.68	-178.50 ± 0.70	-99.80 ± 0.70	21.19 ± 0.08	20.46 ± 0.75	19.90 ± 0.70	15.95		Sb,Cab
86722	17 43 15.6433	+21 36 33.153	44.14 ± 0.88	-123.10 ± 1.10	-628.00 ± 1.00	23.88 ± 0.04	25.58 ± 0.89	26.50 ± 0.60	23.95		Sb
87579	17 53 29.9367	+21 19 31.050	41.05 ± 1.04	-71.40 ± 1.00	57.00 ± 0.90	-13.77 ± 0.10	-12.70 ± 0.90				
88601	18 05 27.2855	+02 30 00.358	196.66 ± 0.84	276.30 ± 2.30	-1091.80 ± 2.30	-6.97 ± 0.10	-9.30 ± 0.63	-10.40 ± 0.50			Sb
88622	18 05 37.4564	+04 39 25.822	41.81 ± 0.59	-26.00 ± 1.10	-316.70 ± 1.10	-119.09 ± 0.10	-119.88 ± 0.72	-119.90 ± 0.20			
88972	18 09 37.4165	+38 27 27.997	90.71 ± 0.30	-318.90 ± 1.40	-467.80 ± 1.40	-19.64 ± 0.07	-19.92 ± 0.22	-20.00 ± 0.10	-19.42	-19.1	
						-19.41 ± 0.04					
89937	18 21 03.3826	+72 43 58.235	124.10 ± 0.87	531.21 ± 1.03	-349.71 ± 0.94	32.02 ± 0.26	32.43 ± 0.82	32.40 ± 0.60			Sb
90656	18 29 52.4073	-01 49 05.173	53.72 ± 0.91	173.30 ± 0.80	-193.50 ± 0.90	-54.81 ± 0.12	-55.68 ± 0.57	-55.70 ± 0.10	-54.75	-54.1	
90790	18 31 18.9597	-18 54 31.722	75.47 ± 0.70	-138.80 ± 1.10	-195.50 ± 1.10	-43.14 ± 0.06	-44.10 ± 1.30		-43.13	-42.8	
91009	18 33 55.7728	+51 43 08.905	61.15 ± 0.68	186.00 ± 1.30	-325.90 ± 1.30	-24.50	-24.50				Sb,Cab
91438	18 38 53.4005	-21 03 06.736	76.42 ± 0.46	-74.10 ± 0.70	-152.50 ± 0.70		36.71 ± 0.29	36.60 ± 0.10	37.10	37.4	
92043	18 45 39.7254	+20 32 46.708	52.06 ± 0.24	-9.00 ± 0.30	-336.20 ± 0.40	22.59 ± 0.27	22.48 ± 0.45	22.40 ± 0.20	23.04	24.0	
92200	18 47 27.2503	-03 38 23.391	70.05 ± 1.17	-132.60 ± 1.20	-276.30 ± 1.20	15.21 ± 0.19	16.20 ± 1.50		15.54		
92283	18 48 29.2256	+10 44 43.620	59.31 ± 0.83	126.90 ± 1.30	-437.20 ± 1.20	-7.57 ± 0.09	-7.71 ± 1.83	-7.70 ± 0.10		-6.1	
93017	18 57 01.6105	+32 54 04.585	67.25 ± 0.37	201.96 ± 0.28	-145.47 ± 0.35	-45.82 ± 0.69	-48.20 ± 0.25	-48.60 ± 0.20			Sb
93871	19 07 02.0420	+07 36 57.156	40.35 ± 1.41	-321.70 ± 1.30	-761.80 ± 1.40	8.53 ± 0.19	12.00				
94346	19 12 11.3578	+57 40 19.133	49.96 ± 0.32	217.50 ± 0.90	408.60 ± 0.90	-27.22 ± 0.05	-26.50 ± 1.00				
95319[★]	19 23 34.0126	+33 13 19.078	63.44 ± 0.35	79.30 ± 1.20	162.40 ± 1.20	-21.55	-21.70 ± 0.16	-22.00 ± 0.10	-21.51	-21.2	RV
95995	19 31 07.9736	+58 35 09.637	58.94 ± 0.64	-508.90 ± 0.90	-396.80 ± 1.00	11.40	11.80 ± 0.10	11.80 ± 0.10			Sb

It follows in the next page

Table A.1 It cames from the previous page

						Radial Velocity					
HIP	α	δ	π	$\mu_\alpha \times \cos\delta$	μ_δ	*Thiswork*	*KH*07	*NO*04	*NI*02	*VF*05	Notes
	(h,m,s)	(^{o},',")	(mas)	(mas/yr)	(mas/yr)	(km/s)	(km/s)	(km/s)	(km/s)	(km/s)	
(1)	(2)	(3)	(4)	(5)	(6)	(7)	(8)	(9)	(10)	(11)	(12)
96085	19 32 06.7047	-11 16 29.792	56.72 ± 0.72	236.70 ± 1.10	18.60 ± 1.10	-48.83 ± 0.09	-49.26 ± 0.16	-49.50 ± 0.20	-48.86	-48.3	
96100	19 32 21.5908	+69 39 40.232	173.77 ± 0.18	599.20 ± 1.90	-1734.70 ± 2.00	26.58 ± 0.04	26.64 ± 0.16	26.30 ± 0.10	26.69	26.9	
96183	19 33 25.5531	+21 50 25.186	48.63 ± 0.63	-21.30 ± 0.90	-204.70 ± 0.90	10.70 ± 0.80	11.00 ± 2.83	11.00 ± 0.10	11.41	11.7	
96285	19 34 39.8401	+04 34 57.059	69.32 ± 1.55	524.50 ± 1.40	311.30 ± 1.40	-59.10 ± 0.24	-56.80 ± 1.20				
97944	19 54 17.7456	-23 56 27.854	71.17 ± 0.42	-123.10 ± 0.70	-410.40 ± 0.70	-5.10	-5.70 ± 3.37	-6.10 ± 1.00			Sb
98677	20 02 34.1558	+15 35 31.471	52.70 ± 0.65	-161.70 ± 1.40	-581.10 ± 1.30	19.68 ± 0.80	20.00 ± 1.48	20.00 ± 0.10	20.39	21.0	
98698	20 02 47.0447	+03 19 34.278	77.75 ± 0.53	-88.20 ± 1.10	121.60 ± 1.10	-31.19 ± 0.11	-28.90 ± 1.20		-30.30		
98819	20 04 06.2247	+17 04 12.624	56.28 ± 0.35	-392.50 ± 1.10	-407.60 ± 1.00	3.89 ± 0.90 5.39 ± 0.07 4.13 ± 0.13	4.88 ± 0.22	4.80 ± 0.10	4.76	4.2	
98828	20 04 10.0452	+25 47 24.827	45.54 ± 0.77	-76.20 ± 1.20	-39.30 ± 1.10	-7.58 ± 0.10	-7.10 ± 1.40				
99240	20 08 43.6084	-66 10 55.446	163.71 ± 0.17	1211.20 ± 0.90	-1131.00 ± 0.90		-21.90 ± 0.53	-21.90 ± 0.10		-19.3	
99316	20 09 34.3037	+16 48 20.757	42.30 ± 0.99	3.90 ± 1.40	167.90 ± 1.40	-31.10 ± 0.12	-32.60				
99452	20 11 06.0744	+16 11 16.799	49.07 ± 0.65	-413.10 ± 1.20	398.20 ± 1.10	-49.78 ± 0.80	-49.00 ± 0.70		-49.29	-49.0	
99461	20 11 11.9381	-36 06 04.366	166.24 ± 0.27	458.40 ± 1.10	-1569.30 ± 1.10		-129.41 ± 0.53	-129.40 ± 0.10		-126.9	
99711*	20 13 59.8451	-00 52 00.757	51.76 ± 0.78	-62.70 ± 0.90	262.00 ± 1.10	-20.58 ± 0.80	-11.30 ± 13.44	-11.30 ± 0.20	-10.74	-10.1	
99764	20 14 28.1911	-07 16 55.110	49.33 ± 1.45	12.50 ± 2.20	-270.70 ± 2.40	7.07 ± 0.22					
99825	20 15 17.3909	-27 01 58.716	112.23 ± 0.30	1241.90 ± 0.70	-180.80 ± 0.70		-54.73 ± 0.38	-54.80 ± 0.20		-55.1	
101345	20 32 23.6956	-09 51 12.181	40.97 ± 0.33	307.20 ± 0.70	103.70 ± 0.70	8.93 ± 0.08	9.40 ± 1.91	9.40 ± 0.10	9.54	10.0	
101955	20 39 37.7092	+04 58 19.265	59.80 ± 3.42	873.90 ± 1.60	90.60 ± 1.50	-39.20	-41.90 ± 1.20				Sb
101997	20 40 11.7558	-23 46 25.923	69.54 ± 0.40	500.20 ± 0.90	460.80 ± 0.90	-41.82 ± 0.06	-42.11 ± 2.62	-42.10 ± 0.20	-41.99	-41.6	
102485	20 46 05.7330	-25 16 15.231	68.13 ± 0.27	-51.95 ± 0.24	-156.56 ± 0.21		25.59 ± 2.74	20.30 ± 3.80			
103256	20 55 06.8608	+13 10 36.307	44.62 ± 0.94	552.10 ± 1.30	377.40 ± 1.20	-41.65 ± 0.13	-38.20 ± 1.10				
104092	21 05 19.7454	+07 04 09.474	66.41 ± 0.95	80.10 ± 1.30	-564.20 ± 1.30	-66.85 ± 0.15	-67.47 ± 0.71	-67.50 ± 0.10			
104214	21 06 53.9434	+38 44 57.898	286.83 ± 6.77	4168.30 ± 6.56	3269.11 ± 12.07	-64.82 ± 0.09 -66.10 ± 0.08	-66.46 ± 0.49	-66.50 ± 0.10	-65.73		
104217	21 06 55.2648	+38 44 31.400	285.89 ± 0.55	4117.10 ± 2.00	3128.00 ± 2.00	-64.17 ± 0.15 -63.61 ± 0.15	-64.90 ± 0.10	-65.30 ± 0.10	-64.02		
104239	21 07 10.3807	-13 55 22.547	56.89 ± 0.60	382.30 ± 0.90	-39.90 ± 0.80	-33.27 ± 0.10	-34.00 ± 2.10			-32.1	
104858	21 14 28.8152	+10 00 25.132	54.09 ± 0.66	39.70 ± 1.30	-304.20 ± 1.20	-15.80	-16.16 ± 0.74	-16.20 ± 0.30			Sb
105038	21 16 32.4674	+09 23 37.772	61.02 ± 0.89	143.40 ± 1.60	-116.70 ± 1.60	-18.23 ± 0.12	-18.78 ± 0.91	-18.80 ± 0.10	-18.07	-17.3	
105152	21 18 02.9749	+00 09 41.686	50.46 ± 1.04	467.70 ± 1.00	-187.50 ± 1.00	-27.43 ± 0.11	-28.09 ± 0.91	-28.10 ± 0.10	-27.43	-26.9	
105858	21 26 26.6056	-65 21 58.314	107.98 ± 0.19	80.57 ± 0.12	800.59 ± 0.14	-31.83 ± 0.07	-29.65 ± 0.20	-29.90 ± 0.20			
106147	21 30 02.7534	-12 30 36.252	54.34 ± 1.18	1020.20 ± 1.20	-259.40 ± 1.20	-84.32 ± 0.23	-81.00 ± 1.60		-84.19		
106400	21 33 01.0691	+62 00 08.824	43.02 ± 0.96	371.80 ± 2.10	193.50 ± 2.00	-11.14 ± 0.10	-10.50 ± 0.60				
107310	21 44 08.5777	+28 44 33.476	45.06 ± 0.43	277.40 ± 2.70	-251.10 ± 2.60	18.11 ± 0.22 15.86 ± 0.44	16.80 ± 0.30	16.20 ± 0.30			
107350	21 44 31.3299	+14 46 18.981	55.92 ± 0.45	231.20 ± 1.20	-113.90 ± 1.10	-15.70 ± 0.09 -15.08 ± 0.15	-17.13 ± 0.22	-17.20 ± 0.10	-16.83	-16.2	
108028	21 53 05.3528	+20 55 49.863	43.41 ± 0.75	-4.30 ± 0.90	-100.80 ± 0.90	3.84 ± 0.80					
108156	21 54 45.0401	+32 19 42.851	50.12 ± 0.80	209.30 ± 1.60	-233.30 ± 1.50	-13.96 ± 0.10	-15.40 ± 0.90		-13.25	-12.5	
109176	22 07 00.6661	+25 20 42.402	85.29 ± 0.63	297.40 ± 0.50	26.40 ± 0.50	-5.50	-5.52 ± 12.88	-14.80 ± 18.20			Sb
109378*	22 09 29.8657	-07 32 55.155	46.38 ± 0.48	83.90 ± 0.80	-450.60 ± 0.80	-19.35 ± 0.06	-22.30 ± 0.70		-20.87	-20.4	
109527	22 11 11.9133	+36 15 22.787	43.65 ± 0.53	27.20 ± 1.50	-251.90 ± 1.50	-19.55 ± 0.09	-19.80 ± 1.20		-19.44	-19.0	
110109	22 18 15.6152	-53 37 37.465	72.53 ± 0.36	436.80 ± 0.90	-632.80 ± 0.90	-12.62 ± 0.04	-13.03 ± 0.58	-13.00 ± 0.20			
110778	22 26 34.2753	-16 44 31.697	49.32 ± 1.21	251.10 ± 4.30	-20.60 ± 4.50	4.84 ± 0.12	1.86 ± 1.01	2.10 ± 0.30			
111449	22 34 41.6369	-20 42 29.577	44.09 ± 0.26	221.40 ± 0.70	-145.50 ± 0.70		-3.44 ± 0.80	-5.20 ± 0.90			
111888	22 39 50.7668	+04 06 58.015	41.51 ± 0.77	180.40 ± 1.20	110.40 ± 1.20	14.15 ± 0.10	23.80 ± 0.90				

It follows in the next page

Table A.1 It cames from the previous page

						Radial Velocity					
HIP	α (h,m,s)	δ (^{o},',")	π (mas)	$\mu_\alpha \times \cos\delta$ (mas/yr)	μ_δ (mas/yr)	*Thiswork* (km/s)	*KH*07 (km/s)	*NO*04 (km/s)	*NI*02 (km/s)	*VF*05 (km/s)	Notes
(1)	(2)	(3)	(4)	(5)	(6)	(7)	(8)	(9)	(10)	(11)	(12)
112190	22 43 21.3025	-06 24 02.956	46.47 ± 0.90	-152.60 ± 1.20	-289.40 ± 1.30	-13.86 ± 0.70	-14.10 ± 0.80		-13.80		
112447	22 46 41.5806	+12 10 22.396	61.37 ± 0.20	233.60 ± 0.90	-492.20 ± 0.90	-5.41 ± 0.10	-6.08 ± 0.71	-6.10 ± 0.10	-5.86	-4.5	
112870	22 51 26.3576	+13 58 11.937	46.97 ± 1.01	405.10 ± 0.80	202.60 ± 0.80	1.02 ± 0.13	-1.90 ± 1.30		1.29	-2.1	
113357⋆	22 57 27.9805	+20 46 07.796	64.09 ± 0.38	207.90 ± 0.70	59.80 ± 0.60	-31.32 ± 0.05	-33.69 ± 0.22	-33.70 ± 0.10	-33.23	-32.4	
113576	23 00 16.1209	-22 31 27.648	121.68 ± 0.69	-900.10 ± 1.50	58.60 ± 1.50	16.31 ± 0.18	15.31 ± 0.78	15.30 ± 0.10	16.42		
113718	23 01 51.5444	-03 50 55.444	58.71 ± 0.92	397.50 ± 0.90	-208.20 ± 1.00	-44.73 ± 0.05	-44.70 ± 1.00				Sb
114622	23 13 16.9754	+57 10 06.078	152.77 ± 0.29	2074.50 ± 0.70	295.40 ± 0.70	-17.52 ± 0.07	-19.10 ± 2.26	-19.10 ± 0.10	-18.56	-19.2	
						-18.59 ± 0.07					
						-18.47 ± 0.05					
						-18.40 ± 0.07					
114886	23 16 18.1579	+30 40 12.746	41.64 ± 0.72	358.30 ± 1.10	90.20 ± 1.00	9.88 ± 0.15	8.30 ± 2.20		9.99	10.1	
115331	23 21 36.5128	+44 05 52.378	46.47 ± 0.53	636.20 ± 0.80	218.70 ± 0.90	3.37 ± 0.09	3.03 ± 0.29	3.00 ± 0.10			
115341	23 21 44.4519	+45 10 33.807	48.82 ± 0.93	195.90 ± 1.10	-71.00 ± 1.10	-13.86 ± 0.12					
115445	23 23 04.8947	-10 45 51.278	52.27 ± 0.86	452.40 ± 0.80	260.60 ± 0.80	35.06 ± 0.12	33.41 ± 1.25	33.40 ± 0.10	34.00	34.4	
116613	23 37 58.4882	+46 11 57.972	42.85 ± 0.42	356.90 ± 1.20	-12.00 ± 1.20	-0.65 ± 0.09	-0.30 ± 0.51	-0.30 ± 0.20	-0.17	0.2	
116771	23 39 57.0409	+05 37 34.650	72.91 ± 0.15	376.30 ± 0.30	-436.50 ± 0.30	5.55 ± 0.03	5.39 ± 0.53	5.40 ± 0.10	5.66	6.6	
117712	23 52 25.3197	+75 32 40.518	91.82 ± 0.30	325.80 ± 1.00	45.60 ± 1.10	1.70	4.50 ± 2.62	4.50 ± 0.10			Sb,Cab
120005	09 14 24.6984	+52 41 10.954	156.20 ± 8.63	-1560.80 ± 0.80	-660.60 ± 0.90	13.17 ± 0.32	12.00 ± 0.10	11.90 ± 0.10	12.50		

† Star with uncertainty in the parallax larger than 10 milliarcsec

⋆ Star with known planets

Table A.2: Membership criteria for the Local Association candidate stars. (Convergence Point: 5.98 hours, -35.15 degrees; U =-11.6 km/s, V = -21.0 km/s, W = -11.4 km/s; Age: 20-150 Myr)

		Kinematics							Lithium	CaII H,K		ROSAT-data		Rotation		
HIP	$(B-V)$	U (km/s)	V (km/s)	W (km/s)	V_{Total} (km/s)	V_T (km/s)	$PV^\star$ (km/s)	$\rho_c^\star$ (km/s)	EW(LiI) (mÅ)	R'_{HK} (log)	Age (Gyr)	L_X/L_{Bol} (log)	Age (Gyr)	Prot (days)	Age (Gyr)	[Fe/H]
(1)	(2)	(3)	(4)	(5)	(6)	(7)	(8)	(9)	(10)	(11)	(12)	(13)	(14)	(15)	(16)	(17)
Probable Non-members																
3979	0.68	-15.58 ± 0.32	-25.43 ± 0.42	-0.53 ± 0.18	29.83	29.83	5.48 Y	-7.01 Y	35.84 ± 3.72	-4.92 [4]	5.04					-0.19
7751	0.88	-4.19 ± 0.16	-18.73 ± 0.14	-18.60 ± 0.07	26.72	15.16	-0.06 Y	10.19 N	2.14 ± 4.65	-4.94 [1]	5.49			30 [13]	3.46	-0.23
12929	1.18	-14.65 ± 0.21	-22.21 ± 0.58	-8.39 ± 0.12	27.90	27.82	4.30 Y	11.59 Y	34.29 ± 6.13	-4.57 [3]	0.97					
26779	0.84	-13.82 ± 0.10	-23.07 ± 0.18	-14.40 ± 0.13	30.50	30.44	-1.69 Y	0.68 Y	13.54 ± 4.49	-4.55 [1]	0.84	-4.72	0.66	11 [2]	0.62	0.16
69357	0.86	-10.90 ± 0.42	-33.09 ± 0.98	-1.65 ± 0.19	34.88	36.13	5.33 Y	11.26 N	21.43 ± 4.56	-4.60 [1]	1.14	-5.34	2.02			-0.15
79755	1.32	-9.71 ± 0.15	-29.99 ± 0.22	3.82 ± 0.22	31.75	32.24	-17.23 N	-26.32 N		-4.58 [3]	1.03	-4.72	2.45			
108156	0.93	-2.70 ± 0.16	-21.94 ± 0.18	-24.19 ± 0.49	32.77	35.10	-13.76 N	-23.30 N	18.73 ± 4.88	-4.68 [1]	1.79	-5.33	2.04			-0.08
115341	1.06	-9.89 ± 0.30	-20.49 ± 0.19	-9.14 ± 0.28	24.52	23.37	0.44 Y	-11.71 Y	18.15 ± 5.52	-4.73 [1]	2.31	-4.75	0.99			
Doubtful Members																
19422	0.96	-7.92 ± 0.26	-23.86 ± 0.23	-17.19 ± 0.22	30.46	28.17	-4.37 Y	-8.04 Y	4.54 ± 5.02	-4.86 [3]	4.08					-0.06
37288	1.40	-12.25 ± 0.17	-22.15 ± 0.27	-12.50 ± 0.39	28.23	28.58	0.31 Y	20.51 Y	43.42 ± 7.27	-4.72 [3]	2.2					
57494	1.17	-14.43 ± 0.52	-26.95 ± 0.44	3.59 ± 0.33	30.78	23.66	6.46 N	3.76 N	14.26 ± 6.09	-4.80 [1]	3.2					
62523	0.71	-18.16 ± 0.20	-21.36 ± 0.23	-8.35 ± 0.05	29.25	30.17	5.74 Y	-12.14 Y	22.48 ± 3.85	-4.43 [1]	0.37	-5.08	0.83			0.08
72146	0.93	-6.08 ± 0.09	-30.02 ± 0.48	-6.84 ± 0.10	31.38	38.31	-4.74 Y	-25.49 N	8.69 ± 4.89	-4.84 [1]	3.72					
73695	0.59	-17.06 ± 0.32	-26.77 ± 0.41	-2.37 ± 0.42	31.83	46.30	-1.67 Y	-38.12 N	29.62 ± 3.30	-4.60 [3]	1.16	-3.96	0.12			-0.19
105038	1.04	-10.74 ± 0.16	-20.02 ± 0.16	-4.74 ± 0.25	23.21	18.27	-0.34 Y	-11.30 N	12.14 ± 5.40	-4.69 [1]	1.89					-0.10
Probable Members																
544	0.75	-15.02 ± 0.15	-21.38 ± 0.14	-10.12 ± 0.12	28.02	27.92	3.44 Y	-7.12 Y	79.89 ± 4.05	-4.320 [3]	0.16	-4.35	0.32			0.12
7576	0.79	-13.31 ± 0.25	-18.41 ± 0.42	-11.14 ± 0.12	25.31	24.45	2.34 Y	9.95 Y	117.41 ± 4.25	-4.29 [1]	0.13	-4.43	0.44			-0.03
13402	0.88	-15.30 ± 0.07	-21.81 ± 0.11	-9.21 ± 0.06	28.19	28.78	4.06 Y	19.44 Y	182.52 ± 4.63	-4.33 [1]	0.17	-4.12	0.30	6.6 [12]	0.24	0.10
18859	0.51	-7.98 ± 0.18	-28.15 ± 0.21	-11.89 ± 0.15	31.58	37.55	-1.77 Y	26.94 N	96.79 ± 2.98	-4.291 [4]	0.13	-4.16	0.12			-0.01
46843	0.79	-9.93 ± 0.13	-22.89 ± 0.26	-5.64 ± 0.18	25.58	24.18	-4.59 Y	4.17 Y	192.41 ± 4.24	-4.08 [1]	0.02	-3.93	0.22	6 [2]	0.23	
54155	0.79	-15.14 ± 0.38	-28.39 ± 0.44	-0.70 ± 0.42	32.18	26.27	2.33 Y	6.12 N	103.69 ± 4.22	-4.34 [1]	0.18	-3.65	0.12			-0.09
54745	0.62	-16.07 ± 0.23	-23.41 ± 0.29	-11.04 ± 0.12	30.47	30.87	1.94 Y	-6.30 Y	88.31 ± 3.44	-4.27 [1]	0.11	-4.52	0.29	7.6 [12]	0.59	0.08
63742	0.86	-8.87 ± 0.15	-23.28 ± 0.51	-19.50 ± 0.22	31.64	29.87	-6.54 N	-5.26 Y	140.60 ± 4.56	-4.34 [4]	0.19	-4.25	0.38			
65515	0.81	-15.76 ± 0.24	-18.47 ± 0.18	-8.52 ± 0.08	25.73	29.12	2.85 Y	-18.87 N	39.95 ± 4.33	-4.22 [1]	0.07	-4.36	0.36			-0.10
75809	0.65	-14.73 ± 0.22	-25.95 ± 0.17	-2.33 ± 0.14	29.93	32.31	-9.56 N	-21.82 N	141.10 ± 3.59	-4.41 [1]	0.32	-4.01	0.15			-0.29
75829	0.78	-14.16 ± 0.26	-25.03 ± 0.18	-2.30 ± 0.14	28.85	31.11	-9.19 N	-21.02 N	127.81 ± 4.19	-4.41 [4]	0.31	-3.79	0.15			0.07
77408	0.80	-17.81 ± 0.10	-27.25 ± 0.44	-12.44 ± 0.13	34.85	34.04	3.56 Y	-23.96 Y	10.37 ± 4.30	-4.35 [1]	0.2	-4.40	0.43			-0.05
86346	1.18	-6.86 ± 0.68	-24.72 ± 0.30	-11.76 ± 0.46	28.22	16.54	-2.27 Y	-14.83 N	28.19 ± 6.25	-3.96 [11]		-2.90	0.10†	1.8 [14]		
107350	0.59	-13.92 ± 0.13	-20.05 ± 0.10	-11.10 ± 0.18	26.81	26.73	2.55 Y	-15.61 Y	91.91 ± 3.30	-4.48 [1]	0.53	-4.40	0.24	4.7 [12]	0.3	-0.01

† Upper limit

⋆ 'Y', 'N' labels indicate if the star satisfies or not the criteria.

Table A.3: Membership criteria for the Hyades candidate stars. (Convergence Point: 6.40 hours, 6.50 degrees; U =-39.7 km/s, V = -17.7 km/s, W = -2.4 km/s; Age: 600 Myr)

		Kinematics							Lithium	CaII H,K		ROSAT-data		Rotation		
HIP	$(B-V)$	U (km/s)	V (km/s)	W (km/s)	V_{Total} (km/s)	V_T (km/s)	$PV^\star$ (km/s)	$\rho_c^\star$ (km/s)	EW(LiI) (mÅ)	R'_{HK} (log)	Age (Gyr)	L_X/L_{Bol} (log)	Age (Gyr)	Prot (days)	Age (Gyr)	[Fe/H]
(1)	(2)	(3)	(4)	(5)	(6)	(7)	(8)	(9)	(10)	(11)	(12)	(13)	(14)	(15)	(16)	(17)
Probable Non-members																
4148	0.90	-36.34 ± 0.32	-20.72 ± 0.20	6.50 ± 0.06	42.33	41.64	-4.63 N	-2.13 Y		-4.83 [1]	3.64	-5.22	2.04			-0.15
17420	0.93	-30.35 ± 0.18	-14.81 ± 0.12	-4.58 ± 0.16	34.08	31.28	-0.89 Y	21.33 Y	4.20 ± 4.91	-5.04 [1]	7.35	-5.04	1.45			-0.12
19335	0.52	-33.23 ± 0.26	-15.64 ± 0.23	-8.05 ± 0.16	37.60	36.64	-6.08 N	26.37 Y	93.12 ± 3.01	-4.401 [2]	0.30	-4.40	0.16	2.6 [12]	0.22	0.07
40035	0.49	-37.17 ± 0.16	-19.18 ± 0.13	-12.77 ± 0.16	43.73	45.72	-10.54 N	38.19 Y	31.97 ± 2.88	-4.81 [5]	3.27					-0.22
43726	0.67	-40.82 ± 0.19	-20.43 ± 0.08	-11.53 ± 0.20	47.08	52.25	-7.81 N	40.40 N	31.42 ± 3.66	-4.66 [2]	1.60	-5.25	0.89	15 [2]	0.16	0.09
47592	0.52	-40.79 ± 0.14	-27.27 ± 0.09	6.96 ± 0.09	49.56	40.25	4.49 N	21.86 N	28.83 ± 3.01	-4.86 [5]	4.14					-0.05
66147	1.02	-42.27 ± 0.72	-20.27 ± 0.40	4.78 ± 0.20	47.12	48.65	0.86 Y	-13.46 N	7.38 ± 5.34	-4.70 [1]	1.99	-4.89	1.28			0.07
67275	0.50	-34.92 ± 0.13	-19.03 ± 0.07	-11.90 ± 0.30	41.51	37.27	-4.35 N	-11.29 N	2.73 ± 2.91	-4.90 [1]	4.78	-5.12	0.36	4 [2]		0.25
90790	0.86	-38.06 ± 0.07	-24.73 ± 0.15	5.31 ± 0.07	45.69	50.10	-10.42 N	-48.90 Y	1.64 ± 4.56	-4.90 [1]	4.78	-5.23	1.81			-0.15
Doubtful Members																
18774	1.12	-48.75 ± 0.44	-17.60 ± 0.36	-7.18 ± 0.18	52.33	51.33	-5.37 N	15.56 Y		-4.56 [1]	0.90	-5.23	2.74			
21482	1.08	-39.25	-17.55	-1.59	43.02	43.50	0.67 Y	36.58 Y	42.40 ± 5.60	-4.06 [4]	0.01	-3.01	0.09			
25220	1.10	-38.68 ± 0.10	-14.25 ± 0.21	6.81 ± 0.28	41.77	44.58	9.34 N	42.33 Y	13.25 ± 5.69	-4.13 [1]	0.03	-4.62	1.15			
43587	0.86	-37.07 ± 0.17	-18.04 ± 0.11	-7.70 ± 0.23	41.94	47.93	-0.55 Y	35.99 N	34.60 ± 4.58	-5.10 [4]						0.35
44248	0.45	-44.62	-14.29	-9.63	47.83	50.80	7.55 N	33.02 Y	18.80 ± 2.73	-4.55 [4]	0.83	-5.21	0.30			0.13
48411	1.22	-44.17 ± 0.84	-19.52 ± 0.14	-7.99 ± 0.65	48.95	52.39	-2.47 Y	32.29 N	37.12 ± 6.32	-4.68 [4]	1.77					
63257	1.06	-37.22 ± 1.32	-17.31 ± 0.81	-2.20 ± 0.17	41.11	41.18	-0.49 Y	-6.97 Y		-4.78 [5]	2.93					
69526	1.07	-36.30 ± 0.62	-14.54 ± 0.24	-5.67 ± 0.26	39.51	38.12	1.95 Y	-12.93 Y	12.10 ± 5.57	-4.28 [1]	0.12	-4.88	1.38			
96085	0.92	-50.34 ± 0.14	-14.85 ± 0.13	-4.80 ± 0.23	52.71	62.49	6.43 N	-59.60 N		-4.52 [1]	0.69					-0.06
Probable Members																
1803	0.65	-36.58 ± 0.45	-14.94 ± 0.20	-0.15 ± 0.10	39.52	39.40	1.72 Y	-1.13 Y	67.36 ± 3.61	-4.36 [1]	0.22	-4.59	0.34	7.7 [12]	0.52	0.22
12709	1.08	-47.52	-15.55	-3.70	50.13	46.75	2.77 Y	26.78 Y	21.09 ± 5.63	-4.48 [4]	0.52	-4.53	0.83			
13976	0.94	-43.59 ± 0.71	-19.85 ± 0.77	-0.38 ± 0.62	47.90	49.55	0.85 Y	31.46 Y		-4.40 [1]	0.30	-4.72	0.75	10.2 [14]		0.18
16134	1.27	-46.71 ± 0.40	-19.24 ± 0.18	-7.47 ± 0.30	51.06	47.04	1.80 Y	29.81 Y	19.12 ± 6.54	-4.61 [1]	1.21	-4.29	0.98			
42074	0.81	-36.00 ± 0.24	-20.75 ± 0.12	-1.08 ± 0.27	41.56	35.84	-2.61 Y	29.93 N	15.34 ± 4.34	-4.454 [4]	0.44	-4.76	0.69			0.03
42333	0.64	-43.52 ± 0.42	-19.37 ± 0.17	-12.32 ± 0.45	49.20	57.06	-7.33 N	46.20 N	46.42 ± 3.56	-4.40 [1]	0.30	-4.78	0.46			0.04
46580	1.00	-41.11	-13.60	-0.27	43.30	43.08	4.77 N	29.81 Y	6.68 ± 5.23	-4.50 [1]	0.61	-4.65	0.94	13.6 [13]		-0.04
72848	0.83	-36.20 ± 0.19	-13.45 ± 0.10	-14.34 ± 0.27	41.20	31.56	2.39 Y	-16.80 N	11.00 ± 4.44	-4.52 [1]	0.69	-4.77	0.69			0.09
94346	0.80	-44.05 ± 0.30	-22.10 ± 0.06	-15.52 ± 0.10	51.67	46.88	-11.21 N	-19.88 N	5.13 ± 4.29	-4.52 [10]	0.69	-4.68	0.56			
104239	0.89	-42.25 ± 0.25	-17.98 ± 0.08	-4.90 ± 0.29	46.18	49.04	0.16 Y	-37.14 Y	10.84 ± 4.69	-4.496 [3]	0.59	-4.52	0.55			0.02
116613	0.65	-33.85 ± 0.39	-16.38 ± 0.20	-12.13 ± 0.19	39.51	38.26	-10.05 N	-2.12 Y	30.39 ± 3.58	-4.555 [4]	0.87	-4.54	0.30			0.12

⋆ 'Y', 'N' labels indicate if the star satisfies or not the criteria.

Table A.4: Membership criteria for the Ursa Major MG candidate stars. (Convergence Point: 20.55 hours, -38.10 degrees; U =14.9 km/s, V = 1.0 km/s, W = -10.7 km/s; Age: 300 Myr)

		Kinematics							Lithium	CaII H,K		ROSAT-data		Rotation		
HIP	$(B-V)$	U (km/s)	V (km/s)	W (km/s)	V_{Total} (km/s)	V_T (km/s)	$PV^\star$ (km/s)	$\rho_c^\star$ (km/s)	EW(LiI) (mÅ)	R'_{HK} (log)	Age (Gyr)	L_X/L_{Bol} (log)	Age (Gyr)	Prot (days)	Age (Gyr)	[Fe/H]
(1)	(2)	(3)	(4)	(5)	(6)	(7)	(8)	(9)	(10)	(11)	(12)	(13)	(14)	(15)	(16)	(17)
Probable Non-members																
27072	0.49	18.18 ± 0.13	4.44 ± 0.13	-11.67 ± 0.09	22.06	20.82	1.62 Y	-6.32 Y	68.82 ± 2.90	-4.78 [7]	2.93					-0.09
33277	0.60	13.53	5.66	-4.98	15.48	2.72	3.47 N	-2.48 N	15.28 ± 3.35	-4.94 [3]	5.45					-0.13
73996	0.45	16.71 ± 0.39	-1.81 ± 0.27	-18.15 ± 0.75	24.74	23.13	-1.39 Y	-3.54 Y		-4.85 [3]	3.95	-5.34	0.50			0.05
74702	0.82	9.28 ± 0.17	1.13 ± 0.09	-14.68 ± 0.16	17.40	17.04	0.34 Y	-2.35 Y		-4.35 [1]	0.20	-5.11	1.34			-0.09
Doubtful Members																
27913	0.59	13.63 ± 0.30	2.46 ± 0.06	-7.40 ± 0.05	15.70	12.78	1.27 Y	-10.00 Y	102.91 ± 3.30	-4.49 [1]	0.57	-4.54	0.30	5.2 [12]	0.36	-0.01
36827	0.87	6.34 ± 0.13	6.30 ± 0.13	-11.69 ± 0.32	14.72	10.01	7.72 N	-6.82 Y	53.47 ± 4.59	-4.24 [1]	0.08	-4.49	0.61			-0.26
37349	0.96	25.33 ± 0.14	-2.41 ± 0.17	-7.36 ± 0.11	26.49	24.24	-9.54 N	-17.59 Y	8.58 ± 5.02	-4.46 [1]	0.47	-4.87	1.17			-0.05
80337	0.63	13.23 ± 0.10	-1.03 ± 0.06	-1.40 ± 0.06	13.34	5.50	1.65 N	3.70 N	35.52 ± 3.49	-4.53 [7]	0.69	-4.62	0.37	8.5 [12]	0.68	0.05
60866	1.16	23.76 ± 0.72	1.69 ± 0.19	-16.49 ± 0.39	28.97	29.02	0.36 Y	-5.58 Y	26.68 ± 6.05	-5.14 [1]						
80686	0.55	12.80	5.30	-5.99	15.09	17.66	3.89 N	12.53 Y	116.12 ± 3.15	-4.65 [1]	1.52	-4.59	0.29	13 [13]	0.24	-0.08
96183	0.75	21.40 ± 0.49	-0.95 ± 0.69	-7.63 ± 0.16	22.74	21.54	-6.61 N	10.26 Y		-4.75 [4]	2.56					0.11
108028	0.92	7.78 ± 0.25	-1.68 ± 0.71	-8.53 ± 0.38	11.67	12.04	-2.91 N	5.66 Y	27.80 ± 4.85	-4.40 [1]	0.30	-4.33	0.60			
Probable Members																
5944	0.58	17.87 ± 0.17	-3.60 ± 0.14	0.16 ± 0.14	18.23	11.82	5.46 N	-2.74 N	95.70 ± 3.29	-4.47 [1]	0.50	-4.68	0.39			-0.07
8486	0.62	18.93 ± 1.21	2.03 ± 0.22	-2.55 ± 0.45	19.21	19.35	1.82 Y	-5.05 Y	91.56 ± 3.46	-4.19 [1]	0.05	-4.35	0.27			-0.11
42438	0.61	10.69 ± 0.06	0.24 ± 0.07	-10.55 ± 0.07	15.02	13.07	2.25 N	-11.65 Y	106.36 ± 3.41	-4.38 [1]	0.26	-4.45	0.29	5 [2]	0.29	-0.20
71395	0.98	16.90 ± 0.32	-4.47 ± 0.12	-20.53 ± 0.19	26.96	24.75	-5.66 N	-2.33 N	12.30 ± 5.12	-4.45 [1]	0.43	-4.54	0.70			0.02
72659	0.72	4.99 ± 0.04	1.99 ± 0.02	-1.35 ± 0.07	5.54	5.25	1.33 N	0.75 Y	99.03 ± 3.92	-4.36 [2]	0.23	-4.37	0.37	6.2 [12]	0.29	-0.10
102485	0.43	19.67 ± 2.91	-5.05 ± 1.06	-11.47 ± 2.21	23.32	50.17	1.39 Y	48.86 N		-4.40 [5]	0.31	-5.06	0.30			0.00

⋆ 'Y', 'N' labels indicate if the star satisfies or not the criteria.

Table A.5: Membership criteria for the IC 2391 MG candidate stars. (Convergence Point: 5.82 hours, -12.44 degrees; U =-20.6 km/s, V = -15.7 km/s, W = -9.1 km/s; Age: 35-55 Myr)

		Kinematics							Lithium	CaII H,K		ROSAT-data		Rotation		
HIP	$(B-V)$	U (km/s)	V (km/s)	W (km/s)	V_{Total} (km/s)	$V_T^\star$ (km/s)	$PV^\star$ (km/s)	ρ_c (km/s)	EW(LiI) (mÅ)	R'_{HK} (log)	Age (Gyr)	L_X/L_{Bol} (log)	Age (Gyr)	Prot (days)	Age (Gyr)	[Fe/H]
(1)	(2)	(3)	(4)	(5)	(6)	(7)	(8)	(9)	(10)	(11)	(12)	(13)	(14)	(15)	(16)	(17)
Probable Non-members																
8362	0.79	-24.86 ± 0.13	-16.48 ± 0.11	-5.36 ± 0.07	30.30	29.81	4.72 N	0.58 Y	7.98 ± 4.22	-5.05 [1]	7.54	-4.96	0.89	23 [2]	2.53	0.02
18267	0.73	-21.33 ± 0.62	-24.22 ± 0.41	-5.06 ± 0.34	32.66	40.76	3.16 Y	30.95 N		-4.89 [4]	4.67	-5.17	1.03			-0.01
25119	0.94	-26.59 ± 0.17	-26.68 ± 0.40	-12.84 ± 0.14	39.80	56.71	0.30 Y	54.40 N	10.76 ± 4.93	-4.88 [4]	4.42	-5.65	3.46			-0.23
54810	1.23	-24.97 ± 0.54	-20.40 ± 0.31	3.09 ± 0.32	32.39	27.57	3.24 N	3.73 N		-4.50 [1]	0.61	-5.07	2.34			
Doubtful Members																
11072	0.61	-17.46 ± 0.27	-15.84 ± 0.27	-4.79 ± 0.15	24.06	26.58	-1.79 Y	17.04 Y	35.24 ± 3.39	-4.99 [5]	6.32	-4.51	0.14	19.3 [13]	3.25	-0.06
19832	1.18	-16.71 ± 0.23	-17.91 ± 0.93	-12.15 ± 0.25	27.34	27.13	-5.37 N	24.67 Y	25.86 ± 6.13	-4.66 [1]	1.61					
22449	0.48	-25.65 ± 0.07	-14.77 ± 0.03	4.37 ± 0.04	29.92	25.13	14.35 N	22.89 Y	12.88 ± 2.82	-4.79 [3]	3.04	-4.99	0.32			-0.03
34567	0.70	-21.68	-18.03	-15.92	32.39	37.46	2.59 Y	27.44 N	54.66 ± 3.82	-4.46 [4]	0.47	-4.45	0.32			0.00
40170	1.21	-17.68 ± 0.78	-20.66 ± 1.22	-10.07 ± 0.74	29.00	29.90	-3.70 N	9.55 Y	23.26 ± 6.43	-5.15 [1]						
53486	0.93	-16.63 ± 0.29	-14.39 ± 0.22	-6.15 ± 0.21	22.83	22.40	-0.94 Y	4.32 Y		-4.59 [1]	1.08	-4.59	0.67			-0.03
75201	1.30	-28.10 ± 0.47	-17.90 ± 0.61	0.50 ± 0.48	33.32	37.79	10.37 N	-28.78 N	16.31 ± 6.77	-4.54 [1]	0.79					
76051	0.77	-27.90 ± 4.87	-16.55 ± 8.59	-18.44 ± 6.25	37.31	25.02	0.45 Y	-20.80 N		-4.67 [4]	1.69					
95319	0.81	-21.00	-14.04	-2.91	25.43	24.42	5.82 N	-21.16 Y	22.77 ± 4.31	-5.08 [3]						0.16
Probable Members																
19076	0.64	-25.68 ± 0.09	-13.46 ± 0.12	-6.61 ± 0.07	29.74	24.74	4.18 N	18.14 N	44.90 ± 3.53	-4.30 [1]	0.14	-4.61	0.34			0.04
22263	0.62	-24.11 ± 0.08	-8.65 ± 0.07	-3.06 ± 0.08	25.80	39.73	8.25 N	38.27 N	55.79 ± 3.47	-4.511 [2]	0.65	-4.73	0.44	7.6 [12]	0.57	0.00
29568	0.70	-20.82 ± 0.12	-10.26 ± 0.11	-7.01 ± 0.10	24.24	43.31	1.05 Y	42.23 N	51.29 ± 3.79	-4.39 [1]	0.28	-4.29	0.28			-0.01
59280	0.80	-28.62 ± 0.50	-22.55 ± 0.40	-7.13 ± 0.10	37.13	37.79	-1.89 Y	-7.77 Y	26.16 ± 4.26	-4.56 [1]	0.90	-5.24	1.26			0.14
66252	1.16	-27.83 ± 0.34	-14.63 ± 0.39	-17.03 ± 0.22	35.76	31.50	0.34 Y	-12.54 N	65.40 ± 6.06	-3.89 [1]		-3.05	0.15	3.9 [13]		
71743	0.73	-22.30 ± 0.18	-6.93 ± 0.27	-13.83 ± 0.15	27.14	18.29	-0.15 Y	-10.56 N	34.70 ± 3.96	-4.51 [1]	0.65	-4.86	0.68			0.04

⋆ 'Y', 'N' labels indicate if the star satisfies or not the criteria.

Table A.6: Membership criteria for the Castor MG candidate stars. (Convergence Point: 4.57 hours, -18.44 degrees; U =-10.7 km/s, V = -8.0 km/s, W = -9.7 km/s; Age: 200 Myr)

		Kinematics							Lithium	CaII H,K		ROSAT-data		Rotation		
HIP	$(B-V)$	U (km/s)	V (km/s)	W (km/s)	V_{Total} (km/s)	V_T (km/s)	$PV\star$ (km/s)	$\rho_c^\star$ (km/s)	EW(LiI) (mÅ)	R'_{HK} (log)	Age (Gyr)	L_X/L_{Bol} (log)	Age (Gyr)	Prot (days)	Age (Gyr)	[Fe/H]
(1)	(2)	(3)	(4)	(5)	(6)	(7)	(8)	(9)	(10)	(11)	(12)	(13)	(14)	(15)	(16)	(17)
Doubtful Members																
12110	1.06	-12.52 ± 0.22	-8.05 ± 0.20	-11.63 ± 0.13	18.89	17.47	0.99 Y	15.06 Y		-4.40 [1]	0.30	-4.81	1.16			0.06
67105	1.09	-4.32 ± 0.14	-10.06 ± 0.30	-13.51 ± 0.10	17.39	13.24	-7.30 N	-9.43 Y	5.15 ± 5.68	-4.39 [1]	0.28	-5.17	2.15			
109176	0.45	-14.69	-7.00	-6.39	17.48	16.40	5.19 N	-4.54 Y	74.47 ± 2.73	-5.06 [9]	7.72	-5.76	0.89			-0.05
Probable Members																
29067	1.25	-7.16 ± 0.46	-7.69 ± 0.40	-9.98 ± 0.49	14.49	14.33	0.89 Y	-0.57 Y	37.82 ± 6.47	-4.40 [1]	0.30					
45383	1.00	-13.47 ± 0.48	-4.33 ± 0.44	-0.52 ± 0.45	14.16	8.75	5.68 N	2.96 N	8.68 ± 5.25	-4.31 [1]	0.15	-3.93	0.33			
110778	0.61	-17.08 ± 0.67	-5.03 ± 0.47	-17.11 ± 0.45	24.69	23.47	5.97 N	0.43 Y	83.22 ± 3.43	-4.43 [1]	0.37	-4.19	0.18			-0.17
117712	0.96	-15.75	-6.48	-1.20	17.07	15.32	8.18 N	3.64 Y		-4.55 [3]	0.86	-4.56	0.64			-0.32

⋆ 'Y', 'N' labels indicate if the star satisfies or not the criteria.

Table A.7: Properties of the stars classified as Other young discs stars

		Kinematics			Lithium	Ca II H,K		X-ray		Rotation		
HIP	$(B-V)$	U (km/s)	V (km/s)	W (km/s)	EW Li I (mÅ)	R'_{HK} (log)	*Age* (Gyr)	L_X/L_{Bol} (log)	*Age* (Gyr)	*Prot* (Days)	*Age* (Gyr)	[Fe/H]
(1)	(2)	(3)	(4)	(5)	(6)	(7)	(8)	(9)	(10)	(11)	(12)	(13)
1692	1.31	-18.78 ± 8.10	-1.08 ± 3.74	-18.51 ± 1.00								
3810	0.52	7.43	-10.88	-18.45		-4.92 [4]	5.07	-6.35	1.88			-0.07
3998	1.22	3.40 ± 0.27	-14.96 ± 0.68	-23.70 ± 0.68	21.94 ± 6.34	-4.96 [3]	5.80	-4.53	1.18			
4845	1.10	5.05 ± 0.32	-13.10 ± 0.62	-13.53 ± 0.26	4.35 ± 5.90	-4.54 [1]	0.79					
7235	0.75	-10.89 ± 0.18	-26.44 ± 0.29	0.94 ± 0.08		-4.72 [1]	2.20	-5.29	1.45			-0.04
7918	0.61	-38.63 ± 0.28	-31.20 ± 0.26	-0.07 ± 0.07	7.60 ± 3.42	-4.99 [3]	6.36					0.06
8275	1.02	-11.10 ± 0.15	0.75 ± 0.30	-20.62 ± 0.19	4.53 ± 5.34	-4.51 [1]	0.65					
8768	1.40	-35.88 ± 0.45	-28.55 ± 0.38	-1.87 ± 0.22	26.69 ± 7.20	-4.59 [1]	1.08	-4.52	1.92			
9829	0.65	6.34 ± 0.41	-12.38 ± 0.35	-9.20 ± 0.41	6.47 ± 3.57	-4.98 [4]	6.13					-0.20
10337	1.37	-32.70 ± 1.18	-21.64 ± 0.83	10.03 ± 0.50	13.06 ± 7.18	-4.68 [1]	1.79	-4.49	1.27			
13081	0.83	-24.79 ± 0.60	-26.53 ± 0.99	-1.49 ± 0.19		-4.58 [4]	1.00	-4.56	0.48			-0.08
13642	0.90	-40.49 ± 0.35	-21.47 ± 0.71	-16.62 ± 0.17		-5.11 [3]						0.21
14150	0.70	-18.54 ± 0.13	-22.45 ± 0.28	-5.69 ± 0.10		-4.85 [4]	4.01					0.12
15442	0.64	-25.57 ± 0.22	-30.64 ± 0.57	-6.09 ± 0.24	5.90 ± 3.56	-4.75 [1]	2.55					-0.20
15457	0.67	-21.03 ± 0.73	-4.33 ± 0.04	-4.02 ± 0.68	38.88 ± 3.68	-4.42 [2]	0.35	-4.62	0.40	9.4 [12]	0.70	0.11
16852	0.57	1.66 ± 0.18	-15.51 ± 0.12	-42.40 ± 0.19	46.48 ± 3.22	-5.05 [3]	7.59			17.6 [13]	3.50	-0.04
23835	0.64	-26.31 ± 0.08	-23.11 ± 0.13	27.54 ± 0.19	13.06 ± 3.55	-5.13 [4]						-0.16
27435	0.62	-18.69 ± 0.10	-29.66 ± 0.12	-12.38 ± 0.07	33.59 ± 3.46	-4.97 [4]	6.00					-0.22
29525	0.66	3.04 ± 0.76	-25.79 ± 0.37	-6.62 ± 0.16	39.19 ± 3.65	-4.33 [1]	0.17	-4.78	0.55	7.8 [14]		-0.10
29650	0.45	-33.85 ± 0.13	-18.52 ± 0.12	-16.37 ± 0.16	4.90 ± 2.72	-4.71 [4]	2.13	-5.30	0.51			0.07
30422	0.45	-15.95	-4.07	-2.82	4.66 ± 2.72	-4.58 [4]	0.99	-5.05	0.40			
33560	1.07	14.67 ± 0.37	-8.13 ± 0.36	-1.26 ± 0.19	58.70 ± 5.62	-4.14 [1]	0.03	-3.37	0.22			
37279	0.43	5.48	-8.48	-18.84	2.10 ± 2.65	-4.78 [2]	2.89	-6.12	0.99	3.0 [2]		0.00
42808	0.93	-25.93 ± 0.12	-7.93 ± 0.10	-0.82 ± 0.07	69.52 ± 4.89	-4.48 [1]	0.53	-4.41	0.57			-0.03
44897	0.58	-30.64 ± 0.14	-14.03 ± 0.16	4.33 ± 0.16	28.44 ± 3.29	-4.47 [1]	0.50	-4.74	0.36	10.0 [2]	1.15	0.03
45038	0.49	-1.13 ± 0.08	-9.16 ± 0.11	1.93 ± 0.09		-5.31 [3]		-6.09	1.32			-0.05
45333	0.59	8.64	-7.61	-9.46	60.35 ± 3.32	-5.07 [4]						-0.13
45343	1.36	-39.13 ± 1.18	-13.70 ± 0.58	-21.71 ± 1.08		-4.56 [3]	0.91	-4.59	2.37			
46509	0.46	0.94 ± 0.36	-7.33 ± 0.22	11.37 ± 0.35	3.36 ± 2.77	-4.83 [3]	3.61	-4.96	0.27			-0.01
46816	0.89	-20.11 ± 0.33	-4.35 ± 0.25	-10.13 ± 0.28	202.25 ± 4.72	-3.66 [1]		-3.03	0.08			-0.21
47080	0.76	-36.76	-17.35	-15.85	10.43 ± 4.11	-4.57 [1]	0.95	-5.11	0.83	18.0 [2]	1.72	0.33
48113	0.61	11.12 ± 0.72	-5.54 ± 0.13	17.93 ± 0.84	28.30 ± 3.41	-5.04 [3]	7.39					0.13

Table A.7 Continued

		Kinematics			Lithium	Ca II H,K		X-ray		Rotation		
HIP	$(B-V)$	U (km/s)	V (km/s)	W (km/s)	EW Li I (mÅ)	R'_{HK} (log)	*Age* (Gyr)	L_X/L_{Bol} (log)	*Age* (Gyr)	*Prot* (Days)	*Age* (Gyr)	[Fe/H]
(1)	(2)	(3)	(4)	(5)	(6)	(7)	(8)	(9)	(10)	(11)	(12)	(13)
49699	0.97	-8.69 ± 0.11	-7.09 ± 0.13	4.27 ± 0.09	11.26 ± 5.09	-5.00 [4]	6.58					0.04
49908	1.33	-8.81 ± 0.10	-20.71 ± 0.05	-36.38 ± 0.11	37.55 ± 6.82	-5.00 [1]	6.60	-5.09	3.46	6.0 [14]		
49986	1.29	-2.20 ± 0.07	-12.46 ± 0.15	-2.99 ± 0.15	14.13 ± 6.75	-4.41 [11]	0.32	-4.47	3.86			
51459	0.52	-13.58 ± 0.05	-1.99 ± 0.05	1.82 ± 0.05	56.71 ± 3.02	-4.78 [3]	2.97	-5.51	1.02			-0.05
53721	0.61	-24.18 ± 0.09	-2.38 ± 0.05	0.74 ± 0.08	16.15 ± 3.42	-4.91 [3]	4.93					0.03
54426	0.98	-6.42 ± 0.48	-3.54 ± 0.21	-41.94 ± 0.22	2.23 ± 5.12	-4.77 [1]	2.80					
54906	0.83	-10.70 ± 0.25	1.19 ± 0.15	-4.76 ± 0.11	5.05 ± 4.42	-5.06 [4]	7.72					-0.27
56242	0.58	-21.34 ± 0.67	-30.27 ± 0.94	-20.26 ± 0.47	58.86 ± 3.26	-4.92 [2]	5.16	-5.95	2.09	14.0 [12]	2.21	-0.02
56997	0.73	7.85 ± 0.04	-16.01 ± 0.06	-3.74 ± 0.06	7.26 ± 3.95	-4.55 [2]	0.82	-5.16	1.08	17.1 [12]	1.70	-0.03
61941	0.38	-35.51 ± 0.27	-6.47 ± 0.31	-18.47 ± 0.58	43.96 ± 2.44	-4.50 [11]	0.61	-4.79	0.18			
62505	0.93	4.37 ± 0.36	5.64 ± 0.50	4.00 ± 0.28	12.13 ± 4.92	-4.57 [5]	0.96	-4.68	0.68			
64241	0.47	-39.00 ± 0.61	-9.53 ± 0.22	-13.70 ± 0.24	12.33 ± 2.81	-4.53 [2]	0.74	-4.91	0.21	3.0 [12]		-0.21
65343	1.40	-49.45 ± 0.89	-11.19 ± 0.22	-34.57 ± 0.20	46.18 ± 7.24	-4.59 [11]	1.08	-5.10	3.06			
65352	0.80	3.20 ± 0.18	4.04 ± 0.28	31.80 ± 0.15		-5.07 [4]	7.81					-0.30
66886	1.25	-35.59 ± 0.52	-21.62 ± 0.99	-38.36 ± 0.13		-4.67 [4]	1.67					
67422	1.22	-20.07 ± 0.21	-25.35 ± 0.27	-13.95 ± 0.09	6.49 ± 6.30	-4.68 [1]	1.79	-4.57	1.09			-0.35
68030	0.51	-29.60 ± 0.29	-20.32 ± 0.25	-1.46 ± 0.20	32.74 ± 2.95	-4.92 [10]	5.13					-0.41
68184	1.03	-2.56 ± 0.07	-10.09 ± 0.07	-26.64 ± 0.08	19.60 ± 5.39							0.10
68337	1.16	-29.65 ± 0.39	-16.50 ± 0.30	-50.29 ± 0.21	6.46 ± 6.02	-4.72 [1]	2.20					
68682	0.75	14.92 ± 0.26	-13.83 ± 0.20	-19.46 ± 0.30	5.62 ± 4.04	-4.87 [3]	4.25					-0.02
69972	1.03	-43.04 ± 0.24	-11.54 ± 0.24	-34.89 ± 0.29	25.50 ± 5.35	-5.01 [5]	6.79					0.22
72603	0.41	-24.54 ± 0.14	-8.16 ± 0.15	-12.07 ± 0.10	71.44 ± 2.54	-4.58 [11]	1.01	-5.05	0.30			-0.09
75253	0.97	-0.44 ± 0.16	-19.12 ± 0.55	-12.74 ± 0.28	30.26 ± 5.10	-4.83 [1]	3.64					0.11
75277	0.79	-19.79 ± 0.52	-11.30 ± 0.30	7.04 ± 0.75	11.75 ± 4.25	-4.90 [4]	4.81					-0.07
75722	0.91	2.08 ± 0.33	-19.22 ± 0.42	-34.75 ± 0.47	15.80 ± 4.81	-5.18 [3]		-4.53	0.57			0.18
76602	0.51	-1.70 ± 0.30	-0.50 ± 0.35	-5.43 ± 0.40	65.11 ± 2.97	-4.79 [4]	3.10					0.11
76603	0.49	1.72 ± 0.40	-1.48 ± 0.41	-4.63 ± 0.56	73.03 ± 2.88	-4.86 [4]	4.12					0.00
77052	0.67	18.73 ± 0.10	-7.24 ± 0.11	11.28 ± 0.09	26.13 ± 3.69	-4.89 [7]	4.61	-5.29	1.10			0.06
81300	0.83	1.00 ± 0.07	-0.38 ± 0.04	-28.39 ± 0.10	15.43 ± 4.43	-4.73 [1]	2.31	-5.08	1.19	21.3 [12]	2.00	0.05
85561	1.24	-33.73 ± 0.18	-21.14 ± 0.72	14.61 ± 0.66	2.79 ± 6.51	-4.40 [1]	0.30					
86400	0.95	20.44 ± 0.07	0.70 ± 0.09	12.03 ± 0.07	24.20 ± 5.01	-4.76 [1]	2.67	-5.58	3.15	33.5 [12]		-0.16
87579	0.96	-13.61 ± 0.17	-9.89 ± 0.11	4.23 ± 0.27	3.65 ± 5.06	-4.43 [1]	0.37	-4.74	1.04			
88601	0.83	7.29 ± 0.11	-19.30 ± 0.10	-18.97 ± 0.10	7.40 ± 4.44	-4.86 [1]	4.11	-4.88	0.76	19.7 [12]	1.76	0.04
90656	1.10	-42.67 ± 0.15	-32.80 ± 0.15	-25.17 ± 0.38	39.46 ± 5.71							0.19

Table A.7 Continued

		Kinematics			Lithium	Ca II H,K		X-ray		Rotation		
HIP	$(B-V)$	U (km/s)	V (km/s)	W (km/s)	EW Li I (mÅ)	R'_{HK} (log)	*Age* (Gyr)	L_X/L_{Bol} (log)	*Age* (Gyr)	*Prot* (Days)	*Age* (Gyr)	[Fe/H]
(1)	(2)	(3)	(4)	(5)	(6)	(7)	(8)	(9)	(10)	(11)	(12)	(13)
98698	1.11	-22.88 ± 0.09	-16.92 ± 0.10	15.71 ± 0.10	29.15 ± 5.74	-4.69 [2]	1.91	-5.11	2.03	29.3 [12]		
98828	0.93	3.69 ± 0.17	-9.96 ± 0.12	4.92 ± 0.15	16.57 ± 4.89	-4.81 [1]	3.34					
99240	0.75	-48.79 ± 0.08	-13.38 ± 0.06	-14.92 ± 0.06	24.75 ± 4.07	-5.00 [7]	6.60					0.30
99316	0.80	-29.52 ± 0.36	-15.73 ± 0.28	14.22 ± 0.30		-5.08 [4]						
99452	0.82	-31.69 ± 0.45	-27.29 ± 0.69	61.66 ± 0.73	13.97 ± 4.40	-5.09 [4]						-0.09
99764	1.37	14.87 ± 0.38	-17.35 ± 0.67	-14.35 ± 0.45	10.96 ± 7.36	-4.71 [1]	2.09					
105152	1.03	-36.58 ± 0.50	-32.18 ± 0.32	-24.89 ± 0.85	8.82 ± 5.39	-5.11 [3]	8.53					-0.09
106400	1.16	-41.62 ± 1.05	-18.29 ± 0.21	-13.82 ± 0.40	22.26 ± 6.02	-3.98 [1]	0.01	-3.68				
111449	0.45	-16.42 ± 0.40	-21.61 ± 0.32	-10.08 ± 0.77		-4.55 [5]	0.83	-5.05	0.31			0.00
113357	0.65	-15.42 ± 0.12	-28.13 ± 0.05	14.43 ± 0.06	12.20 ± 3.58	-5.07 [2]				37.0 [2]	8.49	0.18
116771	0.51	-7.82 ± 0.03	-26.07 ± 0.07	-26.35 ± 0.06	24.82 ± 2.96	-5.11 [3]		-6.15	1.59			-0.05
120005	1.40	-44.78 ± 1.97	-17.49 ± 1.11	-22.54 ± 1.75	3.47 ± 7.15	-4.39 [1]	0.28	-4.59	2.09			

Table A.8: Properties of the stars non-members of moving groups

		Kinematics			Lithium	Ca II H,K		X-ray		Rotation		
HIP	$(B-V)$	U (km/s)	V (km/s)	W (km/s)	EW Li I (*m*Å)	R'_{HK} (log)	*Age* (Gyr)	L_X/L_{Bol} (log)	*Age* (Gyr)	*Prot* (Days)	*Age* (Gyr)	[Fe/H]
(1)	(2)	(3)	(4)	(5)	(6)	(7)	(8)	(9)	(10)	(11)	(12)	(13)
171	0.65	-8.36	-76.17	-33.38		-4.85 [3]	3.96	-5.89	3.23			-0.52
910	0.48	18.82 ± 0.26	-12.66 ± 0.23	-19.95 ± 0.09	28.53 ± 2.83	-4.79 [5]	3.04					-0.34
1499	0.69	-31.47 ± 0.42	-38.69 ± 0.45	-1.61 ± 0.17	9.01 ± 3.75	-5.06 [4]	7.70					0.17
1532	1.23	18.83 ± 0.70	-26.56 ± 0.85	1.71 ± 0.38	42.26 ± 6.47							
1598	0.62	18.02 ± 0.47	10.64 ± 0.58	-33.64 ± 0.52	32.07 ± 3.46	-4.98 [4]	6.21					-0.41
1599	0.56	-71.53 ± 0.12	-4.39 ± 0.04	-45.35 ± 0.08	39.59 ± 3.20	-4.84 [7]	3.79					-0.17
2941	0.72	-85.72	-52.37	-23.99		-4.90 [2]	4.83					
3093	0.85	39.89 ± 0.31	-19.53 ± 0.52	8.50 ± 0.53	10.50 ± 4.53	-4.99 [2]	6.43			48.0 [12]	8.25	0.14
3206	0.96	17.95 ± 0.22	-82.78 ± 0.50	-27.33 ± 0.76		-5.02 [3]	6.96	-5.41	2.20			0.12
3418	1.10	43.02 ± 0.53	-30.44 ± 0.18	-12.44 ± 0.60	6.29 ± 5.70	-4.71 [3]	2.04					
3535	1.02	29.79 ± 0.50	-36.44 ± 0.66	-36.23 ± 0.80	32.96 ± 5.32	-5.05 [3]	7.59					0.22
3765	0.88	-1.26 ± 0.16	-47.44 ± 0.28	-13.30 ± 0.35		-5.41 [1]				38.0 [12]	5.21	-0.22
3821	0.57				27.12 ± 3.24	-4.96 [3]	5.83	-6.24	3.56			-0.19
5286	1.11	4.43 ± 0.47	-28.76 ± 0.87	-41.33 ± 0.94	12.06 ± 5.79	-4.59 [1]	1.08					
5336	0.68	-42.40	-157.40	-35.23		-4.91 [3]	4.90					-0.81
5799	0.45	-33.17 ± 0.25	21.12 ± 0.18	-9.34 ± 0.16	9.47 ± 2.70	-5.46 [3]		-5.32	0.44			-0.33
5957	1.35	-23.43 ± 1.53	-48.75 ± 1.48	10.24 ± 0.29	32.64 ± 7.15	-4.78 [3]	2.89					
6290	1.34	15.32 ± 1.05	33.23 ± 0.98	36.63 ± 1.70		-4.40 [1]	0.30					
6917	0.98	-45.69	-31.09	-22.23		-4.56 [4]	0.88	-4.63	0.58			-0.32
7339	0.68	50.88 ± 0.30	-4.15 ± 0.22	1.12 ± 0.14		-5.02 [4]	6.99					
7513	0.54	28.77 ± 0.04	-22.50 ± 0.02	-14.28 ± 0.07	31.01 ± 3.10	-5.04 [3]	7.26	-5.98	1.24			0.11
7981	0.83	34.82 ± 0.52	-24.97 ± 0.45	2.61 ± 0.60	3.69 ± 4.44	-5.19 [1]				35.0 [2]	4.87	-0.04
8102	0.71	18.71 ± 0.01	29.42 ± 0.02	12.80 ± 0.04		-4.96 [2]	5.82	-6.86	16.30	34.0 [2]	5.95	-0.46
9269	0.79	8.32 ± 0.25	-60.07 ± 0.61	-11.59 ± 0.46		-5.13 [4]						0.15
10138	0.82	-99.05 ± 0.38	-77.08 ± 0.22	-31.44 ± 0.12	2.31 ± 4.35	-4.68 [1]	1.79			30.0 [13]	3.83	-0.22
10416	1.05	17.30 ± 0.35	-17.85 ± 0.44	-2.60 ± 0.26		-4.30 [1]	0.14	-4.66	0.99			-0.06
10644	0.60	-35.30	-47.96	11.12	38.93 ± 3.37	-4.64 [3]	1.47	-5.05	0.65			
10798	0.73	-11.03 ± 0.08	26.81 ± 0.15	-9.94 ± 0.04	0.76 ± 3.95	-4.86 [7]	4.11					-0.46
11452	1.41	-16.43 ± 0.30	10.70 ± 0.22	8.56 ± 0.30	61.17 ± 7.23							
11565	1.22	-59.01 ± 1.29	-27.82 ± 0.65	-0.90 ± 0.63		-4.58 [1]	1.01					
12114	0.97	-76.46 ± 0.20	0.41 ± 0.03	32.01 ± 0.17	1.15 ± 5.07	-4.96 [2]	5.82			45.0 [12]		
12777	0.50	-30.27 ± 0.05	1.28 ± 0.05	-0.85 ± 0.02	69.56 ± 2.92	-5.07 [3]	7.92	-5.92	1.46			0.04

Table A.8 Continued

		Kinematics			Lithium	Ca II H,K		X-ray		Rotation		
HIP	$(B-V)$	U (km/s)	V (km/s)	W (km/s)	EW Li I (m Å)	R'_{HK} (log)	*Age* (Gyr)	L_X/L_{Bol} (log)	*Age* (Gyr)	*Prot* (Days)	*Age* (Gyr)	[Fe/H]
(1)	(2)	(3)	(4)	(5)	(6)	(7)	(8)	(9)	(10)	(11)	(12)	(13)
12843	0.48				14.25 ± 2.85	-4.52 [5]	0.71	-4.80	0.25			-0.07
13258	1.23	11.52 ± 0.26	-62.02 ± 1.17	6.66 ± 0.28	33.57 ± 6.38	-4.76 [1]	2.67					
14286	0.67	-71.34 ± 1.28	-85.48 ± 1.32	-29.36 ± 0.47	3.47 ± 3.68	-4.99 [4]	6.36					-0.26
14632	0.59	-75.90 ± 0.10	-15.61 ± 0.12	21.45 ± 0.08	54.94 ± 3.33	-5.00 [3]	6.58					0.13
14879	0.50	-38.59 ± 0.29	16.45 ± 0.07	29.26 ± 0.10	12.88 ± 2.93	-4.90 [5]	4.79	-4.50	0.12			-0.19
15099	0.89	5.75 ± 0.56	-62.45 ± 1.20	8.88 ± 0.47	5.34 ± 4.71	-4.84 [3]	3.82					-0.04
15330	0.64	-70.01 ± 0.20	-46.56 ± 0.13	15.82 ± 0.11	2.83 ± 3.53	-4.86 [1]	4.11	-5.71	2.15			-0.22
15371	0.59	-69.72 ± 0.17	-46.46 ± 0.09	15.85 ± 0.06	4.36 ± 3.31	-4.79 [7]	3.06					-0.23
15510	0.70	-79.86 ± 0.08	-96.10 ± 0.07	-34.11 ± 0.07		-4.98 [7]	6.22	-6.70	10.59			-0.34
15673	1.01	42.65 ± 0.26	-14.07 ± 0.25	-40.49 ± 1.05	22.95 ± 5.31	-4.54 [1]	0.79					
15919	1.15	48.04 ± 0.69	-29.02 ± 0.36	-21.33 ± 0.69	20.02 ± 5.95	-4.60 [1]	1.14	-5.12	1.99			
16537	0.89	-3.60 ± 0.03	7.06 ± 0.01	-20.70 ± 0.03	7.30 ± 4.69	-4.62 [1]	1.28	-4.80	0.94	11.3 [12]	0.61	-0.04
17147	0.54	-111.06 ± 0.39	-89.27 ± 1.11	-42.84 ± 0.60	8.46 ± 3.11	-4.92 [10]	5.13					-0.79
17496	1.18	-89.58 ± 0.51	-6.83 ± 0.35	-16.85 ± 0.74	16.62 ± 6.15	-4.71 [3]	2.06					
17651	0.43	35.18 ± 0.20	-22.45 ± 0.14	-20.85 ± 0.23	0.51 ± 2.66	-4.68 [5]	1.83	-6.88	3.70			0.04
18324	0.85	-59.46 ± 0.54	-16.91 ± 0.75	12.98 ± 0.25		-5.03 [3]	7.11					-0.32
18413	0.67	33.35 ± 0.27	16.10 ± 0.38	-5.75 ± 0.12	12.72 ± 3.67	-4.93 [4]	5.25					-0.10
19849	0.81	96.26 ± 0.08	-12.27 ± 0.03	-41.12 ± 0.08		-5.38 [1]				43.0 [2]	7.30	-0.23
20917	1.34	33.30 ± 0.14	6.86 ± 0.13	14.26 ± 0.08	55.68 ± 6.90	-4.62 [1]	1.28	-4.45	1.25			
22498	1.34	-69.12 ± 1.06	-1.81 ± 1.71	19.17 ± 0.58	27.95 ± 6.93	-4.55 [11]	0.84	-4.96	1.88			
23311	1.07	4.64 ± 0.12	-54.29 ± 0.21	-10.90 ± 0.05	29.34 ± 5.56	-5.29 [1]		-5.90	5.25	47.0 [2]		0.30
23693	0.52	-6.12 ± 0.05	2.55 ± 0.24	-1.51 ± 0.18	75.41 ± 3.00	-4.49 [1]	0.57	-5.02	0.52			-0.12
23786	0.79	-28.29 ± 0.86	-44.02 ± 0.94	2.34 ± 0.40	5.04 ± 4.26	-4.49 [1]	0.57	-5.07	1.22			-0.17
24786	0.56	-37.98 ± 0.14	-44.72 ± 0.25	20.22 ± 0.42	27.63 ± 3.20	-4.98 [5]	6.17					-0.08
24813	0.61	-76.26 ± 0.05	-34.97 ± 0.18	4.41 ± 0.02	29.94 ± 3.42	-5.01 [3]	6.81					0.10
24819	1.01	-84.37 ± 0.21	-56.47 ± 0.43	13.01 ± 0.82		-4.53 [1]	0.74					
24874	1.03	-8.38 ± 0.55	10.71 ± 0.18	30.86 ± 0.71	22.59 ± 5.39	-4.14 [1]	0.03	-4.91	1.46			0.09
25623	1.14	74.23 ± 0.30	-2.04 ± 0.28	-18.18 ± 0.39	30.00 ± 5.89	-4.60 [1]	1.14					-0.20
26505	0.82	47.65 ± 0.74	20.43 ± 0.60	-47.67 ± 0.61	4.71 ± 4.39	-5.16 [4]						-0.31
27207	0.84	21.36 ± 1.10	-74.47 ± 1.20	13.76 ± 0.31	6.32 ± 4.49	-5.04 [3]	7.39					-0.02
28103	0.35	-6.01 ± 0.41	8.23 ± 0.34	1.62 ± 0.18	22.18 ± 2.33	-4.78 [11]	2.93	-5.75	0.64			
28267	0.71	-106.69 ± 0.22	-92.53 ± 0.34	-37.64 ± 0.13	5.55 ± 3.87	-5.06 [4]	7.70					-0.09
29271	0.72	18.97 ± 0.06	-30.21 ± 0.17	-11.64 ± 0.10	11.36 ± 3.91	-4.94 [7]	5.49	-6.72	8.88			0.08
29432	0.64	61.84 ± 0.20	-12.69 ± 0.50	11.15 ± 0.20	13.08 ± 3.53	-4.97 [4]	6.11					-0.09

Table A.8 Continued

		Kinematics			Lithium	Ca II H,K		X-ray		Rotation		
HIP	$(B-V)$	U (km/s)	V (km/s)	W (km/s)	EW Li I (m Å)	R'_{HK} (log)	*Age* (Gyr)	L_X/L_{Bol} (log)	*Age* (Gyr)	*Prot* (Days)	*Age* (Gyr)	[Fe/H]
(1)	(2)	(3)	(4)	(5)	(6)	(7)	(8)	(9)	(10)	(11)	(12)	(13)
29800	0.44	-13.07 ± 0.57	7.80 ± 0.21	14.32 ± 0.11	13.04 ± 2.67	-4.51 [1]	0.65	-4.98	0.32			-0.14
29860	0.60	-15.87 ± 0.09	16.53 ± 0.19	-9.46 ± 0.12	43.55 ± 3.35	-5.00 [2]	6.62			20.0 [2]	3.63	-0.08
32010	1.02	49.16 ± 0.14	-19.57 ± 0.59	-1.36 ± 0.16	4.00 ± 5.35	-4.38 [1]	0.26	-5.04	1.91			-0.18
32423	0.97	18.90 ± 0.34	35.10 ± 0.91	-52.65 ± 1.21	11.43 ± 5.09	-4.64 [1]	1.44					-0.18
32439	0.52				44.74 ± 3.01	-5.02 [3]	7.05	-6.53	4.34			-0.16
32480	0.56	25.61 ± 0.07	8.92 ± 0.09	-2.76 ± 0.06	70.00 ± 3.17	-4.99 [3]	6.32					0.09
32919	1.22	-40.58 ± 0.44	-43.65 ± 0.88	-31.68 ± 0.71	30.23 ± 6.33	-5.06 [1]	7.72					
32984	1.07	0.47 ± 0.08	13.15 ± 0.08	-19.76 ± 0.10	15.91 ± 5.55	-4.36 [1]	0.22	-4.84	1.36			-0.02
33373	1.10	-53.29 ± 0.19	-49.11 ± 1.73	10.55 ± 0.23	25.23 ± 5.73	-4.51 [1]	0.65					
33537	0.64	25.58 ± 0.05	14.29 ± 0.14	4.37 ± 0.16	2.24 ± 3.52	-4.94 [4]	5.40					-0.33
33955	1.09	34.33 ± 0.23	7.57 ± 0.25	-27.68 ± 0.50		-4.74 [4]	2.43	-5.15	2.35			-0.17
34017	0.59	-18.07 ± 0.09	-77.69 ± 0.59	-9.00 ± 0.15	24.82 ± 3.32	-4.94 [3]	5.54					-0.11
35136	0.57	-79.85 ± 0.06	-1.63 ± 0.12	32.37 ± 0.07	17.60 ± 3.24	-4.93 [4]	5.25					-0.33
36357	0.93	9.05 ± 0.13	10.60 ± 0.20	14.78 ± 0.29	6.40 ± 4.88	-4.38 [1]	0.25	-5.00	1.46			
36366	0.33	22.75 ± 8.04	13.51 ± 1.01	9.86 ± 3.17	31.29 ± 2.26	-4.66 [11]	1.61	-5.35	0.36			
36439	0.46	25.58 ± 0.11	-15.42 ± 0.16	-4.26 ± 0.13	31.70 ± 2.77	-5.31 [3]						-0.35
36551	1.14	-47.20 ± 0.28	-52.83 ± 0.66	12.47 ± 0.18		-4.44 [1]	0.40					
38382	0.60	27.94	2.47	-19.69	22.01 ± 3.36	-4.88 [5]	4.49			9.7 [14]	0.99	-0.02
38657	0.97	30.56 ± 0.27	-36.15 ± 0.79	-15.14 ± 0.18	24.29 ± 5.10	-5.15 [4]						0.09
38784	0.72	-8.99 ± 0.12	8.77 ± 0.12	-38.09 ± 0.23	8.08 ± 3.92	-4.84 [3]	3.75	-5.84	2.95			-0.14
38931	1.01	-3.54 ± 0.18	5.97 ± 0.11	-12.82 ± 0.28		-5.05 [4]	7.52	-5.23	2.43			-0.23
39064	0.83	45.98 ± 0.46	-52.11 ± 1.06	-14.95 ± 0.19	9.21 ± 4.41	-5.11 [4]						-0.04
39157	0.72	-13.31	-88.96	-29.79	6.29 ± 3.91	-4.92 [3]	5.04					-0.48
40118	0.66	-48.25 ± 0.29	-60.95 ± 0.69	-39.98 ± 0.68	11.67 ± 3.64	-4.85 [3]	3.92					-0.30
40375	1.19	-39.30 ± 0.51	3.93 ± 0.32	-19.41 ± 0.63	15.10 ± 6.16	-4.56 [4]	0.87					
40671	1.09	-21.87 ± 0.32	-83.58 ± 2.26	-38.22 ± 1.26	24.01 ± 5.66	-4.64 [1]	1.44					
40693	0.77	28.41 ± 0.21	-60.96 ± 0.17	-9.88 ± 0.10	8.03 ± 4.12	-4.99 [5]	6.43	-5.90	3.32			-0.04
40843	0.48	-24.26 ± 0.08	-38.80 ± 0.21	7.19 ± 0.09	62.43 ± 2.82	-5.19 [3]	9.83					-0.22
41484	0.62	20.11 ± 0.13	-38.97 ± 0.39	-22.89 ± 0.12	30.59 ± 3.47	-4.91 [4]	5.00					-0.01
41926	0.78	-75.43 ± 0.41	6.06 ± 0.13	-24.57 ± 0.17		-4.95 [7]	5.67					-0.37
42173	0.69	-33.42 ± 0.86	-36.33 ± 0.82	-0.79 ± 0.96	98.98 ± 3.77	-4.48 [3]	0.53	-4.80	0.51			0.08
42430	0.87	-62.62 ± 0.64	-27.29 ± 0.31	13.98 ± 0.36	24.67 ± 4.63	-5.03 [5]	7.18	-5.52	1.60			0.30
42499	0.82	18.00 ± 1.09	-30.28 ± 0.89	-29.05 ± 0.80	4.59 ± 4.38	-4.99 [3]	6.39					-0.36
42525	0.58	-49.27 ± 0.40	-2.01 ± 0.44	34.20 ± 0.50	70.66 ± 3.45							

Table A.8 Continued

		Kinematics			Lithium	Ca II H,K		X-ray		Rotation		
HIP	$(B-V)$	U (km/s)	V (km/s)	W (km/s)	EW Li I (m Å)	R'_{HK} (log)	*Age* (Gyr)	L_X/L_{Bol} (log)	*Age* (Gyr)	*Prot* (Days)	*Age* (Gyr)	[Fe/H]
(1)	(2)	(3)	(4)	(5)	(6)	(7)	(8)	(9)	(10)	(11)	(12)	(13)
43557	0.63	19.51	-25.38	4.81	3.19 ± 3.51	-4.67 [1]	1.70	-4.93	0.52			-0.14
44075	0.52	-48.67 ± 0.14	-91.58 ± 0.18	69.61 ± 0.25	±	-4.78 [5]	2.94					-0.90
45170	0.74	-75.01	-1.37	1.41	±	-4.85 [4]	3.89	-5.60	1.59			-0.30
45617	0.99	24.59 ± 0.65	-35.93 ± 0.60	-17.17 ± 0.62	3.65 ± 5.18	-4.51 [1]	0.65					0.07
45839	1.15	-39.21 ± 0.79	-36.68 ± 0.36	-16.62 ± 1.22	18.50 ± 6.01	-4.78 [4]	2.90					
45963	1.04	-24.69	-43.60	-30.49	±	-4.10 [4]	0.02	-3.11	0.05			
49081	0.67	-56.14 ± 0.13	-44.12 ± 0.19	20.90 ± 0.13	17.99 ± 3.66	-4.97 [3]	6.02					0.19
49366	0.91	-12.45 ± 0.41	4.06 ± 0.16	-20.89 ± 0.38		-4.54 [1]	0.79	-5.05	1.41			-0.14
50125	1.11	22.51 ± 0.35	-82.97 ± 2.48	10.69 ± 0.90	5.62 ± 5.77	-4.81 [4]	3.30					
50384	0.50	-51.29 ± 0.29	-29.25 ± 0.18	4.33 ± 0.23	53.08 ± 2.92	-5.02 [3]	6.96					-0.39
50505	0.68	12.09 ± 0.13	-27.44 ± 0.31	2.47 ± 0.12	5.29 ± 3.71	-5.00 [4]	6.60					-0.18
51248	0.59	20.38 ± 0.25	-91.34 ± 0.91	22.88 ± 0.34	14.63 ± 3.33	-4.91 [3]	4.88					-0.40
51502	0.39	-10.86 ± 1.92	5.56 ± 2.44	-1.22 ± 2.03		-4.55 [11]	0.84	-4.94	0.30			-0.30
51525	1.35	-40.54 ± 0.52	-50.66 ± 0.92	5.20 ± 0.27	27.67 ± 6.93	-4.88 [1]	4.44	-4.59	1.38			
51933	0.53	69.87 ± 0.66	-35.35 ± 0.39	-36.38 ± 0.32	49.82 ± 3.05	-4.85 [5]	3.93					-0.21
52369	0.63	34.72 ± 0.42	9.05 ± 0.12	-10.15 ± 0.11	27.56 ± 3.50	-4.83 [5]	3.58					-0.10
54646	1.33	38.38 ± 0.35	2.45 ± 0.06	-2.01 ± 0.16	54.96 ± 6.84	-4.86 [1]	4.11					
54651	1.08	-107.88 ± 2.12	-20.98 ± 0.19	26.81 ± 0.13		-4.94 [4]	5.47					
54677	1.13	94.05 ± 2.75	-2.09 ± 0.38	-19.65 ± 0.42	21.42 ± 5.90	-4.73 [5]	2.35					
54966	1.34	43.38 ± 18.37	-22.70 ± 7.29	-18.94 ± 10.14	26.16 ± 6.87							
55210	0.74	77.36 ± 1.12	8.89 ± 0.28	31.03 ± 0.31	2.29 ± 4.01	-4.94 [10]	5.49					-0.22
55848	1.04	-62.03 ± 1.62	-12.75 ± 0.31	-9.85 ± 0.37	4.09 ± 5.41							0.24
56452	0.80	-47.58 ± 0.17	19.65 ± 0.05	12.37 ± 0.10	18.93 ± 4.26	-4.86 [7]	4.11					-0.32
56809	0.58	-50.90 ± 1.01	-27.36 ± 0.46	-36.02 ± 0.40	34.53 ± 3.27	-5.07 [3]	7.83					-0.17
56829	0.98	-29.95	34.34	1.33		-4.34 [11]	0.19	-4.22	0.53			
57443	0.66	-59.64 ± 0.15	-38.48 ± 0.10	5.17 ± 0.05	0.95 ± 3.63	-4.95 [7]	5.67			24.0 [13]	3.81	-0.27
57757	0.56	40.39	3.45	6.65	18.12 ± 3.18	-4.99 [6]	6.41	-5.75	0.84			0.14
57939	0.74	277.96 ± 0.94	-157.18 ± 0.57	-13.57 ± 0.33		-4.90 [2]	4.71			31.0 [2]	4.71	-1.22
59000	1.37	20.65 ± 0.47	-42.11 ± 0.62	-0.88 ± 0.77	45.91 ± 7.16	-4.12 [1]	0.03	-3.68	0.44			
59750	0.46	53.11 ± 0.98	-71.06 ± 1.28	-60.92 ± 1.20	10.35 ± 2.78	-4.65 [2]	1.53	-5.81	1.69	7.0 [2]		-0.76
61317	0.59				8.51 ± 3.31	-4.85 [3]	3.96					-0.16
61901	1.09	22.47 ± 0.24	-22.12 ± 0.21	18.62 ± 0.10		-5.02 [4]	6.98					
62207	0.55	-41.67 ± 0.19	6.94 ± 0.08	75.31 ± 0.09	38.10 ± 3.16	-4.98 [3]	6.24					-0.50
63366	0.81	-74.85 ± 1.47	-34.15 ± 0.64	17.35 ± 0.30	8.40 ± 4.32	-4.88 [3]	4.37					-0.30

Table A.8 Continued

		Kinematics			Lithium	Ca II H,K		X-ray		Rotation		
HIP	$(B-V)$	U (km/s)	V (km/s)	W (km/s)	EW Li I (m Å)	R'_{HK} (log)	*Age* (Gyr)	L_X/L_{Bol} (log)	*Age* (Gyr)	*Prot* (Days)	*Age* (Gyr)	[Fe/H]
(1)	(2)	(3)	(4)	(5)	(6)	(7)	(8)	(9)	(10)	(11)	(12)	(13)
64394	0.59	-49.98 ± 0.08	11.49 ± 0.03	7.59 ± 0.05	61.55 ± 3.30	-5.06 [1]	7.72	-5.67	1.38	12.4 [12]	1.67	0.07
64792	0.59	-38.05 ± 0.18	1.68 ± 0.08	-18.68 ± 0.13	93.75 ± 3.31	-4.44 [2]	0.41	-4.42	0.16	3.0 [2]	0.13	0.21
64797	0.89	35.45 ± 0.29	7.42 ± 0.10	1.92 ± 0.08	0.52 ± 4.69	-4.63 [1]	1.36	-5.04	1.47	18.8 [12]	1.50	-0.16
64924	0.71	-23.92 ± 0.04	-47.07 ± 0.10	-32.13 ± 0.05	13.36 ± 3.86	-5.00 [2]	6.62			29.0 [2]	4.55	0.06
65721	0.71	13.33 ± 0.09	-51.59 ± 0.24	-2.70 ± 0.14	56.23 ± 3.84	-5.07 [3]	7.89					-0.06
69414	0.75	23.91 ± 0.13	-43.67 ± 0.46	18.25 ± 0.19	16.33 ± 4.03	-5.08 [4]						-0.11
69701	0.51	24.48 ± 0.26	-36.99 ± 0.18	-12.82 ± 0.34	19.37 ± 2.99	-4.68 [2]	1.81	-4.89	0.13	7.6 [12]	1.71	-0.01
69962	1.41	21.86 ± 0.64	-34.68 ± 1.19	-17.56 ± 0.86	36.21 ± 7.26	-4.80 [1]	3.20					
70016	0.85	-43.38 ± 0.67	-47.22 ± 0.87	6.94 ± 0.28		-5.05 [3]	7.44					-0.17
70218	1.23	-23.39 ± 0.20	-51.71 ± 0.52	-19.00 ± 0.20	22.27 ± 6.37	-4.44 [1]	0.40	-4.63	1.51			
70319	0.64	21.80 ± 0.34	-15.14 ± 0.22	-38.29 ± 0.28	3.40 ± 3.52	-4.96 [2]	5.80			22.0 [2]	3.56	-0.29
71284	0.37	2.22 ± 0.09	16.31 ± 0.11	-5.31 ± 0.23	3.93 ± 2.41	-5.48 [3]		-5.55	0.68			-0.33
71681	0.90	-28.33 ± 0.42	2.86 ± 0.43	13.34 ± 0.46	30.82 ± 4.76	-4.92 [7]	5.13			42.0 [13]	6.07	0.15
71683	0.90	-29.87 ± 0.08	1.29 ± 0.08	12.34 ± 0.07	19.38 ± 4.76	-5.00 [7]	6.60					0.19
72237	1.32	62.48 ± 0.74	-55.13 ± 1.06	25.84 ± 0.23	11.65 ± 6.87	-4.56 [1]	0.87					
72567	0.59	5.09 ± 0.14	9.71 ± 0.16	-6.64 ± 0.11	112.06 ± 3.32	-4.34 [1]	0.19	-4.65	0.33			-0.04
72875	0.99	-68.61 ± 1.49	-68.13 ± 1.61	13.05 ± 1.12		-4.45 [1]	0.43					-0.23
72981	1.17	5.18 ± 0.53	-59.04 ± 3.67	0.82 ± 0.32	112.96 ± 9.71							
73184	1.08	47.75 ± 0.18	-21.90 ± 0.10	-32.74 ± 0.28	23.84 ± 5.63	-4.63 [1]	1.36			44.6 [13]		0.10
73457	1.37	24.74 ± 0.59	-35.60 ± 1.31	-16.43 ± 1.01	67.94 ± 7.13	-4.63 [5]	1.34					
73786	1.41	-58.06 ± 0.37	-73.38 ± 3.61	-57.43 ± 0.53	8.09 ± 8.12	-5.12 [3]						
74537	0.76	-86.28 ± 0.35	-101.23 ± 0.91	-14.28 ± 0.33		-5.11 [4]						
75542	1.06	-161.25 ± 1.44	-22.71 ± 1.94	-4.35 ± 1.59		-4.88 [1]	4.44					-0.35
75718	0.82	20.60 ± 0.36	-20.24 ± 0.48	-18.15 ± 0.53	28.38 ± 4.38	-4.98 [3]	6.19					0.01
76375	0.95	-44.23 ± 0.37	-64.51 ± 0.40	-27.23 ± 0.38		-5.14 [3]						0.26
76779	1.29	7.84 ± 0.20	11.99 ± 0.33	-0.76 ± 0.17	37.26 ± 6.67	-4.78 [1]	2.93	-5.29	4.40			
77257	0.60				25.80 ± 3.35	-5.00 [2]	6.67	-6.21	2.36	18.0 [12]	3.00	0.04
78072	0.49	56.89 ± 0.12	-33.91 ± 0.08	-24.71 ± 0.09	28.46 ± 2.88	-5.11 [3]		-6.77	4.38			-0.13
78709	0.76	-101.33 ± 1.37	-14.21 ± 0.19	13.46 ± 0.87		-5.03 [3]	7.11					-0.07
78775	0.73	-36.14	-58.79	-18.25		-4.97 [3]	6.04					-0.49
78843	1.06	48.75 ± 0.39	-10.39 ± 0.25	-22.99 ± 0.93	12.13 ± 5.50	-5.02 [5]	6.90					
79190	0.84	33.82 ± 0.10	-10.82 ± 0.09	21.36 ± 0.23		-4.94 [7]	5.49					-0.36
79492	0.77	50.99 ± 1.03	-12.68 ± 0.53	-16.44 ± 0.78	13.07 ± 4.13	-4.93 [3]	5.32					-0.07
79672	0.65	27.36 ± 0.11	-14.35 ± 0.11	-22.03 ± 0.17	25.60 ± 3.58	-4.87 [3]	4.25			23.7 [12]	3.86	0.04

Table A.8 Continued

		Kinematics			Lithium	Ca II H,K		X-ray		Rotation		
HIP	$(B-V)$	U (km/s)	V (km/s)	W (km/s)	EW Li I (m Å)	R'_{HK} (log)	*Age* (Gyr)	L_X/L_{Bol} (log)	*Age* (Gyr)	*Prot* (Days)	*Age* (Gyr)	[Fe/H]
(1)	(2)	(3)	(4)	(5)	(6)	(7)	(8)	(9)	(10)	(11)	(12)	(13)
80366	0.96	5.05 ± 0.12	-30.28 ± 0.74	6.80 ± 0.19	5.05 ± 5.04	-4.60 [1]	1.14					-0.26
80644	1.23	-21.06 ± 0.22	-39.81 ± 0.66	-14.69 ± 0.22	24.05 ± 6.36	-4.84 [3]	3.82					
80725	0.85	-54.63 ± 0.57	-10.99 ± 0.15	12.45 ± 0.53	6.07 ± 4.50	-4.51 [1]	0.65	-5.07	1.39			
81375	0.83	6.86 ± 0.59	13.25 ± 0.25	1.44 ± 0.36	7.71 ± 4.44	-5.00 [4]	6.51	-4.80	0.66			0.17
82588	0.76	85.11 ± 0.55	-112.93 ± 1.45	9.12 ± 0.18	200.57 ± 4.07	-4.39 [1]	0.28	-4.40	0.36	11.1 [12]	0.75	-0.05
83591	1.14	46.65 ± 0.21	-63.49 ± 0.73	20.70 ± 0.11	17.64 ± 5.92							-0.62
83601	0.57	2.75 ± 0.17	-30.34 ± 0.24	-19.71 ± 0.15	90.95 ± 3.24	-4.50 [1]	0.61	-4.90	0.44	7.6 [12]	0.77	0.03
84195	0.92	22.73 ± 0.22	9.42 ± 0.11	-2.30 ± 0.26	13.44 ± 4.86	-4.99 [4]	6.37					
84478	1.14	-0.68 ± 0.13	-33.84 ± 0.13	-7.07 ± 0.04	15.10 ± 5.91	-4.66 [2]	1.63	-4.97	2.18	18.0 [12]		
84720	0.78	-6.22 ± 0.08	33.42 ± 0.21	-31.36 ± 0.23	7.29 ± 4.19	-4.94 [7]	5.49					-0.27
84862	0.61	25.49 ± 0.24	-80.78 ± 0.12	-63.65 ± 0.10		-4.96 [3]	5.91					-0.26
85235	0.76	1.59 ± 0.08	-49.84 ± 0.09	5.49 ± 0.12		-4.93 [10]	5.31					-0.33
85295	1.35	0.01 ± 0.15	-52.91 ± 0.26	-9.92 ± 0.05	28.77 ± 6.92	-4.72 [1]	2.20	-4.95	2.68			
85810	0.65	-31.01	-49.90	-1.88	33.56 ± 3.59	-4.46 [1]	0.46	-5.83	1.92			0.09
86036	0.59	35.97	-4.43	-22.33	61.79 ± 3.31	-4.76 [1]	2.67	-5.04	0.55			-0.17
86722	0.78	67.13 ± 1.05	-28.04 ± 0.90	-1.06 ± 0.27	7.55 ± 4.20	-5.09 [4]	8.32					-0.34
88622	0.60	-78.72 ± 0.32	-88.27 ± 0.43	-38.62 ± 0.26		-4.61 [3]	1.23	-5.31	1.07			-0.49
88972	0.88	16.61 ± 0.11	-31.28 ± 0.07	0.33 ± 0.08	12.59 ± 4.66	-4.96 [2]	5.76			42.0 [12]	6.24	-0.05
89937	0.50	3.64 ± 0.10	39.90 ± 0.24	-3.15 ± 0.18	29.09 ± 2.94	-4.90 [11]	4.78	-6.16	2.29			-0.40
91009	1.17	18.22	-17.57	-28.39	4.29 ± 6.06	-3.66 [1]		-3.06	0.10			
91438	0.65	38.24 ± 0.10	-2.15 ± 0.08	-4.50 ± 0.05	24.36 ± 3.61	-4.89 [7]	4.61	-5.76	2.55			-0.24
92043	0.47	37.18 ± 0.20	1.21 ± 0.22	-8.01 ± 0.08		-4.90 [3]	4.74	-5.27	0.29			0.04
92200	1.23	23.39 ± 0.25	-10.67 ± 0.34	-0.75 ± 0.10	6.96 ± 6.37	-4.65 [1]	1.52					
92283	1.06	14.11 ± 0.30	-23.24 ± 0.29	-25.33 ± 0.38	20.56 ± 5.52	-4.68 [1]	1.79					0.06
93017	0.56	-15.02 ± 0.30	-37.95 ± 0.60	-27.23 ± 0.19	42.51 ± 3.18	-4.87 [2]	4.34	-5.67	1.39	16.0 [2]	3.21	-0.15
93871	1.06	70.55 ± 2.26	-66.91 ± 2.56	-7.61 ± 0.33	1.12 ± 5.55							
95995	0.85	45.27	3.20	27.64		-5.05 [4]	7.48					-0.26
96100	0.79	31.40 ± 0.07	43.23 ± 0.05	-18.93 ± 0.06	0.78 ± 4.21	-4.83 [2]	3.67	-5.59	2.66	27.0 [2]	3.37	-0.16
96285	1.19	-69.51 ± 0.63	-14.56 ± 0.60	-13.72 ± 0.51	29.42 ± 6.18	-5.08 [1]						
97944	1.03	3.24	-28.81	0.37	±	-4.58 [5]	1.03	-4.70	0.49			
98677	0.73	52.84 ± 0.70	-15.60 ± 0.77	-17.19 ± 0.26	13.84 ± 3.97	-4.83 [3]	3.61					-0.30
98819	0.60	42.36 ± 0.27	-20.31 ± 0.17	9.52 ± 0.12	53.60 ± 3.37	-4.80 [2]	3.16	-5.88	2.01	13.5 [12]	1.75	0.04
99461	0.85	-118.41 ± 0.09	-51.77 ± 0.08	47.08 ± 0.07		-5.39 [1]						-0.44
99711	0.94	-22.84 ± 0.59	4.19 ± 0.58	22.21 ± 0.38	8.15 ± 4.95	-4.60 [1]	1.14	-5.07	1.49			-0.05

Table A.8 Continued

		Kinematics			Lithium	Ca II H,K		X-ray		Rotation		
HIP	$(B-V)$	U (km/s)	V (km/s)	W (km/s)	EW Li I (m Å)	R'_{HK} (log)	*Age* (Gyr)	L_X/L_{Bol} (log)	*Age* (Gyr)	*Prot* (Days)	*Age* (Gyr)	[Fe/H]
(1)	(2)	(3)	(4)	(5)	(6)	(7)	(8)	(9)	(10)	(11)	(12)	(13)
99825	0.89	-73.00 ± 0.19	-11.63 ± 0.06	-18.69 ± 0.17	14.56 ± 4.70	-5.05 [5]	7.50					-0.02
101345	0.69	-18.58 ± 0.24	18.86 ± 0.15	-28.04 ± 0.23	48.37 ± 3.76	-5.15 [3]						0.04
101955	1.34	-68.74	-16.82	-37.14	0.87 ± 6.94	-4.97 [3]	6.08	-4.36	1.31			
101997	0.72	-58.88 ± 0.18	20.34 ± 0.21	4.22 ± 0.14		-4.93 [7]	5.31					-0.28
103256	1.01	-81.52 ± 1.33	-8.01 ± 0.56	-8.59 ± 0.52	18.34 ± 5.29	-4.50 [1]	0.61					
104092	1.15	-15.09 ± 0.31	-76.68 ± 0.42	3.91 ± 0.40	23.52 ± 5.95	-5.23 [1]						
104214	1.15	-94.40 ± 2.10	-54.60 ± 0.26	-8.28 ± 0.45		-4.76 [2]	2.72			37.9 [12]		
104217	1.29	-92.19 ± 0.18	-53.34 ± 0.11	-9.41 ± 0.06		-4.89 [2]	4.62			48.0 [12]		
104858	0.51	5.77	-28.95	-10.05	44.03 ± 2.96	-4.91 [4]	4.86					-0.15
105858	0.48	-14.30 ± 0.05	44.80 ± 0.06	7.01 ± 0.05	45.15 ± 2.84	-4.49 [5]	0.57					-0.64
109378	0.75	5.01 ± 0.17	-49.87 ± 0.42	-7.53 ± 0.25	4.65 ± 4.06	-5.10 [3]						0.20
109527	0.82	14.04 ± 0.27	-25.35 ± 0.14	-17.31 ± 0.37	12.56 ± 4.36	-4.41 [1]	0.32	-4.88	0.70			0.16
110109	0.59	-29.52 ± 0.13	-42.13 ± 0.24	6.19 ± 0.06	22.21 ± 3.32	-4.86 [7]	4.11	-6.18	3.45			-0.19
111888	0.89	-20.60 ± 0.50	13.18 ± 0.16	-13.63 ± 0.16	29.77 ± 4.69	-4.59 [1]	1.08	-4.97	1.52			
112190	0.97	22.56 ± 0.60	-27.20 ± 0.58	7.55 ± 0.57	17.36 ± 5.11	-4.93 [4]	5.22					-0.10
112447	0.50	3.87 ± 0.08	-31.77 ± 0.14	-27.86 ± 0.14	43.13 ± 2.91	-5.28 [3]						-0.18
112870	0.85	-45.31 ± 1.01	1.20 ± 0.12	-5.99 ± 0.17	3.65 ± 4.54	-4.97 [3]	5.96					-0.47
113576	1.32	34.84 ± 0.19	16.95 ± 0.11	0.11 ± 0.19	26.85 ± 6.80	-4.63 [1]	1.36					
113718	0.94	-28.52 ± 0.37	-47.12 ± 0.42	16.73 ± 0.35	15.17 ± 4.94	-5.09 [4]						
114622	1.01	-52.91 ± 0.12	-39.48 ± 0.05	-14.27 ± 0.04		-5.10 [3]		-6.46	12.36			0.09
114886	0.91	-41.75 ± 0.74	-1.78 ± 0.24	-10.97 ± 0.19	8.63 ± 4.79	-5.11 [1]						-0.05
115331	0.81	-66.57 ± 0.77	-16.76 ± 0.25	-2.91 ± 0.10	49.87 ± 4.31	-4.15 [1]	0.04	-4.61	0.55			-0.01
115445	0.89	-40.46 ± 0.78	19.41 ± 0.13	-38.17 ± 0.16	2.95 ± 4.69	-4.70 [1]	1.99					-0.29

B
Tables of Chapter 4

B.1 Tables

Results produced in the framework of this work are only available in the electronic version of the corresponding paper or at the CDS via anonymous ftp to cdsarc.u-strasbg.fr (130.79.128.5) or via
`http://cdsarc.u-strasbg.fr/viz-bin/qcat?J/A+A/541/A40`

Table B.1 lists the stars in the SWDs (stars with known debris discs) and SWODs (stars without debris discs) samples, as well as their properties: HIP number (column 1); HD number (column 2); Hipparcos spectral-type (column 3); distance in parsec (column 4); logAge(yr) (column 5); [Fe/H] and its reference (column 6); and references for debris disc detection (column 7). References for [Fe/H] are: (a) this work; (b) Valenti & Fischer (2005); (c) Nordström et al. (2004); metallicities taken from (b) and (c) are set on the metallicity scale of this work as described in Section 4.3.2. References in column 6 are as follows: (1) Habing et al. (2001); (2) Spangler et al. (2001); (3) Chen et al. (2005); (4) Beichman et al. (2006a); (5) Bryden et al. (2006); (6) Moór et al. (2006); (7) Smith et al. (2006); (8) Rhee et al. (2007); (9) Trilling et al. (2008); (10) Kóspál et al. (2009); (11) Plavchan et al. (2009); (12) Tanner et al. (2009); (13) Koerner et al. (2010); (14) Moór et al. (2011).

Table B.2 contains: HIP number (column 1); HD number (column 2); Hipparcos spectral-type (column 3); effective temperature in kelvin (column 4); logarithm of the surface gravity in cms^{-2} (column 5); microturbulent velocity in kms^{-1} (column 6); final metallicity in dex (column 7); mean iron abundance derived from Fe I lines (column 8) in the usual scale ($A(Fe) = \log[(N_{Fe}/N_H) + 12]$); number of Fe I lines used (column 9); mean iron abundance derived from Fe II lines (column 10); number of Fe II lines used (column 11); and spectrograph (column 12). Each measured quantity is accompanied by its corresponding uncertainty.

Table B.1: The SWDs and SWODs samples.

HIP	HD	SpType	V	distance (pc)	log(Age) (yr)	[Fe/H]† (dex)	Ref
Stars with known debris discs.							
171	224930	G3V	5.80	12.17	9.60	-0.72 (a)	13
490	105	G0V	7.51	39.39	8.34	-0.03 (b)	2
544	166	K0V	6.07	13.67	9.16	0.15 (a)	5
682	377	G2V	7.59	39.08	8.34	0.12 (b)	6
1481	1466	F8/G0	7.46	41.55	8.34	-0.22 (c)	7
1598	1562	G0	6.97	24.80	9.79	-0.32 (a)	13
1599	1581	F9V	4.23	8.59	9.58	-0.29 (a)	9
2843	3296	F5	6.72	45.05		0.02 (c)	9
3810	4676	F8V	5.07	23.45	9.71	0.00 (c)	13
4148	5133	K2V	7.15	14.17	9.56	-0.16 (b)	13
5336	6582	G5V	5.17	7.55	9.69	-0.89 (a)	13
5862	7570	F8V	4.97	15.10	9.62	0.17 (a)	10
5944	7590	G0	6.59	23.20	8.70	-0.02 (a)	11
6878	8907	F8	6.66	34.77	8.78	-0.09 (b)	6
7576	10008	G5	7.66	23.96	8.10	0.08 (a)	11
8102	10700	G8V	3.49	3.65	9.77	-0.43 (a)	1
11160	15060	F5	7.02	75.99		-0.08 (c)	14
12623	16739	F9V	4.91	24.19	9.83	0.21 (c)	13
13402	17925	K1V	6.05	10.35	8.24	0.08 (a)	1
13642	18143	K2	7.52	23.52		0.35 (a)	13
15371	20807	G1V	5.24	12.03	9.49	-0.16 (a)	9
16852	22484	F9V	4.29	13.97	9.88	-0.07 (a)	9
17439	23484	K1V	6.99	16.03	8.88	0.04 (b)	13
18859	25457	F5V	5.38	18.84	9.06	-0.04 (c)	6
19335	25998	F7V	5.52	21.00	9.36	0.08 (c)	4
22263	30495	G3V	5.49	13.27	9.08	0.04 (a)	1
22295	32195	F7V	8.14	61.01		-0.07 (c)	14
23693	33262	F7V	4.71	11.64	8.76	-0.15 (c)	5
23816	33081	F7V	7.04	50.61		-0.13 (c)	14
24205	33636	G0	7.00	28.37	9.56	-0.15 (b)	9
24947	35114	F6V	7.39	48.31		-0.12 (c)	14
25486	35850	F7V	6.30	27.04	7.29	-0.09 (b)	2
26779	37394	K1V	6.21	12.28	8.93	0.14 (a)	12
27072	38393	F7V	3.59	8.93	9.47	-0.09 (a)	8
27980	39833	G0III	7.65	41.22		0.20 (c)	8
29568	43162	G5V	6.37	16.72	8.45	0.00 (a)	10
31711	48189	G1/G2V	6.15	21.29	8.02	-0.18 (c)	11
32480	48682	G0V	5.24	16.72	9.80	0.16 (a)	4

Table B.1 Continued

HIP	HD	SpType	V	distance (pc)	log(Age) (yr)	[Fe/H]† (dex)	Ref
32775	50571	F7III-IV	6.11	33.62	8.93	0.08 (c)	6
33690	53143	K0IV-V	6.81	18.33	8.92	0.28 (a)	6
34819	55052	F5IV	5.85	109.77		0.07 (c)	8
36515	59967	G3V	6.66	21.82	8.39	-0.19 (c)	11
36827	60491	K2V	8.16	24.56	7.92	-0.18 (a)	13
36906	60234	G0	7.68	133.87		0.15 (c)	8
36948	61005	G3/G5V	8.23	35.35	8.27	-0.13 (c)	8
42333	73350	G0	6.74	23.98	8.48	0.07 (a)	11
42430	73752	G3/G5V	5.05	19.38	9.86	0.39 (c)	8
42438	72905	G1.5V	5.63	14.35	8.41	-0.02 (a)	2
43625	75616	F5	6.92	35.42		-0.26 (c)	9
43726	76151	G3V	6.01	17.39	9.20	0.23 (a)	12
50384	89125	F8V	5.81	22.82	9.84	-0.27 (a)	13
52462	92945	K1V	7.72	21.40	8.45	-0.15 (b)	3
56830	101259	G6/G8V	6.40	63.09		-0.72 (b)	9
59422	105912	F5	6.95	49.68		-0.01 (c)	9
60025	107067	F8	8.69	65.96	9.22	-0.03 (c)	2
60074	107146	G2V	7.04	27.46	8.28	-0.07 (b)	6
60582	108102	F8	8.12	95.15	8.00	-0.07 (c)	2
62207	110897	G0V	5.95	17.38	9.80	-0.53 (a)	9
63584	113337	F6V	6.01	36.89		0.13 (c)	8
66704	119124	F8V	6.31	25.33	8.38	-0.16 (c)	3
66765	118972	K1V	6.92	15.65	8.60	-0.11 (b)	9
66781	119332	K0IV-V	7.77	24.63		-0.07 (a)	13
68101	121384	G8V	6.00	38.70		-0.53 (b)	8
68380	122106	F8V	6.36	77.52		0.20 (c)	6
68593	122652	F8	7.16	39.29	9.47	-0.02 (b)	8
69682	124718	G5V	8.89	63.17		-0.03 (c)	8
69989	125451	F5IV	5.41	26.10		0.07 (c)	2
70344	126265	G2III	7.21	70.42		0.12 (c)	8
72848	131511	K2V	6.00	11.51	8.84	0.13 (a)	13
73869	134319	G5	8.40	44.74	8.20	-0.15 (b)	2
74702	135599	K0	6.92	15.85	8.31	-0.13 (a)	11
74975	136202	F8III-IV	5.04	25.38	9.92	0.02 (c)	13
76375	139323	K3V	7.65	22.38		0.30 (b)	8
76635	139590	G0V	7.50	55.77		0.08 (c)	8
76829	139664	F5IV-V	4.64	17.44		-0.05 (c)	1
79492	145958	G8V	6.68	23.79	9.73	-0.09 (b)	13
81800	151044	F8V	6.48	29.33	9.82	-0.03 (b)	1
85235	158633	K0V	6.44	12.80	9.73	-0.44 (a)	4

Table B.1 Continued

HIP	HD	SpType	V	distance (pc)	log(Age) (yr)	[Fe/H]† (dex)	Ref
88399	164249	F5V	7.01	48.15		-0.07 (c)	6
88745	165908	F7V	5.05	15.64	9.37	-0.60 (a)	13
89770	169666	F5	6.68	53.22		0.02 (c)	6
90936	170773	F5V	6.22	36.98	8.44	0.00 (c)	6
93815	177171	F7	5.17	56.72		0.01 (c)	7
94050	177996	K1V	7.89	33.84	8.33	-0.23 (c)	2
94858	180134	F7	6.36	45.07		-0.12 (c)	7
95270	181327	F5/F6V	7.04	51.81		0.14 (c)	6
96258	184960	F7V	5.71	25.11		-0.17 (c)	2
99273	191089	F5V	7.18	52.22		-0.09 (c)	6
99316	191499	K0	7.56	23.64		-0.16 (a)	13
102626	197890	K0V	9.44	52.19		-1.49 (c)	11
103389	199260	F7V	5.70	21.97	8.48	-0.11 (c)	4
104239	200968	K1V	7.12	17.58	9.47	-0.01 (a)	13
105184	202628	G5V	6.75	24.42	9.47	-0.02 (b)	13
105388	202917	G5V	8.65	42.97	7.18	0.03 (b)	2
107022	205536	G8V	7.07	22.02	9.91	-0.04 (b)	8
107350	206860	G0V	5.96	17.88	8.73	-0.20 (a)	9
107412	206893	F5V	6.69	38.34	8.68	-0.01 (c)	6
107649	207129	G2V	5.57	15.99	9.84	-0.06 (b)	1
108028	208038	K0	8.18	23.04	8.48	-0.02 (a)	13
108809	209253	F6/F7V	6.63	30.14	8.39	-0.03 (b)	2
110753	212695	F5	6.94	46.49		-0.02 (c)	9
111170	213429	F7V	6.15	25.41	9.56	0.02 (c)	14
114236	218340	G3	8.44	56.59		0.09 (a)	7
114924	219623	F7V	5.58	20.50		-0.03 (c)	4
114948	219482	F7V	5.64	20.54	8.59	-0.15 (c)	4
117712	223778	K3V	6.36	10.89	8.93	-0.68 (c)	13
	3670	F5V	8.23			-0.07 (c)	14
Stars without debris discs.							
394	225239	G2V	6.09	39.18		-0.41 (c)	
462	63	F5	7.13	50.66		-0.09 (c)	
910	693	F5V	4.89	18.75	9.48	-0.32 (c)	
1573	1539	F5	7.03	43.69		-0.04 (c)	
2802	3302	F6V	5.51	34.82	8.50	0.04 (c)	
3170	3823	G1V	5.89	24.96	9.63	-0.26 (b)	
3185	3795	G3/G5V	6.14	28.89	9.82	-0.49 (b)	
3236	3861	F5	6.52	33.44	9.25	0.05 (b)	
3559	4307	G2V	6.15	31.00	9.89	-0.22 (b)	
3765	4628	K2V	5.74	7.45		-0.24 (a)	

Table B.1 Continued

HIP	HD	SpType	V	distance (pc)	log(Age) (yr)	[Fe/H]† (dex)	Ref
3909	4813	F7IV-V	5.17	15.75	2.93	-0.16 (a)	
7601	10800	G2V	5.88	27.38	9.09	-0.11 (c)	
7981	10476	K1V	5.24	7.53		-0.03 (a)	
8486	11131	G0	6.72	22.56	7.72	-0.03 (a)	
10306	13555	F5V	5.23	28.87		-0.21 (c)	
10798	14412	G8V	6.33	12.67	9.61	-0.46 (a)	
11072	14802	G2V	5.19	21.96	9.80	-0.06 (a)	
11548	15335	G0V	5.89	31.41		-0.24 (b)	
11783	15798	F5V	4.74	26.70	9.26	-0.26 (c)	
12114	16160	K3V	5.79	7.18		-0.19 (a)	
12777	16895	F7V	4.10	11.13	9.90	0.12 (a)	
14632	19373	G0V	4.05	10.54	9.82	0.11 (a)	
15330	20766	G2V	5.53	12.01	9.61	-0.21 (a)	
15457	20630	G5Vvar	4.84	9.14	8.54	0.09 (a)	
17378	23249	K0IV	3.52	9.04		0.03 (b)	
19855	26913	G5IV	6.94	21.06	8.45	-0.11 (c)	
22449	30652	F6V	3.19	8.07	9.48	-0.01 (b)	
23311	32147	K3V	6.22	8.71		0.29 (a)	
24786	34721	G0V	5.96	25.03	9.79	-0.24 (a)	
24813	34411	G0V	4.69	12.63	9.83	0.08 (a)	
25278	35296	F8V	5.00	14.39	8.41	-0.09 (c)	
27913	39587	G0V	4.39	8.66	8.75	-0.09 (a)	
28954	41593	K0	6.76	15.27	8.70	0.19 (a)	
29271	43834	G5V	5.08	10.20	9.74	0.12 (a)	
32984	50281	K3V	6.58	8.71		-0.02 (b)	
33277	50692	G0V	5.74	17.24	9.74	-0.11 (a)	
34017	52711	G4V	5.93	19.13	9.74	-0.14 (a)	
35136	55575	G0V	5.54	16.89	9.72	-0.36 (a)	
36439	58855	F6V	5.35	20.24		-0.23 (c)	
37283	60912	F5	6.89	45.50		-0.07 (c)	
37853	63077	G0V	5.36	15.21	9.55	-0.72 (c)	
38172	63333	F5	7.09	43.08		-0.38 (c)	
39780	67228	G2IV	5.30	23.29	9.69	0.19 (b)	
39903	68456	F5V	4.74	19.98	8.09	-0.17 (c)	
40843	69897	F6V	5.13	18.27		-0.39 (a)	
41226	70843	F5	7.06	46.30		0.14 (b)	
41484	71148	G5V	6.32	22.25		0.01 (a)	
41573	71640	F5	7.40	44.74		-0.18 (c)	
41926	72673	K0V	6.38	12.21	9.75	-0.40 (b)	
42074	72760	G5	7.32	21.14	8.03	0.01 (a)	

Table B.1 Continued

HIP	HD	SpType	V	distance (pc)	log(Age) (yr)	[Fe/H]† (dex)	Ref
42808	74576	K2V	6.58	11.14	8.73	-0.16 (a)	
44728	77967	F0	6.61	43.25		-0.36 (c)	
44897	78366	F9V	5.95	19.19	8.70	0.03 (b)	
45699	80218	F5	6.61	40.65		-0.21 (c)	
47403	83451	F5	7.12	49.04		-0.06 (c)	
47436	83525	F5	6.90	48.97		-0.07 (c)	
47592	84117	G0V	4.93	15.01	9.62	-0.21 (a)	
48113	84737	G2V	5.08	18.37	9.87	0.10 (a)	
48768	86147	F5	6.70	47.01		-0.01 (c)	
50366	88984	F5	7.30	51.15		-0.21 (c)	
51459	90839	F8V	4.82	12.78	9.47	-0.15 (a)	
52574	93081	F5	7.09	48.38		-0.22 (c)	
53252	94388	F6V	5.23	30.81	9.54	0.24 (c)	
54745	97334	G0V	6.41	21.93	8.03	-0.01 (a)	
55666	99126	F5	6.94	49.75		-0.09 (c)	
56186	100067	F5	7.17	39.95		-0.32 (c)	
56452	100623	K0V	5.96	9.56	9.61	-0.38 (a)	
56997	101501	G8Vvar	5.31	9.61	8.91	0.01 (a)	
57507	102438	G5V	6.48	17.47	9.72	-0.28 (b)	
57757	102870	F8V	3.59	10.93	9.81	0.09 (a)	
57939	103095	G8Vp	6.42	9.09	9.67	-1.12 (a)	
58268	103773	F5	6.73	46.45		0.05 (c)	
58803	104731	F6V	5.15	25.32	8.56	-0.01 (c)	
61100	109011	K2V	8.08	25.10		-0.34 (a)	
61578	109756	F5	6.95	48.52		-0.15 (c)	
62523	111395	G7V	6.29	16.93	8.57	0.22 (a)	
62636	111545	F5	6.99	47.76		-0.02 (c)	
63033	112164	G2IV	5.89	40.10		0.20 (c)	
63742	113449	G5V	7.69	21.70	8.28	-0.17 (a)	
64394	114710	G0V	4.23	9.13	9.89	0.11 (a)	
64408	114613	G3V	4.85	20.67		0.18 (b)	
64792	115383	G0Vs	5.19	17.56	8.61	0.24 (a)	
65515	116956	G9IV-V	7.29	21.59	7.84	0.03 (a)	
65530	117043	G6V	6.50	21.17		0.29 (a)	
67195	120005	F5	6.51	43.73		0.05 (c)	
67620	120690	G5V	6.43	19.47	9.31	0.05 (a)	
69040	123691	F2	6.80	53.02		-0.08 (c)	
69090	122862	G1V	6.02	28.50	9.82	-0.15 (b)	
70497	126660	F7V	4.04	14.53	9.03	-0.08 (c)	
70873	127334	G5V	6.36	23.74		0.25 (b)	

Table B.1 Continued

HIP	HD	SpType	V	distance (pc)	log(Age) (yr)	[Fe/H]† (dex)	Ref
71743	128987	G6V	7.24	23.67	8.81	0.01 (a)	
72130	130460	F5	7.22	49.12		-0.01 (c)	
72567	130948	G2V	5.86	18.17	8.28	-0.01 (b)	
72573	133002	F9V	5.63	43.29		-0.41 (c)	
73996	134083	F5V	4.93	19.55	9.60	0.05 (b)	
74605	136064	F9IV	5.15	25.34	9.46	-0.03 (c)	
77372	141128	F5	7.00	49.24		-0.19 (c)	
77408	141272	G8V	7.44	21.29	8.29	-0.14 (a)	
77760	142373	F9V	4.60	15.89	9.87	-0.50 (a)	
77801	142267	G0IV	6.07	17.35	9.60	-0.50 (a)	
77838	143105	F5	6.76	48.66		0.03 (c)	
78072	142860	F6V	3.85	11.25		-0.17 (b)	
79672	146233	G1V	5.49	13.90	9.63	0.04 (a)	
81300	149661	K2V	5.77	9.75	9.36	0.05 (a)	
82588	152391	G8V	6.65	17.25	8.44	0.04 (a)	
84862	157214	G0V	5.38	14.33	9.77	-0.41 (a)	
88972	166620	K2V	6.38	11.02	9.76	-0.07 (b)	
89348	168151	F5V	4.99	22.92	9.62	-0.17 (c)	
90485	169830	F8V	5.90	36.60	9.81	0.09 (b)	
91120	171886	F5	7.16	49.43		-0.30 (c)	
91438	172051	G5V	5.85	13.08	9.66	-0.21 (a)	
92043	173667	F6V	4.19	19.21	9.68	0.12 (b)	
93252	176441	F5	7.06	46.77		-0.16 (c)	
93858	177565	G8V	6.15	16.95	9.78	0.07 (b)	
94346	180161	G8V	7.04	20.02	8.84	0.18 (a)	
94981	181655	G8V	6.29	25.39	9.79	0.02 (b)	
95149	181321	G1/G2V	6.48	18.83	8.39	-0.21 (c)	
96100	185144	K0V	4.67	5.75	9.56	-0.26 (a)	
96895	186408	G2V	5.99	21.08	9.84	0.02 (a)	
97675	187691	F8V	5.12	19.19	9.85	0.13 (b)	
98066	188376	G3/G5III	4.70	25.99	9.87	0.06 (c)	
98819	190406	G1V	5.80	17.77	9.50	0.12 (a)	
98959	189567	G2V	6.07	17.73	9.61	-0.22 (b)	
99240	190248	G5IV-Vvar	3.55	6.11	9.82	0.36 (a)	
99461	191408	K2V	5.32	6.02		-0.40 (b)	
100017	193664	G3V	5.91	17.57	9.58	-0.14 (b)	
101983	196378	F8V	5.11	24.66	9.57	-0.39 (b)	
101997	196761	G8/K0V	6.36	14.38	9.72	-0.30 (b)	
102485	197692	F5V	4.13	14.68	8.49	0.03 (c)	
103931	200433	F5	6.91	47.37		-0.05 (c)	

Table B.1 Continued

HIP	HD	SpType	V	distance (pc)	log(Age) (yr)	[Fe/H]† (dex)	Ref
105202	202884	F5	7.27	41.81		-0.27 (c)	
105858	203608	F6V	4.21	9.26	8.76	-0.84 (a)	
109422	210302	F6V	4.94	18.28	9.55	0.09 (b)	
109821	210918	G5V	6.23	22.05		-0.09 (b)	
110649	212330	F9V	5.31	20.56		0.00 (b)	
112447	215648	F7V	4.20	16.30		-0.20 (b)	
113829	217813	G5V	6.65	24.72		0.02 (b)	
114622	219134	K3Vvar	5.57	6.55		0.10 (b)	
115220	219983	F2	6.64	48.73		-0.12 (c)	
115331	220182	K1V	7.36	21.52	7.56	0.11 (a)	
116250	221420	G2V	5.82	31.44		0.33 (b)	
116613	222143	G5	6.58	23.33	9.08	0.14 (a)	
116745	222237	K3V	7.09	11.42		-0.24 (b)	
116771	222368	F7V	4.13	13.71		-0.13 (a)	
116906	222582	G5	7.68	41.77		-0.03 (b)	

Table B.2: Basic physical parameters and metallicities, for the stars measured in this work.

HIP	HD	SpType	$T_{\rm eff}$ (K)	$\log g$ ($\rm cms^{-2}$)	ξ_t ($\rm kms^{-1}$)	[Fe/H] dex	$\langle A(\rm Fe\ I)\rangle$	$n_{\rm I}$	$\langle A(\rm Fe\ II)\rangle$	$n_{\rm II}$	Spec.†
(1)	(2)	(3)	(4)	(5)	(6)	(7)	(8)	(9)	(10)	(11)	(12)
Stars with known debris discs											
171	224930	G3V	5491 ± 31	4.75 ± 0.12	0.92 ± 0.40	-0.72 ± 0.08	6.78 ± 0.11	52	6.78 ± 0.12	12	4
544	166	K0V	5575 ± 51	4.68 ± 0.14	1.05 ± 0.25	0.15 ± 0.05	7.65 ± 0.06	57	7.65 ± 0.06	13	4
1598	1562	G0	5603 ± 36	4.30 ± 0.12	0.67 ± 0.27	-0.32 ± 0.06	7.18 ± 0.07	58	7.18 ± 0.09	12	1
1599	1581	F9V	5809 ± 39	4.24 ± 0.12	1.30 ± 0.30	-0.29 ± 0.06	7.21 ± 0.08	59	7.22 ± 0.10	13	5
5336	6582	G5V	5291 ± 32	4.57 ± 0.11	0.82 ± 0.42	-0.89 ± 0.08	6.61 ± 0.11	55	6.62 ± 0.12	12	4
5862	7570	F8V	6111 ± 35	4.42 ± 0.10	1.35 ± 0.17	0.17 ± 0.03	7.67 ± 0.04	50	7.67 ± 0.04	13	6
5944	7590	G0	5951 ± 39	4.65 ± 0.11	1.04 ± 0.38	-0.02 ± 0.05	7.48 ± 0.06	48	7.48 ± 0.08	11	1
7576	10008	G5	5293 ± 68	4.90 ± 0.19	0.39 ± 0.45	0.08 ± 0.06	7.58 ± 0.07	53	7.58 ± 0.10	9	1
8102	10700	G8V	5312 ± 137	4.59 ± 0.13	0.15 ± 0.69	-0.43 ± 0.15	7.07 ± 0.24	63	7.07 ± 0.20	11	4
13402	17925	K1V	5103 ± 47	4.51 ± 0.17	0.87 ± 0.22	0.08 ± 0.06	7.58 ± 0.05	45	7.58 ± 0.09	12	4
13642	18143	K2V	5162 ± 54	4.54 ± 0.15	0.31 ± 0.38	0.35 ± 0.03	7.86 ± 0.03	53	7.85 ± 0.05	10	1
15371	20807	G1V	5874 ± 40	4.64 ± 0.11	0.87 ± 0.27	-0.16 ± 0.05	7.34 ± 0.06	61	7.34 ± 0.07	13	5
16852	22484	F9V	5979 ± 56	4.68 ± 0.17	1.22 ± 0.19	-0.07 ± 0.03	7.43 ± 0.03	59	7.43 ± 0.04	13	4
22263	30495	G3V	5852 ± 25	4.64 ± 0.08	0.94 ± 0.22	0.04 ± 0.03	7.54 ± 0.04	63	7.54 ± 0.04	13	4
26779	37394	K1V	5265 ± 44	4.69 ± 0.12	0.56 ± 0.38	0.14 ± 0.05	7.64 ± 0.06	56	7.63 ± 0.08	11	4
27072	38393	F7V	6259 ± 36	4.44 ± 0.09	1.51 ± 0.16	-0.09 ± 0.04	7.41 ± 0.05	33	7.41 ± 0.05	10	5
29568	43162	G5V	5619 ± 40	4.65 ± 0.12	1.04 ± 0.23	0.00 ± 0.04	7.50 ± 0.06	56	7.50 ± 0.06	12	6
32480	48682	G0V	6132 ± 26	4.67 ± 0.07	1.10 ± 0.18	0.16 ± 0.03	7.66 ± 0.03	55	7.66 ± 0.04	11	1
33690	53143	K0IV-V	5521 ± 43	4.65 ± 0.11	0.73 ± 0.26	0.28 ± 0.04	7.78 ± 0.05	57	7.79 ± 0.05	11	6
36827	60491	K2V	5079 ± 61	4.59 ± 0.15	0.59 ± 0.43	-0.18 ± 0.10	7.32 ± 0.12	45	7.31 ± 0.17	11	1
42333	73350	G0	5818 ± 90	4.42 ± 0.27	1.34 ± 0.30	0.07 ± 0.07	7.57 ± 0.10	56	7.57 ± 0.11	12	1
42438	72905	G1.5Vb	5893 ± 53	4.49 ± 0.18	1.30 ± 0.27	-0.02 ± 0.05	7.48 ± 0.07	50	7.48 ± 0.08	13	1
43726	76151	G3V	5859 ± 24	4.77 ± 0.07	0.65 ± 0.30	0.23 ± 0.03	7.73 ± 0.04	57	7.73 ± 0.03	12	1
50384	89125	F8V	6118 ± 49	4.29 ± 0.14	1.15 ± 0.23	-0.27 ± 0.06	7.23 ± 0.08	29	7.23 ± 0.09	11	1
62207	110897	G0V	5789 ± 55	4.29 ± 0.17	1.29 ± 0.44	-0.53 ± 0.10	6.97 ± 0.13	53	6.97 ± 0.15	11	1
66781	119332	K0IV-V	5154 ± 90	4.55 ± 0.21	0.34 ± 0.44	-0.07 ± 0.11	7.44 ± 0.12	51	7.43 ± 0.18	8	1
72848	131511	K2V	5319 ± 50	4.73 ± 0.13	0.57 ± 0.38	0.13 ± 0.05	7.63 ± 0.06	53	7.63 ± 0.07	13	4
74702	135599	K0	5277 ± 70	4.17 ± 0.23	1.15 ± 0.19	-0.13 ± 0.10	7.37 ± 0.08	45	7.37 ± 0.17	4	2
85235	158633	K0V	5210 ± 44	4.51 ± 0.13	0.02 ± 0.49	-0.44 ± 0.07	7.06 ± 0.07	63	7.06 ± 0.11	11	4
88745	165908	F7V	5938 ± 38	4.17 ± 0.10	1.51 ± 0.27	-0.60 ± 0.07	6.90 ± 0.09	41	6.90 ± 0.11	11	3
99316	191499	G8V	5220 ± 62	4.42 ± 0.15	0.51 ± 0.37	-0.16 ± 0.09	7.35 ± 0.12	57	7.34 ± 0.13	11	1
104239	200968	K1V	5239 ± 115	4.67 ± 0.28	1.10 ± 0.51	-0.01 ± 0.13	7.49 ± 0.17	55	7.49 ± 0.21	10	1
107350	206860	G0V	5750 ± 36	4.27 ± 0.12	1.47 ± 0.32	-0.20 ± 0.06	7.30 ± 0.08	30	7.30 ± 0.08	4	1
108028	208038	K0	4965 ± 27	4.58 ± 0.09	0.61 ± 0.26	-0.02 ± 0.02	7.48 ± 0.03	59	7.47 ± 0.05	10	1
114236	218340	G3V	5888 ± 30	4.48 ± 0.08	0.89 ± 0.18	0.09 ± 0.03	7.59 ± 0.04	49	7.59 ± 0.04	13	6

Table B.2 Continued

HIP	HD	SpType	$T_{\rm eff}$ (K)	$\log g$ ($\rm cms^{-2}$)	ξ_t ($\rm kms^{-1}$)	[Fe/H] dex	$\langle A(\rm Fe\ I)\rangle$	$n_{\rm I}$	$\langle A(\rm Fe\ II)\rangle$	$n_{\rm II}$	Spec.[†]
(1)	(2)	(3)	(4)	(5)	(6)	(7)	(8)	(9)	(10)	(11)	(12)
Stars with known planets and debris discs											
7978	10647	F8V	6101 ± 40	4.49 ± 0.11	1.38 ± 0.16	-0.09 ± 0.04	7.41 ± 0.05	32	7.41 ± 0.06	9	6
14954	19994	F8V	6140 ± 31	4.35 ± 0.09	1.44 ± 0.12	0.19 ± 0.03	7.69 ± 0.03	34	7.69 ± 0.04	8	3
15510	20794	G8V	5386 ± 31	4.53 ± 0.08	0.26 ± 0.40	-0.34 ± 0.06	7.16 ± 0.09	56	7.16 ± 0.08	12	5
16537	22049	K2V	5061 ± 25	4.65 ± 0.09	0.37 ± 0.35	-0.08 ± 0.05	7.42 ± 0.05	55	7.41 ± 0.08	12	4
27435	38858	G4V	5660 ± 20	4.36 ± 0.06	0.97 ± 0.11	-0.27 ± 0.03	7.23 ± 0.03	42	7.23 ± 0.04	6	2
40693	69830	K0V	5400 ± 40	4.57 ± 0.10	0.48 ± 0.44	0.00 ± 0.05	7.50 ± 0.07	63	7.50 ± 0.07	13	4
64924	115617	G5V	5400 ± 40	4.57 ± 0.10	0.48 ± 0.44	0.00 ± 0.05	7.50 ± 0.07	63	7.50 ± 0.07	13	4
65721	117176	G5V	5546 ± 39	4.09 ± 0.12	1.13 ± 0.21	-0.03 ± 0.05	7.47 ± 0.07	59	7.47 ± 0.07	11	1
71395	128311	K0	4906 ± 9	4.32 ± 0.03	0.88 ± 0.06	0.04 ± 0.02	7.54 ± 0.02	61	7.54 ± 0.02	12	1
99711	192263	K0V	4920 ± 49	4.65 ± 0.13	0.66 ± 0.30	-0.01 ± 0.07	7.50 ± 0.06	61	7.48 ± 0.13	10	1
Stars with known planets but without known debris discs											
3093	3651	K0V	5196 ± 31	4.49 ± 0.11	0.01 ± 0.35	0.20 ± 0.03	7.71 ± 0.03	53	7.70 ± 0.05	13	4
6379	7924	K0	5233 ± 43	4.50 ± 0.16	0.54 ± 0.21	-0.20 ± 0.07	7.30 ± 0.04	54	7.30 ± 0.13	9	3
7513	9826	F8V	6153 ± 42	4.28 ± 0.12	1.47 ± 0.20	0.11 ± 0.04	7.61 ± 0.05	49	7.61 ± 0.06	13	4
10138	13445	K0V	5168 ± 55	4.56 ± 0.12	0.49 ± 0.44	-0.20 ± 0.05	7.32 ± 0.06	57	7.32 ± 0.08	12	5
49699	87883	K0V	5000 ± 30	4.62 ± 0.07	0.30 ± 0.22	0.14 ± 0.03	7.65 ± 0.03	62	7.62 ± 0.05	12	1
43587	75732	G8V	6140 ± 31	4.35 ± 0.09	1.44 ± 0.12	0.19 ± 0.03	7.69 ± 0.03	42	7.69 ± 0.04	10	4
53721	95128	G0V	5789 ± 33	4.26 ± 0.11	1.07 ± 0.23	-0.03 ± 0.04	7.47 ± 0.06	61	7.47 ± 0.06	13	4
57443	102365	G3/G5V	5524 ± 40	4.29 ± 0.13	0.81 ± 0.30	-0.37 ± 0.07	7.13 ± 0.08	56	7.13 ± 0.09	12	5
78459	143761	G2V	5793 ± 25	4.28 ± 0.08	0.93 ± 0.17	-0.17 ± 0.05	7.34 ± 0.05	46	7.34 ± 0.06	12	1
79248	145675	K0V	5312 ± 72	4.43 ± 0.24	0.52 ± 0.50	0.46 ± 0.06	7.97 ± 0.11	54	7.96 ± 0.10	11	1
80337	147513	G3/G5V	5917 ± 35	4.61 ± 0.11	0.96 ± 0.28	0.10 ± 0.04	7.60 ± 0.05	64	7.60 ± 0.05	13	5
83389	154345	G8V	5461 ± 35	4.59 ± 0.09	0.57 ± 0.46	-0.06 ± 0.05	7.44 ± 0.07	53	7.44 ± 0.07	8	3
95319	182488	G8V	5452 ± 63	4.64 ± 0.16	0.66 ± 0.37	0.16 ± 0.06	7.66 ± 0.07	56	7.66 ± 0.08	10	3
96901	186427	G5V	5680 ± 62	4.37 ± 0.21	0.89 ± 0.16	0.01 ± 0.06	7.51 ± 0.06	53	7.51 ± 0.09	10	3
109378	210277	G0	5531 ± 30	4.25 ± 0.09	0.83 ± 0.14	0.20 ± 0.03	7.70 ± 0.04	43	7.70 ± 0.04	4	2
113357	217014	G5V	5710 ± 20	4.15 ± 0.16	1.10 ± 0.09	0.11 ± 0.03	7.61 ± 0.03	52	7.61 ± 0.06	10	3
Comparison sample											
3765	4628	K2V	5014 ± 37	4.67 ± 0.11	0.35 ± 0.40	-0.24 ± 0.02	7.27 ± 0.04	61	7.26 ± 0.07	12	4
3909	4813	F7IV-V	6150 ± 29	4.27 ± 0.08	1.33 ± 0.17	-0.16 ± 0.04	7.34 ± 0.04	43	7.34 ± 0.06	9	3
7981	10476	K1V	5262 ± 69	4.65 ± 0.17	0.71 ± 0.50	-0.03 ± 0.09	7.47 ± 0.12	55	7.48 ± 0.13	12	4
8486	11131	G0V	5864 ± 29	4.63 ± 0.07	0.94 ± 0.17	-0.03 ± 0.03	7.47 ± 0.04	57	7.48 ± 0.04	13	6
10798	14412	G8V	5359 ± 25	4.59 ± 0.07	0.48 ± 0.39	-0.46 ± 0.05	7.04 ± 0.06	62	7.04 ± 0.06	11	4
11072	14802	G2V	5853 ± 49	3.99 ± 0.15	1.28 ± 0.15	-0.06 ± 0.05	7.44 ± 0.06	43	7.44 ± 0.08	9	6
12114	16160	K3V	4857 ± 52	4.54 ± 0.12	0.04 ± 0.43	-0.19 ± 0.10	7.32 ± 0.09	59	7.30 ± 0.16	9	1
12777	16895	F7V	6304 ± 76	4.54 ± 0.20	1.38 ± 0.35	0.12 ± 0.05	7.62 ± 0.06	43	7.62 ± 0.07	12	4
14632	19373	G0V	5975 ± 67	4.14 ± 0.21	1.32 ± 0.16	0.11 ± 0.05	7.61 ± 0.06	60	7.61 ± 0.08	13	4
15330	20766	G2V	5719 ± 29	4.63 ± 0.08	0.87 ± 0.18	-0.21 ± 0.04	7.29 ± 0.05	54	7.29 ± 0.06	13	5
15457	20630	G5Vvar	5718 ± 50	4.52 ± 0.12	0.94 ± 0.26	0.09 ± 0.04	7.59 ± 0.06	61	7.59 ± 0.06	13	4
23311	32147	K3V	4746 ± 30	4.55 ± 0.09	0.50 ± 0.25	0.29 ± 0.02	7.80 ± 0.02	60	7.79 ± 0.05	10	4
24786	34721	G0V	5716 ± 70	3.54 ± 0.25	1.22 ± 0.27	-0.24 ± 0.09	7.26 ± 0.12	39	7.26 ± 0.14	5	2
24813	34411	G0V	5871 ± 36	4.40 ± 0.11	1.24 ± 0.19	0.08 ± 0.04	7.58 ± 0.05	62	7.59 ± 0.05	13	4
27913	39587	G0V	5813 ± 26	4.45 ± 0.08	1.12 ± 0.18	-0.09 ± 0.04	7.41 ± 0.05	43	7.41 ± 0.05	12	4
28954	41593	K0	5515 ± 31	4.67 ± 0.09	1.01 ± 0.32	0.19 ± 0.04	7.69 ± 0.06	52	7.70 ± 0.05	12	1
29271	43834	G8V	5649 ± 37	4.60 ± 0.10	0.80 ± 0.31	0.12 ± 0.05	7.62 ± 0.06	62	7.62 ± 0.06	13	5
33277	50692	G0V	5870 ± 31	4.57 ± 0.09	0.83 ± 0.23	-0.11 ± 0.04	7.39 ± 0.05	54	7.39 ± 0.05	11	1
34017	52711	G4V	5797 ± 37	4.20 ± 0.11	0.98 ± 0.18	-0.14 ± 0.05	7.36 ± 0.06	62	7.36 ± 0.07	13	1
35136	55575	G0V	5821 ± 46	4.29 ± 0.13	1.32 ± 0.22	-0.36 ± 0.06	7.14 ± 0.07	59	7.14 ± 0.09	13	1
40843	69897	F6V	6041 ± 69	3.79 ± 0.18	1.51 ± 0.35	-0.39 ± 0.09	7.11 ± 0.10	42	7.11 ± 0.13	13	1
41484	71148	G5V	5838 ± 39	4.58 ± 0.12	1.30 ± 0.33	0.01 ± 0.05	7.51 ± 0.06	57	7.52 ± 0.07	12	1
42074	72760	G5	5203 ± 40	4.62 ± 0.09	0.66 ± 0.37	0.01 ± 0.06	7.52 ± 0.07	52	7.51 ± 0.08	10	1
42808	74576	K2V	4915 ± 45	4.48 ± 0.11	1.05 ± 0.28	-0.16 ± 0.09	7.35 ± 0.11	51	7.34 ± 0.14	9	5
47592	84117	G0V	5991 ± 62	4.21 ± 0.17	1.89 ± 0.36	-0.21 ± 0.08	7.29 ± 0.10	36	7.29 ± 0.11	6	2
48113	84737	G2V	5821 ± 25	4.06 ± 0.08	1.15 ± 0.12	0.10 ± 0.03	7.60 ± 0.03	57	7.60 ± 0.04	11	1
51459	90839	F8V	6050 ± 28	4.29 ± 0.08	1.28 ± 0.15	-0.15 ± 0.04	7.35 ± 0.04	62	7.35 ± 0.05	13	4
54745	97334	G0V	5865 ± 45	4.46 ± 0.13	1.48 ± 0.34	-0.01 ± 0.06	7.49 ± 0.07	44	7.49 ± 0.08	10	1
56452	100623	K0V	5139 ± 53	4.55 ± 0.12	0.70 ± 0.28	-0.38 ± 0.07	7.12 ± 0.08	58	7.12 ± 0.11	10	4
56997	101501	G8V	5591 ± 49	4.60 ± 0.14	0.93 ± 0.20	0.01 ± 0.04	7.50 ± 0.04	63	7.51 ± 0.06	13	4
57757	102870	F8V	6044 ± 40	4.02 ± 0.12	1.41 ± 0.18	0.09 ± 0.04	7.59 ± 0.05	60	7.59 ± 0.06	12	4
57939	103095	G8V	5144 ± 77	4.05 ± 0.20	0.77 ± 0.49	-1.12 ± 0.25	6.38 ± 0.30	33	6.38 ± 0.39	6	1
61100	109011	K2V	4925 ± 48	4.38 ± 0.12	1.07 ± 0.29	-0.34 ± 0.11	7.16 ± 0.12	36	7.16 ± 0.17	8	1
62523	111395	G7V	5677 ± 33	4.65 ± 0.08	0.64 ± 0.20	0.22 ± 0.03	7.72 ± 0.04	58	7.72 ± 0.03	12	1
63742	113449	G5V	5050 ± 55	4.51 ± 0.13	0.96 ± 0.28	-0.17 ± 0.10	7.33 ± 0.12	49	7.33 ± 0.15	8	1
64394	114710	G0V	6023 ± 40	4.24 ± 0.11	1.03 ± 0.20	0.11 ± 0.03	7.61 ± 0.03	62	7.61 ± 0.05	13	4
64792	115383	G0Vs	6133 ± 50	4.63 ± 0.13	1.30 ± 0.26	0.24 ± 0.04	7.74 ± 0.05	53	7.74 ± 0.05	13	1
65515	116956	G9IV-V	5214 ± 34	4.65 ± 0.08	0.93 ± 0.31	0.03 ± 0.05	7.53 ± 0.07	49	7.53 ± 0.07	8	1
65530	117043	G6V	5610 ± 38	4.38 ± 0.11	0.73 ± 0.17	0.29 ± 0.03	7.79 ± 0.04	58	7.79 ± 0.03	13	1
67620	120690	G5V	5720 ± 33	4.63 ± 0.09	0.60 ± 0.39	0.05 ± 0.04	7.55 ± 0.06	49	7.54 ± 0.05	11	3
71743	128987	G6V	5511 ± 123	4.86 ± 0.29	0.80 ± 0.48	0.01 ± 0.11	7.51 ± 0.12	48	7.51 ± 0.16	5	2
77408	141272	G8V	5191 ± 31	4.64 ± 0.07	0.87 ± 0.21	-0.14 ± 0.05	7.37 ± 0.07	49	7.36 ± 0.08	10	1
77760	142373	F9V	5802 ± 65	4.14 ± 0.19	2.00 ± 0.38	-0.50 ± 0.07	7.00 ± 0.09	50	7.00 ± 0.11	13	1
77801	142267	G0IV	5698 ± 53	4.39 ± 0.17	1.14 ± 0.40	-0.50 ± 0.10	7.00 ± 0.13	42	7.00 ± 0.14	9	3
79672	146233	G1V	5804 ± 81	4.43 ± 0.20	1.01 ± 0.24	0.04 ± 0.06	7.54 ± 0.09	59	7.54 ± 0.09	12	4
81300	149661	K2V	5192 ± 57	4.65 ± 0.16	0.33 ± 0.46	0.05 ± 0.06	7.55 ± 0.07	55	7.55 ± 0.10	11	4
82588	152391	G8V	5442 ± 51	4.62 ± 0.16	0.34 ± 0.43	0.04 ± 0.05	7.54 ± 0.05	41	7.54 ± 0.07	13	1

Table B.2 Continued

HIP	HD	SpType	$T_{\rm eff}$ (K)	$\log g$ ($\rm cms^{-2}$)	ξ_t ($\rm kms^{-1}$)	[Fe/H] dex	$\langle A$(Fe I)$\rangle$	$n_{\rm I}$	$\langle A$(Fe II)$\rangle$	$n_{\rm II}$	Spec.†
(1)	(2)	(3)	(4)	(5)	(6)	(7)	(8)	(9)	(10)	(11)	(12)
84862	157214	G0V	5663 ± 34	4.40 ± 0.12	1.32 ± 0.34	-0.41 ± 0.05	7.09 ± 0.07	48	7.09 ± 0.08	10	3
91438	172051	G5V	5638 ± 27	4.65 ± 0.08	0.94 ± 0.29	-0.21 ± 0.04	7.29 ± 0.06	60	7.29 ± 0.06	13	5
94346	180161	G8	5344 ± 59	4.55 ± 0.12	0.71 ± 0.35	0.18 ± 0.06	7.68 ± 0.09	53	7.68 ± 0.08	10	1
96100	185144	K0V	5329 ± 72	4.54 ± 0.20	0.98 ± 0.35	-0.26 ± 0.12	7.24 ± 0.13	60	7.24 ± 0.18	13	4
96895	186408	G2V	5760 ± 74	4.35 ± 0.24	1.05 ± 0.18	0.02 ± 0.06	7.52 ± 0.08	53	7.52 ± 0.10	10	3
98819	190406	G1V	6067 ± 32	4.64 ± 0.08	1.20 ± 0.22	0.12 ± 0.03	7.62 ± 0.05	41	7.62 ± 0.04	5	2
99240	190248	G5IV-V	5603 ± 35	4.37 ± 0.11	0.87 ± 0.20	0.36 ± 0.02	7.86 ± 0.03	56	7.86 ± 0.02	13	5
105858	203608	F6V	5910 ± 38	4.12 ± 0.06	2.60 ± 0.20	-0.84 ± 0.04	6.66 ± 0.02	42	6.66 ± 0.07	13	5
115331	220182	K1V	5455 ± 48	4.65 ± 0.15	0.72 ± 0.26	0.11 ± 0.04	7.61 ± 0.05	39	7.61 ± 0.07	12	1
116613	222143	G5	5795 ± 35	4.41 ± 0.11	1.00 ± 0.27	0.14 ± 0.04	7.64 ± 0.06	61	7.64 ± 0.06	13	1
116771	222368	F7V	6221 ± 92	4.37 ± 0.22	2.38 ± 0.39	-0.13 ± 0.04	7.37 ± 0.10	55	7.37 ± 0.12	13	4

†Spectrograph: **(1)** CAHA/FOCES; **(2)** TNG/SARG; **(3)** NOT/FIES; **(4)** S^4N-McD **(5)** S^4N-FEROS; **(6)** ESO/FEROS ST-ECF Science Archive

B.2 Results of the Kolmogorov-Smirnov tests

Table B.3: Results of the K-S tests performed in this work.

Sample 1	Sample 2	n_1	n_2	$n_{\rm eff}$	H_0‡	p	D
SWDs⋆	SWODs⋆	35	58	22	0	0.94	0.11
SWDs♯	SWODs♯	107	145	62	0	0.09	0.16
SWDPs	SWODs	29	145	24	1	$\sim10^{-3}$	0.40
SWDPs	SWDs	29	107	23	1	7×10^{-3}	0.34
SWDPs	SWPs	29	120	24	0	0.49	0.17
SWPs	SWODs	120	145	66	1	$\sim10^{-11}$	0.43
SWPs	SWDs	120	107	57	1	$\sim10^{-10}$	0.44

‡ 0: Accept null hypothesis; 1: Reject null hypothesis
⋆: Homogeneous samples; ♯: Full samples
†: Only stars with giant planets considered

The Kolmogorov-Smirnov test (hereafter K-S test) is widely used to study the significance of the difference between two data samples (e.g. Peacock 1983). It is based on the maximum deviation between the empirical distribution functions of both samples

$$D = max|F_1(x) - F_2(x)|, \tag{B.1}$$

where $F_1(x)$ and $F_2(x)$ are the empirical distribution functions of the first and second samples respectively, and are given by

$$F(x) = \frac{n(x_i \leq x)}{N}. \tag{B.2}$$

The K-S test tests the null hypothesis H_0 that $F_1(x)$=$F_2(x)$, i.e., both samples come from the same underlying continuous distribution, which is accepted if

$$max|F_1(x) - F_2(x)| < C_{\frac{\alpha}{2},n_1,n_2} \tag{B.3}$$

where n_1 and n_2 are the sizes of the samples, α is the confidence level, and C the corresponding critical values of the K-S distribution.

Through this paper, we perform several K-S tests between the different samples studied. Results are given in Table B.3, where the "asymptotic p value" is also given. It provides an estimate of the likelihood of the null hypothesis and is reasonable accurate for samples sizes for which

$$n_{\text{eff}} = \frac{n_1 \times n_2}{n_1 + n_2} \geq 4. \tag{B.4}$$

All the tests were made at a confidence level α=0.02.

C

Predicted fluxes for the DUNES targets

Table C.1 gives the predicted fluxes for the DUNES targets at *Herschel* PACS 70, 100, and 160 μm and SPIRE 50, 350 and 500 μm. All fluxes are given in mJy with their corresponding uncertainties. Predictions are based on PHOENIX models calculated for each star with its corresponding stellar parameters and normalizing to B, V, I_c, and J, H, K_s 2MASS.

Table C.1: Predicted fluxes for the DUNES targets.

HIP	70 μm (mJy)	100 μm (mJy)	160 μm (mJy)	250 μm (mJy)	350 μm (mJy)	500 μm (mJy)
171	17.94 ± 2.20	8.79 ± 1.08	3.43 ± 0.42	1.41 ± 0.17	0.72 ± 0.09	0.35 ± 0.04
439	22.86 ± 5.73	11.20 ± 2.81	4.38 ± 1.10	1.79 ± 0.45	0.91 ± 0.23	0.45 ± 0.11
544	14.30 ± 1.71	7.01 ± 0.84	2.74 ± 0.33	1.12 ± 0.13	0.57 ± 0.07	0.28 ± 0.03
910	27.35 ± 2.71	13.40 ± 1.33	5.24 ± 0.52	2.14 ± 0.21	1.09 ± 0.11	0.54 ± 0.05
950	18.01 ± 1.90	8.82 ± 0.93	3.45 ± 0.36	1.41 ± 0.15	0.72 ± 0.08	0.35 ± 0.04
1475	29.77 ± 8.04	14.59 ± 3.94	5.70 ± 1.54	2.33 ± 0.63	1.19 ± 0.32	0.58 ± 0.16
1599	63.95 ± 7.17	31.34 ± 3.52	12.24 ± 1.37	5.01 ± 0.56	2.56 ± 0.29	1.25 ± 0.14
1803	8.86 ± 0.92	4.34 ± 0.45	1.70 ± 0.18	0.70 ± 0.07	0.35 ± 0.04	0.17 ± 0.02
2072	30.02 ± 2.37	14.71 ± 1.16	5.75 ± 0.45	2.35 ± 0.19	1.20 ± 0.09	0.59 ± 0.05
2762	21.50 ± 2.37	10.53 ± 1.16	4.11 ± 0.45	1.69 ± 0.19	0.86 ± 0.09	0.42 ± 0.05
2941	22.62 ± 2.89	11.08 ± 1.42	4.33 ± 0.55	1.77 ± 0.23	0.90 ± 0.12	0.44 ± 0.06
3093	21.57 ± 3.04	10.57 ± 1.49	4.13 ± 0.58	1.69 ± 0.24	0.86 ± 0.12	0.42 ± 0.06
3497	8.58 ± 0.88	4.21 ± 0.43	1.64 ± 0.17	0.67 ± 0.07	0.34 ± 0.03	0.17 ± 0.02
3765	29.98 ± 4.67	14.69 ± 2.29	5.74 ± 0.89	2.35 ± 0.37	1.20 ± 0.19	0.59 ± 0.09
3810	20.34 ± 2.13	9.97 ± 1.04	3.89 ± 0.41	1.60 ± 0.17	0.81 ± 0.08	0.40 ± 0.04
3821[‡]	132.86 ± 23.67	65.1 ± 11.6	25.43 ± 4.53	10.42 ± 1.86	5.31 ± 0.95	2.6 ± 0.46
3909	20.60 ± 2.29	10.09 ± 1.12	3.94 ± 0.44	1.62 ± 0.18	0.82 ± 0.09	0.40 ± 0.04
4148	9.02 ± 1.31	4.42 ± 0.64	1.73 ± 0.25	0.71 ± 0.10	0.36 ± 0.05	0.18 ± 0.03
5799	20.50 ± 2.20	10.04 ± 1.08	3.92 ± 0.42	1.61 ± 0.17	0.82 ± 0.09	0.40 ± 0.04
5862	26.66 ± 3.19	13.06 ± 1.56	5.10 ± 0.61	2.09 ± 0.25	1.07 ± 0.13	0.52 ± 0.06
7513	58.86 ± 6.11	28.84 ± 2.99	11.27 ± 1.17	4.62 ± 0.48	2.35 ± 0.24	1.15 ± 0.12

It follows in the next page

Table C.1 It cames from the previous page

HIP	70 μm (mJy)	100 μm (mJy)	160 μm (mJy)	250 μm (mJy)	350 μm (mJy)	500 μm (mJy)
7751*	29.81 ± 5.52	14.61 ± 2.7	5.71 ± 1.06	2.34 ± 0.43	1.19 ± 0.22	0.58 ± 0.11
7918	30.55 ± 3.69	14.97 ± 1.81	5.85 ± 0.71	2.40 ± 0.29	1.22 ± 0.15	0.60 ± 0.07
7978	15.36 ± 1.67	7.52 ± 0.82	2.94 ± 0.32	1.20 ± 0.13	0.61 ± 0.07	0.30 ± 0.03
7981	40.53 ± 5.89	19.86 ± 2.89	7.76 ± 1.13	3.18 ± 0.46	1.62 ± 0.24	0.79 ± 0.11
8768	8.80 ± 2.16	4.31 ± 1.06	1.68 ± 0.41	0.69 ± 0.17	0.35 ± 0.09	0.17 ± 0.04
8903	96.00 ± 6.33	47.04 ± 3.10	18.38 ± 1.21	7.53 ± 0.50	3.84 ± 0.25	1.88 ± 0.12
10138	18.41 ± 2.56	9.02 ± 1.25	3.52 ± 0.49	1.44 ± 0.20	0.74 ± 0.10	0.36 ± 0.05
10644	44.74 ± 5.19	21.92 ± 2.54	8.56 ± 0.99	3.51 ± 0.41	1.79 ± 0.21	0.88 ± 0.10
10798	12.85 ± 1.46	6.30 ± 0.72	2.46 ± 0.28	1.01 ± 0.11	0.51 ± 0.06	0.25 ± 0.03
11452	9.21 ± 2.23	4.51 ± 1.09	1.76 ± 0.43	0.72 ± 0.17	0.37 ± 0.09	0.18 ± 0.04
11964	11.04 ± 2.66	5.41 ± 1.30	2.11 ± 0.51	0.87 ± 0.21	0.44 ± 0.11	0.22 ± 0.05
12114	33.88 ± 5.29	16.60 ± 2.59	6.49 ± 1.01	2.66 ± 0.42	1.36 ± 0.21	0.66 ± 0.10
12444	12.02 ± 1.10	5.89 ± 0.54	2.30 ± 0.21	0.94 ± 0.09	0.48 ± 0.04	0.24 ± 0.02
12777	59.91 ± 6.28	29.36 ± 3.08	11.47 ± 1.20	4.70 ± 0.49	2.40 ± 0.25	1.17 ± 0.12
12843	41.42 ± 4.57	20.29 ± 2.24	7.93 ± 0.87	3.25 ± 0.36	1.66 ± 0.18	0.81 ± 0.09
13402	18.21 ± 2.68	8.92 ± 1.31	3.49 ± 0.51	1.43 ± 0.21	0.73 ± 0.11	0.36 ± 0.05
14879	88.22 ± 10.32	43.23 ± 5.05	16.89 ± 1.97	6.92 ± 0.81	3.53 ± 0.41	1.73 ± 0.20
14954	24.58 ± 2.77	12.05 ± 1.36	4.71 ± 0.53	1.93 ± 0.22	0.98 ± 0.11	0.48 ± 0.05
15330	21.13 ± 2.63	10.35 ± 1.29	4.05 ± 0.50	1.66 ± 0.21	0.85 ± 0.11	0.41 ± 0.05
15371	24.71 ± 2.87	12.11 ± 1.41	4.73 ± 0.55	1.94 ± 0.23	0.99 ± 0.12	0.48 ± 0.06
15457	45.21 ± 5.36	22.16 ± 2.63	8.65 ± 1.03	3.55 ± 0.42	1.81 ± 0.21	0.89 ± 0.11
15510	80.75 ± 10.55	39.57 ± 5.17	15.46 ± 2.02	6.33 ± 0.83	3.23 ± 0.42	1.58 ± 0.21
15799	9.94 ± 1.30	4.87 ± 0.64	1.90 ± 0.25	0.78 ± 0.10	0.40 ± 0.05	0.19 ± 0.02

It follows in the next page

Table C.1 It cames from the previous page

HIP	70 μm (mJy)	100 μm (mJy)	160 μm (mJy)	250 μm (mJy)	350 μm (mJy)	500 μm (mJy)
16134	10.04 ± 2.35	4.92 ± 1.15	1.92 ± 0.45	0.79 ± 0.18	0.40 ± 0.09	0.20 ± 0.05
16245	23.95 ± 2.33	11.74 ± 1.14	4.59 ± 0.45	1.88 ± 0.18	0.96 ± 0.09	0.47 ± 0.05
16852	57.58 ± 6.35	28.21 ± 3.11	11.02 ± 1.22	4.51 ± 0.50	2.30 ± 0.25	1.13 ± 0.12
17420	9.17 ± 1.33	4.49 ± 0.65	1.76 ± 0.26	0.72 ± 0.10	0.37 ± 0.05	0.18 ± 0.03
17439	8.56 ± 1.16	4.19 ± 0.57	1.64 ± 0.22	0.67 ± 0.09	0.34 ± 0.05	0.17 ± 0.02
17651	39.17 ± 3.93	19.19 ± 1.92	7.50 ± 0.75	3.07 ± 0.31	1.57 ± 0.16	0.77 ± 0.08
19849	87.71 ± 12.36	42.98 ± 6.06	16.79 ± 2.37	6.88 ± 0.97	3.51 ± 0.49	1.72 ± 0.24
19884	9.69 ± 1.93	4.75 ± 0.95	1.85 ± 0.37	0.76 ± 0.15	0.39 ± 0.08	0.19 ± 0.04
21770	27.95 ± 2.88	13.69 ± 1.41	5.35 ± 0.55	2.19 ± 0.23	1.12 ± 0.12	0.55 ± 0.06
22263	20.19 ± 2.28	9.89 ± 1.11	3.86 ± 0.44	1.58 ± 0.18	0.81 ± 0.09	0.40 ± 0.05
22449	143.40 ± 13.37	70.28 ± 6.55	27.45 ± 2.56	11.24 ± 1.05	5.74 ± 0.54	2.81 ± 0.26
23311	25.72 ± 4.46	12.60 ± 2.19	4.92 ± 0.85	2.02 ± 0.35	1.03 ± 0.18	0.50 ± 0.09
23693	35.82 ± 3.69	17.55 ± 1.81	6.86 ± 0.71	2.81 ± 0.29	1.43 ± 0.15	0.70 ± 0.07
24186	11.31 ± 2.96	5.54 ± 1.45	2.17 ± 0.57	0.89 ± 0.23	0.45 ± 0.12	0.22 ± 0.06
25110	20.85 ± 2.09	10.21 ± 1.02	3.99 ± 0.40	1.63 ± 0.16	0.83 ± 0.08	0.41 ± 0.04
27072	84.28 ± 8.52	41.30 ± 4.17	16.13 ± 1.63	6.61 ± 0.67	3.37 ± 0.34	1.65 ± 0.17
27288	39.02 ± 3.00	19.12 ± 1.47	7.47 ± 0.57	3.06 ± 0.24	1.56 ± 0.12	0.76 ± 0.06
27887	9.73 ± 1.41	4.77 ± 0.69	1.86 ± 0.27	0.76 ± 0.11	0.39 ± 0.06	0.19 ± 0.03
28103	55.67 ± 4.76	27.28 ± 2.33	10.66 ± 0.91	4.37 ± 0.37	2.23 ± 0.19	1.09 ± 0.09
28442	9.89 ± 2.00	4.85 ± 0.98	1.89 ± 0.38	0.78 ± 0.16	0.40 ± 0.08	0.19 ± 0.04
29271	34.31 ± 4.32	16.81 ± 2.12	6.57 ± 0.83	2.69 ± 0.34	1.37 ± 0.17	0.67 ± 0.08
29568	10.39 ± 1.16	5.09 ± 0.57	1.99 ± 0.22	0.81 ± 0.09	0.42 ± 0.05	0.20 ± 0.02
32439	17.50 ± 1.61	8.58 ± 0.79	3.35 ± 0.31	1.37 ± 0.13	0.70 ± 0.06	0.34 ± 0.03

It follows in the next page

Table C.1 It cames from the previous page

HIP	70 μm (mJy)	100 μm (mJy)	160 μm (mJy)	250 μm (mJy)	350 μm (mJy)	500 μm (mJy)
32480	17.53 ± 2.03	8.59 ± 1.00	3.36 ± 0.39	1.38 ± 0.16	0.70 ± 0.08	0.34 ± 0.04
33277	14.97 ± 1.58	7.34 ± 0.77	2.87 ± 0.30	1.17 ± 0.12	0.60 ± 0.06	0.29 ± 0.03
34017	13.09 ± 1.44	6.42 ± 0.71	2.51 ± 0.28	1.03 ± 0.11	0.52 ± 0.06	0.26 ± 0.03
34065	20.25 ± 2.21	9.92 ± 1.08	3.88 ± 0.42	1.59 ± 0.17	0.81 ± 0.09	0.40 ± 0.04
35136	17.96 ± 1.87	8.80 ± 0.92	3.44 ± 0.36	1.41 ± 0.15	0.72 ± 0.08	0.35 ± 0.04
36366	42.65 ± 3.79	20.90 ± 1.86	8.16 ± 0.73	3.34 ± 0.30	1.71 ± 0.15	0.84 ± 0.07
36439	19.62 ± 1.90	9.61 ± 0.93	3.76 ± 0.36	1.54 ± 0.15	0.78 ± 0.08	0.38 ± 0.04
36850	231.10 ± 14.65	113.20 ± 7.18	44.23 ± 2.80	18.12 ± 1.15	9.24 ± 0.59	4.53 ± 0.29
37279	1292.00 ± 126.11	633.00 ± 61.78	247.30 ± 24.14	101.30 ± 9.89	51.67 ± 5.04	25.32 ± 2.47
37288	4.59 ± 1.10	2.25 ± 0.54	0.88 ± 0.21	0.36 ± 0.09	0.18 ± 0.04	0.09 ± 0.02
38382	27.40 ± 3.14	13.43 ± 1.54	5.25 ± 0.60	2.15 ± 0.25	1.10 ± 0.13	0.54 ± 0.06
38784*	8.7 ± 1.17	4.26 ± 0.57	1.66 ± 0.22	0.68 ± 0.09	0.35 ± 0.05	0.17 ± 0.02
40035	16.26 ± 1.39	7.97 ± 0.68	3.11 ± 0.27	1.28 ± 0.11	0.65 ± 0.06	0.32 ± 0.03
40693	16.80 ± 2.17	8.23 ± 1.06	3.22 ± 0.42	1.32 ± 0.17	0.67 ± 0.09	0.33 ± 0.04
40843	23.07 ± 2.24	11.30 ± 1.10	4.42 ± 0.43	1.81 ± 0.18	0.92 ± 0.09	0.45 ± 0.04
42430	33.91 ± 4.51	16.62 ± 2.21	6.49 ± 0.86	2.66 ± 0.35	1.36 ± 0.18	0.66 ± 0.09
42438	18.41 ± 1.89	9.02 ± 0.93	3.52 ± 0.36	1.44 ± 0.15	0.74 ± 0.08	0.36 ± 0.04
43587	18.53 ± 2.69	9.08 ± 1.32	3.55 ± 0.52	1.45 ± 0.21	0.74 ± 0.11	0.36 ± 0.05
43726	12.94 ± 1.45	6.34 ± 0.71	2.48 ± 0.28	1.01 ± 0.11	0.52 ± 0.06	0.25 ± 0.03
44075	15.15 ± 1.41	7.43 ± 0.69	2.90 ± 0.27	1.19 ± 0.11	0.61 ± 0.06	0.30 ± 0.03
44248	53.40 ± 5.78	26.17 ± 2.83	10.22 ± 1.11	4.19 ± 0.45	2.14 ± 0.23	1.05 ± 0.11
44897	12.42 ± 1.15	6.08 ± 0.56	2.38 ± 0.22	0.97 ± 0.09	0.50 ± 0.05	0.24 ± 0.02
45038	29.52 ± 3.54	14.47 ± 1.73	5.65 ± 0.68	2.32 ± 0.28	1.18 ± 0.14	0.58 ± 0.07

It follows in the next page

Table C.1 It cames from the previous page

HIP	70 μm (mJy)	100 μm (mJy)	160 μm (mJy)	250 μm (mJy)	350 μm (mJy)	500 μm (mJy)
45170	11.54 ± 1.32	5.65 ± 0.65	2.21 ± 0.25	0.90 ± 0.10	0.46 ± 0.05	0.23 ± 0.03
45333	24.96 ± 3.02	12.23 ± 1.48	4.78 ± 0.58	1.96 ± 0.24	1.00 ± 0.12	0.49 ± 0.06
45617	11.10 ± 1.71	5.44 ± 0.84	2.13 ± 0.33	0.87 ± 0.13	0.44 ± 0.07	0.22 ± 0.03
46509	31.37 ± 2.86	15.37 ± 1.40	6.00 ± 0.55	2.46 ± 0.22	1.26 ± 0.11	0.61 ± 0.06
46580	9.57 ± 1.49	4.69 ± 0.73	1.83 ± 0.28	0.75 ± 0.12	0.38 ± 0.06	0.19 ± 0.03
47080	27.59 ± 4.00	13.52 ± 1.96	5.28 ± 0.77	2.16 ± 0.31	1.10 ± 0.16	0.54 ± 0.08
47592	27.33 ± 3.08	13.39 ± 1.51	5.23 ± 0.59	2.14 ± 0.24	1.09 ± 0.12	0.54 ± 0.06
48113	28.40 ± 3.30	13.91 ± 1.61	5.44 ± 0.63	2.23 ± 0.26	1.14 ± 0.13	0.56 ± 0.07
49081	23.33 ± 2.89	11.43 ± 1.41	4.47 ± 0.55	1.83 ± 0.23	0.93 ± 0.12	0.46 ± 0.06
49908	65.18 ± 15.88	31.94 ± 7.78	12.48 ± 3.04	5.11 ± 1.25	2.61 ± 0.64	1.28 ± 0.31
49986	11.57 ± 2.94	5.67 ± 1.44	2.22 ± 0.56	0.91 ± 0.23	0.46 ± 0.12	0.23 ± 0.06
50384	12.53 ± 1.20	6.14 ± 0.59	2.40 ± 0.23	0.98 ± 0.09	0.50 ± 0.05	0.25 ± 0.02
50505	8.28 ± 0.85	4.06 ± 0.42	1.59 ± 0.16	0.65 ± 0.07	0.33 ± 0.03	0.16 ± 0.02
51459	29.40 ± 3.02	14.41 ± 1.48	5.63 ± 0.58	2.31 ± 0.24	1.18 ± 0.12	0.58 ± 0.06
51502	16.07 ± 1.16	7.88 ± 0.57	3.08 ± 0.22	1.26 ± 0.09	0.64 ± 0.05	0.32 ± 0.02
53721	28.76 ± 3.59	14.09 ± 1.76	5.51 ± 0.69	2.26 ± 0.28	1.15 ± 0.14	0.56 ± 0.07
53910	96.66 ± 6.04	47.36 ± 2.96	18.50 ± 1.16	7.58 ± 0.47	3.87 ± 0.24	1.90 ± 0.12
54646	13.86 ± 3.09	6.79 ± 1.51	2.65 ± 0.59	1.09 ± 0.24	0.55 ± 0.12	0.27 ± 0.06
54872	108.40 ± 7.05	53.11 ± 3.45	20.75 ± 1.35	8.50 ± 0.55	4.34 ± 0.28	2.12 ± 0.14
56242	9.11 ± 0.82	4.46 ± 0.40	1.74 ± 0.16	0.71 ± 0.06	0.36 ± 0.03	0.18 ± 0.02
56452	20.25 ± 2.74	9.92 ± 1.34	3.88 ± 0.52	1.59 ± 0.21	0.81 ± 0.11	0.40 ± 0.05
56997	30.50 ± 3.79	14.94 ± 1.85	5.84 ± 0.72	2.39 ± 0.30	1.22 ± 0.15	0.60 ± 0.07
57443	37.49 ± 4.71	18.37 ± 2.31	7.18 ± 0.90	2.94 ± 0.37	1.50 ± 0.19	0.73 ± 0.09

It follows in the next page

Table C.1 It cames from the previous page

HIP	70 μm (mJy)	100 μm (mJy)	160 μm (mJy)	250 μm (mJy)	350 μm (mJy)	500 μm (mJy)
57507	9.94 ± 1.06	4.87 ± 0.52	1.90 ± 0.20	0.78 ± 0.08	0.40 ± 0.04	0.19 ± 0.02
57632	143.80 ± 9.25	70.44 ± 4.53	27.52 ± 1.77	11.27 ± 0.72	5.75 ± 0.37	2.82 ± 0.18
57757	99.23 ± 10.41	48.62 ± 5.10	18.99 ± 1.99	7.78 ± 0.82	3.97 ± 0.42	1.95 ± 0.20
57939	16.23 ± 1.97	7.96 ± 0.97	3.11 ± 0.38	1.27 ± 0.15	0.65 ± 0.08	0.32 ± 0.04
58345	16.00 ± 2.95	7.84 ± 1.44	3.06 ± 0.56	1.26 ± 0.23	0.64 ± 0.12	0.31 ± 0.06
59199	40.19 ± 3.47	19.69 ± 1.70	7.69 ± 0.66	3.15 ± 0.27	1.61 ± 0.14	0.79 ± 0.07
59774	42.54 ± 3.37	20.85 ± 1.65	8.14 ± 0.64	3.34 ± 0.26	1.70 ± 0.13	0.83 ± 0.07
61053*	8.56 ± 0.91	4.19 ± 0.45	1.64 ± 0.18	0.67 ± 0.07	0.34 ± 0.04	0.17 ± 0.02
61174	36.51 ± 3.46	17.89 ± 1.69	6.99 ± 0.66	2.86 ± 0.27	1.46 ± 0.14	0.72 ± 0.07
61317	61.56 ± 6.98	30.16 ± 3.42	11.78 ± 1.34	4.83 ± 0.55	2.46 ± 0.28	1.21 ± 0.14
61874	1.15 ± 0.33	0.56 ± 0.16	0.22 ± 0.06	0.09 ± 0.03	0.05 ± 0.01	0.02 ± 0.01
61941	150.20 ± 13.28	73.60 ± 6.51	28.75 ± 2.54	11.78 ± 1.04	6.01 ± 0.53	2.94 ± 0.26
62145*	9.07 ± 1.58	4.44 ± 0.77	1.74 ± 0.30	0.71 ± 0.12	0.36 ± 0.06	0.18 ± 0.03
62207	12.65 ± 1.17	6.20 ± 0.57	2.42 ± 0.22	0.99 ± 0.09	0.51 ± 0.05	0.25 ± 0.02
62523	11.12 ± 1.31	5.45 ± 0.64	2.13 ± 0.25	0.87 ± 0.10	0.44 ± 0.05	0.22 ± 0.03
64241	44.79 ± 4.31	21.95 ± 2.11	8.57 ± 0.82	3.51 ± 0.34	1.79 ± 0.17	0.88 ± 0.08
64394	56.28 ± 6.19	27.58 ± 3.03	10.77 ± 1.18	4.41 ± 0.48	2.25 ± 0.25	1.10 ± 0.12
64792	20.94 ± 2.36	10.26 ± 1.16	4.01 ± 0.45	1.64 ± 0.19	0.84 ± 0.09	0.41 ± 0.05
64797	15.50 ± 2.23	7.60 ± 1.09	2.97 ± 0.43	1.22 ± 0.18	0.62 ± 0.09	0.30 ± 0.04
64924	50.41 ± 6.23	24.70 ± 3.05	9.65 ± 1.19	3.95 ± 0.49	2.02 ± 0.25	0.99 ± 0.12
65026	16.69 ± 4.20	8.18 ± 2.06	3.19 ± 0.80	1.31 ± 0.33	0.67 ± 0.17	0.33 ± 0.08
65109	66.61 ± 4.72	32.64 ± 2.31	12.75 ± 0.90	5.22 ± 0.37	2.66 ± 0.19	1.31 ± 0.09
65378‡	151.12 ± 23.64	74.05 ± 11.58	28.93 ± 4.53	11.85 ± 1.85	6.04 ± 0.94	2.96 ± 0.46

It follows in the next page

Table C.1 It cames from the previous page

HIP	70 μm (mJy)	100 μm (mJy)	160 μm (mJy)	250 μm (mJy)	350 μm (mJy)	500 μm (mJy)
65530	9.69 ± 1.12	4.75 ± 0.55	1.85 ± 0.21	0.76 ± 0.09	0.39 ± 0.05	0.19 ± 0.02
65721	38.51 ± 5.08	18.87 ± 2.49	7.37 ± 0.97	3.02 ± 0.40	1.54 ± 0.20	0.75 ± 0.10
66249	42.76 ± 3.36	20.95 ± 1.65	8.19 ± 0.64	3.35 ± 0.26	1.71 ± 0.13	0.84 ± 0.07
67153	38.20 ± 3.48	18.72 ± 1.71	7.31 ± 0.67	3.00 ± 0.27	1.53 ± 0.14	0.75 ± 0.07
67155	19.21 ± 4.78	9.41 ± 2.34	3.68 ± 0.92	1.51 ± 0.38	0.77 ± 0.19	0.38 ± 0.09
67275	34.91 ± 3.93	17.10 ± 1.92	6.68 ± 0.75	2.74 ± 0.31	1.40 ± 0.16	0.68 ± 0.08
67422[†]	13.14 ± 2.71	6.44 ± 1.33	2.51 ± 0.52	1.03 ± 0.21	0.53 ± 0.11	0.26 ± 0.05
67620	9.24 ± 1.11	4.53 ± 0.54	1.77 ± 0.21	0.72 ± 0.09	0.37 ± 0.04	0.18 ± 0.02
68184[‡]	17.93 ± 3.62	8.78 ± 1.77	3.43 ± 0.69	1.41 ± 0.29	0.72 ± 0.15	0.35 ± 0.07
68682	11.72 ± 1.45	5.74 ± 0.71	2.24 ± 0.28	0.92 ± 0.11	0.47 ± 0.06	0.23 ± 0.03
69965	12.33 ± 1.20	6.04 ± 0.59	2.36 ± 0.23	0.97 ± 0.09	0.49 ± 0.05	0.24 ± 0.02
70319	11.38 ± 1.15	5.58 ± 0.56	2.18 ± 0.22	0.89 ± 0.09	0.46 ± 0.05	0.22 ± 0.02
70497	59.22 ± 6.40	29.02 ± 3.14	11.34 ± 1.23	4.64 ± 0.50	2.37 ± 0.26	1.16 ± 0.13
70857	8.40 ± 1.01	4.11 ± 0.50	1.61 ± 0.19	0.66 ± 0.08	0.34 ± 0.04	0.16 ± 0.02
71181	9.89 ± 1.53	4.85 ± 0.75	1.89 ± 0.29	0.78 ± 0.12	0.40 ± 0.06	0.19 ± 0.03
71284	34.70 ± 3.28	17.01 ± 1.61	6.64 ± 0.63	2.72 ± 0.26	1.39 ± 0.13	0.68 ± 0.06
71681	536.40 ± 80.77	262.80 ± 39.57	102.70 ± 15.46	42.05 ± 6.33	21.45 ± 3.23	10.51 ± 1.58
71683	761.80 ± 94.70	373.30 ± 46.41	145.80 ± 18.13	59.72 ± 7.42	30.47 ± 3.79	14.93 ± 1.86
71908	77.56 ± 5.95	38.00 ± 2.91	14.84 ± 1.14	6.08 ± 0.47	3.10 ± 0.24	1.52 ± 0.12
72567	12.34 ± 1.28	6.05 ± 0.63	2.36 ± 0.24	0.97 ± 0.10	0.49 ± 0.05	0.24 ± 0.02
72603	17.31 ± 1.62	8.48 ± 0.79	3.31 ± 0.31	1.36 ± 0.13	0.69 ± 0.06	0.34 ± 0.03
72659	84.08 ± 16.25	41.20 ± 7.96	16.09 ± 3.11	6.59 ± 1.27	3.36 ± 0.65	1.65 ± 0.32
72848	17.50 ± 2.56	8.58 ± 1.25	3.35 ± 0.49	1.37 ± 0.20	0.70 ± 0.10	0.34 ± 0.05

It follows in the next page

Table C.1 It cames from the previous page

HIP	70 μm (mJy)	100 μm (mJy)	160 μm (mJy)	250 μm (mJy)	350 μm (mJy)	500 μm (mJy)
73100	14.27 ± 1.21	6.99 ± 0.59	2.73 ± 0.23	1.12 ± 0.09	0.57 ± 0.05	0.28 ± 0.02
73182	41.28 ± 10.07	20.23 ± 4.93	7.90 ± 1.93	3.24 ± 0.79	1.65 ± 0.40	0.81 ± 0.20
73184	48.12 ± 8.19	23.58 ± 4.01	9.21 ± 1.57	3.77 ± 0.64	1.93 ± 0.33	0.94 ± 0.16
73470	7.22 ± 1.78	3.54 ± 0.87	1.38 ± 0.34	0.57 ± 0.14	0.29 ± 0.07	0.14 ± 0.03
73695	43.42 ± 5.33	21.28 ± 2.61	8.31 ± 1.02	3.40 ± 0.42	1.74 ± 0.21	0.85 ± 0.10
73996	22.94 ± 2.01	11.24 ± 0.98	4.39 ± 0.38	1.80 ± 0.16	0.92 ± 0.08	0.45 ± 0.04
75312	28.92 ± 3.15	14.17 ± 1.54	5.54 ± 0.60	2.27 ± 0.25	1.16 ± 0.13	0.57 ± 0.06
76267	100.80 ± 7.73	49.37 ± 3.78	19.28 ± 1.48	7.90 ± 0.61	4.03 ± 0.31	1.98 ± 0.15
77052	17.11 ± 2.25	8.39 ± 1.10	3.28 ± 0.43	1.34 ± 0.18	0.68 ± 0.09	0.34 ± 0.04
77257	51.61 ± 5.77	25.29 ± 2.83	9.88 ± 1.11	4.05 ± 0.45	2.06 ± 0.23	1.01 ± 0.11
77622	33.74 ± 2.49	16.53 ± 1.22	6.46 ± 0.48	2.65 ± 0.20	1.35 ± 0.10	0.66 ± 0.05
77760	59.68 ± 6.03	29.24 ± 2.95	11.42 ± 1.15	4.68 ± 0.47	2.39 ± 0.24	1.17 ± 0.12
78072	67.26 ± 6.96	32.96 ± 3.41	12.87 ± 1.33	5.27 ± 0.55	2.69 ± 0.28	1.32 ± 0.14
78459	23.48 ± 2.42	11.51 ± 1.19	4.50 ± 0.46	1.84 ± 0.19	0.94 ± 0.10	0.46 ± 0.05
78775	10.98 ± 1.26	5.38 ± 0.62	2.10 ± 0.24	0.86 ± 0.10	0.44 ± 0.05	0.22 ± 0.03
79248	10.63 ± 1.45	5.21 ± 0.71	2.04 ± 0.28	0.83 ± 0.11	0.43 ± 0.06	0.21 ± 0.03
79607	27.58 ± 5.71	13.51 ± 2.80	5.28 ± 1.09	2.16 ± 0.45	1.10 ± 0.23	0.54 ± 0.11
80686	29.75 ± 3.33	14.58 ± 1.63	5.69 ± 0.64	2.33 ± 0.26	1.19 ± 0.13	0.58 ± 0.06
80725	9.57 ± 1.27	4.69 ± 0.62	1.83 ± 0.24	0.75 ± 0.10	0.38 ± 0.05	0.19 ± 0.03
82860	26.66 ± 2.85	13.06 ± 1.40	5.10 ± 0.54	2.09 ± 0.22	1.07 ± 0.11	0.52 ± 0.06
83389	8.18 ± 0.93	4.01 ± 0.46	1.57 ± 0.18	0.64 ± 0.07	0.33 ± 0.04	0.16 ± 0.02
84140	13.98 ± 3.56	6.85 ± 1.75	2.68 ± 0.68	1.10 ± 0.28	0.56 ± 0.14	0.27 ± 0.07
84862	24.68 ± 2.90	12.09 ± 1.42	4.72 ± 0.56	1.94 ± 0.23	0.99 ± 0.12	0.48 ± 0.06

It follows in the next page

Table C.1 It cames from the previous page

HIP	70 μm (mJy)	100 μm (mJy)	160 μm (mJy)	250 μm (mJy)	350 μm (mJy)	500 μm (mJy)
85235	12.87 ± 1.59	6.31 ± 0.78	2.46 ± 0.30	1.01 ± 0.12	0.51 ± 0.06	0.25 ± 0.03
85295	20.75 ± 4.90	10.17 ± 2.40	3.97 ± 0.94	1.63 ± 0.38	0.83 ± 0.20	0.41 ± 0.10
86036	23.98 ± 2.85	11.75 ± 1.40	4.59 ± 0.55	1.88 ± 0.22	0.96 ± 0.11	0.47 ± 0.06
86201	26.74 ± 2.43	13.10 ± 1.19	5.12 ± 0.47	2.10 ± 0.19	1.07 ± 0.10	0.52 ± 0.05
86614	34.46 ± 3.62	16.89 ± 1.77	6.60 ± 0.69	2.70 ± 0.28	1.38 ± 0.14	0.68 ± 0.07
86796	28.04 ± 3.56	13.74 ± 1.74	5.37 ± 0.68	2.20 ± 0.28	1.12 ± 0.14	0.55 ± 0.07
88601	134.60 ± 20.64	65.94 ± 10.11	25.76 ± 3.95	10.55 ± 1.62	5.38 ± 0.82	2.64 ± 0.40
88745	35.20 ± 3.52	17.25 ± 1.73	6.74 ± 0.67	2.76 ± 0.28	1.41 ± 0.14	0.69 ± 0.07
88972	16.64 ± 2.42	8.15 ± 1.19	3.18 ± 0.46	1.30 ± 0.19	0.67 ± 0.10	0.33 ± 0.05
89042	19.79 ± 2.34	9.70 ± 1.15	3.79 ± 0.45	1.55 ± 0.18	0.79 ± 0.09	0.39 ± 0.05
89348	22.21 ± 2.23	10.88 ± 1.09	4.25 ± 0.43	1.74 ± 0.18	0.89 ± 0.09	0.44 ± 0.04
89937	109.80 ± 10.99	53.80 ± 5.38	21.01 ± 2.10	8.61 ± 0.86	4.39 ± 0.44	2.15 ± 0.22
91009	9.92 ± 2.17	4.86 ± 1.07	1.90 ± 0.42	0.78 ± 0.17	0.40 ± 0.09	0.19 ± 0.04
91768	19.93 ± 5.11	9.77 ± 2.51	3.82 ± 0.98	1.56 ± 0.40	0.80 ± 0.21	0.39 ± 0.10
92043	44.66 ± 4.37	21.88 ± 2.14	8.55 ± 0.84	3.50 ± 0.34	1.79 ± 0.18	0.88 ± 0.09
93017	29.04 ± 3.15	14.23 ± 1.55	5.56 ± 0.60	2.28 ± 0.25	1.16 ± 0.13	0.57 ± 0.06
95995	13.67 ± 1.83	6.70 ± 0.90	2.62 ± 0.35	1.07 ± 0.14	0.55 ± 0.07	0.27 ± 0.04
96100	60.78 ± 8.65	29.78 ± 4.24	11.63 ± 1.66	4.77 ± 0.68	2.43 ± 0.35	1.19 ± 0.17
96441	28.35 ± 2.74	13.89 ± 1.34	5.43 ± 0.53	2.22 ± 0.21	1.13 ± 0.11	0.56 ± 0.05
96895	12.42 ± 1.37	6.09 ± 0.67	2.38 ± 0.26	0.97 ± 0.11	0.50 ± 0.06	0.24 ± 0.03
97649	693.80 ± 48.25	339.90 ± 23.64	132.80 ± 9.24	54.39 ± 3.78	27.75 ± 1.93	13.60 ± 0.95
97944	23.61 ± 4.03	11.57 ± 1.98	4.52 ± 0.77	1.85 ± 0.32	0.94 ± 0.16	0.46 ± 0.08
98959	12.31 ± 1.36	6.03 ± 0.66	2.36 ± 0.26	0.97 ± 0.11	0.49 ± 0.05	0.24 ± 0.03

It follows in the next page

Table C.1 It cames from the previous page

HIP	70 μm (mJy)	100 μm (mJy)	160 μm (mJy)	250 μm (mJy)	350 μm (mJy)	500 μm (mJy)
99240	140.30 ± 19.11	68.75 ± 9.37	26.86 ± 3.66	11.00 ± 1.50	5.61 ± 0.76	2.75 ± 0.37
99461	52.04 ± 9.46	25.50 ± 4.64	9.96 ± 1.81	4.08 ± 0.74	2.08 ± 0.38	1.02 ± 0.19
99825	30.53 ± 4.69	14.96 ± 2.30	5.85 ± 0.90	2.39 ± 0.37	1.22 ± 0.19	0.60 ± 0.09
101955	12.34 ± 2.66	6.05 ± 1.31	2.36 ± 0.51	0.97 ± 0.21	0.49 ± 0.11	0.24 ± 0.05
101997	11.52 ± 1.38	5.64 ± 0.68	2.20 ± 0.26	0.90 ± 0.11	0.46 ± 0.06	0.23 ± 0.03
102333	23.46 ± 2.05	11.50 ± 1.00	4.49 ± 0.39	1.84 ± 0.16	0.94 ± 0.08	0.46 ± 0.04
102485	47.05 ± 4.39	23.05 ± 2.15	9.01 ± 0.84	3.69 ± 0.34	1.88 ± 0.18	0.92 ± 0.09
103389	12.24 ± 1.12	6.00 ± 0.55	2.34 ± 0.21	0.96 ± 0.09	0.49 ± 0.04	0.24 ± 0.02
104214	103.40 ± 21.25	50.66 ± 10.41	19.79 ± 4.07	8.11 ± 1.67	4.14 ± 0.85	2.03 ± 0.42
104217	85.65 ± 20.30	41.97 ± 9.95	16.39 ± 3.88	6.72 ± 1.59	3.43 ± 0.81	1.68 ± 0.40
104858	38.19 ± 4.04	18.71 ± 1.98	7.31 ± 0.77	2.99 ± 0.32	1.53 ± 0.16	0.75 ± 0.08
105312	10.85 ± 1.26	5.32 ± 0.62	2.08 ± 0.24	0.85 ± 0.10	0.43 ± 0.05	0.21 ± 0.02
105858	57.11 ± 5.80	27.98 ± 2.84	10.93 ± 1.11	4.48 ± 0.45	2.28 ± 0.23	1.12 ± 0.11
106696	8.33 ± 1.14	4.08 ± 0.56	1.59 ± 0.22	0.65 ± 0.09	0.33 ± 0.05	0.16 ± 0.02
107310	41.88 ± 4.68	20.52 ± 2.29	8.02 ± 0.90	3.28 ± 0.37	1.68 ± 0.19	0.82 ± 0.09
107350	12.61 ± 1.17	6.18 ± 0.57	2.41 ± 0.22	0.99 ± 0.09	0.50 ± 0.05	0.25 ± 0.02
107649	16.93 ± 1.79	8.29 ± 0.88	3.24 ± 0.34	1.33 ± 0.14	0.68 ± 0.07	0.33 ± 0.03
108870	116.60 ± 20.58	57.15 ± 10.09	22.33 ± 3.94	9.14 ± 1.61	4.67 ± 0.82	2.29 ± 0.40
109176	70.42 ± 6.62	34.51 ± 3.24	13.48 ± 1.27	5.52 ± 0.52	2.82 ± 0.27	1.38 ± 0.13
109378	9.44 ± 1.14	4.62 ± 0.56	1.81 ± 0.22	0.74 ± 0.09	0.38 ± 0.05	0.19 ± 0.02
109422	26.62 ± 2.90	13.05 ± 1.42	5.10 ± 0.55	2.09 ± 0.23	1.07 ± 0.12	0.52 ± 0.06
110109	22.36 ± 2.65	10.96 ± 1.30	4.28 ± 0.51	1.75 ± 0.21	0.89 ± 0.11	0.44 ± 0.05
110649	24.51 ± 3.06	12.01 ± 1.50	4.69 ± 0.59	1.92 ± 0.24	0.98 ± 0.12	0.48 ± 0.06

It follows in the next page

Table C.1 It cames from the previous page

HIP	70 μm (mJy)	100 μm (mJy)	160 μm (mJy)	250 μm (mJy)	350 μm (mJy)	500 μm (mJy)
110778	20.17 ± 2.07	9.89 ± 1.02	3.86 ± 0.40	1.58 ± 0.16	0.81 ± 0.08	0.40 ± 0.04
111449	16.50 ± 1.75	8.09 ± 0.86	3.16 ± 0.33	1.29 ± 0.14	0.66 ± 0.07	0.32 ± 0.03
112117	11.20 ± 1.03	5.49 ± 0.51	2.14 ± 0.20	0.88 ± 0.08	0.45 ± 0.04	0.22 ± 0.02
112447	53.54 ± 5.59	26.23 ± 2.74	10.25 ± 1.07	4.20 ± 0.44	2.14 ± 0.22	1.05 ± 0.11
113283	26.52 ± 4.67	13.00 ± 2.29	5.08 ± 0.90	2.08 ± 0.37	1.06 ± 0.19	0.52 ± 0.09
113357	19.91 ± 2.41	9.76 ± 1.18	3.81 ± 0.46	1.56 ± 0.19	0.80 ± 0.10	0.39 ± 0.05
113576	21.81 ± 5.22	10.69 ± 2.56	4.17 ± 1.00	1.71 ± 0.41	0.87 ± 0.21	0.43 ± 0.10
114948	12.99 ± 1.27	6.37 ± 0.62	2.49 ± 0.24	1.02 ± 0.10	0.52 ± 0.05	0.25 ± 0.02
116745	12.06 ± 1.85	5.91 ± 0.91	2.31 ± 0.35	0.95 ± 0.15	0.48 ± 0.07	0.24 ± 0.04
116771	56.23 ± 6.09	27.55 ± 2.98	10.76 ± 1.16	4.41 ± 0.48	2.25 ± 0.24	1.10 ± 0.12
120005	29.27 ± 7.27	14.34 ± 3.56	5.60 ± 1.39	2.30 ± 0.57	1.17 ± 0.29	0.57 ± 0.14

$*$ 2MASS J magnitude without a reliable photometric error. Not used in the computations.

$\star$ 2MASS H magnitude is an upper limit. Not used in the computations.

† 2MASS K_s magnitude is an upper limit. Not used in the computations.

‡ 2MASS K_s magnitude without a reliable photometric error. Not used in the computations.

Bibliography

Aarnio, A. N., Weinberger, A. J., Stassun, K. G., Mamajek, E. E., & James, D. J. 2008, AJ, 136, 2483

Aibéo, A., Ferreira, J. M., & Lima, J. J. G. 2007, A&A, 473, 501

Alibert, Y., Mordasini, C., & Benz, W. 2004, A&A, 417, L25

Allende Prieto, C., Barklem, P. S., Lambert, D. L., & Cunha, K. 2004, A&A, 420, 183

Ammler-von Eiff, M. & Guenther, E. W. 2009, A&A, 508, 677

Anosova, J. P. & Orlov, V. V. 1991, A&A, 252, 123

Antoja, T., Figueras, F., Fernández, D., & Torra, J. 2008, A&A, 490, 135

Asiain, R., Figueras, F., Torra, J., & Chen, B. 1999, A&A, 341, 427

Aumann, H. H., Beichman, C. A., Gillett, F. C., et al. 1984, ApJ, 278, L23

Backman, D. E. & Paresce, F. 1993, in Protostars and Planets III, ed. E. H. Levy & J. I. Lunine, 1253–1304

Baliunas, S., Sokoloff, D., & Soon, W. 1996, ApJ, 457, L99

Barbier-Brossat, M. & Figon, P. 2000, A&AS, 142, 217

Barnes, S. A. 2007, ApJ, 669, 1167

Barnes, III, T. G., Moffett, T. J., & Slovak, M. H. 1986, PASP, 98, 223

Barrado y Navascués, D. 1998, A&A, 339, 831

Barrado y Navascués, D., Fernandez-Figueroa, M. J., Garcia Lopez, R. J., de Castro, E., & Cornide, M. 1997, A&A, 326, 780

Barrado y Navascués, D., Stauffer, J. R., Song, I., & Caillault, J. 1999, ApJ, 520, L123

Basri, G., Laurent, R., & Walter, F. M. 1985, ApJ, 298, 761

Beavers, W. I., Eitter, J. J., Ketelsen, D. A., & Oesper, D. A. 1979, PASP, 91, 698

Beichman, C. A., Bryden, G., Rieke, G. H., et al. 2005, ApJ, 622, 1160

Beichman, C. A., Bryden, G., Stapelfeldt, K. R., et al. 2006a, ApJ, 652, 1674

BIBLIOGRAPHY

Beichman, C. A., Tanner, A., Bryden, G., et al. 2006b, ApJ, 639, 1166

Benítez, N., Maíz-Apellániz, J., & Canelles, M. 2002, Physical Review Letters, 88, 081101

Bertone, E., Buzzoni, A., Chávez, M., & Rodríguez-Merino, L. H. 2004, AJ, 128, 829

Bessell, M. S. 1979, PASP, 91, 589

Bessell, M. S. 1990, PASP, 102, 1181

Boesgaard, A. M. 1991, ApJ, 370, L95

Boesgaard, A. M. & Friel, E. D. 1990, ApJ, 351, 467

Bond, J. C., Tinney, C. G., Butler, R. P., et al. 2006, MNRAS, 370, 163

Boss, A. P. 1997, Science, 276, 1836

Boss, A. P. 2002, ApJ, 567, L149

Boss, A. P. 2006, ApJ, 643, 501

Bovy, J., Hogg, D. W., & Roweis, S. T. 2009, ApJ, 700, 1794

Brott, I. & Hauschildt, P. H. 2005, in ESA Special Publication, Vol. 576, The Three-Dimensional Universe with Gaia, ed. C. Turon, K. S. O'Flaherty, & M. A. C. Perryman, 565

Bryden, G., Beichman, C. A., Carpenter, J. M., et al. 2009, ApJ, 705, 1226

Bryden, G., Beichman, C. A., Trilling, D. E., et al. 2006, ApJ, 636, 1098

Bubar, E. J. & King, J. R. 2010, AJ, 140, 293

Butler, R. P., Marcy, G. W., Vogt, S. S., et al. 2003, ApJ, 582, 455

Butler, R. P., Marcy, G. W., Williams, E., Hauser, H., & Shirts, P. 1997, ApJ, 474, L115

Castelli, F. & Kurucz, R. L. 2003, in IAU Symposium, Vol. 210, Modelling of Stellar Atmospheres, ed. N. Piskunov, W. W. Weiss, & D. F. Gray, 20P

Chavero, C., Gómez, M., Whitney, B. A., & Saffe, C. 2006, A&A, 452, 921

Chen, C. H., Patten, B. M., Werner, M. W., et al. 2005, ApJ, 634, 1372

Chereul, E., Crézé, M., & Bienaymé, O. 1999, A&AS, 135, 5

Cohen, M., Wheaton, W. A., & Megeath, S. T. 2003, AJ, 126, 1090

Currie, T. 2009, ApJ, 694, L171

Cutispoto, G., Messina, S., & Rodonò, M. 2001, A&A, 367, 910

Cutri, R. M., Skrutskie, M. F., van Dyk, S., et al. 2003, 2MASS All Sky Catalog of point sources., ed. Cutri, R. M., Skrutskie, M. F., van Dyk, S., Beichman, C. A., Carpenter, J. M., Chester, T., Cambresy, L., Evans, T., Fowler, J., Gizis, J., Howard, E., Huchra, J., Jarrett, T., Kopan, E. L., Kirkpatrick, J. D., Light, R. M., Marsh, K. A., McCallon, H., Schneider, S., Stiening, R., Sykes, M., Weinberg, M., Wheaton, W. A., Wheelock, S., & Zacarias, N.

Dehnen, W. 1998, AJ, 115, 2384

Dermott, S. F., Kehoe, T. J. J., Durda, D. D., Grogan, K., & Nesvorný, D. 2002, in ESA Special Publication, Vol. 500, Asteroids, Comets, and Meteors: ACM 2002, ed. B. Warmbein, 319–322

Dodson-Robinson, S. E., Beichman, C. A., Carpenter, J. M., & Bryden, G. 2011, AJ, 141, 11

Donahue, R. A. 1993, PhD thesis, New Mexico State University, University Park.

Dumusque, X., Santos, N. C., Udry, S., Lovis, C., & Bonfils, X. 2011a, A&A, 527, A82

Dumusque, X., Udry, S., Lovis, C., Santos, N. C., & Monteiro, M. J. P. F. G. 2011b, A&A, 525, A140

Duncan, D. K., Vaughan, A. H., Wilson, O. C., et al. 1991, ApJS, 76, 383

Eggen, O. J. 1958a, MNRAS, 118, 65

Eggen, O. J. 1958b, MNRAS, 118, 154

Eggen, O. J. 1959a, The Observatory, 79, 182

Eggen, O. J. 1959b, The Observatory, 79, 88

Eggen, O. J. 1964, Royal Greenwich Observatory Bulletin, 84, 111

Eggen, O. J. 1965, The Observatory, 85, 191

Eggen, O. J. 1969, PASP, 81, 553

Eggen, O. J. 1971a, PASP, 83, 271

Eggen, O. J. 1971b, PASP, 83, 251

Eggen, O. J. 1975, PASP, 87, 37

Eggen, O. J. 1984, AJ, 89, 1358

Eggen, O. J. 1987, in NATO ASIC Proc. 207: The Galaxy, ed. G. Gilmore & B. Carswell, 211–227

Eggen, O. J. 1989, PASP, 101, 366

Eggen, O. J. 1991, AJ, 102, 2028

Eggen, O. J. 1992, AJ, 104, 1493

Eggen, O. J. 1994, in Galactic and Solar System Optical Astrometry, ed. L. V. Morrison & G. F. Gilmore, 191

Eggen, O. J. 1995, AJ, 110, 2862

Eggen, O. J. & Sandage, A. R. 1959, MNRAS, 119, 255

Eiroa, C., Fedele, D., Maldonado, J., et al. 2010, A&A, 518, L131

Eiroa, C., Marshall, J. P., Mora, A., et al. 2011, A&A, 536, L4

Eker, Z., Ak, N. F., Bilir, S., et al. 2008, MNRAS, 389, 1722

ESA, ed. 1997, ESA Special Publication, Vol. 1200, The HIPPARCOS and TYCHO catalogues. Astrometric and photometric star catalogues derived from the ESA HIPPARCOS Space Astrometry Mission

Famaey, B., Pont, F., Luri, X., et al. 2007, A&A, 461, 957

Famaey, B., Siebert, A., & Jorissen, A. 2008, A&A, 483, 453

Favata, F., Barbera, M., Micela, G., & Sciortino, S. 1995, A&A, 295, 147

Feltzing, S. & Holmberg, J. 2000a, A&A, 357, 153

Feltzing, S. & Holmberg, J. 2000b, A&A, 357, 153

Fischer, D. A. & Valenti, J. 2005, ApJ, 622, 1102

Fleming, T. A., Schmitt, J. H. M. M., & Giampapa, M. S. 1995, ApJ, 450, 401

Flower, P. J. 1996, ApJ, 469, 355

Francis, C. & Anderson, E. 2009, New A, 14, 615

Frandsen, S. & Lindberg, B. 1999, in Astrophysics with the NOT, ed. H. Karttunen & V. Piirola, 71

Fuhrmann, K. 2004, Astronomische Nachrichten, 325, 3

Fuhrmann, K. 2008, MNRAS, 384, 173

Gaidos, E. J., Henry, G. W., & Henry, S. M. 2000, AJ, 120, 1006

Gálvez, M. C., Montes, D., Fernández-Figueroa, M. J., & López-Santiago, J. 2006, Ap&SS, 304, 59

Garnett, D. R. & Kobulnicky, H. A. 2000, ApJ, 532, 1192

Gautier, III, T. N., Rieke, G. H., Stansberry, J., et al. 2007, ApJ, 667, 527

Ghezzi, L., Cunha, K., Schuler, S. C., & Smith, V. V. 2010a, ApJ, 725, 721

Ghezzi, L., Cunha, K., Smith, V. V., et al. 2010b, ApJ, 720, 1290

Gomes, R. S. 2003, Icarus, 161, 404

González Hernández, J. I., Israelian, G., Santos, N. C., et al. 2010, ApJ, 720, 1592

Gratton, R. G., Bonanno, G., Bruno, P., et al. 2001, Experimental Astronomy, 12, 107

Gray, R. O., Corbally, C. J., Garrison, R. F., et al. 2006, AJ, 132, 161

Gray, R. O., Corbally, C. J., Garrison, R. F., McFadden, M. T., & Robinson, P. E. 2003, AJ, 126, 2048

Greaves, J. S., Fischer, D. A., & Wyatt, M. C. 2006, MNRAS, 366, 283

Greaves, J. S., Fischer, D. A., Wyatt, M. C., Beichman, C. A., & Bryden, G. 2007, MNRAS, 378, L1

Griffin, M. J., Abergel, A., Abreu, A., et al. 2010, A&A, 518, L3

Griffin, R. F. 1998, The Observatory, 118, 223

Guedel, M., Guinan, E. F., & Skinner, S. L. 1997, ApJ, 483, 947

Gurnett, D. A., Ansher, J. A., Kurth, W. S., & Granroth, L. J. 1997, Geophys. Res. Lett., 24, 3125

Gustafsson, B., Edvardsson, B., Eriksson, K., et al. 2008, A&A, 486, 951

Habing, H. J., Dominik, C., Jourdain de Muizon, M., et al. 2001, A&A, 365, 545

Hall, J. C., Lockwood, G. W., & Skiff, B. A. 2007, AJ, 133, 862

Hartmann, L. 2000, Accretion Processes in Star Formation, Cambridge University Press

Hauck, B. & Mermilliod, M. 1997, VizieR Online Data Catalog, 2215, 0

Hekker, S. & Meléndez, J. 2007, A&A, 475, 1003

Henry, T. J., Soderblom, D. R., Donahue, R. A., & Baliunas, S. L. 1996, AJ, 111, 439

Høg, E., Fabricius, C., Makarov, V. V., et al. 2000, A&A, 355, L27

Hollenbach, D., Gorti, U., Meyer, M., et al. 2005, ApJ, 631, 1180

Hormuth, F., Brandner, W., Hippler, S., Janson, M., & Henning, T. 2007, A&A, 463, 707

Hubickyj, O., Bodenheimer, P., & Lissauer, J. J. 2005, Icarus, 179, 415

Humes, D. H. 1980, J. Geophys. Res., 85, 5841

Hünsch, M., Schmitt, J. H. M. M., Sterzik, M. F., & Voges, W. 1999, A&AS, 135, 319

Ida, S. & Lin, D. N. C. 2004, ApJ, 616, 567

Jenkins, J. S., Jones, H. R. A., Tinney, C. G., et al. 2006, MNRAS, 372, 163

Jewitt, D. C. & Luu, J. X. 2000, Protostars and Planets IV, 1201

Jianke, L. & Collier Cameron, A. 1993, MNRAS, 261, 766

Johnson, D. R. H. & Soderblom, D. R. 1987, AJ, 93, 864

Jura, M. 2003, ApJ, 584, L91

Kapteyn, J. C. 1905, Brit. Assoc. Adv. Sci. Rep., 302, 257

Kaufer, A., Stahl, O., Tubbesing, S., et al. 1999, The Messenger, 95, 8

Kawaler, S. D. 1989, ApJ, 343, L65

Kenyon, S. J. & Bromley, B. C. 2005, AJ, 130, 269

Kharchenko, N. V., Scholz, R.-D., Piskunov, A. E., Röser, S., & Schilbach, E. 2007, Astronomische Nachrichten, 328, 889

King, J. R., Villarreal, A. R., Soderblom, D. R., Gulliver, A. F., & Adelman, S. J. 2003, AJ, 125, 1980

Klement, R., Fuchs, B., & Rix, H.-W. 2008, ApJ, 685, 261

Koerner, D. W., Kim, S., Trilling, D. E., et al. 2010, ApJ, 710, L26

Kóspál, Á., Ardila, D. R., Moór, A., & Ábrahám, P. 2009, ApJ, 700, L73

Kraft, R. P. 1967, ApJ, 150, 551

Lachaume, R., Dominik, C., Lanz, T., & Habing, H. J. 1999, A&A, 348, 897

Levison, H. F. & Morbidelli, A. 2003, Nature, 426, 419

Li, J. Z. & Hu, J. Y. 1998, A&AS, 132, 173

Li, J. Z., Hu, J. Y., & Chen, W. P. 2000, A&A, 356, 157

López-Santiago, J., Micela, G., & Montes, D. 2009, A&A, 499, 129

López-Santiago, J., Montes, D., Crespo-Chacón, I., & Fernández-Figueroa, M. J. 2006, ApJ, 643, 1160

López-Santiago, J., Montes, D., Gálvez-Ortiz, M. C., et al. 2010, A&A, 514, A97

Maíz-Apellániz, J. 2001, ApJ, 560, L83

Makarov, V. V. 2007, ApJS, 169, 105

Maldonado, J., Eiroa, C., Villaver, E., Montesinos, B., & Mora, A. 2012, A&A, 541, A40

Maldonado, J., Martínez-Arnáiz, R. M., Eiroa, C., Montes, D., & Montesinos, B. 2010, A&A, 521, A12

Mamajek, E. E. 2006, AJ, 132, 2198

Mamajek, E. E. 2007, in IAU Symposium, Vol. 237, IAU Symposium, ed. B. G. Elmegreen & J. Palous, 442–442

Mamajek, E. E. & Hillenbrand, L. A. 2008, ApJ, 687, 1264

Martínez-Arnáiz, R., Maldonado, J., Montes, D., Eiroa, C., & Montesinos, B. 2010, A&A, 520, A79

Mason, B. D., Wycoff, G. L., Hartkopf, W. I., Douglass, G. G., & Worley, C. E. 2001, AJ, 122, 3466

Matteucci, F. & Greggio, L. 1986, A&A, 154, 279

Matteucci, F. & Recchi, S. 2001, ApJ, 558, 351

Matteucci, F., Spitoni, E., Recchi, S., & Valiante, R. 2009, A&A, 501, 531

Matthews, B. C., Sibthorpe, B., Kennedy, G., et al. 2010, A&A, 518, L135

Mayor, M., Marmier, M., Lovis, C., et al. 2011, ArXiv e-prints

Mayor, M., Udry, S., Naef, D., et al. 2004, A&A, 415, 391

Meibom, S., Mathieu, R. D., & Stassun, K. G. 2009, ApJ, 695, 679

Meléndez, J., Asplund, M., Gustafsson, B., & Yong, D. 2009, ApJ, 704, L66

Messina, S., Rodonò, M., & Guinan, E. F. 2001, A&A, 366, 215

Montes, D. 2010, in Highlights of Astronomy XV, Proceedings of the IAU XXVII General Assembly, August 03 - 14, 2009 Rio de Janeiro, Brazil

Montes, D., Fernandez-Figueroa, M. J., Cornide, M., & de Castro, E. 1996, A&A, 312, 221

Montes, D., López-Santiago, J., Fernández-Figueroa, M. J., & Gálvez, M. C. 2001a, A&A, 379, 976

Montes, D., López-Santiago, J., Gálvez, M. C., et al. 2001b, MNRAS, 328, 45

Montesinos, B., Thomas, J. H., Ventura, P., & Mazzitelli, I. 2001, MNRAS, 326, 877

Moór, A., Ábrahám, P., Derekas, A., et al. 2006, ApJ, 644, 525

Moór, A., Pascucci, I., Kóspál, Á., et al. 2011, ApJS, 193, 4

Mordasini, C., Alibert, Y., & Benz, W. 2009, A&A, 501, 1139

Mordasini, C., Alibert, Y., Benz, W., Klahr, H., & Henning, T. 2012, ArXiv e-prints

Moro-Martín, A., Carpenter, J. M., Meyer, M. R., et al. 2007, ApJ, 658, 1312

Nesvorný, D., Jenniskens, P., Levison, H. F., et al. 2010, ApJ, 713, 816

Neuhaeuser, R., Torres, G., Sterzik, M. F., & Randich, S. 1997, A&A, 325, 647

Nidever, D. L., Marcy, G. W., Butler, R. P., Fischer, D. A., & Vogt, S. S. 2002, ApJS, 141, 503

Nilsson, R., Liseau, R., Brandeker, A., et al. 2010, A&A, 518, A40

Nordström, B., Mayor, M., Andersen, J., et al. 2004, A&A, 418, 989

Noyes, R. W., Hartmann, L. W., Baliunas, S. L., Duncan, D. K., & Vaughan, A. H. 1984, ApJ, 279, 763

O'Brien, D. P., Morbidelli, A., & Bottke, W. F. 2007, Icarus, 191, 434

Pascucci, I., Gorti, U., Hollenbach, D., et al. 2006, ApJ, 651, 1177

Pasquini, L., Döllinger, M. P., Weiss, A., et al. 2007, A&A, 473, 979

Peacock, J. A. 1983, MNRAS, 202, 615

Pfeiffer, M. J., Frank, C., Baumueller, D., Fuhrmann, K., & Gehren, T. 1998, A&AS, 130, 381

Pilbratt, G. L., Riedinger, J. R., Passvogel, T., et al. 2010, A&A, 518, L1

Pizzolato, N., Maggio, A., Micela, G., Sciortino, S., & Ventura, P. 2003, A&A, 397, 147

Plavchan, P., Werner, M. W., Chen, C. H., et al. 2009, The Astrophysical Journal, 698, 1068

Poglitsch, A., Waelkens, C., Geis, N., et al. 2010, A&A, 518, L2

Pollack, J. B., Hubickyj, O., Bodenheimer, P., et al. 1996, Icarus, 124, 62

Porto de Mello, G. F. & da Silva, L. 1997, ApJ, 482, L89

Pourbaix, D., Tokovinin, A. A., Batten, A. H., et al. 2004, A&A, 424, 727

Proctor, R. A. 1869, Royal Society of London Proceedings Series I, 18, 169

Prosser, C. F., Shetrone, M. D., Dasgupta, A., et al. 1995, PASP, 107, 211

Radick, R. R., Thompson, D. T., Lockwood, G. W., Duncan, D. K., & Baggett, W. E. 1987, ApJ, 321, 459

Ramírez, I., Asplund, M., Baumann, P., Meléndez, J., & Bensby, T. 2010, A&A, 521, A33

Ramírez, I., Meléndez, J., & Asplund, M. 2009, A&A, 508, L17

Raskin, G., van Winckel, H., Hensberge, H., et al. 2011, A&A, 526, A69

Raymond, S. N., Armitage, P. J., Moro-Martín, A., et al. 2011, A&A, 530, A62

Reach, W. T., Morris, P., Boulanger, F., & Okumura, K. 2003, Icarus, 164, 384

Reid, I. N., Hawley, S. L., & Gizis, J. E. 1995, AJ, 110, 1838

Rhee, J. H., Song, I., Zuckerman, B., & McElwain, M. 2007, ApJ, 660, 1556

Ribas, I., Guinan, E. F., Güdel, M., & Audard, M. 2005, ApJ, 622, 680

Rice, W. K. M. & Armitage, P. J. 2003, ApJ, 598, L55

Rieke, G. H., Su, K. Y. L., Stansberry, J. A., et al. 2005, ApJ, 620, 1010

Rocha-Pinto, H. J. & Maciel, W. J. 1998, MNRAS, 298, 332

Ruden, S. P. 1999, in NATO ASIC Proc. 540: The Origin of Stars and Planetary Systems, ed. C. J. Lada & N. D. Kylafis, 643

Saar, S. H. & Osten, R. A. 1997, MNRAS, 284, 803

Saffe, C., Gómez, M., & Chavero, C. 2005, A&A, 443, 609

Saffe, C., Gómez, M., Pintado, O., & González, E. 2008, A&A, 490, 297

Santos, N. C., Israelian, G., & Mayor, M. 2001, A&A, 373, 1019

Santos, N. C., Israelian, G., & Mayor, M. 2004, A&A, 415, 1153

Schroeder, D. J., ed. 2000, Astronomical optics

Schuster, W. J. & Nissen, P. E. 1989, A&A, 221, 65

Schütz, O., Meeus, G., & Sterzik, M. F. 2005, A&A, 431, 175

Shu, F. H., Adams, F. C., & Lizano, S. 1987, ARA&A, 25, 23

Siegler, N., Muzerolle, J., Young, E. T., et al. 2007, ApJ, 654, 580

Siess, L., Dufour, E., & Forestini, M. 2000, A&A, 358, 593

Simon, T. & Fekel, Jr., F. C. 1987, ApJ, 316, 434

Sinclair, J. A., Helling, C., & Greaves, J. S. 2010, MNRAS, 409, L49

Skiff, B. A. 2009, VizieR Online Data Catalog, 1, 2023

Skuljan, J., Cottrell, P. L., & Hearnshaw, J. B. 1997, in ESA Special Publication, Vol. 402, Hipparcos - Venice '97, 525–530

Skuljan, J., Hearnshaw, J. B., & Cottrell, P. L. 1999, MNRAS, 308, 731

Skumanich, A. 1972, ApJ, 171, 565

Smith, P. S., Hines, D. C., Low, F. J., et al. 2006, ApJ, 644, L125

Soderblom, D. R. 1983, ApJS, 53, 1

Soderblom, D. R. 2010, ARA&A, 48, 581

Soderblom, D. R., Duncan, D. K., & Johnson, D. R. H. 1991, ApJ, 375, 722

Soderblom, D. R., Jones, B. F., Balachandran, S., et al. 1993, AJ, 106, 1059

Soderblom, D. R., Laskar, T., Valenti, J. A., Stauffer, J. R., & Rebull, L. M. 2009, AJ, 138, 1292

Soderblom, D. R. & Mayor, M. 1993a, ApJ, 402, L5

Soderblom, D. R. & Mayor, M. 1993b, AJ, 105, 226

Soderblom, D. R., Oey, M. S., Johnson, D. R. H., & Stone, R. P. S. 1990, AJ, 99, 595

Sousa, S. G., Santos, N. C., Israelian, G., Mayor, M., & Udry, S. 2011, A&A, 533, A141

Sousa, S. G., Santos, N. C., Mayor, M., et al. 2008, A&A, 487, 373

Spangler, C., Sargent, A. I., Silverstone, M. D., Becklin, E. E., & Zuckerman, B. 2001, ApJ, 555, 932

Stauffer, J. R., Caillault, J.-P., Gagne, M., Prosser, C. F., & Hartmann, L. W. 1994, ApJS, 91, 625

Steele, P. R., Burleigh, M. R., Dobbie, P. D., et al. 2011, MNRAS, 416, 2768

Stern, R. A., Schmitt, J. H. M. M., & Kahabka, P. T. 1995, ApJ, 448, 683

Sterzik, M. F. & Schmitt, J. H. M. M. 1997, AJ, 114, 1673

Strom, R. G., Malhotra, R., Ito, T., Yoshida, F., & Kring, D. A. 2005, Science, 309, 1847

Su, K. Y. L., Rieke, G. H., Stansberry, J. A., et al. 2006, ApJ, 653, 675

Takeda, Y., Honda, S., Kawanomoto, S., Ando, H., & Sakurai, T. 2010, A&A, 515, A93

Takeda, Y., Kawanomoto, S., Honda, S., Ando, H., & Sakurai, T. 2007, A&A, 468, 663

Takeda, Y., Ohkubo, M., & Sadakane, K. 2002, PASJ, 54, 451

Takeda, Y., Sato, B., Kambe, E., et al. 2005, PASJ, 57, 109

Tanner, A., Beichman, C., Bryden, G., Lisse, C., & Lawler, S. 2009, ApJ, 704, 109

Taylor, B. J. 2000, A&A, 362, 563

Timmes, F. X., Woosley, S. E., & Weaver, T. A. 1995, ApJS, 98, 617

Torres, C. A. O., Quast, G. R., de La Reza, R., da Silva, L., & Melo, C. H. F. 2003, in Astronomical Society of the Pacific Conference Series, Vol. 287, Galactic Star Formation Across the Stellar Mass Spectrum, ed. J. M. De Buizer & N. S. van der Bliek, 439–444

Torres, C. A. O., Quast, G. R., Melo, C. H. F., & Sterzik, M. F. 2008, Young Nearby Loose Associations, ed. Reipurth, B., 757

Trilling, D. E., Bryden, G., Beichman, C. A., et al. 2008, ApJ, 674, 1086

Trilling, D. E., Stansberry, J. A., Stapelfeldt, K. R., et al. 2007, ApJ, 658, 1289

Tull, R. G., MacQueen, P. J., Sneden, C., & Lambert, D. L. 1995, PASP, 107, 251

Udry, S., Mayor, M., Benz, W., et al. 2006, A&A, 447, 361

Udry, S., Mayor, M., Maurice, E., et al. 1999a, in Astronomical Society of the Pacific Conference Series, Vol. 185, IAU Colloq. 170: Precise Stellar Radial Velocities, ed. J. B. Hearnshaw & C. D. Scarfe, 383

Udry, S., Mayor, M., & Queloz, D. 1999b, in Astronomical Society of the Pacific Conference Series, Vol. 185, IAU Colloq. 170: Precise Stellar Radial Velocities, ed. J. B. Hearnshaw & C. D. Scarfe, 367

Valenti, J. A. & Fischer, D. A. 2005, ApJS, 159, 141

van Leeuwen, F. v. 2007, Hipparcos, the New Reduction of the Raw Data (XXXII, 449 p., Hardcover, ISBN: 978-1-4020-6341-1: Astrophysics and Space Science Library , Vol. 350)

Vaughan, A. H. & Preston, G. W. 1980, PASP, 92, 385

Vitense, C., Krivov, A. V., Kobayashi, H., & Löhne, T. 2012, A&A, 540, A30

Voges, W., Aschenbach, B., Boller, T., et al. 1999, A&A, 349, 389

Voges, W., Aschenbach, B., Boller, T., et al. 2000, IAU Circ., 7432, 1

Vogt, S. S., Butler, R. P., Marcy, G. W., et al. 2005, ApJ, 632, 638

Weber, E. J. & Davis, L. J. 1967, ApJ, 148, 217

Wielen, R. 1971, A&A, 13, 309

Williams, M. E. K., Freeman, K. C., Helmi, A., & the RAVE collaboration. 2009, in IAU Symposium, Vol. 254, IAU Symposium, ed. J. Andersen, J. Bland-Hawthorn, & B. Nordström, 139–144

Wright, C. O., Egan, M. P., Kraemer, K. E., & Price, S. D. 2003, AJ, 125, 359

Wright, E. L., Eisenhardt, P. R. M., Mainzer, A. K., et al. 2010, AJ, 140, 1868

Wright, J. T., Marcy, G. W., Butler, R. P., & Vogt, S. S. 2004, ApJS, 152, 261

Wright, J. T., Upadhyay, S., Marcy, G. W., et al. 2009, ApJ, 693, 1084

Wyatt, M. C. 2008, ARA&A, 46, 339

Wylie-de Boer, E., Freeman, K., & Williams, M. 2010, AJ, 139, 636

Zhao, J., Zhao, G., & Chen, Y. 2009, ApJ, 692, L113

Zuckerman, B., Bessell, M. S., Song, I., & Kim, S. 2006, ApJ, 649, L115

Zuckerman, B. & Song, I. 2004, ARA&A, 42, 685

Zuckerman, B., Song, I., & Bessell, M. S. 2004, ApJ, 613, L65

Zuckerman, B. & Webb, R. A. 2000, ApJ, 535, 959